

## Self-healing Porous Asphalt: A Combination of Encapsulated Rejuvenator and Induction Heating

Xu, S.

**DOI**

[10.4233/uuid:d6b9b064-ae38-421e-a709-0fcc5a3f028f](https://doi.org/10.4233/uuid:d6b9b064-ae38-421e-a709-0fcc5a3f028f)

**Publication date**

2020

**Document Version**

Final published version

**Citation (APA)**

Xu, S. (2020). *Self-healing Porous Asphalt: A Combination of Encapsulated Rejuvenator and Induction Heating*. [Dissertation (TU Delft), Delft University of Technology]. <https://doi.org/10.4233/uuid:d6b9b064-ae38-421e-a709-0fcc5a3f028f>

**Important note**

To cite this publication, please use the final published version (if applicable). Please check the document version above.

**Copyright**

Other than for strictly personal use, it is not permitted to download, forward or distribute the text or part of it, without the consent of the author(s) and/or copyright holder(s), unless the work is under an open content license such as Creative Commons.

**Takedown policy**

Please contact us and provide details if you believe this document breaches copyrights. We will remove access to the work immediately and investigate your claim.

**Self-healing Porous Asphalt: A Combination of  
Encapsulated Rejuvenator and Induction Heating**



**Self-healing Porous Asphalt: A Combination of  
Encapsulated Rejuvenator and Induction Heating**

**Dissertation**

for the purpose of obtaining the degree of doctor

at Delft University of technology

by the authority of the Rector Magnificus Prof. dr. ir. T. H. J. van der Hagen

chair of the Board for Doctorates

to be defended publicly on

Monday, 23 November 2020 at 15.00 hours

By

**Shi XU**

Master of Engineering in Material Science,  
Wuhan University of Technology, P.R. China,  
born in Hubei, P.R. China.

This dissertation has been approved by the promotor

Promotor: Prof. dr. ir. E. Schlangen

Copromotor: Dr. X. Liu

Composition of the doctoral committee:

Rector Magnificus,	chairperson
Prof. dr. ir. E. Schlangen	Delft University of Technology, promotor
Dr. X. Liu	Delft University of Technology, copromotor

Independent members:

Prof. dr. ir. S.M.J.G. Erkens	Delft University of Technology
Prof. dr. ir. P. Bauer	Delft University of Technology
Prof. dr. Q. Liu,	Wuhan University of Technology
Dr. ir. B.J. Lommerts	Latexfalt B.V.

Other member:

Dr. A. Tabaković	Technological University Dublin
------------------	---------------------------------



This research was financially supported by China Scholarship Council.

Keywords: Self-healing asphalt, Calcium alginate capsules, induction heating, Combined healing system.

Printed by: Ipskamp Printing, The Netherlands

Cover design: Shi Xu

Copy right @ 2020 by S. Xu

ISBN 978-94-6421-138-2

An electronic version of this dissertation is available at

<http://repository.tudelft.nl>

*To my family*



# ACKNOWLEDGEMENTS

I would like to express my appreciations to all dear teachers, colleagues, friends and family who helped me through the journey to a PhD.

First of all, a special gratitude goes to China Scholarship Council (CSC) for sponsoring me to conduct the research presented in this dissertation at the section of Materials and Environment at the faculty of Civil Engineering and Geosciences at Delft University of Technology. Support from the section of Pavement Engineering at the faculty of Civil Engineering and Geosciences at Delft University of Technology, Heijmans and Latexfalt B.V. are greatly appreciated.

I would like to express my sincere gratitude to my promotor Prof. Erik Schlangen. He enlightens me with his unique scientific vision which keeps me always working in the right direction. His office is always open for a sudden discussion, and no matter how busy he is, he is always enthusiastic and tries the best to give the feedback in time. As a professor, he could even drive thousand of miles to pursue a solution for my research. His patience and tolerance are also impressive, which motivate me to think and try innovatively. He is serious in work, while in daily conversations, his sense of humour always makes me happy and relaxed. I will be grateful forever for everything he has done for me and everything I learnt from him, in both life and research.

My special gratitude goes to my co-promotor Dr. Xueyan Liu. His meticulous concern covers every aspect of my research and his professional and constructive suggestions always help me to overcome obstacles. As a supervisor, he is always strict and encourages me to challenge and learn something new, and all these finally become the most precious treasure that will benefit my whole career. Every year, he organises dinner for the Chinese New Year, the traditional dishes and music make me feel at home which is very meaningful for us far away from hometown, and the hospitality of his wife Mrs Li and daughter Liu Liu are greatly appreciated.

I would also like to acknowledge my supervisor Dr. Amir Tabaković. Amir helped me to build the first milestone at the beginning of my PhD research and offered me persistent support even if he no longer worked in TUDelft. He not only

helps me in the research, but also concerns my life, and all these make him much more than a supervisor to me.

Besides my supervisors, I would like to thank all other committee members for my PhD defence: Prof. Kees Vuik, Prof. Sandra Erkens, Prof. Pavol Bauer, Prof. Quantao Liu and Dr. Bert Jan Lommerts.

I would like to thank Martin Megalla who helped me to translate the Summary of this thesis from English to Dutch. Thank you for the friendship and a lot of funs together on business trips. Meanwhile, special thanks go to Dr. Henk Jonkers, Dr. Damian Palin and Renée Mors for the very kindly share of knowledge on self-healing materials. Additionally, the help from Dr. Branko Šavija in modelling and Dr. Oguzhan Copuroglu in microscopy are greatly appreciated.

I would also like to thank people from Heijmans and Latexfalt: Dr. Gerbert van Bochove, Dr. Bert Jan Lommerts, Dr. Sayeda Nahar, Ruud Kurvers, Thomas van der Kwaak for their kind help to my research. In TUDelft, support from Arjan Thijssen, Maiko van Leeuwen, Ton Blom, John van den berg, Marco Poot, Michèle van Aggelen, Jan Willem, Paul Vermeulen are greatly appreciated. I would also like to acknowledge secretaries: Jacqueline van Unen-Berghenegouwen, Iris Batterham, Claire de Bruin, Nynke Verhulst, Claudia Baltussen, for their assistance during my stay in TUDelft.

The help of people from Wuhan University of Technology is greatly appreciated. Special thanks go to Prof. Jianying Yu who lead me to the world of material sciences. I wish also to thank Prof. Shaopeng Wu, Prof. Quantao Liu, Prof. Gang Liu, Prof. Yue Xiao, Dr. Liantong Mo. I wish also to thank Jian Qiu (Lili Wu) and Yuan Zhang (Hailing Zhang) who offered me a warm welcome in the Netherlands and helped me a lot in getting used to the life in Delft. Thank you for all the kind help!

I would like to thank my officemates: Hongzhi Zhang, Wenjuan Lyu, Xuhui Liang, Zhi Wan, Xingliang Yao, Zainab Aldin and Kamel Arbi. It is a great pleasure to share my research life in room 6.06 with you.

My special thanks go to Xu Ma, Leyang Lyu and Xueer Tang, Stefan Chaves Figueiredo and Bianca Fraga Silva, Claudia Romero Rodriguez and Fernando Mendonca Filho, Yu Chen, Yading Xu, Yidong Gan, Ze Chang and Lu cheng, Emanuele Rossi, Marija Nedeljković and Patrick Holthuizen. Thank you for the friendship, wonderful presentations in group meetings and happiness in lunchtime and coffee break.

My appreciation extends to other colleagues in Microlab. Special thanks to Dr. Guang Ye for organising special events for Chinese colleagues for our traditional festivals. I would also like to thank Farhad Pargar, Jeannette van den Bos, Amir

Zomorodian, Yask Kulshreshtha, Kuba Pawlowicz, Albina Kostiuhenko and Bart Hendrix for the joyful moments together. A very special gratitude goes to my Chinese colleagues for all beautiful memories: Hua Dong, Jiayi Chen (Wenqin Shi), Tianshi Lu, Peng Gao, Yong Zhang, Hao Huang (Ha Ni), Bei Wu, Xuliang Hou (Ying Yang), Zhipei Chen, Xiaowei Ouyang (Cui Wei), Yibing Zuo, Zhenming Li (Na Yu), Shizhe Zhang, Boyu Chen, Zhiyuan Xu, Yu Zhang. Thank you all for the friendship and support!

I would also like to acknowledge other colleagues in the section of Pavement Engineering in TUDelft. Thank you, Prof. Tom Scarpas, Dr. Martin van de Ven, Dr. Lambert Houben, Dr. Kumar Anupam, Dr. Katerina Varveri, Cor Kasbergen, Dr. Ruxin Jing, Pavlatos Nikiforos, Dr. Chao Xing, Dr. Meng Zhang, Dr. Naipeng Tang, Greet Leegwater, Hong Zhang, Tianchi Tang, Haopeng Wang, Zhaojie Sun, Panos Apostolidis, Peng Lin, Yi Zhang, Shisong Ren and Lili Ma. Colleagues from pavement section is another big family for me who are always friendly and enthusiastic to help. I will forever remember the moments we working together, sharing ideas and our journey in conferences.

My special thanks go to the visiting scholars who shared their experiences in TUDelft. Special thanks to Prof. Yingzi Yang, her words 'Every effort you make will become a precious asset in the future' always motivate me and make me strong. Thank you, Pro. Jiangxiong Wei, Dr. Yun Huang, Prof. Weidong Huang, Prof. Dae-wook Park, Dr. José Norambuena-Contreras, Dr. Alvaro Gonzalez Dr. Yuqing Zhang, Dr. Fan Gu, Jiahua Liu, Dr. Min Bai. I really learnt a lot from all of you.

I wish also to thank the people I met in conferences: Prof. Sybrand van der Zwaag, Dr. Santiago Garcia, Prof. Lijun Sun, Prof. Feipeng Xiao, Prof. Hui Li, Prof. Dawei Wang, Prof. Jun Yang, Prof. Xianhua Chen, Dr. Zhen Leng, Dr. Pengfei Liu, Dr. Guoyang lu, Prof. Ningxu Han, Giovanni Anglani and all other people who shared their precious experience and exchanged ideas with me.

Many thanks to my friends: Haixin Fang, Kai Li, Ran Shang, Tao Iyu, Kai Zhang, Xiangming Liu, Yuguang Yang, Zhou Zhou, Hongxiao Guo, Wei Fang, Fanxiang Xu, Langzi Chang, Liangfu Wei. Thank you for the friendship and the beautiful memories in Delft.

Finally, I want to express my deepest love to my parents, my wife and my daughter. My parents, thank you for bringing me up, teaching me everything, giving me unlimited support with infinite love. My wife, Qiling Wang, thank you for giving up everything, joining me all the way to the Netherlands and supporting me unconditionally. My daughter, Yahan Xu, thank you for coming to the world and bringing me the ultimate happiness. It is so proud to watch you grow up, to learn

everything little by little, and your smile are always so cute. Special thanks to my mother-in-law Mrs Qiu for her kind help to carry my family in the Netherlands. To all my dear family, I cannot achieve all these without you, I love you all and my appreciation is truly beyond words.

Shi Xu (许实)

October 2020

Delft



# CONTENTS

<b>CHAPTER 1</b>	<b>GENERAL INTRODUCTION</b>	<b>1</b>
1.1.	Research background	2
1.1.1.	Ravelling in porous asphalt	2
1.1.2.	Development of self-healing asphalt	3
1.1.3.	Alginate and its encapsulation abilities	4
1.2.	Research objective	5
1.3.	Research approach	6
1.4.	Thesis outline	7
	References	8
<b>CHAPTER 2</b>	<b>SELF-HEALING ASPHALT: LITERATURE REVIEW</b>	<b>13</b>
2.1.	Self-healing materials: an introduction to the concept and principle	14
2.2.	The intrinsic healing capacity of bituminous materials	16
2.2.1.	The concept of self-healing in bituminous materials	16
2.2.2.	Influence factors on self-healing effect of asphalt pavement	18
2.3.	Extrinsic healing methods for asphalt pavement	21
2.3.1.	Thermally induced healing methods	22
2.3.2.	Embedded rejuvenator encapsulation methods	34
2.4.	Concluding remarks	47
	References	49
<b>CHAPTER 3</b>	<b>DETERMINATION OF PROPER REJUVENATOR TYPE AND AMOUNT FOR THE CAPSULE HEALING SYSTEM</b>	<b>61</b>
3.1.	Introduction	62
3.2.	Materials and methods	65
3.2.1.	Materials	65
3.2.2.	Test methods	66
3.3.	Results and discussion	72
3.3.1.	Physical properties	72
3.3.2.	Rheological properties	75
3.3.3.	Chemical properties	79

3.4. Conclusions	81
References	83
<b>CHAPTER 4 PREPARATION AND OPTIMIZATION OF THE CALCIUM ALGINATE CAPSULES</b>	<b>87</b>
4.1. Introduction	88
4.2. Materials and methods	88
4.2.1. Preparation of calcium alginate capsules	88
4.2.2. Characterization of calcium alginate capsules	90
4.3. Results and discussions	93
4.3.1. Capsule morphology	93
4.3.2. Microstructure	94
4.3.3. Thermal stability	95
4.3.4. Mechanical resistance	96
4.3.5. Volumetric composition	98
4.4. Conclusions	100
References	101
<b>CHAPTER 5 EVALUATION OF THE HEALING EFFECT OF CALCIUM ALGINATE CAPSULES IN POROUS ASPHALT</b>	<b>103</b>
5.1. Introduction	104
5.2. Materials and methods	104
5.2.1. Materials and asphalt mixture design	104
5.2.2. laboratory ageing process	106
5.2.3. Beam sample preparation for asphalt mastic and mortar	107
5.2.4. Three point bending test for asphalt mastic/mortar samples	108
5.2.5. Preparation of porous asphalt concrete slabs	109
5.2.6. Semi-circular bending and healing test for porous asphalt concrete samples	110
5.2.7. Bending and healing programme	112
5.3. Results and discussions	116
5.3.1. Fracture faces characterization	116
5.3.2. Mechanical response of the tested samples	118
5.3.3. Healing efficiency	122
5.4. Conclusions	125
References	127
<b>CHAPTER 6 SELF-HEALING SYSTEM EVALUATION IN POROUS ASPHALT</b>	<b>129</b>

6.1. Introduction	130
6.2. Materials and methods	131
6.2.1. Mixture design and sample preparation	131
6.2.2. Asphalt binder and mixture characterization	134
6.2.3. Mechanical property tests	136
6.2.4. Fatigue property tests	138
6.2.5. Healing procedure design and healing efficiency evaluation	142
6.3. Results and discussions	148
6.3.1. Material study	148
6.3.2. Mechanical properties	150
6.3.3. Fatigue properties	154
6.3.4. Healing efficiency	160
6.4. Conclusions	163
References	165
<b>CHAPTER 7 CONCLUSIONS AND RECOMMENDATIONS</b>	<b>167</b>
7.1. Conclusions and prospects	168
7.1.1. Calcium alginate capsules encapsulating rejuvenator	168
7.1.2. Evaluation of self-healing systems in porous asphalt	169
7.2. Recommendations for future work	171
7.3. References	172
<b>APPENDIX A</b>	<b>173</b>
<b>APPENDIX B</b>	<b>181</b>
<b>APPENDIX C</b>	<b>185</b>
<b>SUMMARY</b>	<b>191</b>
<b>SAMENVATTING</b>	<b>193</b>
<b>CURRICULUM VITAE</b>	<b>197</b>
<b>LIST OF PUBLICATIONS</b>	<b>199</b>



# 1

## GENERAL INTRODUCTION

*This chapter introduces the background and objective of this research. The advantages and issues in porous asphalt and the concept of self-healing asphalt are presented. Then, the healing agent encapsulation prospect with alginate is presented. Finally, the outline of this thesis is given.*

## 1.1. RESEARCH BACKGROUND

### 1.1.1. RAVELLING IN POROUS ASPHALT

In the Netherlands, the concept of Zeer Open Asphalt Beton (ZOAB), which is known as Porous Asphalt (PA) in the rest of world, was proposed and first applied in 1972 [1]. With a void content above 20%, PA shows advantages in noise reduction, comfortable driving and reducing of splash and spray during rainfall, which led to a fast implementation in the asphalt pavement design in both the Netherlands and worldwide [2-4]. Figure 1.1 illustrates the water draining advantage of porous asphalt over the standard pavement, which prevents water accumulation on the surface of the pavement and reduces splash. As a result, more than 90% of the highways in the Netherlands are surfaced by the PA mix and the goal is 100% by 2022 [4, 5].



Figure 1.1: Water draining ability of porous asphalt [6].

However, the high void content structure of PA makes the vehicle loadings more likely to create stress concentration at the stone-to-stone regions, thus prone to bitumen stripping [7]. Moreover, the larger void content of PA provides a higher chance to contact the oxygen thus suffering more serious ageing than dense asphalt [8]. These negative effects limit the average service life of PA to around 11 to 12 years, thus it requires more frequent maintenance and reconstruction in comparison to traditional (dense graded) pavement mixtures [9, 10].

Ravelling of porous asphalt, which is a failure at the surface of the pavement occurring within the stone-to-stone contact regions and causing the loss of aggregate particles from the road surface, is the main defect of porous asphalt [11]. It is caused by an increase of stiffness, reduction of relaxation capacity and formation of micro-cracks in the binder due to ageing [12]. If the micro-cracks can be healed in the early

stage, the problem of ravelling can be prevented or delayed, prolonging the service life of porous asphalt [13].

### **1.1.2. DEVELOPMENT OF SELF-HEALING ASPHALT**

As a novel concept, self-healing asphalt stems from the Forum of European National Highway Research Laboratories (FEHRL) goal ‘Forever open road’ – roads that will never be closed for repairs, which aims to produce a sustainable asphalt pavement by using self-healing technology to stimulate and improve the healing capacity of bituminous materials, so that damages (microcracks) can be self-repaired which finally prolongs the service life of asphalt pavement. As such, the inclusion of the self-healing technology into the asphalt pavement design and construction will reduce the maintenance works which not only reduces the need for extra resources (aggregate, bitumen, etc.) but also reduces the emissions of greenhouse gases into the atmosphere [14, 15].

Currently, there are two self-healing technologies, they are: i) thermally induced healing or ii) embedded rejuvenator encapsulation. Both show significant healing effect in the laboratory and are gradually demonstrated in the field application [16-18]:

- i. In a thermally induced healing mechanism, the induction heating achieves crack healing by heating up asphalt with induction energy [19]. To start the healing process, the alternating electromagnetic field generated by the induction coil induces flowing current inside the asphalt with conductive particles, thus heating up the asphalt, melting the asphalt mastic and finally healing the crack [20]. The advantages of induction heating methods include efficient asphalt crack healing and the healing can be repeated [19].
- ii. The healing mechanism of the embedded rejuvenator encapsulation lies in the aged binder rejuvenation with the released rejuvenator. This healing is activated when crack initiates and propagates through the capsule/fibre to trigger the release of rejuvenator, thus the rejuvenator diffuses into the crack surface and softens the aged binder. In this way, the crack can be healed with the flow of asphalt mastic [16, 21].

Existing research has demonstrated the huge potential of using self-healing technology to extend the service life of asphalt pavement. However, limitations of current self-healing asphalt technologies are:

- The heating methods could not solve the problem of bitumen ageing which may cause premature failures in asphalt pavement.
- The damage healing efficiency of the embedded rejuvenation method is very limited.

These issues need to be resolved before the self-healing technology is accepted into asphalt mix design and construction practices. Hence, development of a more efficient and durable self-healing technology in asphalt pavement is needed.

### 1.1.3. ALGINATE AND ITS ENCAPSULATION ABILITIES

Alginates are linear water-soluble polysaccharides comprising of (1-4) linked units of  $\alpha$ -D-mannuronate (G) and  $\beta$ -L-guluronate (M) at different proportions and different distributions within the chains [22]. Their functional properties are strongly related to composition (G/M ratio) and sequence of the uronic acids. The chemical formula for sodium alginate is:  $C_6H_7O_6Na$  and its structural formula is shown in Figure 1.2.

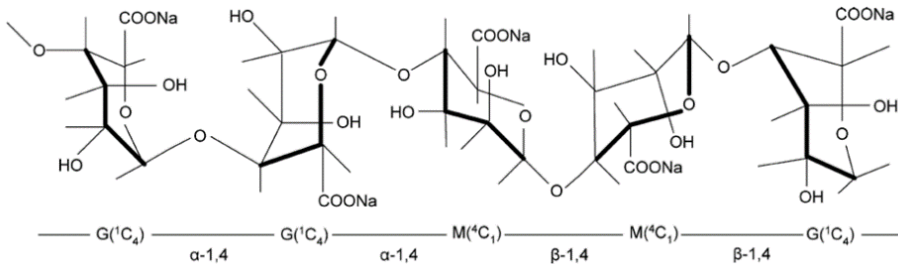


Figure 1.2: Structural formula of Sodium Alginate.

Alginates are present in brown algae and can also be found in metabolic products of bacteria, e.g. pseudomonas and azotobacter [23-25]. Alginates are commonly used as food additives, gelling agents, wound dressings and for drug delivery [26, 27]. The encapsulation mechanism of alginate is shown in Figure 1.3: when dissolved in the liquid solution, doubly charged ions ( $Ca^{2+}$ ) can bind two different alginate strands simultaneously by replacing positively charged sodium ions ( $Na^+$ ) thereby crosslinking and solidifying the solution [28].

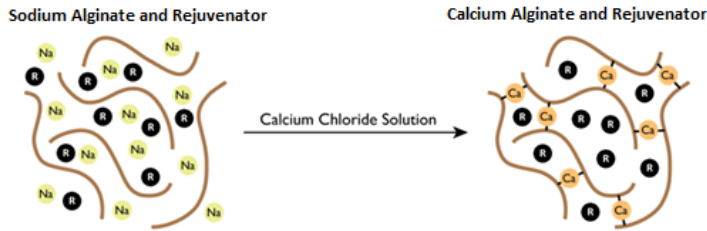


Figure 1.3: Encapsulation of rejuvenator with calcium alginate crosslinking.

Currently, the alginate has been successfully investigated for its use in the field of material self-healing technology. It has been used for the encapsulation of i) bacteria in microcapsules for concrete healing [29] and ii) healing agent (solvents) for thermoplastic composite material healing [30, 31]. Alginate's advantages such as relatively low price and environmentally friendly provide a good prospect for the application in self-healing system for a range of engineering materials, such as asphalt pavement [32]. Hence, the potential use of alginate as a bitumen rejuvenator encapsulating mechanism is explored in this research.

## 1.2. RESEARCH OBJECTIVE

The main objective of this research is to develop a self-healing system that further extends the service life of porous asphalt. To this aim, a combined healing system is designed which includes both induction heating and encapsulated rejuvenator. The combined healing system possesses comprehensive healing mechanisms including sufficient crack healing ability and aged material rejuvenation. Furthermore, the combination of these two technologies will potentially produce positive synergistic effects:

- i. Increased temperature from induction heating will improve the diffusion coefficient of asphalt rejuvenator, thus the rejuvenation efficiency is improved.
- ii. Encapsulated rejuvenator, when released, will restore bitumen healing capacity and soften the aged bitumen which in turn improves the induction healing effect.

Hence, the concept of the combined healing system, incorporating the advantages from both induction heating and encapsulated rejuvenator, is expected

to achieve an enhanced crack healing in porous asphalt which is illustrated in Figure 1.4.

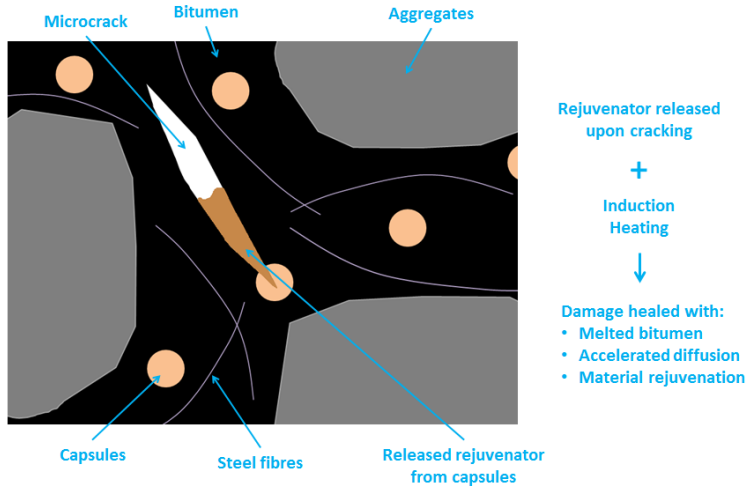


Figure 1.4: Crack healing mechanism of the combined healing system.

### 1.3. RESEARCH APPROACH

To accomplish the research objective above, the development of the combined healing system was conducted in two research stages:

- Stage 1: Development of the capsule healing system

The development of the capsule healing system began with the selection of a proper type of rejuvenator and knowing its ability to restore the lost properties of aged bitumen. Then, the potential rejuvenator encapsulation method was explored in the laboratory which led to the discovery of calcium alginate capsules. Subsequently, the encapsulation method was optimized to achieve a balanced capsule performance in thermal stability, mechanical resistance and rejuvenator content. Finally, the calcium alginate capsules healing system was evaluated in asphalt mastic, mortar and full PA mix.

- Stage 2: Development of the combined healing system

In this stage, full PA mix with the combined healing system was designed by incorporating both the calcium alginate capsules healing system and the induction

healing system. Then, the influence of the combined healing system on the mechanical properties of the PA was investigated. Afterwards, the crack healing efficiency and the fatigue damage healing efficiency of the combined healing system was evaluated, and the results were compared with the single healing systems (capsules or induction) and the reference mix (without extrinsic healing). As a result, the performance of the combined healing system was studied and its advantage over other healing systems was investigated.

#### 1.4. THESIS OUTLINE

Figure 1.5 illustrates the thesis outline. This thesis contains seven chapters that are divided into four parts. The chapters are organized as follows:

**Chapter 1** serves as a general introduction that describes the background, objective, approach and outline of this thesis.

**Chapter 2** presents the literature survey on self-healing asphalt. The general concept and design principle of the self-healing material are described. Then the intrinsic healing capacity of bituminous materials and the extrinsic healing methods for asphalt pavement are reviewed.

**Chapter 3** presents the study on the performance of three different types of bitumen rejuvenator. Based on the physical, rheological and chemical properties of the well-blended rejuvenator-bitumen blends, the optimal type of rejuvenator for capsule healing system is determined and the proper rejuvenator amount is indicated.

**Chapter 4** presents the study on the preparation process of the calcium alginate capsules. The rejuvenator is encapsulated in the calcium alginate capsules and the alginate/rejuvenator (A/R) ratio is adjusted based on the thermal stability and mechanical resistance to achieve the optimum capsule behaviour for the potential use for capsule healing system in porous asphalt.

**Chapter 5** evaluates the performance of the calcium alginate capsules healing system in asphalt mastic, asphalt mortar and full porous asphalt mix. A three-point bending test is used to evaluate the mechanical response of the capsule healing system in asphalt mastic and asphalt mortar, while the semi-circular bending test is used for porous asphalt samples. A bending and healing programme is used to evaluate the healing efficiency of the capsule healing system in all asphalt mix. The influence of asphalt ageing is discussed.

**Chapter 6** presents the development of the combined healing system in porous asphalt. The mechanical properties, fracture resistance and fatigue life of the porous asphalt samples with different healing systems, namely capsule healing system, in-

duction healing system, combined healing system and the reference mix, are evaluated and compared. The healing indices, including the crack healing index and the fatigue healing index, are used to evaluate the healing efficiency of different systems in porous asphalt. The influence of asphalt ageing is also discussed.

**Chapter 7** summaries the research findings of this Ph.D. project and gives recommendations for future studies.

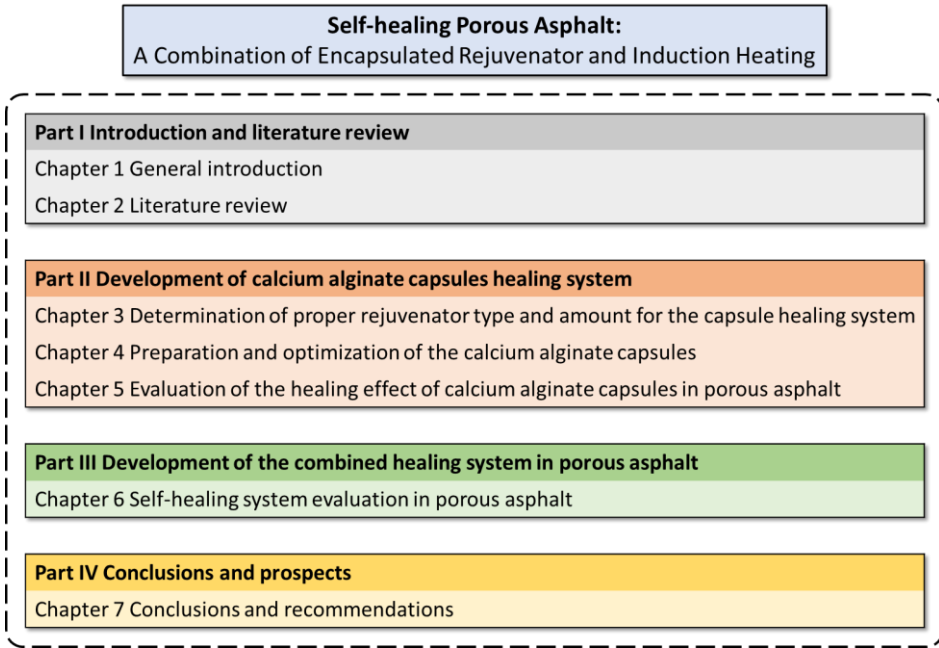


Figure 1.5 Thesis outline.

## REFERENCES

- [1] J.T. Van Der Zwan, T. Goeman, H. Gruis, J. Swart, R. Oldenburger, Porous asphalt wearing courses in the Netherlands: State of the art review, Transportation Research Record (1265) (1990).
- [2] R. McDaniel, W. Thornton, Field evaluation of a porous friction course for noise control, Annual Meeting of the Transportation Research Board, Washington, DC, 2005.

- [3] P. Bolzan, J. Nicholls, G. Huber, Searching for superior performing porous asphalt wearing courses, 80th Transportation Research Board Annual Meeting, Washington DC, 2001.
- [4] J. Swart, Experiences with porous asphalt in the Netherlands. Ministry of transportation, public works and water management, Proceedings of the European conference on porous asphalt. Avon Books, Madrid, Spain, New York, 1997.
- [5] L. Mo, Damage development in the adhesive zone and mortar of porous asphalt concrete, Delft University of Technology, 2010.
- [6] Porous asphalt pavement, 2014. <https://www.slideshare.net/ashifar/porous-asphalt-pavement>.
- [7] S. Xu, X. Liu, A. Tabaković, E. Schlangen, Investigation of the Potential Use of Calcium Alginate Capsules for Self-Healing in Porous Asphalt Concrete, *Materials* 12(1) (2019) 168.
- [8] R. Jing, Ageing of bituminous materials: Experimental and numerical characterization, Delft University of Technology, 2019.
- [9] H. Zhang, H. Li, Y. Zhang, D. Wang, J. Harvey, H. Wang, Performance enhancement of porous asphalt pavement using red mud as alternative filler, *Construction and Building Materials* 160 (2018) 707-713.
- [10] A. Molenaar, E. Hagos, M. Van de Ven, Effects of aging on the mechanical characteristics of bituminous binders in PAC, *Journal of Materials in Civil Engineering* 22(8) (2010) 779-787.
- [11] A. Klomp, Life period of porous asphalt, Dutch Road and Hydraulic Engineering Institute report (1996).
- [12] E.T. Hagos, The effect of aging on binder properties of porous asphalt concrete, Delft University of Technology (2008).
- [13] Q. Liu, Á. García, E. Schlangen, M. van de Ven, Induction healing of asphalt mastic and porous asphalt concrete, *Construction and Building Materials* 25(9) (2011) 3746-3752.
- [14] H. Jahanbakhsh, M.M. Karimi, H. Naseri, F.M. Nejad, Sustainable asphalt concrete containing high reclaimed asphalt pavements and recycling agents:

performance assessment, cost analysis, and environmental impact, *Journal of Cleaner Production* (2019) 118837.

[15] S. Xu, X. Liu, A. Tabaković, E. Schlangen, A novel self-healing system: Towards a sustainable porous asphalt, *Journal of Cleaner Production* (2020) 120815.

[16] S. Xu, A. García, J. Su, Q. Liu, A. Tabaković, E. Schlangen, Self - Healing Asphalt Review: From Idea to Practice, *Advanced Materials Interfaces* (2018) 1800536.

[17] A. Tabaković, E. Schlangen, Self-healing technology for asphalt pavements, *Self-healing Materials*, Springer 2015, pp. 285-306.

[18] P. Ayar, F. Moreno-Navarro, M.C. Rubio-Gámez, The healing capability of asphalt pavements: a state of the art review, *Journal of Cleaner Production* 113 (2016) 28-40.

[19] Q. Liu, *Induction Healing of Porous Asphalt Concrete*, Delft University of Technology, 2012.

[20] Á. García, E. Schlangen, M. van de Ven, D. van Vliet, Induction heating of mastic containing conductive fibers and fillers, *Materials and structures* 44(2) (2011) 499-508.

[21] Y. Xiao, C. Li, M. Wan, X. Zhou, Y. Wang, S. Wu, Study of the diffusion of rejuvenators and its effect on aged bitumen binder, *Applied Sciences* 7(4) (2017) 397.

[22] J. Zlopasa, E. Koenders, S. Picken, Using bio-based polymers for curing cement-based materials, *AMS 14: Proceedings of the 1st Ageing of Materials & Structures Conference*, Delft, The Netherlands, 26-28 May 2014, DCMat Ageing Centre, Delft University of Technology, 2014.

[23] K.I. Draget, G. Skjåk-Bræk, O. Smidsrød, Alginate based new materials, *International journal of biological macromolecules* 21(1-2) (1997) 47-55.

[24] H. Grasdalen, B. Larsen, O. Smisrod, <sup>13</sup>C-NMR studies of monomeric composition and sequence in alginate, *Carbohydrate Research* 89(2) (1981) 179-191.

[25] A. Linker, R.S. Jones, A new polysaccharide resembling alginic acid isolated from pseudomonads, *Journal of Biological Chemistry* 241(16) (1966) 3845-3851.

- [26] B. Balakrishnan, M. Mohanty, P. Umashankar, A. Jayakrishnan, Evaluation of an in situ forming hydrogel wound dressing based on oxidized alginate and gelatin, *Biomaterials* 26(32) (2005) 6335-6342.
- [27] I.R. Matthew, R.M. Browne, J.W. Frame, B.G. Millar, Subperiosteal behaviour of alginate and cellulose wound dressing materials, *Biomaterials* 16(4) (1995) 275-278.
- [28] F. Gu, B. Amsden, R. Neufeld, Sustained delivery of vascular endothelial growth factor with alginate beads, *Journal of Controlled Release* 96(3) (2004) 463-472.
- [29] D. Palin, V. Wiktor, H. Jonkers, Bacteria-based agent for self-healing marine concrete, Proc. 5th Int. Conf. on Self-Healing Materials (Durham, USA), 2015, pp. 2-6.
- [30] M. Prajer, X. Wu, S. Garcia, S. van der Zwaag, Direct and indirect observation of multiple local healing events in successively loaded fibre reinforced polymer model composites using healing agent-filled compartmented fibres, *Composites Science and Technology* 106 (2015) 127-133.
- [31] S.D. Mookhoek, H.R. Fischer, S. van der Zwaag, Alginate fibres containing discrete liquid filled vacuoles for controlled delivery of healing agents in fibre reinforced composites, *Composites Part A: Applied Science and Manufacturing* 43(12) (2012) 2176-2182.
- [32] A. Tabaković, W. Post, D. Cantero, O. Copuroglu, S. Garcia, E. Schlangen, The reinforcement and healing of asphalt mastic mixtures by rejuvenator encapsulation in alginate compartmented fibres, *Smart Materials and Structures* 25(8) (2016) 084003.



# 2

## SELF-HEALING ASPHALT: LITERATURE REVIEW

*In nature, the ability of self-healing is widely developed in biological materials through evolution, for example, healing broken bones, wound healing, etc. Inspired by nature, the concept of self-healing has been integrated into the design of man-made materials aiming to improve their functional sustainability in different fields including asphalt pavement. In the past two decades, emerging self-healing technologies for asphalt pavements, such as embedded rejuvenation encapsulation and induction heating, demonstrated in the laboratory and gradually verified in the field applications, its ability to repair the damage in the asphalt pavement. In turn offering longer lasting and more durable asphalt pavements. In this chapter, the general concept of self-healing materials is explained first. Afterwards, the intrinsic healing capacity of bituminous materials is discussed. Then, a state-of-the-art of self-healing technologies applied in asphalt pavement is presented. Finally, aimed for further improvements of the healing efficiency in asphalt pavement, the future development of self-healing asphalt is discussed.*

## 2.1. SELF-HEALING MATERIALS: AN INTRODUCTION TO THE CONCEPT AND PRINCIPLE

Traditionally, design of an engineering material follows the concept of ‘Damage Prevention’, which is illustrated by van der Zwaag [1] using the schematic diagram presented in Figure 2.1. Following this concept, design of a material that is ‘stronger’ than material A can be achieved with an improvement in the conditions for damage initiation (material B) or with an improvement in the point of onset of damage as well as in the rate of damage formation (material C) [1].

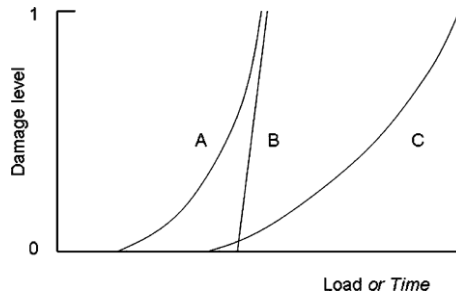


Figure 2.1: Schematic diagram of the damage development of traditional engineering material where the damage level only increases [1].

Other than the traditional material design concept, the self-healing material is designed following the concept of ‘Damage Management’, which is illustrated in Figure 2.2 [1]. Figure 2.2 (a) shows a self-healing material designed with a single healing action in its lifetime, in which the lifespan of this material is extended; Figure 2.2 (b) shows a self-healing material with multiple healing action and failure may occur until running out of effective healing, as such this material can endure more damage cycles in its lifetime; Figure 2.2 (c) shows an ideal self-healing material in which the damage is healed many times and no accumulation of damage to the level of catastrophic failure occurs.

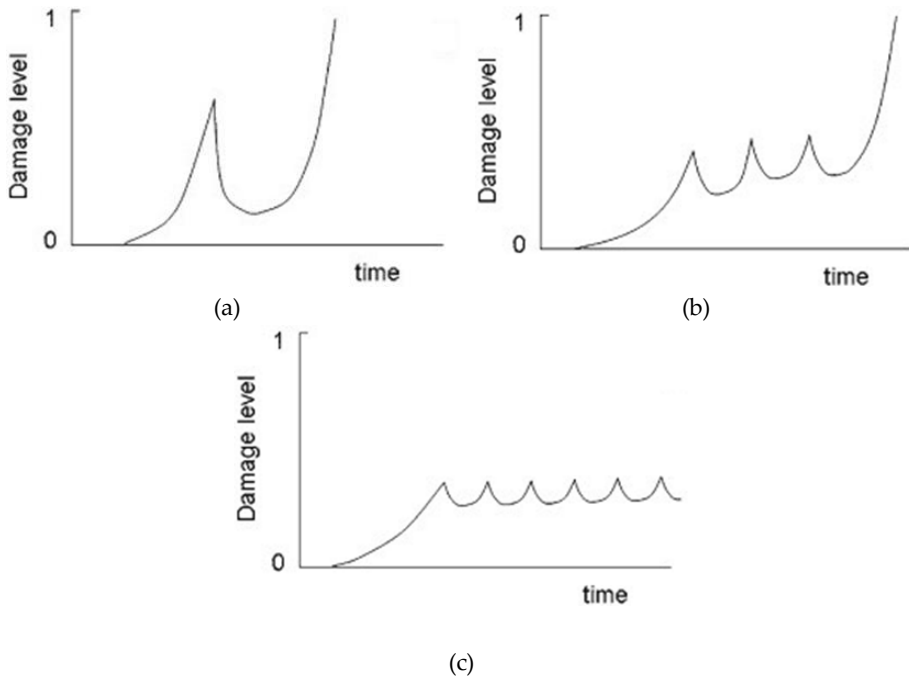


Figure 2.2: Schematic diagram of the damage development in three grades of self-healing materials where the damage level decreases during certain stages of the lifetime [1].

Van der Zwaag indicated that although the 'Damage Prevention' has been a very useful and productive concept, the formation of damage during the lifetime can never be excluded. On the contrary, following the concept of 'Damage Management', self-healing materials have a negative rate of damage formation at one or more stages of their life [1]. Van der Zwaag also pointed out that it will be quite challenging to make a self-healing material, as the various tasks of the atoms in a self-healing material are far more complex than those in classical materials. The self-healing material is no longer just a material but has become a system in itself [1].

Cracking is one of the most common damaging phases in material engineering which can develop from microscopic cracks into macroscopic damages [2-4]. Hager et al [5] summarized the common principle shared by diverse self-healing materials in a crack healing event as the subsequent generation of a 'mobile phase'. Hager et al indicated that a prerequisite for a self-healing of a (mechanical) damage is the generation of a mobile phase, which can close this crack (Figure 2.3). If damage is inflicted on the material (Figure 2.3 (a) and (b)), a crack can occur. The subsequent generation of a 'mobile phase' (Figure 2.3 (c)), triggered either by the occurrence of damage (in the ideal case) or by external stimuli, can heal the damage due to the

directed mass transport towards the damage site and the subsequent local mending reaction (Figure 2.3 (d)). After the healing of the damage, the previously mobile material is immobilised again, resulting in the best case in fully restored mechanical properties (Figure 2.3 (e)) [5].

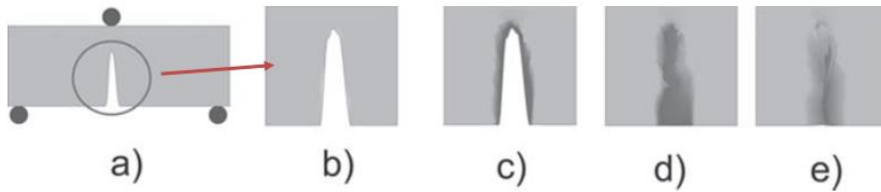


Figure 2.3: Common basic principle of self-healing materials. a) The mechanical load induces a crack; b) detailed view of the crack; c) a ‘mobile phase’ is induced; d) closure of the crack by the ‘mobile phase’; e) immobilisation after healing [5].

In the past two decades, self-healing technologies have been developed and studied in different fields, and asphalt pavement is one of these applications [6, 7]. The intrinsic healing capacity of bituminous material, as well as the emerging extrinsic healing methods, were studied for the common objective of building a more functionally sustainable asphalt pavement.

## 2.2. THE INTRINSIC HEALING CAPACITY OF BITUMINOUS MATERIALS

### 2.2.1. THE CONCEPT OF SELF-HEALING IN BITUMINOUS MATERIALS

With the advantages of cost efficiency, noise reduction, and comfort driving experience, asphalt is widely used as a binding material in pavement engineering. However, after years in service, asphalt concrete deteriorates under cyclic vehicle loadings as well as the environmental effects [8-10]. As a self-healing material, the intrinsic healing capacity of an asphalt allows the damage to repair itself during hot summers and long rest periods, as such the self-healing ability of asphalt mixtures plays an important role in the service life of an asphalt pavement [4, 11].

In 1967, Bazin et al [12] witnessed and reported a temperature-related healing phenomenon in asphalt mix after loadings. Following this work, the healing phenomenon of bituminous material became a research focus for road engineers.

On different scale levels, the asphalt concrete shows different self-healing behaviours. Qiu [4] explained the crack healing in macro and meso levels: at macro level, some of the microcracks can be healed during the rest periods between two axle passages, and also during summer when the temperature is high. At meso level,

healing can be observed both in the cohesive and adhesive regions of asphalt mixtures. Healing is considered to be cohesive when occurring in the bitumen or mastic and to be adhesive when occurring at the bitumen-aggregate interface.

For the explanation of the healing mechanism in bitumen, Qiu [4, 13] summarised the healing in two ways:

i) Physicochemical way

Lytton et al [14] indicated that healing is the reparation of a chemical structure in such a way that micro fatigue damage is decelerated. It is related to the composition and the physicochemical characteristics of bitumen and asphalt mixes.

ii) Mechanical way

Williams et al [15] found that microdamage healing is real and measurable and that it has a significant impact on pavement performance. The stress wave test was used to measure microcrack damage growth and study the healing of asphalt pavements in the field and they found that healing does occur in pavements in the field during rest periods and hence it was concluded that the performance and service life of the pavement can be increased if rest periods are introduced.

The healing phenomenon of bituminous material can also be explained with the molecular interactions within the asphalt binder. In 1981, based on polymer chain dynamics, Wool et al [16] proposed five steps of the healing process for a polymer system: surface arrangement, surface approach, wetting, diffusion and randomization, which are illustrated in Figure 2.4. Wetting is a function of surface energy and is followed by an instantaneous gain in strength. Diffusion and randomization lead to intrinsic healing, which is a time-dependent function. Self-diffusion of random coils of molecules undergoes successive randomization over time [17].

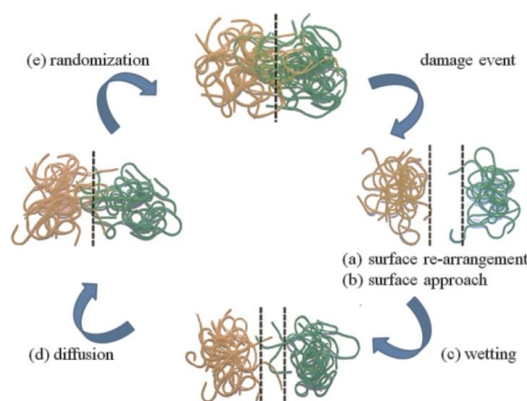


Figure 2.4: Illustration of the principal stages of self-healing mechanism of molecular inter-diffusion [16, 17].

In 1990, Kim et al [18] proved that the healing rate for different asphalt mixtures related to the molecular characteristics of their respective bitumens. That is the methyl hydrogen to carbon ratio and the methylene to methyl group ratio. Later on, Bhasin et al [19] used the asphalt binder molecules' self-diffusivity theory to explain the time-dependent healing effect in asphalt. The term self-diffusivity refers to the diffusion coefficient of a species of molecules of a material within the bulk of that material. Self-diffusivity represents the random motion of molecules in the absence of gradients that cause mass flux. Based on this theory, Bhasin et al [20] used molecular simulation techniques to investigate the correlation of chain length and chain branching to self-diffusivity of binder molecules. The findings were consistent with previous studies and expanded on the understanding of the relationship between molecular architecture, self-diffusivity, and self-healing properties of asphalt binders. Later, Hou et al [21] explained the self-healing mechanism of asphalt by using a Phase-Field model. In this model, the thermodynamic approach and mechanical approach are combined, which provided a better understanding of the healing mechanism of asphalt.

### **2.2.2. INFLUENCE FACTORS ON SELF-HEALING EFFECT OF ASPHALT PAVEMENT**

With the intrinsic healing capacity, an asphalt is able to repair the damage (close cracks), restore its stiffness and strength when subjected to rest periods [4]. Qiu et al [22] investigated the self healing capability of bituminous mastics using a microscopy coupled fracture-healing-refracture test procedure which is illustrated in Figure 2.5. Qiu et al reported that healing of an open crack in asphalt pavement is a viscosity-driven process, which depends on rest period and temperature. Qiu et al also indicated that the healing process includes two phases: crack closure and strength gain. The completion of the crack closure process does not imply a full recovery of the strength.

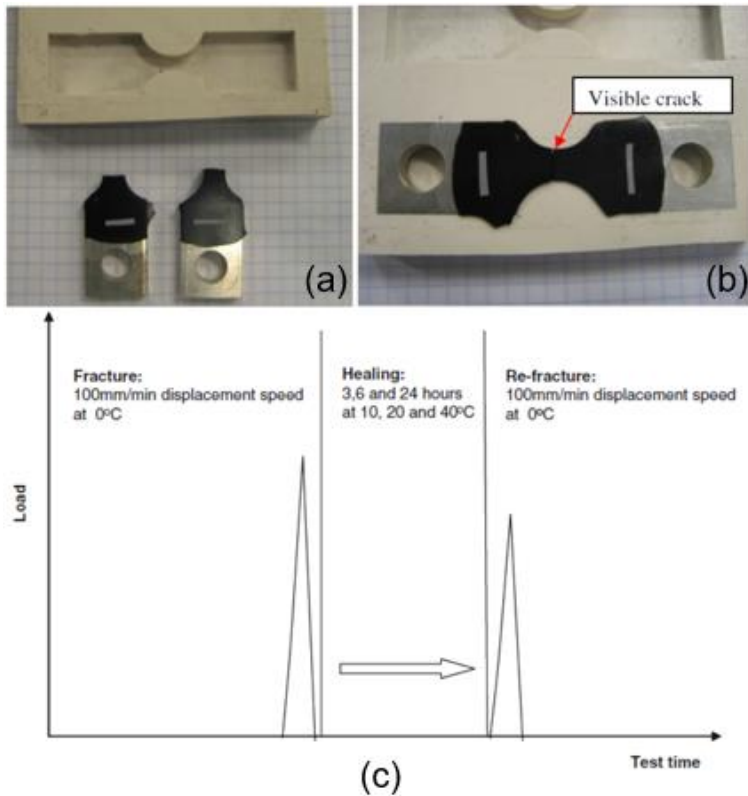


Figure 2.5: Illustration of the fracture-healing-refracture test procedure followed by Qiu et al: (a) the broken pieces from fracture test, (b) placed for healing in a designed mould (b) and (c) the schematic of fracture-healing-refracture test procedure [22].

Figure 2.6 shows the CT-scan images recorded by García [23], which illustrate the crack healing process in an asphalt mastic sample. It was indicated that, the generated crack with a width of 200  $\mu\text{m}$  can be healed with a 50 minutes curing period in an oven at 70°C. García further studied the asphalt mastic healing behaviour with different healing time and temperature and found that asphalt mastic self-healing properties are directly linked to temperature and to the rest periods, and as such it can be classified as a thermally induced self-healing material.

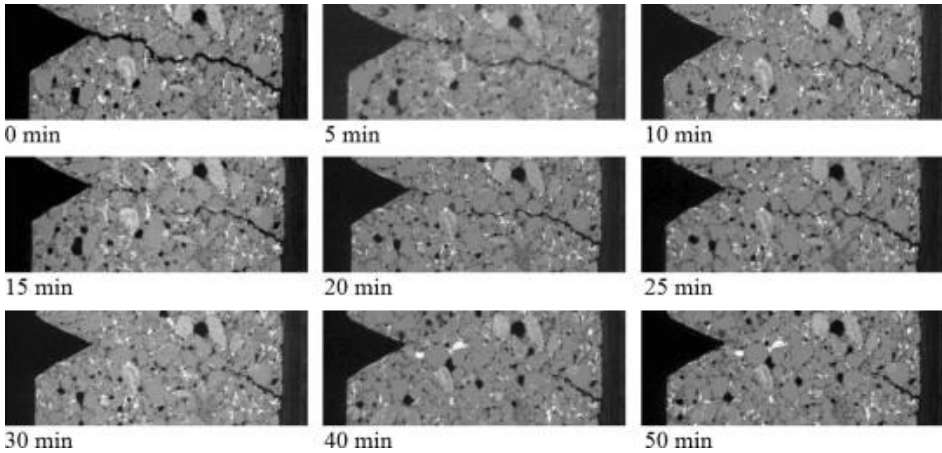


Figure 2.6: CT-Scan images of the crack healing process in an asphalt mastic sample [23].

Riara et al [24] carried out experimental studies to investigate the effect of temperature, moisture ingress and healing agents on the crack healing of asphalt mortar and asphalt concrete. Riara et al indicated that an increase in temperature improves the crack healing effect in both asphalt mortar and mixtures, while the crack healing of asphalt mortar was higher than that of its associated mixtures. In addition, Riara et al found the healing in asphalt mortar is more sensitive to water ingress and changes in temperature, and the spray of healing agents on crack faces can accelerate the healing process.

Based on the activation energy, Sun et al [25] studied the intrinsic healing capacity of asphalt mastic and found that the polymer or nature asphalt additives may have a negative effect on healing. Additionally, Sun et al indicated that different asphalt type, filler type or filler content may influence the healing of asphalt mastic.

More factors influence the healing process in bituminous materials and they can be categorized into bitumen properties, asphalt mix composition and environmental aspects [7, 26]. Tabaković [6] summarised the influencing factors for the healing of asphalt concrete, as presented in Table 2.1.

Table 2.1: Influencing factors for the healing of asphalt concrete [6].

Factors influencing healing	Bitumen properties	Bitumen type
		Chemical compositions
		Viscoelastic properties
		Surface free energy
		Ageing
		Diffusion
		Modifiers
	Asphalt mixture compositions	Bitumen content
		Aggregate structure
		Gradation
		Thickness
	Environmental aspects	Temperature
		Loading history
Rest period		

Although the intrinsic healing capacity of asphalt has been proven, the asphalt intrinsic healing effect is limited by the field condition and is not enough to match the deterioration process [4]. Understanding of the self-healing mechanism and the influencing factors in asphalt pavement may contribute to the evolution of self-healing asphalt and inspire new techniques to accelerate the healing in asphalt, aim for a more sustainable asphalt pavement.

### 2.3. EXTRINSIC HEALING METHODS FOR ASPHALT PAVEMENT

It is well-known that, when asphalt pavements have the ability to repair small cracks, it will considerably decrease maintenance costs, extend the service life and reduce greenhouse gas emission [7]. Therefore, researchers are exploring methods to inspire the potential healing capacity of asphalt. Subsequently, various extrinsic healing methods have been proposed, such as induction healing [27-31], embedded rejuvenator encapsulation [32-39], etc. In particular, some novel methods have been applied in trial sections, such as the induction healing section A58 in the Netherlands [40], European HealRoad project [41] and the microcapsules healing section in China [42]. All these achievements reveal a closer step to the successful large scale application of self-healing technologies in asphalt. This section presents a technical overview of the extrinsic methods related to self-healing asphalt and field applications.

### 2.3.1. THERMALLY INDUCED HEALING METHODS

Asphalt pavement can repair its own damage and recover its strength and fatigue life autonomously during rest periods [43-47]. Researches have demonstrated that temperature is the dominant factor influencing the self-healing properties of asphalt concrete, which means an increase in the test temperature not only increases the self-healing rate but also shortens the total time needed for full healing [4, 48]. Based on this concept, methods including induction heating and microwave heating are developed to achieve self-healing in asphalt concrete by increasing the temperature [31, 49].

#### 2.3.1.1. INDUCTION HEATING

To enhance the self-healing capacity of asphalt concrete through increasing the temperature, an induction heating approach was developed at Delft University of Technology. Figure 2.7 presents the schematic diagram that illustrates the general principle for the induction heating method used in self-healing asphalt. Conductive particles were added to asphalt mixtures and induction heating was applied to increase the healing capacity of asphalt concrete when cracks occurred in asphalt mastic [28, 50-52]. During induction heating, asphalt mortar containing conductive particles are exposed to a high-frequency alternating electromagnetic field, which can induce eddy currents in materials that are electrically and magnetically susceptible. The conductive particles were heated by the induced eddy currents and the heat energy diffuses into the bitumen to increase the temperature. Asphalt mixture can be healed quickly because bitumen behaves as a Newtonian fluid when its temperature is above the softening point of bitumen [23, 53, 54].

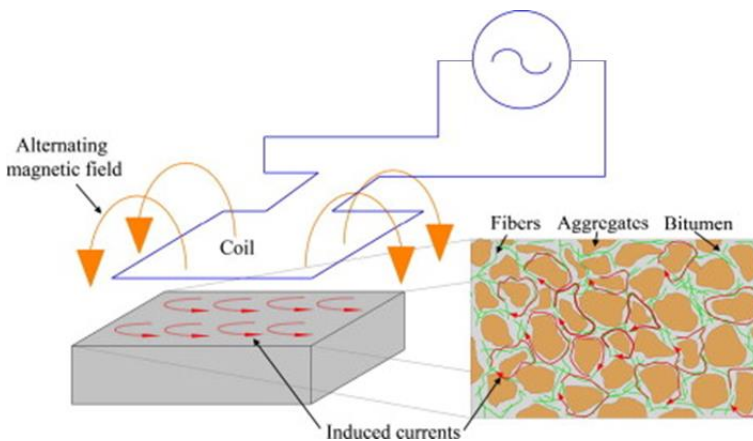


Figure 2.7: Illustration of the induction heating in asphalt concrete [55].

To make asphalt concrete electrically conductive and suitable for induction heating, conductive additives are incorporated into the mixture. Several types of conductive additives are studied in various researches which include metal particles (e.g., steel fibres [26], steel powder [56], steel slag [57], steel grit [58]), carbon-based materials (e.g., carbon fibre [59], graphite [60], and carbon black [61]) and other nonmetallic conductive particles [62]. Among all these additives, steel fibres (wool) were usually used because of the advantage of high conductive efficiency [26, 63, 64]. Long steel fibres are more effective to enhance the conductivity and induction heating speed of asphalt mixture [27], but they are very difficult to mix and tend to form clusters, which will absorb too much bitumen and decrease the mechanical properties of the mixture. Short and thick steel wool fibres with a diameter of 70–130  $\mu\text{m}$  and a length of around 4.2 mm are recommended in the latest research [65]. These steel wool fibres are quite easy to mix with the normal mixing procedure and their optimal content is 6% by volume of bitumen. These steel wool fibres can increase Marshall Stability, residual Marshall Stability ratio, water stability, ravelling resistance, fatigue resistance and low-temperature properties of asphalt mixture. The composite of steel fibres and steel slag (replacing a portion of mineral aggregates with steel slag) can enhance the induction heating speed, the heating homogeneity and thus enhance the induction heating efficiency of asphalt mixture [66]. Figure 2.8 illustrates the steel fibres distribution in an asphalt concrete [67].

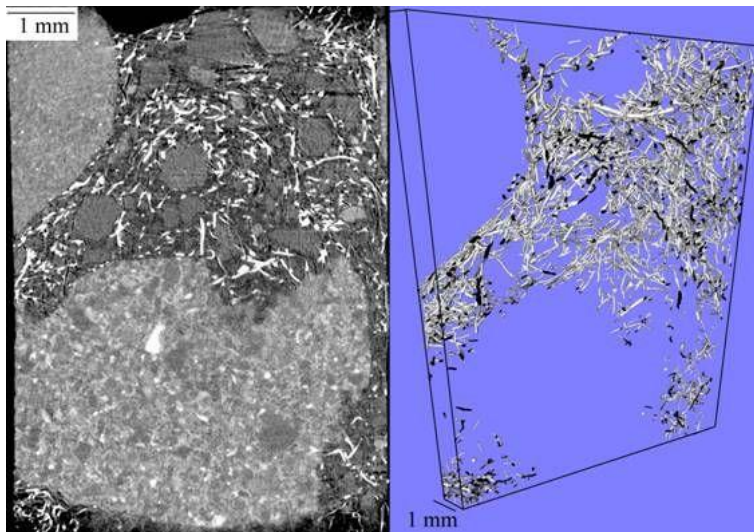


Figure 2.8: Illustration of the steel fibres distribution in an asphalt concrete [67].

Induction heating shows the healing effect on various damaging mechanisms in asphalt concrete, such as cracking, ravelling and fatigue damaging [26]. The crack healing effect is the most reported function of induction heating [7]. The asphalt crack healing with induction heating is usually investigated following a bending and healing programme which is based on Three-Point-Bending (3PB) test [49] or Semi-Circular-Bending (SCB) test [31]. The general principle of this programme is presented in Figure 2.9. With this programme, the healing index can be calculated with equation 2.1:

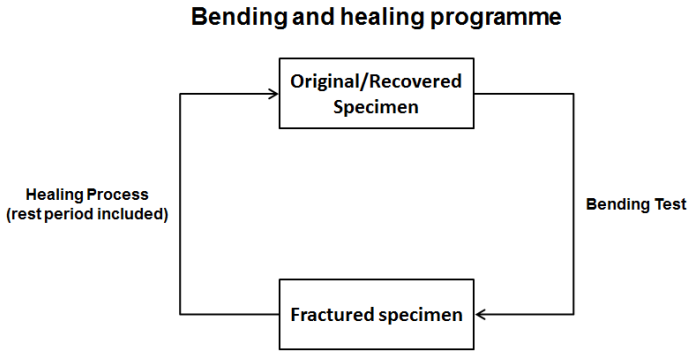


Figure 2.9: General principle of bending and healing programme used for crack healing efficiency evaluation [37].

$$HI = \frac{C_x}{C_1} \times 100\% \quad (2.1)$$

Where:

$HI$  is the healing index (%),

$C_1$  is the initial bending test result;

$C_x$  is the bending test result measured from the  $x$  testing cycle.

In an induction healing effect study on asphalt mastic, Liu reported that the healing can be repeated and can reach a healing index over 70% for 5 healing cycles [26]. Liu indicated that the strength recovery is not complete for two reasons. The crack represents a weak point and the sample suffers some kind of structural damage due to the induction heating. It should be noted that the specimens were completely fractured in two pieces, which might not fit perfectly together anymore.

In the situation of porous asphalt concrete cylinders, the intention is to apply healing at an early stage when there are only just micro-cracks (before major cracks develop).

In an induction heating effect study on porous asphalt concrete, Liu et al found that the maximum strength recovery of the fractured beam is 77.9%, which means the induction heating does not fully (100%) repair damage [29]. One possible reason for the incomplete healing mainly lies in the fact that some aggregates were broken during the test, a damage which cannot be recovered. Another possible reason is the temperature gradient through the depth of the sample. The sample is fully damaged through its thickness, but induction heating tends to only heal the damage in the top part of the beam, where the temperature is higher than in the lower part after induction heating. In the same case study, the strength recovery ratios of the asphalt concrete beam samples at different induction heating temperatures are shown in Figure 2.10 [29]. Liu indicated that the healing of bitumen and asphalt mixtures can be regarded as a thermally activated process of capillary flow and diffusion of the binder. A higher temperature will benefit the healing process while overheating will damage the structure. Swelling of the mortar can be observed in the samples heated to 95°C. Binder drainage may also occur in these overheated samples, and that can also offset the beneficial effect of heating (self-healing). Based on this result, it is concluded that the optimal heating temperature is 85°C.

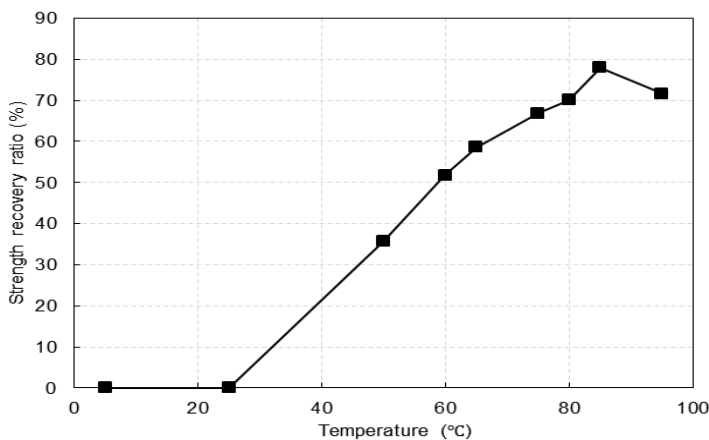


Figure 2.10: Strength recovery ratios of the samples at different heating temperatures [65].

Liu et al used a three-step-method to test the induction heating activated healing of fatigue damage in asphalt beams: (1) fatigue testing at 15°C, 10 Hz and with 600 microstrains was performed on asphalt beams until the complex modulus dropped to half of its initial value; (2) the fatigue damaged beams were heated to

different temperatures, and (3) finally the heated beams were cooled to 15°C and tested again under fatigue until the complex modulus dropped to the same value as the first fatigue testing [65]. The second fatigue life is a healing indication caused by resting and induction heating. The healing index fatigue life extension ratio can be defined as the second fatigue life divided by the original fatigue life.

To explore the effect of heating temperature on the healing rates of asphalt mixture, the fatigue life extensions of the fatigue damaged samples with different heating temperatures were investigated. Liu et al found that the healing ratio increases dramatically with the increasing heating temperature due to the faster flow of bitumen and obtains the maximum healing ratio before decreasing. After 87°C, a decrease of fatigue life extension ratio can be found where Liu et al explained as the overheating effect which caused the geometry damage. In this case, the asphalt mortar suffered excess expansion due to overheating and the swelling problem showed up in the sample. The optimal induction heating temperature for the beams 87°C and the maximum fatigue life extension ratio of the samples is 56.2% [65]. To quantify the effect of the microstrain amplitude on the healing rates of the samples, Liu et al investigated the fatigue life extension ratios of the samples with different microstrain amplitudes in fatigue testing and the results are presented in Figure 2.11. Figure 2.11 shows that the sample obtained the maximum fatigue life extension ratio at 400 microstrains. At a lower microstrain amplitude, a great amount of energy was dissipated during fatigue testing and the samples suffered significant damage. Thus, the fatigue life extension ratios are decreased at a lower microstrain amplitude. At higher microstrain amplitudes, bigger cracks were generated in the fatigue testing which is more difficult to heal. Liu et al concluded that the healing ratio of asphalt concrete with induction heating is dependent on the damage extent and crack size.

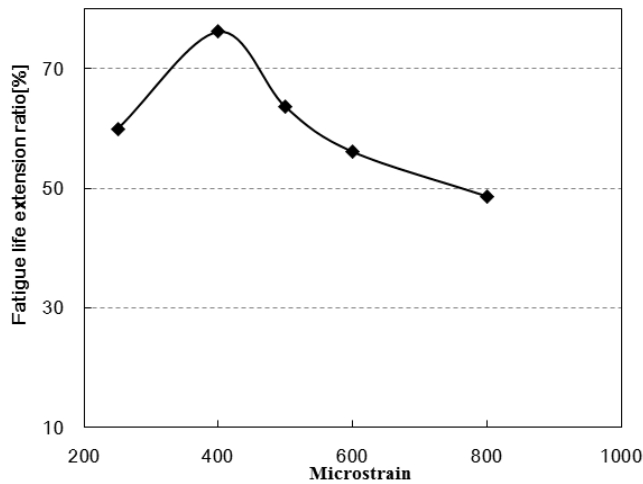


Figure 2.11: Fatigue life extension ratios of the samples under different microstrain amplitudes [65].

To examine the possibility of multiple instances of induction heating, Liu et al [66] designed a damaging, heating-and-resting, and re-damaging programme: A strain amplitude of 300 microstrains at a frequency of 8 Hz was applied to the porous asphalt concrete beams for 50,000 cycles; Then, samples were induction heated to 85°C and rested for 18 h for the first time; After that, another 50,000 cycles of fatigue loading were applied to the beams, followed by a second heating and resting process. Finally, the beam fatigue life was measured. Figure 2.12 compares the original fatigue curve and the modified fatigue curve for the sample with multiple instances of induction heating to show the fatigue life extension caused by induction heating. The original fatigue life of the sample is 95,700 cycles. With four instances of damage loading of 50,000 cycles followed by four instances of induction heating and resting, the modified fatigue life is 277,720, which is 2.9 times the original fatigue life; the fatigue life extension ratio was 190% in this case. Even though this research does not fully optimize when to heat the pavement and heating frequency, multiple instances of heating definitely can greatly extend the fatigue life of asphalt concrete.

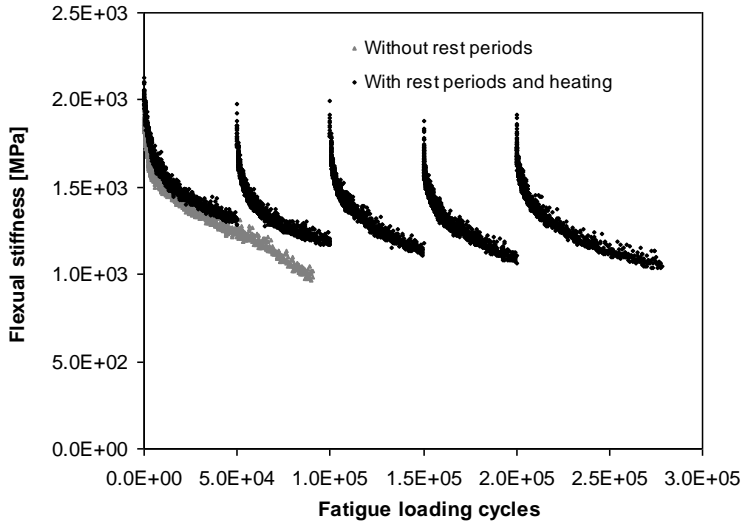


Figure 2.12: Fatigue life extension of the sample caused by multiple induction heating [68].

García et al [69] examined the induction healing properties of dense asphalt concrete. The results show that the minimum induction heated temperature for healing asphalt concrete is at approximately  $50^{\circ}\text{C}$ , and the maximum efficiency can be reached at around  $100^{\circ}\text{C}$ . However, the maximum healing efficiency is only 0.6 due to the deformation of samples during induction heating. Additionally, García et al developed a semi-empirical model to explain asphalt healing through the capillary theory and fitted to the results. In that study, García et al also reported a temperature gradient between the upper and lower layers of the asphaltic material created by induction heating, and this could make the healing not uniform. Besides, to simulate better the conditions in an asphalt concrete pavement, García et al suggested the test samples should be introduced in a mould before healing.

Based on the Arrhenius equation, García et al [27] developed a model to define induction heating in asphalt mastic and validated with experimental works. García et al discovered that the main parameters affecting induction heating are heat gains from the Joule losses in the fibres and heat losses from the thermal radiation, convection with air and conduction with other layers of the pavement. Additionally, it was found that heat gains depend mainly on the radius of the fibres, and other parameters that have a great influence on the heating are the frequency and intensity of the applied alternating magnetic field. García et al indicated that this model could be used to predict the needed induction heating time to obtain a full healing recovery of asphalt mastic.

A similar cyclic induction healing effect on dense asphalt was reported by Dai et al [70]. Dai et al found that bending test can increase the electrical resistivity by generating the internal damage or cracks. As such, the electrical resistivity of the samples decreases with bending-healing cycles because of the accumulated crack opening in the samples. In the same study, Dai et al compared the healing effect of the asphalt concrete samples healed with three different temperatures: 60°C, 80°C and 100°C, and found that the 100°C heating temperature could be the optimum option for the induction healing.

Menozi et al [71] conducted indirect tensile fatigue tests on Marshall test specimens to investigate the repair of microcracks in dense asphalt with induction heating. The indirect tensile fatigue tests were performed under 10°C and the loadings were set as 35% of the ultimate tensile strength of the test samples. The results showed that induction healing can only heal cracks of a certain width, and as such, there is an optimum moment for healing cracks in asphalt mixture. Menozi et al also indicated that permanent deformations can not be healed with induction heating and an excess of temperature during induction heating degrades the bitumen, which may affect its capacity for healing the mixture.

Apostolidis et al [72] studied the use of steel fibres and iron powders in induction heating of an asphalt mortar. It was indicated that the utilization of steel fibres shows significantly higher thermal, electrical conductivity and induction heating rate in asphalt mortar than one with iron powders, and the combined use of steel fibres and iron powders shows even slightly higher. Additionally, Apostolidis et al [72] developed a finite element model which simulates electro-magneto-thermal phenomena in a real-time system, and used in the simulation of the induction heating in the asphalt mortar. It is believed that the application of numerical simulations to evaluate induction healing behaviour is an effective way to predict the healing effect. To design and optimise an in-situ induction healing system, a three-dimensional finite element model was developed and the methodology schematic is presented in Figure 2.13 [73]. Apostolidis et al indicated that, in field induction healing application, the supplied power and the travelling speed of the induction system are the most influential factors for the development of a quick and highly efficient system.

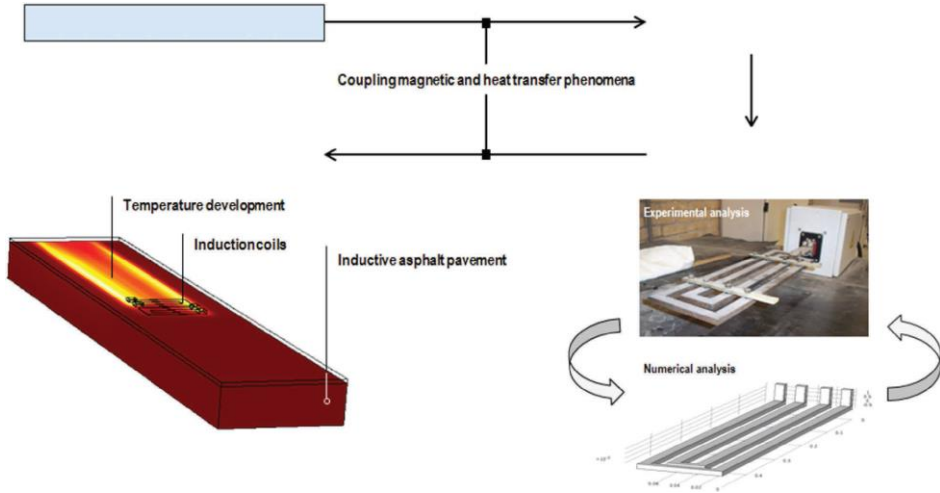


Figure 2.13: The methodology schematic for induction heating [73].

Dinh et al [74] tested the induction healing on reclaimed asphalt pavement (RAP) and found that the optimum steel wool fibres content is 6% by the volume of bitumen which can achieve the maximum thermal and electrical conductivity with a good dispersion. The results also showed that the presence of RAP causes the ineffectiveness of induction heating which resulted in decreasing of the healing performance of recycled asphalt mix at every testing cycle. However, Dinh et al believed that an addition of rejuvenators can enhance the healing performance of the recycled asphalt mix by reducing the RAP binder's viscosity. Therefore, Dinh et al indicated that the combined use of Rejuvenator and steel wool fibres in hot recycle asphalt mixtures may be promising due to its cost-effective strategy and environmental safety.

The first trial section with the induction heating concept was constructed on highway A58 near Vlissingen in the Netherlands in 2010. This trial section showed better ravelling resistance and good healing ratios with induction heating. The first induction heating treatment was applied to it in June 2014 (Figure 2.14).

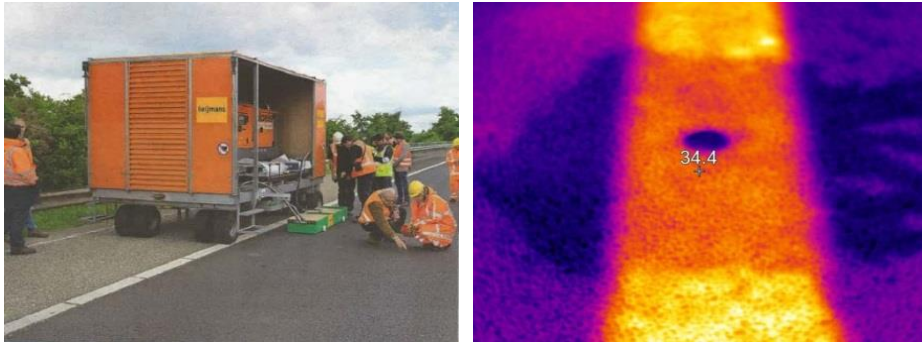


Figure 2.14: Application of Induction heating on Dutch Highway A58.

These findings indicate that induction healing asphalt, being a smart material and an advanced maintenance concept for asphalt pavement, is promising to greatly improve the quality of the pavement, reduce the maintenance activities and extend its service life. However, the clustering problem of the steel fibres in asphalt mixture, the gradient temperature distribution through the depth of the heated asphalt, and the speed of induction heating and the availability of a large-scale induction vehicle limit the widespread of this technique in field applications. Moreover, it is well-known that the intrinsic healing capacity of an asphalt decays with long-term ageing process which may in turn reduce the induction healing effectiveness, and this is investigated in Chapter 6.

### 2.3.1.2. MICROWAVE HEATING

Similar to induction heating, microwave heating is also considered as a promising extrinsic technique to promote self-healing of bituminous materials. Due to its advantages in heating such as fast speed, good uniformity and energy-saving, microwave is widely used in our daily life as well as in food industry, medicine production and other fields [75]. During the heating process, microwave radiation applies alternating electromagnetic fields with higher frequency than induction, in the order of Megahertz, causing a change in the orientation of polar molecules, which results in internal friction and increases the material temperature [76]. In this way, the bitumen begins to flow, so that the damages get healed.

Norambuena-Contreras et al [31] found that Microwave heating increased the temperature of the binder, not the aggregates, and as such normal asphalt mixture can be heated with microwave heating energy. González et al [76] also indicated that asphalt mixtures with aggregates that were naturally heated with microwave radiation could be crack-healed.

However, with some additives, the microwave heating speed can be accelerated significantly. The ferrous particles are the most common materials used to enhance the microwave heating effect in asphalt mixture because they can absorb and conduct more thermal energy than the other components of the mixtures, aggregates and bitumen. Figure 2.15 shows the schematic of the microwave heating effect with and without ferrous particles illustrated by Zhao et al [77], which indicates that addition of ferrite particles can largely increase the microwave heating speed in asphalt concrete.

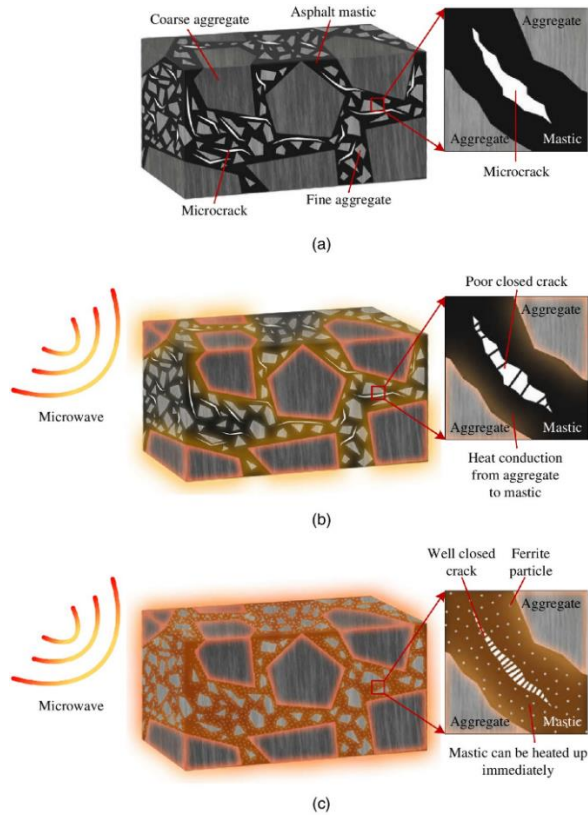


Figure 2.15: The schematic of crack healing with microwave heating: (a) asphalt concrete with microcracks, (b) conventional asphalt concrete heated with microwaves and (c) asphalt concrete containing ferrite particles heated with microwaves [77].

Steel wool fibres are usually used to enhance microwave heating effect in asphalt mixture. In a microwave crack healing study, Gallego et al [30] incorporated steel wool fibres in an asphalt mixture and found these steel wool fibres make it more susceptible to the energy of the microwaves. Then Gallego et al indicated that

the microwave heating requires much less steel fibre content and energy consumption, but shows higher heating efficiency in contrast to the induction heating. Similar results were reported by Norambuena-Contreras et al [78]. In the other study, Norambuena-Contreras et al [31] compared the healing effects from induction heating and microwave heating, which confirmed the higher healing efficiency of the microwave heating but indicated that microwave heating could result in a change in the air voids structure.

In a microwave technique application study, Gao et al [79] found that steel slag possesses a higher microwave heating capacity in contrast to limestone aggregate, which is due to the higher hyperactive ( $\text{Fe}_3\text{O}_4$ ) and active ( $\text{Fe}_2\text{O}_3$  and  $\text{FeS}$ ) content in steel slag. Phan et al [80] used coarse steel slag to replace normal aggregate which also showed an improved microwave healing effect in asphalt mixture. Wang et al [81] reported similar findings and used a numerical model to simulate the microwave heating of asphalt mixture which showed a good correlation with laboratory test results. Sun et al [82] compared the effect of steel fibres and steel slags and reported that the asphalt mixture with steel slag showed a better performance of healing with the microwave as the temperature distribution was more uniform. Sun et al indicated that as the aggregate occupied the main volume of asphalt mixtures, it would be easier for steel slag aggregate to build a uniform temperature distribution.

The use of fine ferrous particles in microwave healing was also investigated. Li et al [57] tested the microwave healing effect of asphalt mixture with steel slags fillers and found that steel slags fillers based asphalt mastics could release more heat than limestone fillers based asphalt mastics under microwave irradiation. Li et al explained this with the higher relative complex permittivity, relative complex permeability and the reflection loss of steel slag filler than limestone filler. In another study, Zhao et al [77] tested the microwave heating with three types of filler additives in asphalt mixture and indicated that NiZn ferrite powders have an excellent microwave absorbing capacity, and an increase in the NiZn ferrite content resulted in a significant increase of the heating speed of asphalt mastic, asphalt matrix, and asphalt concrete.

Except ferrite particles, carbon based materials are also investigated in asphalt mixture for microwave healing. Wang et al [83] reported that carbon fibre, as a modifier, could increase the thermal conductivity and the fracture strength due to fibre reinforcement. Wang et al also indicated that the addition of carbon fibres could achieve superior microwave healing performance in the fracture-healing cycles. Karimi et al [84] proposed the activated carbon as a potentially viable and

robust binder-based conductive component for microwave induced heating and healing of asphalt concrete.

These findings indicate that the microwave healing is a promising method to accelerate the damage healing process in asphalt mixture which has an excellent heating speed, requires fewer additives, and consumes less energy compared to induction heating. However, its overheating, uneven temperature distribution and influence to the voids structure of asphalt concrete limit the application of this technique. Furthermore, the upscaling from laboratory to practical application might be difficult, also from the perspective of safety.

### **2.3.2. EMBEDDED REJUVENATOR ENCAPSULATION METHODS**

It is possible for an asphalt pavement to recover its self-repair mechanism via the addition of bitumen with a higher penetration value or via the addition of a rejuvenating agent [85-88].

A rejuvenator is an engineered cationic emulsion containing maltenes and saturates. The primary purpose of the rejuvenator is to diffuse into the aged binder and restore its original molecular structure to extend the pavement service life. Pavement lifespan is extended by adjusting the properties of the asphalt mix, i.e. reducing its stiffness [86]. Except industrial rejuvenator, Garcia et. al. [89] and Su et al. [90] found that vegetable oil and waste cooking oil can also be used as a rejuvenator. It is possible to use a rejuvenator to heal early stage cracks thereby preventing further crack propagation and pavement failure [91]. In 2010, a research project entitled 'LVO-ZOAB' was carried out by the Ministry of Infrastructures and the Environment (Rijkswaterstaat) of the Netherlands and found that the service life of a porous asphalt can be extended by several years by spraying bitumen rejuvenator on the surface course before the initiation of serious damages [92]. However, this maintenance method only allows the rejuvenator to penetrate no more than 20 mm of the porous surface course, indicating that any damage (cracks) occurring at the bottom of the asphalt layer will not be repaired [93]. A further issue encountered when applying the rejuvenator to the asphalt pavement is the necessity for road closures. The rejuvenators may also cause a significant reduction in the surface friction of the pavement and may be harmful to the environment. The inclusion of a rejuvenator into the asphalt mix via micro-capsules or micro-fibres offers the potential to overcome these problems [36, 90, 94-97].

### 2.3.2.1. EPOXY CAPSULES

Garcia et al [89, 98] successfully produced capsules using porous sand which is used as rejuvenator arraying (absorbing) material, the sand granules are bound together and coated by a hard shell made of an epoxy-cement matrix with a volume percentage of 20.9, 13.1, 24.9 and 13.0% of rejuvenator, porous sand, cement and epoxy, respectively. The capsules obtained have a mean size of 1.60mm. The idea is to substitute part of the sand aggregates in asphalt concrete with the microcapsules. When the stress in capsules embedded in the asphalt reaches a certain threshold value, the capsules break and rejuvenator is released. Figure 2.16 shows epoxy microcapsule morphology.

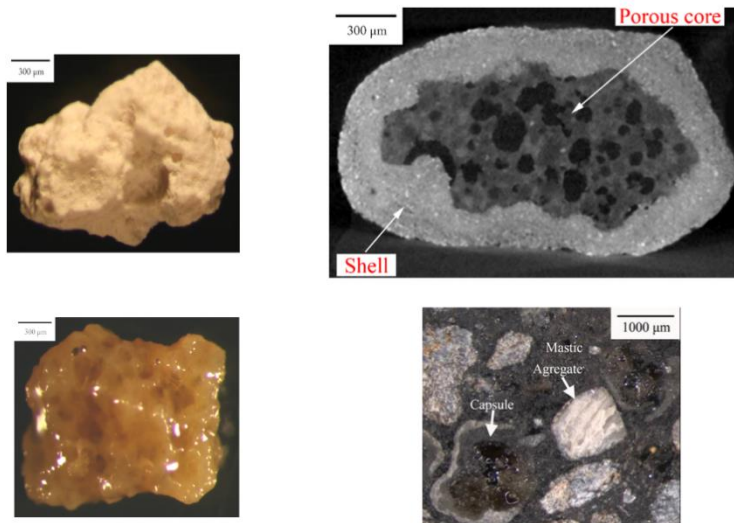


Figure 2.16: Epoxy microcapsule, top left: porous sand, bottom left: rejuvenator saturated sand granule, top right: microscopic image of epoxy microcapsule encapsulating rejuvenator cross-section, bottom right: embedded epoxy microcapsule in asphalt mix [89, 98]

The microcapsule approach presented a solution for the asphalt self-healing process, as it rejuvenates aged binder i.e. recovers its original physical and mechanical properties. However, the downside to this approach is that it works only once, i.e. once the healing material is released from the microcapsule it cannot be replenished [99].

Furthermore, these capsules have limited rejuvenator content which requires large quantities of capsules to achieve an effective healing. The addition of large quantities of capsules into the asphalt mix can reduce the quality of the pavement

which itself may cause premature pavement failure. Garcia et al. [89, 98] and Sun et al. [100] reported that asphalt stiffness was reduced when capsules were added. The possible reason was the release of the rejuvenator.

### 2.3.2.2. POLYMER MELAMINE-FORMALDEHYDE MICROCAPSULES

Polymer Melamine-Formaldehyde (MMF) microcapsules encapsulating rejuvenator are successfully manufactured by Su [35, 97, 101].

These microcapsules were prepared by the in-situ polymerization method using MMF shell. Hydrolyzed styrene maleic anhydride (SMA) was used as an amphiphilic polymeric surfactant. SMA was hydrolyzed by NaOH and absorbed at the interface of the oily droplets. The strong electron negative of rejuvenator droplets reduced the oil/water interfacial tension. Rejuvenator droplets were formed by high-speed stirring. The oil droplets absorbed MMF prepolymer to balance the charge. The concentration polymers were cross-linked and then formed shells under the effects of acid and heat [102].

Figure 2.17 (a, b) shows the morphologies of these microcapsules. The microcapsules keep a regular global shape with a mean size of 100  $\mu\text{m}$ . The core-shell structure can be recognized from a broken microcapsule in Figure 2.17 (c), which means that the oily rejuvenator has been encapsulated by polymeric shell material. Generally, larger microcapsules are easier to break. As a result, the mean size of microcapsules in asphalt needs to be less than 100  $\mu\text{m}$  avoiding squeeze rupture [101]. It has also been found that the 20-50  $\mu\text{m}$  is an ideal size for the self-healing microcapsules in asphalt [35]. Polymer shells can not maintain integrity under an ultimate mechanical strength or thermal stimulation [103]. Therefore, it is important that the microcapsules keep regularity and have the appropriate mean size as well as the shell thickness. The core/shell ratios controlling method has been reported in previous works [35].

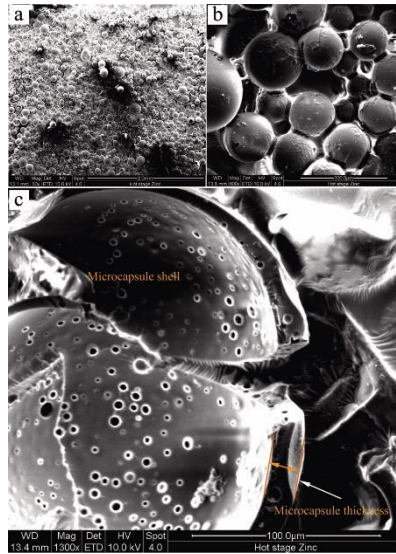


Figure 2.17: SEM morphologies of microcapsules containing rejuvenator, (a, b) microcapsules containing rejuvenator, (c) shell structure of a broken microcapsule.[102]

The microcapsules have been proven to be able to survive under the temperature of 180~200°C [104] The results confirmed that the microcapsules are capable of application in hot mix asphalt. Figure 2.18 (a) shows that fine aggregates and bitumen were mixed together, which asphalt binder is marked with an arrow. Su et al [103] also proved that compatibility of microcapsules with bitumen performed well so that microcracks were not generated by microcapsules departing from the asphalt mixtures, which means an addition of microcapsules will not affect the performance of asphalt. Figure 2.18 (b) shows a fluorescence microscope morphology of microcapsules in asphalt binder. The surface of microcapsules is completely covered by asphalt binder and a fusion of microcapsules and bitumen can also be found. It can also be seen that rupture was not generated at the shell surfaces. The microcapsules survived from agitation in the molten asphalt. Similar results have been reported in other works [105].

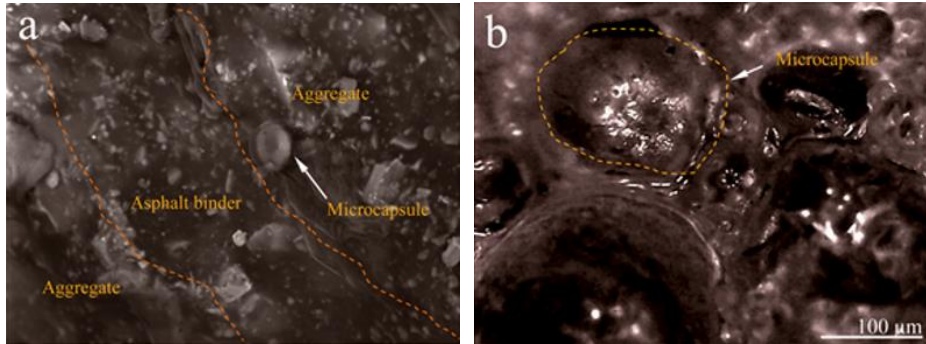


Figure 2.18: Microstructure morphologies of microcapsules in asphalt sample (MB-7) at room temperature state, (a) ESEM morphology of asphalt with aggregate and bitumen binder, and (b) a fluorescence microscope morphology of microcapsules in bitumen binders [102].

When applied in asphalt, agglomeration of microcapsules should be avoided since it may greatly influence the healing effect [106]. Figure 2.19 shows the in-situ fluorescence microscope morphologies of microcapsules dispersing in asphalt samples of MB-3 and MB-7. The microcapsules disperse in asphalt binders homogeneously without adhesion. The shells of these microcapsules have an inorganic/organic composite structure, the electrostatic interaction between particles does not increase the appearance of the phenomenon of agglomeration.

Comparing Figure 2.19 (a) and Figure 2.19 (b), increasing in microcapsules content (3%-7%) also does not affect the dispersion of microcapsules. When the asphalt binder gets aged, the generated microcracks will break microcapsules and release the oily rejuvenator. If the microcapsules are not well dispersed, the healing effect will be limited.

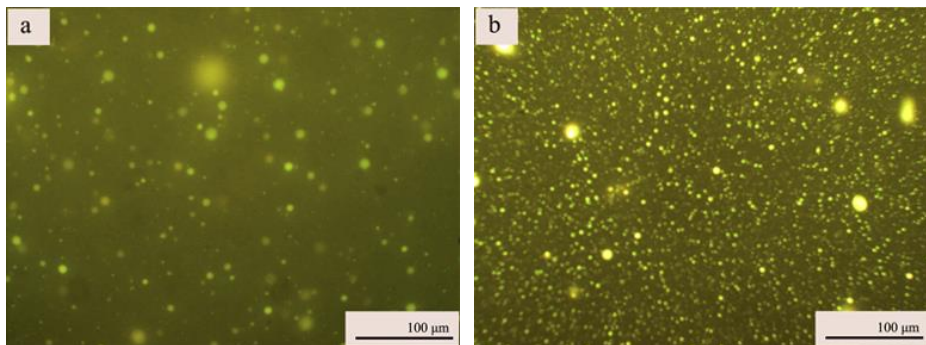


Figure 2.19: In-situ observation of microcapsules dispersing in asphalt binder by a fluorescence microscope: morphologies of (a) MB-3 and (b) MB-7 [102].

Su et al [60] used XCT to investigate the dispersion of microcapsules in asphalt. Since the shell has inorganic nano- $\text{CaCO}_3$ , the shape of microcapsules can be identified due to the density difference between bitumen and inorganic material. Figure 2.20 (a) shows an image of X-ray scanning part of XCT instrument. Figure 2.20 (b) shows an image of the bitumen/microcapsules samples with cylindrical shapes (3.0 wt.%, microcapsules). CT scan is a non-destructive test that allows the user to observe the inside of an object using computer-processed combinations of many X-ray image slices. These slices can be taken from different angles of specific areas of a scanned object. Figure 2.20 (c) shows a typical tomographic slice of bitumen/microcapsules sample. The global shape of microcapsules can be identified and microcapsules are found homogeneously dispersed in asphalt binder. It can also be seen that the microcapsules were covered with inorganic particles due to the density difference.

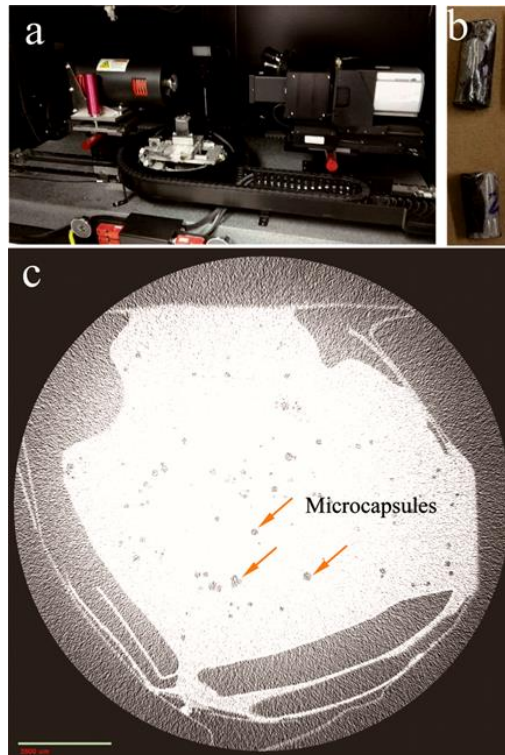


Figure 2.20: XCT investigation of microcapsules in pure bitumen, (a) a photograph of X-ray scanning part of XCT instrument, (b) a photograph of testing microcapsules/bitumen samples with cylindrical shape (3.0 wt.%, microcapsules), and (c) XCT image of microcapsules dispersing in pure bitumen [102].

Su et al [102] also investigated the influence of aggregate on the distribution of microcapsules. Figure 2.21 (a) shows an XCT slice of microcapsules dispersing in the asphalt sample (BM-7) with a microcrack. Figure 2.21 (b) illustrates the 3D-XCT image of the asphalt sample (BM-7). It shows that the microcapsules have a full range distribution in asphalt which is important for effective crack healing.

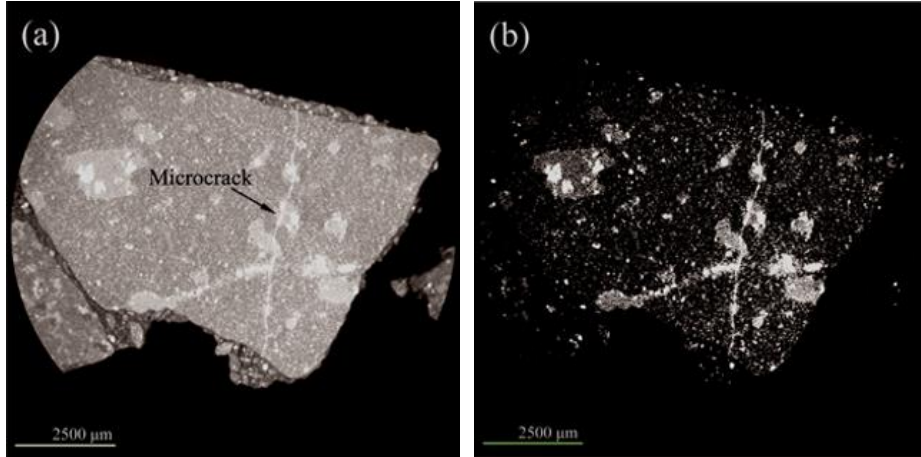


Figure 2.21: XCT images of microcapsules in asphalt binder (BM-7), (a) an XCT slice of microcapsules dispersing in asphalt sample, (b) a 3D-image of microcapsules dispersing in asphalt sample [102].

The mechanism of self-healing of asphalt using microcapsules is clear that oily rejuvenator flows out from microcapsules and fills the whole microcrack through capillarity. As microcapsules are homogeneously distributed, the encapsulated rejuvenator can wet the surface of microcracks. The homogeneous dispersion of microcapsules also will help to disperse the rejuvenator to each damage site [106].

The initial decomposition temperature of microcapsules was affected by the factors including core/shell ratio, morphology and shell material dropping speed [35]. Su et al [102] showed that the microcapsules with nano- $\text{CaCO}_3$ /polymer shells can survive in 180-200°C bitumen. Although microcapsules can safely survive in asphalt, it is still required to prove that microcapsules can resist some comprehensive extreme conditions. Asphalt in the field conditions withstands the external temperature changes. The temperature change cycles may cause the breakdown of microcapsules. This will significantly reduce the possibility of microcapsule rupture only when the microcracks appear.

Su et al [102] used a simulation method to investigate the thermal stability of microcapsules in asphalt binders under an alternating temperature process. Asphalt sample (MB-7) was heated to 50°C and then cooling down to -10°C with a rate of

2°C/min. This process was repeated 50-100 times. After that, a piece of sample was peeled off and heated to 150°C, then the melting bitumen was evenly distributed on glass and observed by a fluorescence microscope. In Figure 2.22 (a), microcapsules still compact particles without rupture dispersing in bitumen. It means that they resist the alternating temperature process repeated for 50 times. With an alternating temperature process repeated for 70 times, as shown in Figure 2.22 (b), it can be found that the particles are brighter and their diameter is increased. It might be because of the rejuvenator penetrating asphalt binder. When an alternating temperature process repeated 100 times, it can be seen the release trace of the rejuvenator in Figure 2.22 (c). Some microcapsules may have been ruptured by the thermal action. It needs to be mentioned that self-healing microcapsules may be broken at different conditions, which will supply a continuous rejuvenator into asphalt binder during the ageing process. This simulated environmental changes implied that microcapsules can survive in asphalt under temperature changes without rupture.

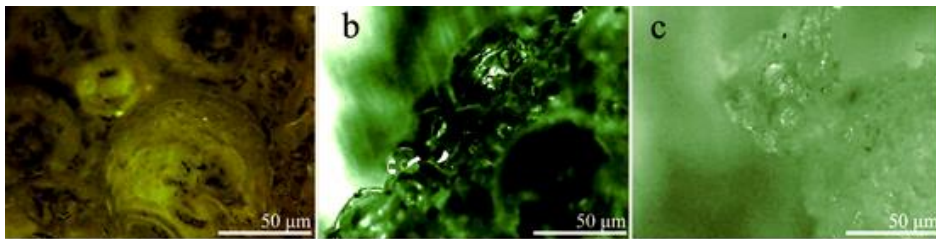


Figure 2.22: Fluorescence microscope morphologies of microcapsules in asphalt binders (MB-7) with a thermal treatment process repeated for different times: (a) 50, (b) 70 and (c) 100 times. One temperature change cycle: heated to 50°C with a rate of 2°C/min and keeping for 10 min, and then decreased the temperature to -10 °C a rate of 2 °C/min [102].

Findings from Su et al indicate that microcapsules encapsulating rejuvenator can be used to enhance the self-healing capability of asphalt. However, the addition of large quantities of microcapsules into the asphalt mix can reduce the quality of the pavement which itself may cause premature pavement failure. Garcia et al [89] and Sun et al [107] reported that the application of microcapsules may reduce the stiffness of asphalt mix. They explained that it is releasing of rejuvenator that softens the asphalt binder. Moreover, this encapsulation technology presents a potential problem for the environment, where material used in production of the capsules: ‘formaldehyde’ in high concentration can be dangerous for human health.

### 2.3.2.3. ALGINATE FIBRES

The compartmented alginate fibre encapsulating rejuvenator is a unique self-healing technology for asphalt pavements, whereby the encapsulated rejuvenator within the asphalt mix is used as the healing catalyst. The principle underpinning this technology is that when micro cracks begin to form within the pavement, they encounter a microcapsule. The fracture energy at the crack-tip will open the capsule, thereby releasing the rejuvenator. The rejuvenator then diffuses with the asphalt binder to seal the crack, preventing its further propagation. Figure 2.23 illustrates the compartmented alginate fibre encapsulating bitumen rejuvenator self-healing concept.

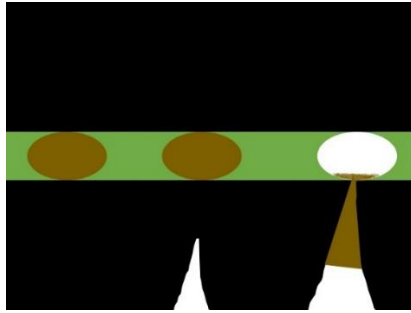


Figure 2.23: Compartmented Alginate Fibres Encapsulating Rejuvenator Concept [37].

Figure 2.23 shows that compartmented fibres comprising of multiple compartments encapsulating bitumen rejuvenator. These were spun from an emulsion of a rejuvenator suspended in a water solution of sodium alginate. To this aim, a 6 wt.% solution of sodium alginate in de-ionized water was prepared. At the same time a 2.5 wt.% poly (ethylene-alt-maleic-anhydride) (PEMA) polymeric surfactant solution was prepared by dissolving the copolymer in the water at 7°C and mixing it for 60min. After the PEMA has been dissolved in the water it was allowed to cool to room temperature ( $20\pm 2^\circ\text{C}$ ) and was added to the rejuvenator in the proportion of 40% PEMA and 60% rejuvenator, forming a healing agent solution. Sodium alginate and PEMA/rejuvenator solutions were then combined in an optimum rejuvenator/alginate proportion of 70:30. The solution was mixed at 200 rpm for 60 seconds. It is important to note that the stirring rate and stirring time can be used to control the size of the rejuvenator droplets in the solution and thus the size of the rejuvenator compartments [94, 108]. If the stirring rate is low and stirring time is short, the droplets will be larger, but if the stirring rate is high and the stirring time is long, the droplets will be smaller.

The emulsion was then spun with a plunger-based lab-scale wet spinning line in a conventional wet spinning process [108, 109] to form the rejuvenator-filled compartmented fibres. A spinneret containing one capillary of 0.5mm diameter and 1.5mm length was used. The extrusion rate was 1.93 cm<sup>3</sup>/min and the take-up speed was 19.1 m/min. The coagulation bath was 0.8m long and contained a 0.45M solution of CaCl<sub>2</sub>·6H<sub>2</sub>O. More details on the fibre preparation and spinning process can be found elsewhere [109]. Figure 2.24 shows an image of a compartmented alginate fibre encapsulating rejuvenator captured by optical microscope technique.



Figure 2.24: An image of a compartmented alginate fibre encapsulating rejuvenator captured by optical microscope. Plane polarized light imaging. The field of view is approximately 3mm [36].

Tabaković et al tested the thermal stability of the alginate fibres and results are presented in Figure 2.25. Figure 2.25 (a) shows the results of the Thermal Gravimetric Analysis (TGA) of the fibre. The compartmented fibres lost 25% of their weight at 270°C and a further weight loss of 9% during the asphalt mixing process (temperatures of 160°C) most likely due to residual water evaporation from the calcium alginate. These results indicate that the alginate fibre can, in principle, resist the high processing temperatures of the asphalt mixing process. Figure 2.25 (b) shows the UTS vs temp. of the optimal (70:30) fibres, the results show to be at the lower end, in the range between 20 and 53 MPa depending on the conditioning temperature. However, its linearity, small change in UTS across the thermal range, indicates the small effect of temperature (high and low) on the fibre properties. These results indicate that the alginate fibre encapsulating rejuvenator can, in principle, resist the high processing temperatures of the asphalt mixing process [36].

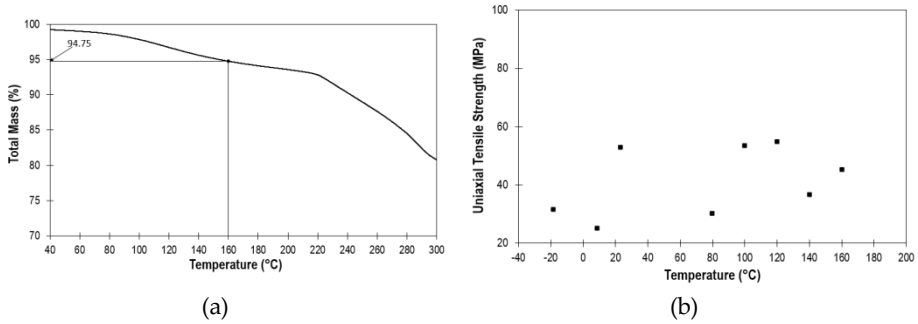


Figure 2.25: Sodium Alginate Compartmented fibres containing rejuvenator; (a) TGA test results and (b) Uniaxial strength vs Temperature [36].

Tabaković et al showed that alginate fibres have great potential as self-healing techniques for asphalt pavements, i.e. they can be inserted into the asphalt mastic mix (fibres can survive asphalt mixing and compaction process) and can increase asphalt mastic mix strength by 36%. The optimum rejuvenator alginate ratio is 70:30 [96]. However, the study showed that fibres have limited healing capacity. The fibres are effective in the healing of microcracks, however, the system is less efficient in the healing of large cracks. Figure 2.26 and Figure 2.27 illustrate the healing efficiency of an asphalt mortar mix with and without fibres. This was explained by low amount of rejuvenator contained in the mix, the rejuvenator alginate ratio was 40:60. Further study showed that with the increase of the rejuvenator alginate ratio in the fibre mix to 70:30 improved healing rate [96]. Tabaković et al [96] also showed that higher amounts of fibre could reduce the healing capacity of the asphalt mix. Figure 2.28 shows that the optimum amount of the fibre in the mix was 5% by volume of the constituents.

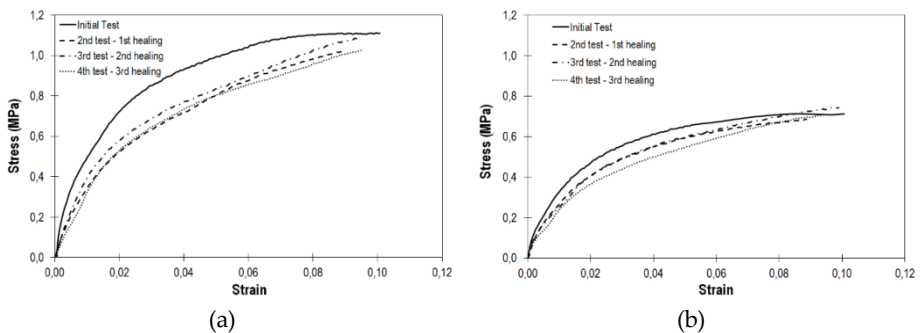


Figure 2.26: Typical 3PB test load vs deflection plots for asphalt mastic mix at 20°C, at varying healing stages: (a) mix containing fibres and (b) mix without fibres [36].

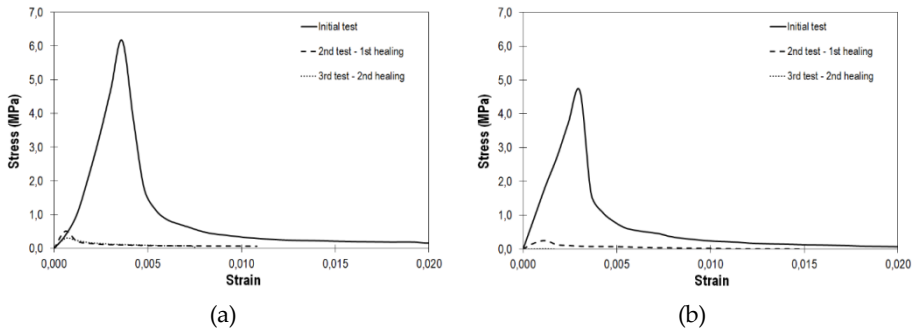


Figure 2.27: Typical 3PB test load vs deflection plots for asphalt mastic mix at -5°C, at varying healing stages: (a) mix containing fibres and (b) mix without fibres [36].

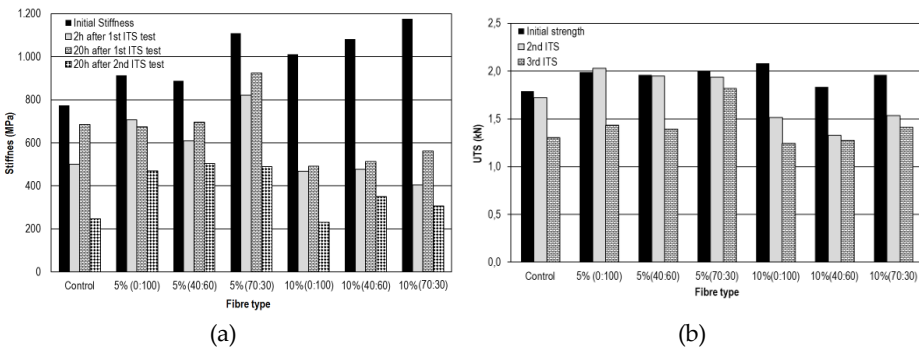


Figure 2.28: Healing efficiency of porous asphalt mix containing varying amounts of fibres in the mix (a) stiffness and (b) tensile strength [110].

Tabakovic et al [110] further demonstrated that optimum healing time for porous asphalt mix using compartmented alginate fibres encapsulating rejuvenator is 20h. Figure 2.29 illustrates successful crack closure (healing) in an asphalt test specimen containing 5% compartmented alginate fibres encapsulating the rejuvenator after 20 h of healing.

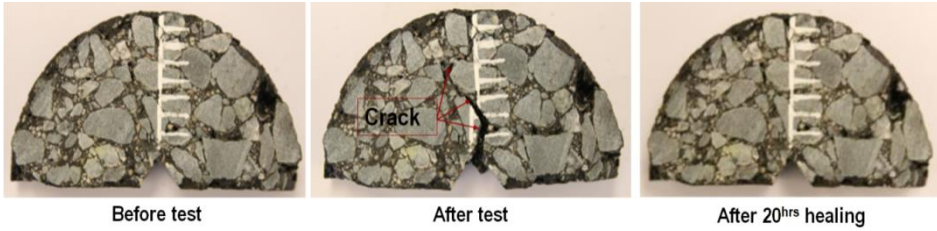
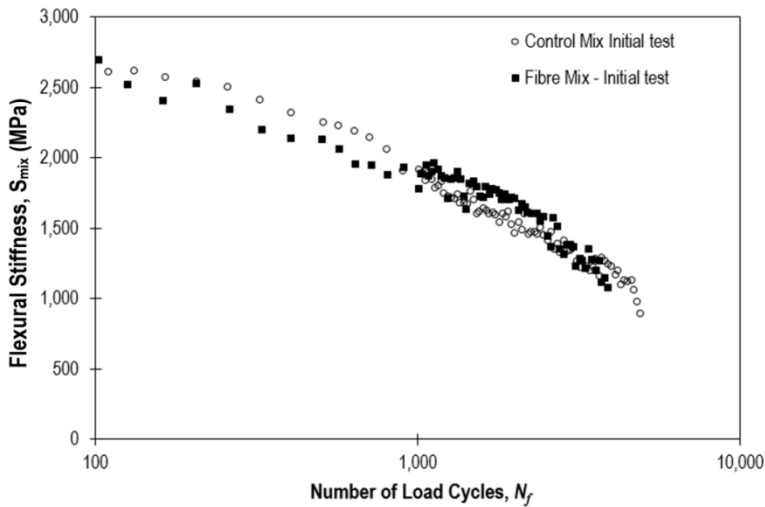


Figure 2.29: SCB test specimen crack closure/healing [110].

Tabakovic et al [110] also studied healing performance a porous asphalt mix containing the fibre healing system subjected to fatigue loading. Figure 2.30 shows the healing efficiency of the porous control mix and fibre mix flexural stiffness ( $S_{mix}$ ). The results show a very close initial test performance (Figure 2.30 (a)). However, Figure 2.30 (b) shows a higher stiffness recovery for the PA fibre mix after 20h healing at 20°C. These results demonstrate the potential benefits of the PA mix containing compartmented alginate fibres encapsulating the rejuvenator.



(a)

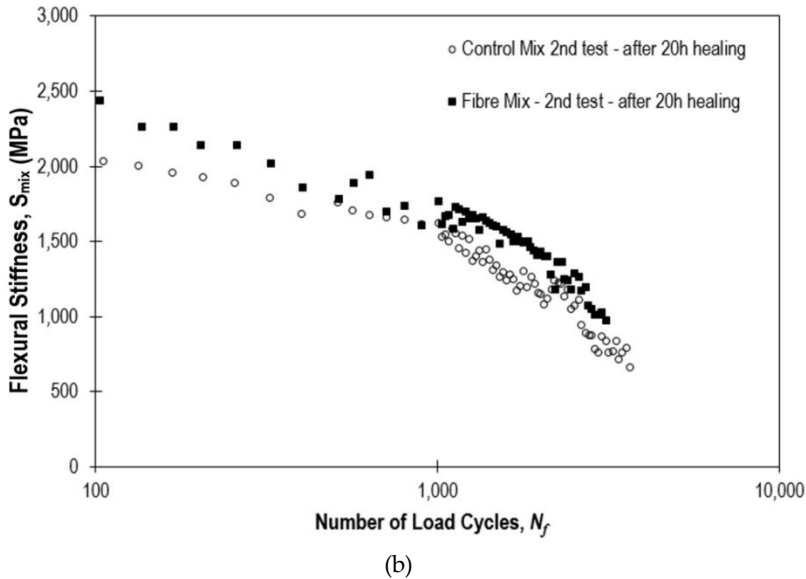


Figure 2.30: 4PBT results: (a) initial test results and (b) test results after 20 h healing at 20 °C [110].

Findings from Tabaković et al indicate that these alginate fibres are capable of healing microcracks within an asphalt mix. However, due to the limit amount of rejuvenator, this self-healing system can only repair small micro-cracks. Besides, studies from Tabaković et al demonstrated that alginate can be used as a very positive material for rejuvenator encapsulation. Hence, based on the alginate materials, utilisation of an encapsulation technology to include a higher content of rejuvenator may have an improved healing effect in asphalt mix, and as such a broader prospect for field application.

Along with this Ph.D. project, other research was also carried out to discover the rejuvenator encapsulation technique using alginate. Successful rejuvenator encapsulations were reported by Shu et al [111, 112], Al-Mansoori et al [113] and Norambuena-Contreras et al [114], and more positive results are expected from the worldwide research.

## 2.4. CONCLUDING REMARKS

Following the literature findings, it has been demonstrated that incorporation of self-healing technology, such as the induction healing or the embedded rejuvenation encapsulation, can help to improve the durability of asphalt pavement which will result in considerable social benefits, both environmental and financial:

- Environmental benefits: the increased sustainability of asphalt pavement with self-healing technology reduces the maintenance works which not only reduces the need of extra resources (aggregate, bitumen, etc.) but also reduces the emissions of greenhouse gases into the atmosphere [115];
- Financial benefits: it was estimated that the Netherlands can save about 90 million euros annually by investing in induction healing asphalt concrete with a 50% extended life span and twice the price compared with standard asphalt concrete [116].

However, in consideration of the drawbacks from thermally induced healing method and embedded rejuvenation encapsulation method, such as the fade of induced healing effect from asphalt ageing and the limited crack healing effect with embedded rejuvenation encapsulation, it is encouraged to develop a new improved healing system which could contribute to a more sustainable asphalt pavement. For this purpose, the combined healing system is developed.

The combined healing system for asphalt pavement is designed following the concept of 'ideal healing' in Figure 2.2 (c). It is expected that, by using the combined healing system, damages from cyclic vehicle loadings can be healed before evolving into a major failure, and this healing event can be repeated, time after time, so that the service life of the asphalt pavement is extended. The induction heating technique, with remarkable crack healing ability and repeatable healing potential, is incorporated in the combined healing system and serves as the major asphalt damage repair mechanism. Although the microwave heating has a higher energy and healing efficiency, it is not adopted mainly due to the uneven heating and overheating which may cause an uncontrolled healing behaviour.

However, the induction heating technique can not reduce the ageing of asphalt and even accelerates the ageing with high temperature, which might result in a stiffer asphalt binder which leads to increased cracking and premature pavement failure. For this reason, encapsulated rejuvenator is also incorporated in the combined healing system to replenish (rejuvenate) aged asphalt binder and reinstate bitumen's healing ability. Alginate is selected as the shell material for rejuvenator encapsulation and the detailed encapsulation procedure is explored and introduced in Chapter 4.

In summary, the limitations of both capsule healing system and induction healing system, as well as the potential synergistic effects motivate to develop a combined healing system to achieve self-healing in asphalt pavement. To this aim, a re-

juvenator encapsulation technology needs to be developed and optimized first. Afterwards, the capsule healing system and induction healing system are combined, and the healing efficiency of the combined healing system are evaluated.

## REFERENCES

- [1] S. van der Zwaag, An introduction to material design principles: Damage prevention versus damage management, *Self healing materials*, Springer2007, pp. 1-18.
- [2] D. Krajcinovic, Damage mechanics, *Mechanics of materials* 8(2-3) (1989) 117-197.
- [3] S. Murakami, *Mechanical modeling of material damage*, (1988).
- [4] J. Qiu, *Self healing of asphalt mixtures: towards a better understanding of the mechanism*, Delft University of Technology, 2012.
- [5] M.D. Hager, P. Greil, C. Leyens, S. van der Zwaag, U.S. Schubert, *Self - healing materials*, *Advanced Materials* 22(47) (2010) 5424-5430.
- [6] A. Tabaković, E. Schlangen, *Self-healing technology for asphalt pavements*, *Self-healing Materials*, Springer2015, pp. 285-306.
- [7] P. Ayar, F. Moreno-Navarro, M.C. Rubio-Gómez, *The healing capability of asphalt pavements: a state of the art review*, *Journal of Cleaner Production* 113 (2016) 28-40.
- [8] S. Ren, X. Liu, H. Wang, W. Fan, S. Erkens, *Evaluation of rheological behaviors and anti-aging properties of recycled asphalts using low-viscosity asphalt and polymers*, *Journal of Cleaner Production* (2020) 120048.
- [9] L. Zhang, Q. Liu, H. Li, J. Norambuena-Contreras, S. Wu, S. Bao, B. Shu, *Synthesis and characterization of multi-cavity Ca-alginate capsules used for self-healing in asphalt mixtures*, *Construction and Building Materials* 211 (2019) 298-307.
- [10] J. Norambuena-Contreras, I. Gonzalez-Torre, *Influence of the microwave heating time on the self-healing properties of asphalt mixtures*, *Applied Sciences* 7(10) (2017) 1076.

- [11] G. Sun, M. Hu, D. Sun, Y. Deng, J. Ma, T. Lu, Temperature induced self-healing capability transition phenomenon of bitumens, *Fuel* 263 (2020) 116698.
- [12] P. Bazin, J. Saunier, *Deformability, fatigue and healing properties of asphalt mixes*, Intl Conf Struct Design Asphalt Pvmnts, 1967.
- [13] J. Qiu, *Self healing of asphalt mixes: literature review*, Delft University of Technology (2008).
- [14] D. Little, R. Lytton, D. Williams, C. Chen, Y. Kim, H. Lee, *Fundamental properties of asphalts and modified asphalts—task K: microdamage healing in asphalt and asphalt concrete*, FHWA Final Report 1 (1998).
- [15] D. Williams, D. Little, R. Lytton, Y. Kim, Y. Kim, *Microdamage healing in asphalt and asphalt concrete, volume II: Laboratory and field testing to assess and evaluate microdamage and microdamage healing*, 2001.
- [16] R. Wool, K. O’connor, A theory crack healing in polymers, *Journal of Applied Physics* 52(10) (1981) 5953-5963.
- [17] S. Nahar, *Phase-separation characteristics of bitumen and their relation to damage-healing*, (2016).
- [18] Y.R. Kim, D.N. Little, F.C. Benson, Chemical and mechanical evaluation on healing mechanism of asphalt concrete (with discussion), *Journal of the Association of Asphalt Paving Technologists* 59 (1990).
- [19] A. Bhasin, D.N. Little, R. Bommavaram, K. Vasconcelos, A framework to quantify the effect of healing in bituminous materials using material properties, *Road Materials and Pavement Design* 9(sup1) (2008) 219-242.
- [20] A. Bhasin, R. Bommavaram, M.L. Greenfield, D.N. Little, Use of molecular dynamics to investigate self-healing mechanisms in asphalt binders, *Journal of Materials in Civil Engineering* 23(4) (2010) 485-492.
- [21] Y. Hou, L. Wang, T. Pauli, W. Sun, Investigation of the asphalt self-healing mechanism using a phase-field model, *Journal of Materials in Civil Engineering* 27(3) (2014) 04014118.
- [22] J. Qiu, M. Van de Ven, S. Wu, J. Yu, A. Molenaar, Evaluating self healing capability of bituminous mastics, *Experimental mechanics* 52(8) (2012) 1163-1171.

- [23] Á. García, Self-healing of open cracks in asphalt mastic, *Fuel* 93 (2012) 264-272.
- [24] M. Riara, P. Tang, L. Mo, W. Hong, M. Chen, S. Wu, Evaluation of moisture and temperature effect on crack healing of asphalt mortar and mixtures using healing agents, *Construction and Building Materials* 177 (2018) 388-394.
- [25] D. Sun, T. Lin, X. Zhu, L. Cao, Calculation and evaluation of activation energy as a self-healing indication of asphalt mastic, *Construction and Building Materials* 95 (2015) 431-436.
- [26] Q. Liu, *Induction Healing of Porous Asphalt Concrete*, Delft University of Technology, 2012.
- [27] Á. García, E. Schlangen, M. van de Ven, Q. Liu, A simple model to define induction heating in asphalt mastic, *Construction and Building Materials* 31 (2012) 38-46.
- [28] Q. Liu, E. Schlangen, Á. García, M. van de Ven, Induction heating of electrically conductive porous asphalt concrete, *Construction and Building Materials* 24(7) (2010) 1207-1213.
- [29] Q. Liu, E. Schlangen, M. van de Ven, Induction healing of porous asphalt concrete beams on an elastic foundation, *Journal of Materials in Civil Engineering* 25(7) (2012) 880-885.
- [30] J. Gallego, M.A. del Val, V. Contreras, A. Páez, Heating asphalt mixtures with microwaves to promote self-healing, *Construction and Building Materials* 42 (2013) 1-4.
- [31] J. Norambuena-Contreras, A. Garcia, Self-healing of asphalt mixture by microwave and induction heating, *Materials & Design* 106 (2016) 404-414.
- [32] T. Al-Mansoori, R. Micaelo, I. Artamendi, J. Norambuena-Contreras, A. Garcia, Microcapsules for self-healing of asphalt mixture without compromising mechanical performance, *Construction and Building Materials* 155 (2017) 1091-1100.
- [33] A. Garcia, J. Jelfs, C.J. Austin, Internal asphalt mixture rejuvenation using capsules, *Construction and Building Materials* 101 (2015) 309-316.
- [34] R. Micaelo, T. Al-Mansoori, A. Garcia, Study of the mechanical properties and self-healing ability of asphalt mixture containing calcium-alginate capsules, *Construction and Building Materials* 123 (2016) 734-744.

- [35] J.-F. Su, J. Qiu, E. Schlangen, Stability investigation of self-healing microcapsules containing rejuvenator for bitumen, *Polymer degradation and stability* 98(6) (2013) 1205-1215.
- [36] A. Tabaković, W. Post, D. Cantero, O. Copuroglu, S. Garcia, E. Schlangen, The reinforcement and healing of asphalt mastic mixtures by rejuvenator encapsulation in alginate compartmented fibres, *Smart Materials and Structures* 25(8) (2016) 084003.
- [37] S. Xu, A. García, J. Su, Q. Liu, A. Tabaković, E. Schlangen, Self - Healing Asphalt Review: From Idea to Practice, *Advanced Materials Interfaces* (2018) 1800536.
- [38] K. Chung, S. Lee, M. Park, P. Yoo, Y. Hong, Preparation and characterization of microcapsule-containing self-healing asphalt, *J. Ind. Eng. Chem. (Amsterdam, Neth.)* 29 (2015) 330-337.
- [39] R.C. Barrasa, V.B. López, C.M.-P. Montoliu, V.C. Ibáñez, J. Pedrajas, J. Santarén, Addressing durability of asphalt concrete by self-healing mechanism, *Procedia-Social and Behavioral Sciences* 162 (2014) 188-197.
- [40] Q. Liu, E. Schlangen, M.F. van de Ven, G. van Bochove, J. van Montfort, Predicting the Performance of the Induction Healing Porous Asphalt Test Section, 7th RILEM International Conference on Cracking in Pavements, Springer, 2012, pp. 1081-1089.
- [41] S. Salih, B. Gómez-Mejjide, M. Aboufoul, A. Garcia, Effect of porosity on infrared healing of fatigue damage in asphalt, *Constr. Build. Mater.* 167 (2018) 716-725.
- [42] J.-F. Su, The world first self-healing asphalt pavement using microcapsules containing rejuvenator., 2017. [www.tjsinogo.cn](http://www.tjsinogo.cn).
- [43] L. Francken, Fatigue performance of a bituminous road mix under realistic test conditions, *Transportation Research Record* (712) (1979).
- [44] M. Castro, J.A. Sánchez, Fatigue and healing of asphalt mixtures: discriminate analysis of fatigue curves, *Transp. Eng. J. ASCE* 132(2) (2006) 168-174.
- [45] D.N. Little, A. Bhasin, Exploring Mechanism of H ealing in Asphalt Mixtures and Quantifying its Impact, *Self healing materials*, Springer2007, pp. 205-218.

[46] D. Williams, D. Little, R. Lytton, Y. Kim, Y. Kim, Microdamage healing in asphalt and asphalt concrete, Volume 2: laboratory and field testing to assess and evaluate microdamage and microdamage healing, Turner-Fairbank Highway Research Center, 2001.

[47] S.I. Sarsam, Crack healing potential of asphalt concrete pavement, International Journal of Scientific Research in Knowledge 3(1) (2015) 001-012.

[48] T.P. Grant, Determination of asphalt mixture healing rate using the Superpave indirect tensile test, University of Florida USA, 2001.

[49] Q. Liu, Á. García, E. Schlangen, M. van de Ven, Induction healing of asphalt mastic and porous asphalt concrete, Construction and Building Materials 25(9) (2011) 3746-3752.

[50] Á. García, E. Schlangen, M. van de Ven, Q. Liu, Electrical conductivity of asphalt mortar containing conductive fibers and fillers, Construction and building materials 23(10) (2009) 3175-3181.

[51] Á. García, E. Schlangen, M. van de Ven, D. van Vliet, Induction heating of mastic containing conductive fibers and fillers, Materials and structures 44(2) (2011) 499-508.

[52] X. Yang, Q. Dai, Z. You, Z. Wang, Integrated experimental-numerical approach for estimating asphalt mixture induction healing level through discrete element modeling of a single-edge notched beam test, J. Mater. Civ. Eng. 27(9) (2014) 04014259.

[53] J. Tang, Q. Liu, S. Wu, Q. Ye, Y. Sun, E. Schlangen, Investigation of the optimal self-healing temperatures and healing time of asphalt binders, Construction and Building Materials 113 (2016) 1029-1033.

[54] S.I. Sarsam, S.A. Barakhas, Influence of load repetitions and heating on micro crack healing of asphalt stabilized subgrade soil, International Journal of Materials Chemistry and Physics, Public science framework, American institute of science 1(3) (2015) 399-405.

[55] Q. Liu, S. Wu, E. Schlangen, Induction heating of asphalt mastic for crack control, Construction and Building Materials 41 (2013) 345-351.

[56] P. Apostolidis, Experimental and numerical investigation of induction heating in asphalt mixes, (2015).

- [57] C. Li, S. Wu, Z. Chen, G. Tao, Y. Xiao, Enhanced heat release and self-healing properties of steel slag filler based asphalt materials under microwave irradiation, *Construction and building materials* 193 (2018) 32-41.
- [58] B. Gómez-Meijide, H. Ajam, P. Lastra-González, A. Garcia, Effect of ageing and RAP content on the induction healing properties of asphalt mixtures, *Construction and Building Materials* 179 (2018) 468-476.
- [59] B. Chen, B. Li, Y. Gao, T.-C. Ling, Z. Lu, Z. Li, Investigation on electrically conductive aggregates produced by incorporating carbon fiber and carbon black, *Construction and Building Materials* 144 (2017) 106-114.
- [60] Z. Wang, Q. Dai, S. Guo, Laboratory performance evaluation of both flake graphite and exfoliated graphite nanoplatelet modified asphalt composites, *Construction and Building Materials* 149 (2017) 515-524.
- [61] H. Jahanbakhsh, M.M. Karimi, B. Jahangiri, F.M. Nejad, Induction heating and healing of carbon black modified asphalt concrete under microwave radiation, *Construction and Building Materials* 174 (2018) 656-666.
- [62] H. Zhang, X.H. Wu, X.L. Wang, Conductivity mechanism of asphalt concrete with the PANI/PP compound conductive fiber, *Materials Science Forum*, Trans Tech Publ, 2011, pp. 69-73.
- [63] H. Ajam, B. Gómez-Meijide, I. Artamendi, A. Garcia, Mechanical and healing properties of asphalt mixes reinforced with different types of waste and commercial metal particles, *Journal of Cleaner Production* 192 (2018) 138-150.
- [64] S. Xu, X. Liu, A. Tabaković, E. Schlangen, The influence of asphalt ageing on induction healing effect on porous asphalt concrete, *RILEM Technical Letters* 3 (2018) 98-103.
- [65] Q. Liu, W. Yu, S. Wu, E. Schlangen, P. Pan, A comparative study of the induction healing behaviors of hot and warm mix asphalt, *Construction and Building Materials* 144 (2017) 663-670.
- [66] Q. Liu, B. Li, E. Schlangen, Y. Sun, S. Wu, Research on the Mechanical, Thermal, Induction Heating and Healing Properties of Steel Slag/Steel Fibers Composite Asphalt Mixture, *Applied Sciences* 7(10) (2017) 1088.

- [67] Q. Liu, E. Schlangen, M.v.d. Ven, Induction Healing of Porous Asphalt Concrete Beams on an Elastic Foundation, *Journal of Materials in Civil Engineering* 25(7) (2013) 880-885.
- [68] Q. Liu, E. Schlangen, M. van de Ven, G. van Bochove, J. van Montfort, Evaluation of the induction healing effect of porous asphalt concrete through four point bending fatigue test, *Construction and Building Materials* 29 (2012) 403-409.
- [69] A. García, M. Bueno, J. Norambuena-Contreras, M.N. Partl, Induction healing of dense asphalt concrete, *Construction and Building Materials* 49 (2013) 1-7.
- [70] Q. Dai, Z. Wang, M.R.M. Hasan, Investigation of induction healing effects on electrically conductive asphalt mastic and asphalt concrete beams through fracture-healing tests, *Construction and Building Materials* 49 (2013) 729-737.
- [71] A. Menozzi, A. Garcia, M.N. Partl, G. Tebaldi, P. Schuetz, Induction healing of fatigue damage in asphalt test samples, *Construction and Building Materials* 74 (2015) 162-168.
- [72] P. Apostolidis, X. Liu, A. Scarpas, C. Kasbergen, M. van de Ven, Advanced evaluation of asphalt mortar for induction healing purposes, *Construction and Building Materials* 126 (2016) 9-25.
- [73] P. Apostolidis, X. Liu, C. Kasbergen, A.T. Scarpas, M. van de Ven, Toward the design of an induction heating system for asphalt pavements with the finite element method, *Transportation Research Record* 2633(1) (2017) 136-146.
- [74] B.H. Dinh, D.-W. Park, T.H.M. Le, Effect of rejuvenators on the crack healing performance of recycled asphalt pavement by induction heating, *Construction and Building Materials* 164 (2018) 246-254.
- [75] X. Zhu, Y. Cai, S. Zhong, J. Zhu, H. Zhao, Self-healing efficiency of ferrite-filled asphalt mixture after microwave irradiation, *Construction and Building Materials* 141 (2017) 12-22.
- [76] A. González, J. Valderrama, J. Norambuena-Contreras, Microwave crack healing on conventional and modified asphalt mixtures with different additives: an experimental approach, *Road Materials and Pavement Design* 20(sup1) (2019) S149-S162.

- [77] H. Zhao, S. Zhong, X. Zhu, H. Chen, High-efficiency heating characteristics of ferrite-filled asphalt-based composites under microwave irradiation, *Journal of Materials in Civil Engineering* 29(6) (2017) 04017007.
- [78] J. Norambuena-Contreras, R. Serpell, G.V. Vidal, A. González, E. Schlangen, Effect of fibres addition on the physical and mechanical properties of asphalt mixtures with crack-healing purposes by microwave radiation, *Construction and Building Materials* 127 (2016) 369-382.
- [79] J. Gao, A. Sha, Z. Wang, Z. Tong, Z. Liu, Utilization of steel slag as aggregate in asphalt mixtures for microwave deicing, *Journal of Cleaner Production* 152 (2017) 429-442.
- [80] T.M. Phan, D.-W. Park, T.H.M. Le, Crack healing performance of hot mix asphalt containing steel slag by microwaves heating, *Construction and Building Materials* 180 (2018) 503-511.
- [81] H. Wang, Y. Zhang, Y. Zhang, S. Feng, G. Lu, L. Cao, Laboratory and numerical investigation of microwave heating properties of asphalt mixture, *Materials* 12(1) (2019) 146.
- [82] Y. Sun, S. Wu, Q. Liu, W. Zeng, Z. Chen, Q. Ye, P. Pan, Self-healing performance of asphalt mixtures through heating fibers or aggregate, *Construction and Building Materials* 150 (2017) 673-680.
- [83] Z. Wang, Q. Dai, D. Porter, Z. You, Investigation of microwave healing performance of electrically conductive carbon fiber modified asphalt mixture beams, *Construction and Building Materials* 126 (2016) 1012-1019.
- [84] M.M. Karimi, H. Jahanbakhsh, B. Jahangiri, F.M. Nejad, Induced heating-healing characterization of activated carbon modified asphalt concrete under microwave radiation, *Construction and Building Materials* 178 (2018) 254-271.
- [85] H.M.R.D. Silva, J.R.M. Oliveira, C.M.G. Jesus, Are totally recycled hot mix asphalts a sustainable alternative for road paving?, *Resources, Conservation and Recycling* 60 (2012) 38– 48.
- [86] J. Brownridge, The role of an asphalt rejuvenator in pavement preservation: use and need for asphalt rejuvenation, 1st International Conf. on Pavement Preservation, Newport Beach, USA., 2010.

[87] A.G. Tabaković, A.; McNally, C. and Gilchrist, M.D., 2010, "The Influence of Recycled Asphalt Pavement on the Fatigue Performance of Asphalt Concrete Base Courses". *ASCE Journal of Materials in Civil Engineering*, Vol. 22, 6, pp. 643 – 650., The influence of recycled asphalt pavement on the fatigue performance of asphalt concrete base courses, *ASCE Journal of Materials in Civil Engineering* 22(6) (2010) 643 - 650.

[88] A. Tabaković, Recycled Asphalt (RA) for Pavements, in: F. Pacheco-Torgal, V.W.Y. Tam, J.A. Labrincha, Y. Ding, J. de Brito (Eds.), *Handbook of Recycled Concrete and Demolition Waste*, Woodhead Publishing 2013, pp. 394 – 419.

[89] A. Garcia, J. Jelfs, C.J. Austin, Internal asphalt mixture rejuvenation using capsules, *Construction and Building Materials* 101 (2015) 8.

[90] J.F. Su, J. Qiu, E. Schlangen, Y.Y. Wang, Investigation the possibility of a new approach of using microcapsules containing waste cooking oil; in-situ rejuvenation, *Construction and Building Materials* 74 (2015) 83–92.

[91] W. Steyn, Potential application of nanotechnology in pavement engineering, *ASCE Journal of Transport Engineering* 135(10) (2009) 764 – 772.

[92] M. Van de Ven, W. Verwaal, E. Schlangen, M. Poot, Y. Zhang, Q. Liu, Test section A50: final report of TU Delft's investigation for INFRAQUEST project LVO-ZOAB, Report 7-11-185-6, Delft University of Technology Delft 2011.

[93] J. Shen, S. Amirghani, J.A. Miller, Effects of rejuvenating agents on superpave mixtures containing reclaimed asphalt pavement, *ASCE Journal of Materials in Civil Engineering* 19(5) (2007) 376–84.

[94] J.F. Su, E. Schlangen, Synthesis and physicochemical properties of high compact microcapsules containing rejuvenator applied in asphalt, *Chemical Engineering Journal* 198-199 (2012) 289-300.

[95] Á. García, E. Schlangen, M. van de Ven, Two ways of closing cracks on asphalt concrete pavements: Microcapsules and Induction Heating, *Key Engineering Materials* 417-418 (2010) 573-576.

[96] A. Tabaković, D. Braak, M. van Gerwen, O. Copuroglu, W. Post, S.J. Garcia, E. Schlangen, The compartmented alginate fibres optimisation for bitumen rejuvenator encapsulation, *Journal of Traffic and Transportation Engineering* 4 (2017).

- [97] J.-F. Su, J. Qiu, E. Schlangen, Y.-Y. Wang, Experimental investigation of self-healing behavior of bitumen/microcapsule composites by a modified beam on elastic foundation method, *Mater. Struct.* 48(12) (2015) 4067-4076.
- [98] A. Garcia, C.J. Austin, J. Jelfs, Mechanical properties of asphalt mixture containing sunflower oil capsules, *Journal of Cleaner Production* 118 (2016) 9.
- [99] J. Qiu, M.F.C. Van de Ven, S. Wu, J. Yu, A.A.A. Molenaar, Investigation of self healing capability of bituminous binders, *Road Materials and Pavement Design; SPECIAL ISSUE ON ASPHALT MATERIALS (ICAM 2009—China)* 10(1) (2009) 81-94.
- [100] D. Sun, J. Hu, X. Zhu, Size optimization and self-healing evaluation of microcapsules in asphalt binder, *Colloid. Polym. Sci.* 293(12) (2015) 3505-3516.
- [101] J.-F. Su, J. Qiu, E. Schlangen, Y.-Y. Wang, Investigation the possibility of a new approach of using microcapsules containing waste cooking oil: In situ rejuvenation for aged bitumen, *Construction and Building Materials* 74 (2015) 83-92.
- [102] J.-F. Su, S. Han, Y.-Y. Wang, E. Schlangen, N.-X. Han, B. Liu, X.-L. Zhang, P. Yang, W. Li, Experimental observation of the self-healing microcapsules containing rejuvenator states in asphalt binder, *Constr. Build. Mater.* 147 (2017) 533-542.
- [103] J.-F. Su, E. Schlangen, Synthesis and physicochemical properties of high compact microcapsules containing rejuvenator applied in asphalt, *Chem. Eng. J.* 198 (2012) 289-300.
- [104] Y.-Y. Wang, J.-F. Su, E. Schlangen, N.-X. Han, S. Han, W. Li, Fabrication and characterization of self-healing microcapsules containing bituminous rejuvenator by a nano-inorganic/organic hybrid method, *Constr. Build. Mater.* 121 (2016) 471-482.
- [105] S.B. Jagtap, M.S. Mohan, P.G. Shukla, Improved performance of microcapsules with polymer nanocomposite wall: Preparation and characterization, *Polymer* 83 (2016) 27-33.
- [106] J.-F. Su, Y.-Y. Wang, N.-X. Han, P. Yang, S. Han, Experimental investigation and mechanism analysis of novel multi-self-healing behaviors of bitumen using microcapsules containing rejuvenator, *Constr. Build. Mater.* 106 (2016) 317-329.
- [107] D. Sun, J. Hu, X. Zhu, Size optimization and self-healing evaluation of microcapsules in asphalt binder, *Colloid Polymer Science* 293 (2015) 12.

- [108] M. Prajer, X. Wu, S.J. Garcia, S. van der Zwaag, Direct and indirect observation of multiple local healing events in successively loaded fibre reinforced polymer model composites using healing agent-filled compartmented fibres, *Composites Science and Technology* 106 (2015) 7.
- [109] S.D. Mookhoek, H.R. Fischer, S. van der Zwaag, Alginate fibres containing discrete liquid filled vacuoles for controlled delivery of healing agents in fibre reinforced composites, *Composites Part A: Applied Science and Manufacturing* 43(12) (2012) 7.
- [110] A. Tabaković, L. Schuyffel, A. Karač, E. Schlangen, An Evaluation of the Efficiency of Compartmented Alginate Fibres Encapsulating a Rejuvenator as an Asphalt Pavement Healing System, *MDPI Applied Sciences* 7(7) (2017) 16.
- [111] B. Shu, S. Wu, L. Dong, Q. Wang, Q. Liu, Microfluidic synthesis of ca-alginate microcapsules for self-healing of bituminous binder, *Materials* 11(4) (2018) 630.
- [112] B. Shu, S. Wu, L. Dong, J. Norambuena-Contreras, Y. Li, C. Li, X. Yang, Q. Liu, Q. Wang, F. Wang, Self-healing capability of asphalt mixture containing polymeric composite fibers under acid and saline-alkali water solutions, *Journal of Cleaner Production* (2020) 122387.
- [113] T. Al-Mansoori, J. Norambuena-Contreras, R. Micaelo, A. Garcia, Self-healing of asphalt mastic by the action of polymeric capsules containing rejuvenators, *Construction and Building Materials* 161 (2018) 330-339.
- [114] J. Norambuena-Contreras, E. Yalcin, A. Garcia, T. Al-Mansoori, M. Yilmaz, R. Hudson-Griffiths, Effect of mixing and ageing on the mechanical and self-healing properties of asphalt mixtures containing polymeric capsules, *Construction and Building Materials* 175 (2018) 254-266.
- [115] H. Jahanbakhsh, M.M. Karimi, H. Naseri, F.M. Nejad, Sustainable asphalt concrete containing high reclaimed asphalt pavements and recycling agents: performance assessment, cost analysis, and environmental impact, *Journal of Cleaner Production* (2019) 118837.
- [116] E. Brinkman, *Self-Healing materials: concept and applications*, The Hague (2010).



# 3

## DETERMINATION OF PROPER REJUVENATOR TYPE AND AMOUNT FOR THE CAPSULE HEALING SYSTEM

*In asphalt, an effective damage healing event of the capsule healing system is accomplished with the damage repairing (e.g., closing cracks) driven by the flow of bitumen which is rejuvenated with the released healing agent. As such, it is important to choose a proper healing agent that has a remarkable ability to restore the lost properties of bitumen from ageing and improve its intrinsic healing capacity to show a sustainable performance after healing. To this aim, three typical types of bitumen rejuvenator and their rejuvenated bitumen were investigated and compared. Finally, the knowledge of an appropriate healing agent type and amount provides a prerequisite for the development of a capsule healing system. Furthermore, the key findings of this chapter help to understand the performance of the rejuvenated bitumen as such provide more scientific base for both encapsulation technique exploration and healing system design in asphalt pavement.*

### 3.1. INTRODUCTION

Asphalt bitumen ageing takes place during the production, transportation and the long term service life of an asphalt pavement, which leads to a bitumen hardening with time and accelerates the damage process due to the environmental (heat, UV light, cold, ice, snow, rain) and physical effects (vehicle loadings) which result in pavement cracking [1-4]. However, a bitumen rejuvenator can be used to reverse this process by restoring the lost properties of aged bitumen, i.e., chemical composition, physical properties and rheological properties [5-7].

Two theories, compositional harmonic and compatibility, explain the aged bitumen rejuvenation process [8]. **The compositional harmonic theory** believes that bitumen is a colloidal solution with a fixed composition of each constituent, and composition changed from ageing can be restored with the introduction of rejuvenator. Figure 3.1 illustrates the typical changes of the chemical composition of bitumen after ageing and rejuvenation. After ageing, the light fractions (maltenes) of the bitumen is reduced due to oxidation and volatilisation. After rejuvenation, the aged bitumen can almost regain its initial characteristics [9-11].

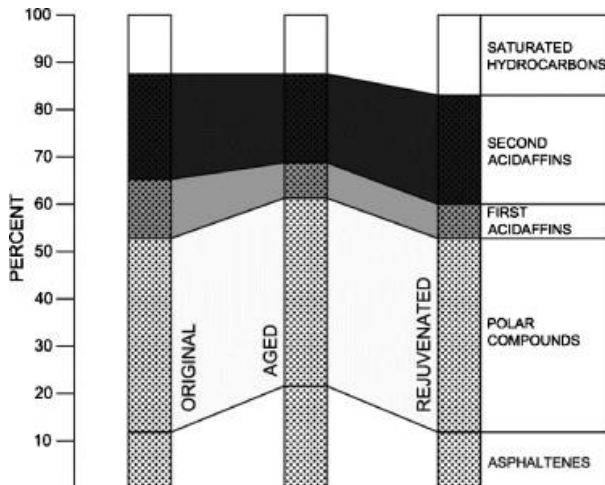


Figure 3.1: Schematic of the typical changes of the chemical composition of a bitumen after ageing and rejuvenation [10].

**The compatibility theory**, assumes that bitumen is a dispersion system, where the asphaltene is homogeneously dispersed in the maltenes, forming a stable system. However, ageing reduces the maltenes content and destroys the stability of the dis-

persion, and the rejuvenator can rebalance the ratio between asphaltene and maltenes so that the dispersion system becomes stable again. Both theories indicate that the use of a rejuvenator replenishes the lost ingredients of the aged bitumen, thus regains its properties to a condition that resembles its virgin state [8].

The type and amount of a rejuvenator have a significant impact on the performance of rejuvenated bitumen [12]. Bitumen with a high penetration level (70/100 or higher) is used in industry to soften the aged bitumen. General rejuvenator types include industrially produced rejuvenator, oily rejuvenator and waster derived rejuvenator, and the recommended dosage ranges from 2% to 20% (by weight of bitumen) which is highly dependent on the rejuvenator type and the characteristics of the aged bitumen (e.g., ageing level) [12-15].

The bitumen rejuvenator can be applied in three ways: i) reclaimed asphalt pavement (RAP), ii) asphalt pavement surface treatment (e.g., fog seal), and iii) embedded rejuvenator encapsulation (e.g., capsules and fibres) [16]. For different rejuvenation purpose, the rejuvenator usage and dosage vary in these applications:

- i. In the application of RAP, a rejuvenation process on old aggregates is always needed before mixing with the fresh material. For such reason, the rejuvenator is usually used to form a low viscosity layer and rejuvenate the aged bitumen of the reclaimed asphalt, and by this means, the recycled asphalt can be reused as part of a new asphalt pavement [9, 17, 18]. The type and amount of rejuvenator need to be properly determined to optimize the performance of pavement with RAP [16, 19]. Although the use of RAP successfully achieves the recycling of aged asphalt, the recycling process involves removal, milling, and crushing of the old pavement, which consumes plenty of resources and energy and may result in a huge delay of traffic [16].
- ii. When an asphalt pavement shows early signs of distress after around 3 to 7 years of service, a fog seal treatment can be employed on the surface layer, thus prevent or delay the damaging process and finally extend the pavement lifespan. The fog seal treatment not only rejuvenates the aged bitumen in the top portion of the surface layer but also seals cracks against intrusion of air and water to prevent serious damages like ravelling [10, 16]. However, the sprayed rejuvenator can penetrate only 5 to 10 mm of a dense surface layer and no more than 20 mm of a porous surface layer, which means the majority depth of asphalt layer cannot be covered. Besides, it is

also reported that some of the fog seal treatment can reduce the skid resistance of an asphalt pavement [20].

- iii. As described in 2.3.2, the rejuvenator can also be encapsulated and embedded in an asphalt pavement (i.e. capsule healing system), thus rejuvenate the aged bitumen and finally heal the damage. Figure 3.2 shows that, with different rejuvenation objectives, the amount of rejuvenator needed for the capsule healing system is much lower than the use in RAP. RAP usually requires the rejuvenated bitumen to behave like the virgin bitumen to mix with new materials. However, the rejuvenation from the capsule healing system works earlier and mainly focuses on accelerating the in-situ crack healing process in asphalt pavement, therefore the rejuvenated bitumen does not need to meet the condition of re-mixing.

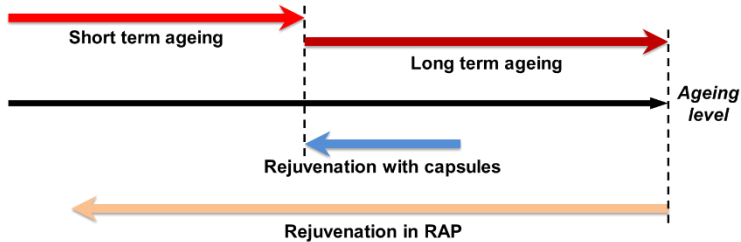


Figure 3.2: The rejuvenation needed in encapsulated rejuvenator and RAP.

In a capsule healing system, it is important to optimise the type and amount of the embedded rejuvenator, since not enough released rejuvenator means insufficient healing and too much released rejuvenator may cause premature failures, i.e., striping and rutting [12, 21]. To this aim, this chapter investigates the effects of various types and dosages of rejuvenators on the physical, rheological and chemical properties of aged bitumen. Figure 3.3 presents the methodology for the study of different rejuvenators. First, laboratory ageing methods including the Rolling Thin-Film Oven (RTFO) and Pressure Aging Vessel (PAV) were employed to prepare bitumen samples with different ageing levels namely origin bitumen (virgin), short-term aged bitumen (after RTFO) and long-term aged bitumen (after RTFO + PAV). Afterwards, the long-term aged bitumen was rejuvenated with different rejuvenator, and the performance of rejuvenated bitumen was evaluated. In some cases, the ageing of rejuvenated bitumen is faster than that of the virgin bitumen [22], therefore the rejuvenated bitumen was exposed to a second long-term ageing process and the properties were investigated. Following this methodology, the rejuvenation effect of

three different types of rejuvenator was studied and ranked, and the recommended type and amount of rejuvenator for the design of a capsule healing system was determined.

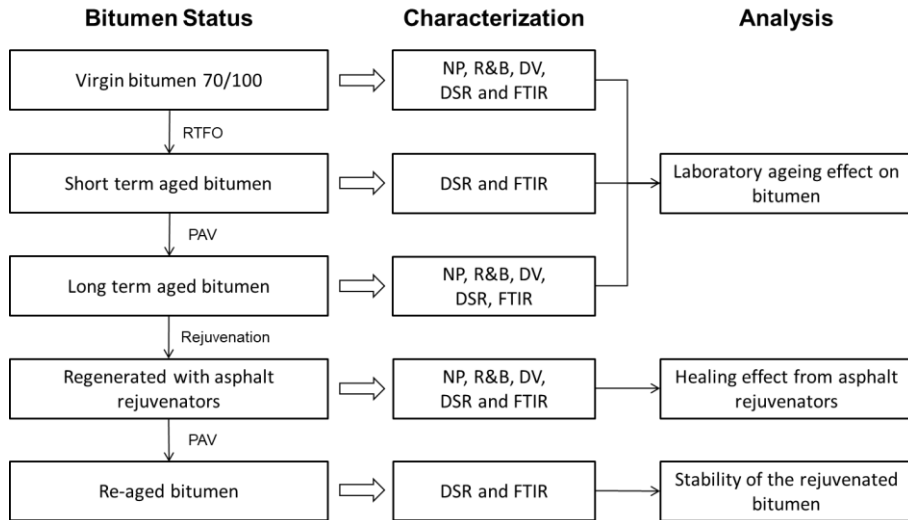


Figure 3.3: Schematic of the research methodology for the rejuvenator study.

### 3.2. MATERIALS AND METHODS

#### 3.2.1. MATERIALS

The bitumen used in this study is the PEN 70/100 bitumen, which is widely applied in the porous asphalt construction in the Netherlands. The specifications and the measured physical properties of the virgin bitumen are shown in Table 3.1.

Table 3.1: Physical properties of the 70/100 bitumen.

Property	Unit	Specification	Measured
Penetration at 25°C	0.1 mm	70-100	73
Softening Point	°C	43-51	48
Dynamic viscosity at 60°C	Pa·S	≥90	-

Figure 3.4 shows the image of the three different rejuvenators, the rejuvenator R20 and rejuvenator B are shown as a black liquid, and the reseed oil presents in a transparent light-yellow liquid. Rejuvenator R20 and rejuvenator B used in this study were provided by Latexfalt B.V., Koudekerk aan den Rijn, the Netherlands.

The rejuvenator R20 is a mix of specific components, which were selected based on specific chemo-physical interactions with the polar functionalities introduced in asphaltene rich domains in an aged multi-phase bitumen system. The rejuvenator R20 is especially suited for high RAP asphalt mixes produced at regular asphalt production temperatures (160°C to 180°C).

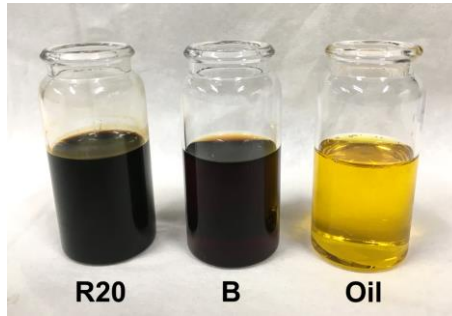


Figure 3.4: Image of three different rejuvenators.

Rejuvenator B is a low viscous liquid rejuvenator, which contains selected components for the re-compatibilization of the various phases in oxidized mastic, also suit for aged polymer modified asphalt and cold rejuvenation. Furthermore, rejuvenator B contains specific components to accelerate the diffusion of the rejuvenating components into aged mastic at ambient temperatures.

The rapeseed oil was purchased from De Smaakspecialist, Ulvenhout, the Netherlands. The major component of the rapeseed oil is unsaturated fat, which includes 27.5% polyunsaturated fat and 65% monounsaturated fat. The measured densities of rejuvenator R20, rejuvenator B and rapeseed Oil are 0.96, 0.93 and 0.90 (g/cm<sup>3</sup>), respectively. In the following description, the three types of rejuvenator, including rejuvenator R20, rejuvenator B and rapeseed oil, are referred as to R, B and O.

### 3.2.2. TEST METHODS

#### 3.2.2.1. BITUMEN AGEING AND REJUVENATION TESTS

Following the European standard EN 12607-1, the Rolling Thin-Film Oven (RTFO) (Figure 3.5 (a)) was employed to simulate the ageing of bitumen during its production process which refers to the short-term ageing process (STA). In the STA test, the virgin bitumen samples were kept in the cylindrical glass bottles designed

for RTFO, and the test was conducted for 75 minutes with the oven temperature maintained at 163°C.

Following the European standard EN 14769, the Pressure Ageing Vessel (PAV) (Figure 3.5 (b)) was employed to simulate the ageing of bitumen after 5 to 10 years in service, which refers to the long-term ageing process (LTA). In the LTA test, the aged bitumen sample from RTFO test was kept a thin oven pan and then heated in the PAV at 100°C under a pressure of 2.1 MPa for 20 hours.

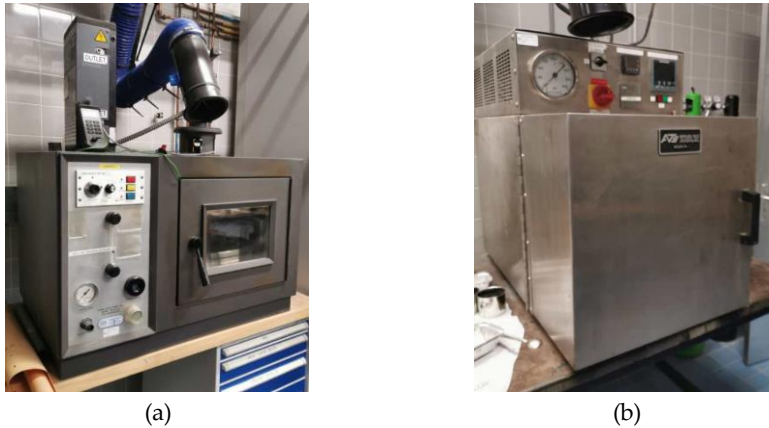


Figure 3.5: The laboratory ageing equipment: (a) RTFO and (b) PAV.

Rejuvenation of long-term aged bitumen is achieved by blending the aged bitumen with rejuvenator, and the rejuvenating procedure is illustrated in Figure 3.6. To this aim, the aged bitumen sample was weighed and contained in an aluminium plate. Then, based on the objective dosage (from 1% to 5% by volume of bitumen where the density of the aged bitumen is assumed to be 1.04 g/cm<sup>3</sup> [23]), the rejuvenator was carefully dropped on the bitumen sample and wetted the surface. Finally, the rejuvenated bitumen was prepared by blending the bitumen and rejuvenator under 140°C for 20 minutes at 300 rpm.

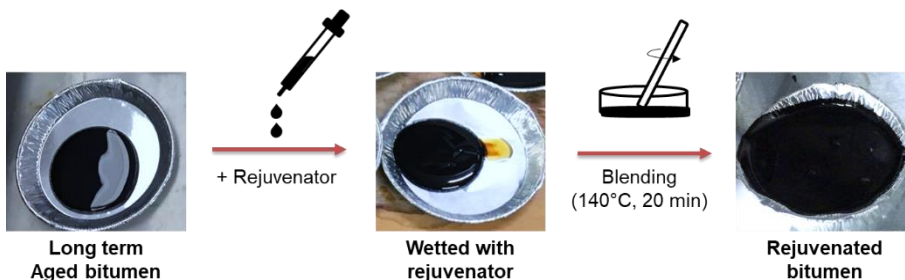


Figure 3.6: The procedure of aged bitumen rejuvenation.

### 3.2.2.2. PHYSICAL PROPERTY TESTS

The physical properties of the bitumen sample were investigated using needle penetration test (NP), ring and ball (R&B) and dynamic viscosity test (DV). Figure 3.7 shows the equipment for physical property tests. The NP and R&B tests (Figure 3.7 (a, b)) were performed following the European standard EN 1426 and EN 1427, respectively. The DV tests were performed with a HAAKE RheoStress 1 viscometer (Figure 3.7 (c)) in Latexfalt B.V., Koudekerk aan den Rijn, the Netherlands, and the viscosity of a bitumen sample was measured every 10°C from 80°C to 160°C, following EN 13302. Except for DV, all the other tests described in this chapter were performed in the laboratory of the pavement engineering section, CEG, TUDelft.

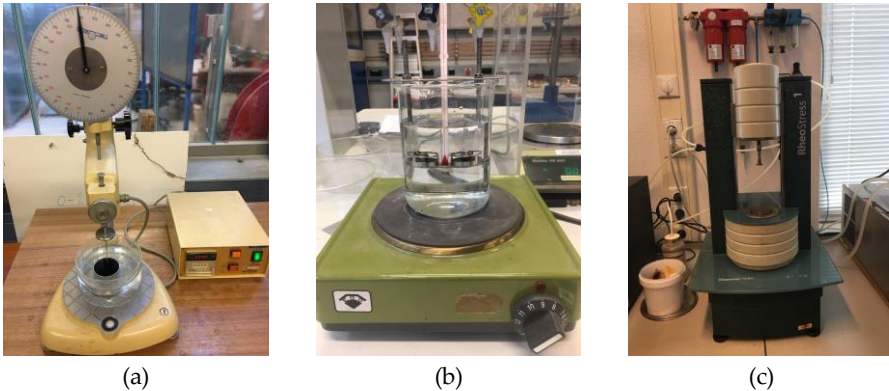


Figure 3.7: The physical property test equipment: (a) penetration test setup, (b) ring and ball test setup and (c) RheoStress viscometer.

### 3.2.2.3. RHEOLOGICAL PROPERTY TEST

Following the European standard EN 14770, The rheological response of the bitumen samples was investigated with a frequency sweep test using a Dynamic Shear Rheometer (DSR) MCR 502 from Anton Paar, Graz, Austria (Figure 3.8).

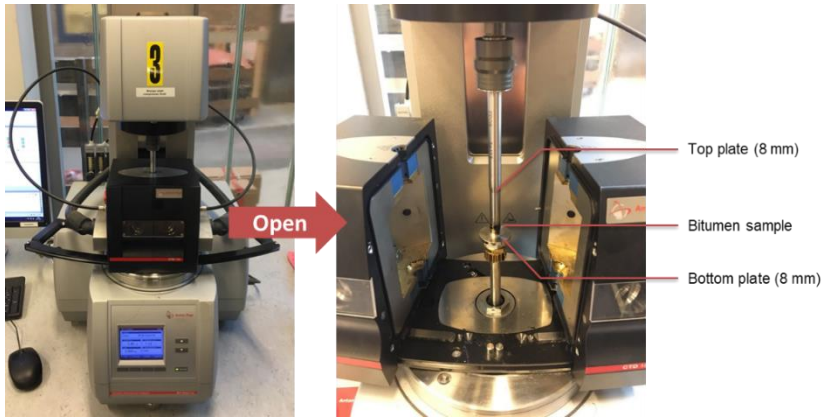


Figure 3.8: The Dynamic Shear Rheometer MCR 502 and the bitumen sample sandwiched between 8 mm parallel plates.

The frequency sweep tests were carried out at five different temperatures: 0, 10, 20, 30 and 40°C, using a range of loading frequency from (0.01 Hz to 50 Hz). The tests were performed with 8 mm parallel plates, and the bitumen sample has a thickness of 2 mm. Based on the time-temperature superposition principle, the curves of complex modulus ( $G^*$ ) and phase angle ( $\delta$ ) at different test temperatures can be obtained, by shifting with Williams–Landel–Ferry equation (3.1), fitting with Symmetrical Sigmoidal equation (3.2) and error minimizing with equation (3.3).

$$\log \alpha_T (T) = \frac{-C_1(T - T_0)}{[C_2 + (T - T_0)]} \tag{3.1}$$

Where:

- $\alpha_T$  is the superposition parameter;
- $T$  is the temperature (°C);
- $T_0$  is the reference temperature (°C);
- $C_1, C_2$  are empirical constants;

$$\log|G^*|_{fit} = \log|G^*|_{min} + \frac{\log|G^*|_{max} - \log|G^*|_{min}}{1 + e^{\beta + \gamma(\log f + \log \alpha_T)}} \tag{3.2}$$

Where:

- $G^*$  is the tested complex modulus (Pa);
- $f$  is the loading frequency (Hz);
- $\beta, \gamma$  are the shifting parameters;
- $\alpha_T$  is the superposition parameter;
- $|G^*|_{max}$  is the assumed maximum complex modulus (Pa);

$|G^*|_{min}$  is the assumed minimum complex modulus (Pa);  
 $|G^*|_{fit}$  is the fitted complex modulus (Pa);

$$\sum_{n=1}^N error = \sum_{n=1}^{\infty} \left( \frac{\log|G^*|_{test} - \log|G^*|_{fit}}{\log|G^*|_{test}} \right)^2 \quad (3.3)$$

Where:

$|G^*|_{test}$  is the tested complex modulus (Pa);  
 $|G^*|_{fit}$  is the fitted complex modulus (Pa);  
 $error$  is the fitting error.

The rutting parameter ( $G^*/\sin\delta$ ) and fatigue parameter ( $G^* \cdot \sin\delta$ ) were deduced from the master curve at 10 rad/s, in which the rutting parameter reflects the irrecoverable deformation of bitumen, and the fatigue parameter represents the loss modulus of the bitumen, therefore they were used to evaluate the rutting resistance and fatigue resistance of the bitumen samples. Besides, the cracking resistance of the bitumen sample was characterized using the black space diagram. In this study, the black space diagram was divided into different crack-sensitive zones based on Glover-Rowe (G-R) parameters (3.4) and R-values (3.5), and the results from master curves were plotted at the frequency of 0.005 rad/s, 15°C [24].

$$GR = \frac{G^* \cdot \cos^2\delta}{\sin\delta} \quad (3.4)$$

Where:

$GR$  is the G-R parameter, which is 180 and 450 in this study;  
 $G^*$  is the complex modulus (kPa);  
 $\delta$  is the phase angle (°).

$$R = \frac{(\log 2) \cdot \log \frac{G^*}{G_g}}{\log \left( 1 - \frac{\delta}{90} \right)} \quad (3.5)$$

Where:

$R$  is the R-value, which is 1, 2, and 3 in this study;  
 $G^*$  is the complex modulus (kPa);  
 $G_g$  is the glassy modulus, assumed to be  $10^9$  (Pa);  
 $\delta$  is the phase angle (°).

### 3.2.2.4. CHEMICAL PROPERTY TEST

Fourier-transform infrared spectroscopy (FTIR) was employed in order to study the change in the bitumen chemical composition caused by the bitumen ageing [25]. The FTIR test was performed using the Spectrum 100 FT-IR spectrometer with Attenuated Total Reflectance (ATR) from PerkinElmer, United States (Figure 3.9), and each bitumen sample was scanned 20 times, at the wavenumbers from 600 to 4000  $\text{cm}^{-1}$  with a resolution of 2  $\text{cm}^{-1}$ .



Figure 3.9: The Spectrum 100 FT-IR spectrometer.

After ageing, the infrared spectra of bitumen may show changes in peak areas at 1030  $\text{cm}^{-1}$  and 1700  $\text{cm}^{-1}$ , which is due to the accumulation of oxidation products during the ageing process, namely carbonyls and sulfoxides [26]. For this reason, the carbonyl index ( $I_c$ ), the sulfoxide index ( $I_s$ ), and the combined ageing index ( $I_c + I_s$ ) are usually used to quantify the ageing level in a bitumen [27], which can be calculated based on the reference area ( $\Sigma A$ ) with the following equations:

$$I_c = \frac{A_{1700}}{\Sigma A} \quad (3.6)$$

$$I_s = \frac{A_{1030}}{\Sigma A} \quad (3.7)$$

$$\Sigma A = A_{(2953,2862)} + A_{1700} + A_{1600} + A_{1460} + A_{1376} + A_{1030} + A_{864} + A_{814} + A_{743} + A_{724} \quad (3.8)$$

Following the experience of Lamontagne et al [25], Zaumanis et al [28] and Jing [29], the reference area ( $\Sigma A$ ) used in this study is derived based on the bitumen characteristics and presented as the highlighted area in Figure 3.10. It is noted that the

carbonyl band is selected between  $1670\text{ cm}^{-1}$  and  $1722\text{ cm}^{-1}$ , to exclude the characteristic peak of the rejuvenator ( $1743\text{ cm}^{-1}$ ) [28]. Besides, the sulfoxide band is selected between  $995\text{ cm}^{-1}$  and  $1047\text{ cm}^{-1}$ .

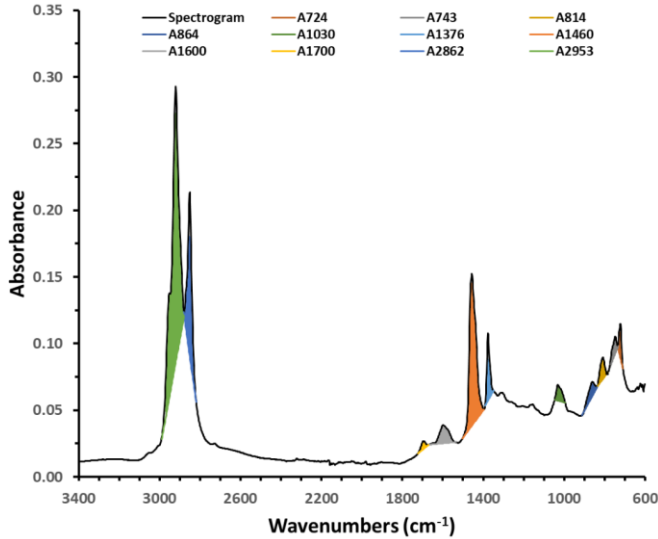


Figure 3.10: The reference areas of FTIR spectrogram.

### 3.3. RESULTS AND DISCUSSION

#### 3.3.1. PHYSICAL PROPERTIES

##### 3.3.1.1. PHYSICAL PROPERTIES OF THE AGED BITUMEN

For the engineering purpose, bitumen is graded based on its penetration level which is described in European standard EN 12591. Table 3.2 shows the bitumen specifications for grades from 20 (0.1 mm) to 100 (0.1 mm) penetration according to EN 12591. In general, ageing leads to a change in bitumen physical properties, e.g., penetration, softening point and viscosity, which results in a decreased grade level, thus the ageing level can be evaluated by referring the bitumen grade to its original (virgin) state.

Table 3.2: The bitumen grade specifications from EN 12591.

Property	Unit	20/30	30/45	35/50	40/60	50/70	70/100
Penetration at 25°C	0.1 mm	20-30	30-45	35-50	40-60	50-70	70-100
Softening Point	°C	55-63	52-60	50-58	48-56	46-54	43-51

The physical properties of the virgin bitumen and the results after the short-term and long-term ageing process are presented in Figure 3.11. Figure 3.11 (a) shows that, after the short-term ageing (STA) process, the penetration and softening point of the PEN 70/100 bitumen were changed from 73 (0.1 mm) and 48°C to 51 (0.1 mm) and 55°C, which indicates a change of bitumen grade to 40/60. While the penetration and softening point of the long-term aged bitumen (LTA) reached 24 and 62, which refers to the PEN 20/30 bitumen. Figure 3.11 (b) shows that the viscosity of the bitumen is increased after ageing, and the bitumen viscosity after LTA is higher than that after STA.

The objective of the rejuvenation effect with a capsule healing system is to improve the intrinsic healing capacity of the aged bitumen without causing premature damages, and as such, the released rejuvenator from capsules should not change the bitumen to a grade lower than its grade after paving. Hence, the STA bitumen grade (40/60) was set as the limit of the rejuvenated bitumen, which was applied in the rejuvenator dosage determination for a capsule healing system.

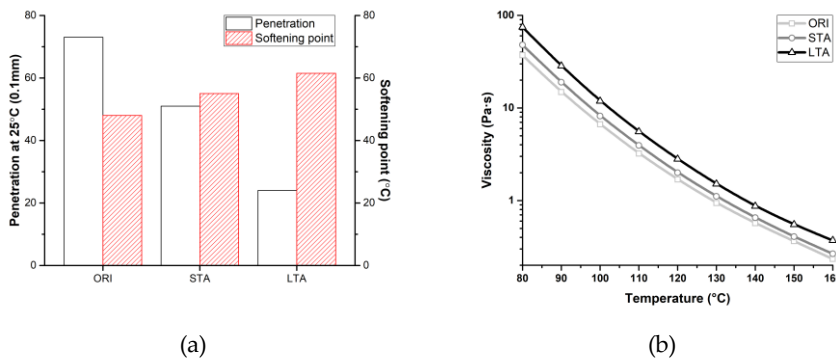


Figure 3.11: Physical properties of the 70/100 bitumen at different ageing levels: (a) Penetration and softening point and (b) dynamic viscosity.

### 3.3.1.2. PHYSICAL PROPERTIES OF THE REJUVENATED BITUMEN

Figure 3.12 shows the penetration, softening point and dynamic viscosity of the long-term aged bitumen rejuvenated with R, B and O (refers to LA\_R, LA\_B and LA\_O), with dosages from 1% to 5% (by volume of bitumen). It is found that rejuvenation of an aged bitumen leads to an increase in penetration (Figure 3.12 (a)) and a decrease in softening point (Figure 3.12 (b)), and this change becomes more significant when a higher dosage of rejuvenator is applied. Among the three types of rejuvenator, O shows the greatest changes in both penetration and softening point, which indicates the highest rejuvenation efficiency, then followed by B and R. Figure 3.12 (c) shows that, when LTA are rejuvenated with 5% of R, B and O (refers to LA\_R5, LA\_B5 and LA\_O5), the dynamic viscosity decreases from LA\_R5, LA\_B5 to LA\_O5, and this agrees with the findings from NP and R&B.

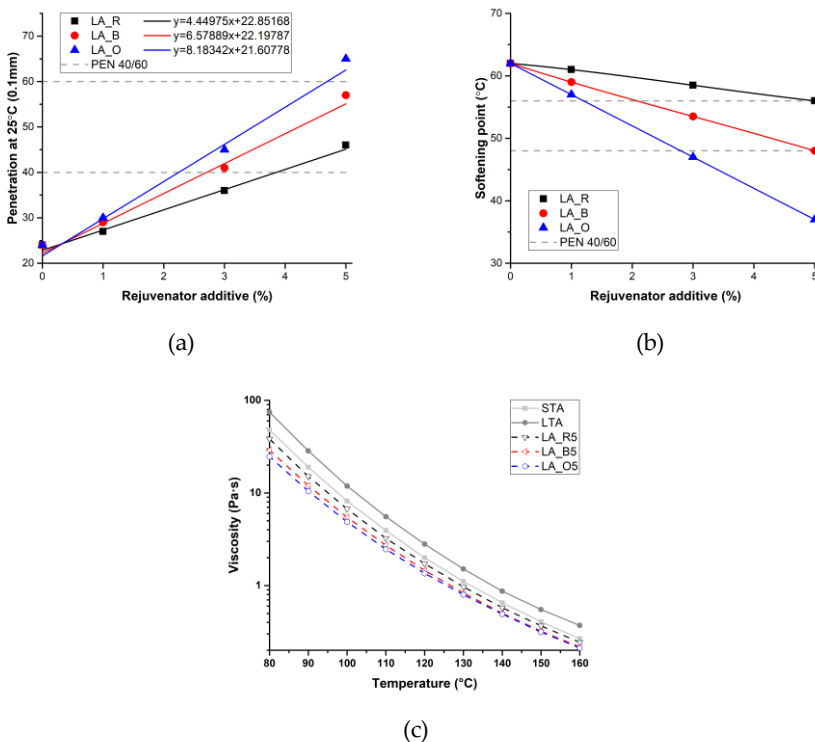


Figure 3.12: The physical properties of the rejuvenated bitumen: (a) penetration, (b) softening point and (c) dynamic viscosity.

Based on the NP and R&B results, the optimum amount of R, B and O can be determined for the application in capsule healing system. The dash-lines in Figure 3.12 (a) and (b) indicate the values for PEN 40/60 bitumen which refers to the objective grade for the rejuvenated bitumen. When the penetration values reach 40 (0.1 mm), the optimum amount of R, B and O are determined following the trend of penetration values with rejuvenator dosages, which are 3.9%, 2.7% and 2.2%, respectively. However, the softening point of the aged bitumen blended with 3.9% R is beyond the upper limit of PEN 40/60, which indicates a better resistance to the temperature changes.

### 3.3.2. RHEOLOGICAL PROPERTIES

#### 3.3.2.1. THE MASTER CURVES OF COMPLEX MODULUS AND PHASE ANGLE

Figure 3.13 shows the master curves of complex modulus and phase angle of the 70/100 bitumen at different ageing levels. Compared to the virgin 70/100 bitumen, STA showed higher complex modulus and lower phase angle, while the LTA showed more significant changes in complex modulus and phase angle.

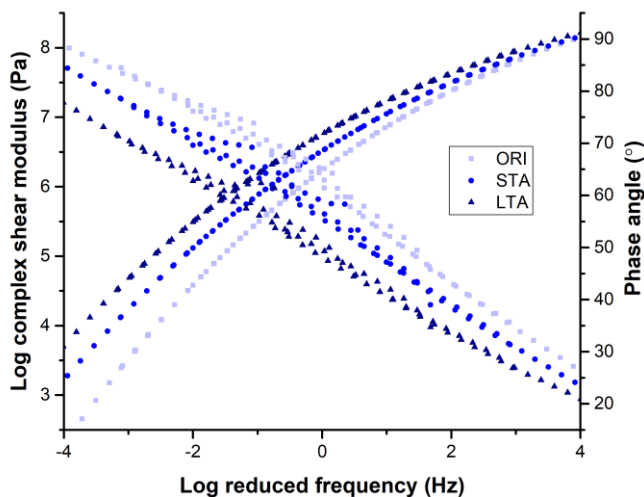


Figure 3.13: Master curves of the 70/100 bitumen at different ageing levels.

Figure 3.14 shows the master curves of the bitumen samples, namely LA\_R3, LA\_B3 and LA\_O3 (with 3% R, B and O, respectively), and their status after re-ageing, namely RA\_R3, RA\_B3 and RA\_O3. The complex modulus and phase angle of

LTA is also plotted as a reference. The complex modulus of LA\_R3 is much higher than LA\_O3, which indicates that the complex modulus of the aged bitumen can be reduced more significantly when blended with O than R. The complex modulus master curve of LA\_B3 generally locates between the curves of LA\_R3 and LA\_O3, which overlaps with LA\_R3 in the low-frequency region and LA\_O3 in high-frequency region, therefore B has an intermediate complex modulus reducing effect. The phase angle of the rejuvenated bitumen samples decreases from LA\_R3, LA\_B3 to LA\_O3, which indicates that the rejuvenator's ability to restore the phase angle decreases from R, B and O.

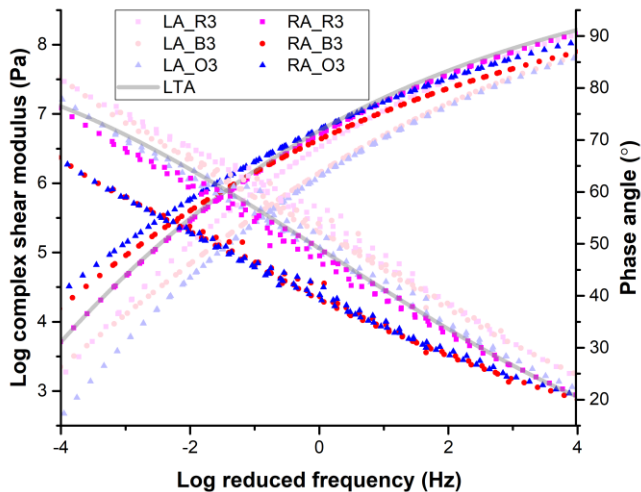


Figure 3.14: Master curves of the rejuvenated bitumen samples and their status after re-aging.

The rejuvenated bitumen becomes brittle after the re-aging process, which can be observed in Figure 3.14 where the complex modulus grows higher and phase angle becomes lower. The LTA samples rejuvenated with B and O all showed significant changes in both complex modulus and phase angle, and their changing amplitude is much greater than those rejuvenated with R. Hence, aged bitumen rejuvenated with R is more difficult to lose its restored properties, thus a more stable behaviour. Figure 3.15 presents the dosage study for R. After rejuvenated with 4% R, both complex modulus and phase angle of LTA can be restored to the level of STA, which means the optimum dosage of R should be around 4%, and this agrees with the optimum dosage obtained from NP tests.

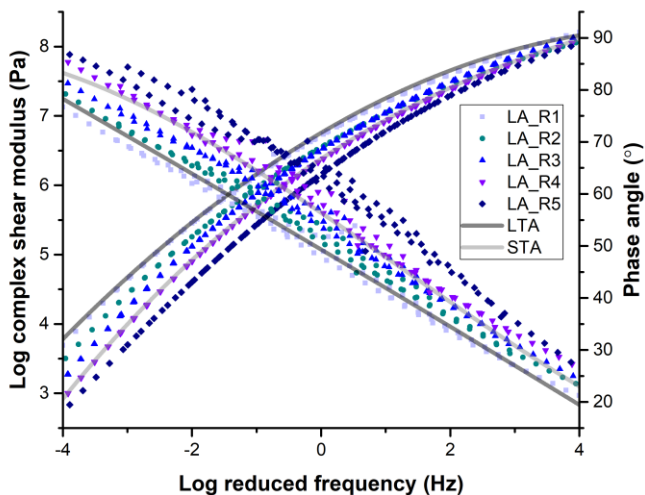


Figure 3.15: Master curves of the bitumen samples rejuvenated with R at a dosage range from 1% to 5%.

### 3.3.2.2. RUTTING AND FATIGUE RESISTANCE

Figure 3.16 shows the rutting parameter and fatigue parameter of the rejuvenated bitumen samples at 20°C and their status after re-ageing, and the results of STA are plotted with dash-lines as references. As shown in Figure 3.16 (a), for the rejuvenated bitumen, the bitumen sample blended with 3% R showed a higher rutting parameter which might be due to LA\_R3 had the highest complex modulus (see Figure 3.14). After re-ageing, all these rejuvenated bitumen samples showed improved rutting resistances, and RA\_O3 became even higher than RA\_R3 as a result of significantly increased modulus for O rejuvenated bitumen.

Figure 3.16 (b) shows that the fatigue parameter for LA\_R3 is much higher than LA\_B3 and LA\_O3, which indicates a lower fatigue resistance. However, the difference of fatigue parameters for three different bitumen samples becomes much lower after re-ageing, which indicates the fatigue resistance of the R rejuvenated bitumen decreases much slower in the ageing process. Besides, the fatigue parameters for all the bitumen samples are below 5 MPa which satisfies the limit of PAV aged bitumen determined in SHRP.

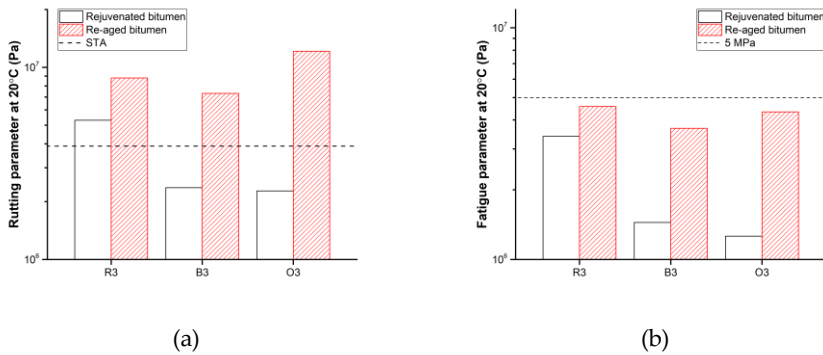


Figure 3.16: The rutting parameter and fatigue parameter for the rejuvenated bitumen and re-aged bitumen.

### 3.3.2.3. BLACK SPACE DIAGRAM

In the black space diagram, a range of G-R values between 180 kPa and 450 kPa can be used to predict the onset and propagation of damage which refers to the damage zone, and the area below is regarded as no block cracking zone [24, 30]. R-values can further divide the black space diagram into different crack-sensitive regions where a higher R-value indicates the greater cracking potential [24].

Figure 3.17 shows the black space diagram of the bitumen samples based on the cracking prediction with G-R parameters and R-values. In general, ageing made the bitumen brittle, which results in a change in black space diagram that drives the data of a bitumen sample moves to the upper left, therefore a higher cracking potential, and this can be found in the development from ORI to LTA. All the tested bitumen samples are located below the damage zone within the region between  $R=1$  and  $R=3$ , which indicates no significant block cracking is expected for these bitumen samples. However, LA\_R3 is in the region between  $R=1$  and  $R=2$ , as such less cracking potential than LA\_B3 and LA\_O3. Furthermore, the bitumen samples blended with B and O showed more significant changes after re-ageing than samples blended with R. Hence, R can better improve the cracking resistance of the aged bitumen, especially after another long-term ageing process.

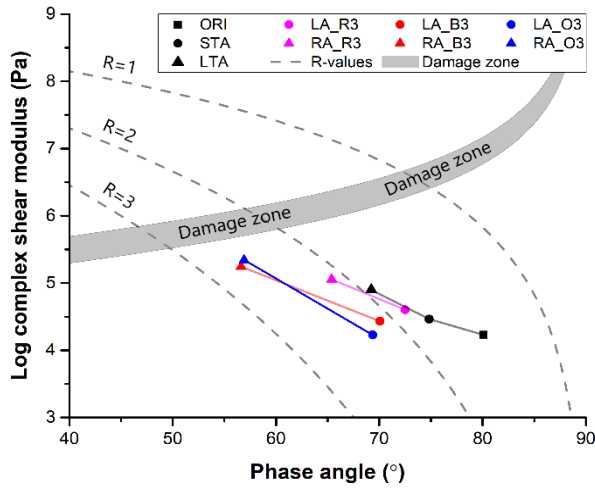


Figure 3.17: The black space diagram at 15°C and 0.005 rad/s divided with R-values.

### 3.3.3. CHEMICAL PROPERTIES

#### 3.3.3.1. CHEMICAL COMPOSITION OF THE AGED BITUMEN AND DIFFERENT REJUVENATORS

Figure 3.18 shows the FTIR spectrogram and the ageing indices of 70/100 bitumen at different ageing levels. Figure 3.18 (a) shows that increased peak area at 1030  $\text{cm}^{-1}$  and 1700  $\text{cm}^{-1}$  are found on STA compared to ORI, which indicates an increased number of carbonyl groups and sulfoxide groups as a result of oxidation, and the changes become more significant for LTA. Figure 3.18 (b) presents the ageing indices of ORI, STA and LTA.

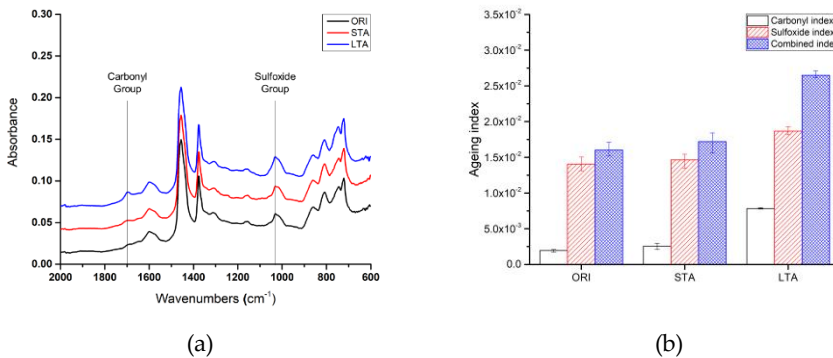


Figure 3.18: FTIR spectrogram of 70/100 bitumen at different ageing levels.

Figure 3.19 shows the chemical composition of three different types of rejuvenator characterized using FTIR. A significant absorbance peak at  $1743\text{ cm}^{-1}$  is found in the spectra for all three types of rejuvenator which is regarded as the characteristic peak for rejuvenator. In the spectrum of rapeseed oil, the absorbance bands at  $1660\text{ cm}^{-1}$  and  $3010\text{ cm}^{-1}$  are due to the alkenyl C=C stretch and the relative C-H stretch from the rich unsaturated fat content [12, 14]. Rejuvenator B shows a similar spectrum to rapeseed oil, and the presence of unsaturated groups can also be detected with the absorbance bands at  $1660\text{ cm}^{-1}$  and  $3010\text{ cm}^{-1}$ . The rejuvenator R20 shows absorbance bands at  $1600\text{ cm}^{-1}$  which might be due to the aromatic C=C bending vibrations from the polar functionalities. Besides, it is also indicated that the chemical composition of rejuvenator R20 very different from rejuvenator B and Oil.

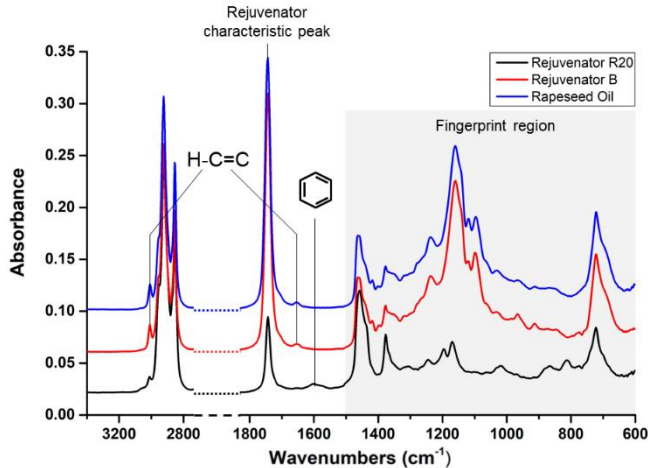


Figure 3.19: The FTIR spectrogram of the three different types of rejuvenator.

### 3.3.3.2. CHEMICAL COMPOSITION OF THE REJUVENATED BITUMEN

The FTIR spectrogram and the combined ageing index of the rejuvenated and the re-aged bitumen samples are shown in Figure 3.20. Figure 3.20 (a) shows the FTIR spectrogram of bitumen samples rejuvenated with R, B and O with the dosages from 1% to 3%. Incorporating a rejuvenator in LTA results in a growth of the absorbance bands at  $1743\text{ cm}^{-1}$ , which is the evidence for the presence of R, B or O. Figure 3.20 (b) shows that LA\_R3 and LA\_B3 have no significant change nor development of new absorbance bands after re-ageing. However, the rejuvenator characteristic

peak of LA\_O3 is largely decreased after re-ageing which might be due to the emissions contained C=O (e.g., aldehydes, ketones) formed from the rapeseed oil degradation [31], thus a less fat content and weaker absorption at the characteristic peak of O ( $1743\text{ cm}^{-1}$ ). Figure 3.20 (c) shows the combined healing index of the rejuvenated and the re-aged bitumen which indicates that, although LA\_R3 shows the highest ageing index, it becomes the lowest after re-ageing, thus a more stable behaviour than LA\_B3 and LA\_O3.

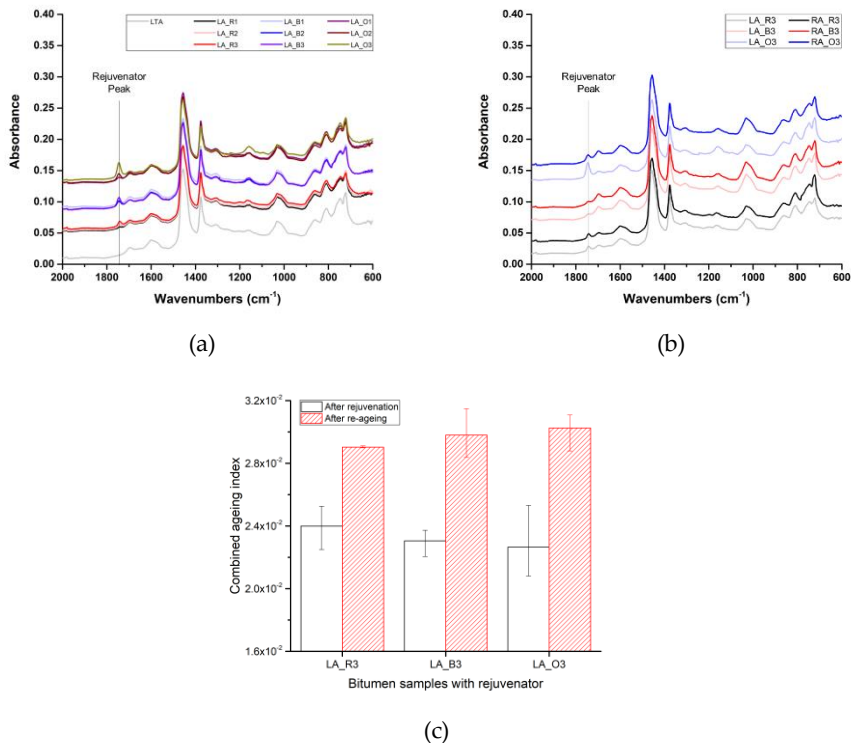


Figure 3.20: The FTIR results of the rejuvenated and the re-aged bitumen samples: (a) the spectrogram of the rejuvenated bitumen, (b) the spectrogram of the re-aged bitumen and (c) their combined ageing index.

### 3.4. CONCLUSIONS

Aimed to optimize the design of a capsule healing system with a proper rejuvenator type and dosage, three different bitumen rejuvenators and their rejuvenated bitumen were evaluated based on the physical properties, the rheological properties and the chemical properties, and the following conclusions can be drawn:

- The laboratory short-term and long-term ageing processes significantly changed the physical, rheological, and chemical properties of the virgin bitumen, namely from the bitumen grade 70/100 to 40/60 with STA, and then to 20/30 with LTA.
- All three types of rejuvenator tested are able to restore the physical properties of the aged bitumen, namely improve the penetration and reduce the softening point and viscosity. However, their efficiency to restore the bitumen physical properties decreases from O, B to R. A similar trend is also found in complex modulus. Finally, based on the penetration values, the optimum dosages for R, B and O are obtained, which are 3.9%, 2.7% and 2.2%, respectively.
- The three types of rejuvenator show different capacity to restore the phase angle of the LTA which decreases from R, B to O, and the phase angle of LTA can be restored to the level of STA with around 4% R. Besides, based on the results from rutting parameter and black space diagram, the rutting and cracking resistance of different types of rejuvenator decreases from R, B to O. Although R rejuvenated bitumen shows lower fatigue resistance, its fatigue resistance is more stable during the ageing process than those rejuvenated with B and O.
- The DSR and FTIR results on re-aged bitumen indicate that the bitumen samples rejuvenated with R showed less change in both rheological properties and chemical properties than those with B and O, thus a more stable behaviour in the long-term service.

Based on these findings, O is determined as the most efficient rejuvenator which can soften the aged bitumen to a required level with the least amount of rejuvenator. R is determined as the best performing rejuvenator since its rejuvenated bitumen showed the best rutting and cracking resistance, and the restored properties are more stable in the next ageing period. Compared with O and R, B showed an intermediate rejuvenation effect, in both efficiency and performance. Nevertheless, as an in-situ damage healing method, the capsule healing system requires the rejuvenated bitumen to work in a more sustainable way, thus the lifespan of a pavement can be extended more significantly. As such, R is determined as the most suitable type of rejuvenator for the capsule healing system and the recommended amount is 3.9% (by volume of bitumen). It is noticed that the preferred rejuvenator type and amount are proposed based on the volume of rejuvenator needed for the

rejuvenation of long-term aged bitumen in the well-blended condition, and these parameters can be altered for the optimization of a specific capsule healing system when more factors need to be considered, such as encapsulation possibility, capsule properties, asphalt mixture behaviours, etc.

## REFERENCES

- [1] H. Zhang, J. Yu, Z. Feng, L. Xue, S. Wu, Effect of aging on the morphology of bitumen by atomic force microscopy, *Journal of Microscopy* 246(1) (2012) 11-19.
- [2] R. Jing, X. Liu, A. Varveri, A. Scarpas, S. Erkens, The effect of ageing on chemical and mechanical properties of asphalt mortar, *Applied Sciences* 8(11) (2018) 2231.
- [3] Y. Zhang, Z. Leng, Quantification of bituminous mortar ageing and its application in ravelling evaluation of porous asphalt wearing courses, *Materials & Design* 119 (2017) 1-11.
- [4] Y. Tong, R. Luo, R.L. Lytton, Moisture and aging damage evaluation of asphalt mixtures using the repeated direct tensional test method, *International Journal of Pavement Engineering* 16(5) (2015) 397-410.
- [5] T. Ma, X. Huang, Y. Zhao, Y. Zhang, Evaluation of the diffusion and distribution of the rejuvenator for hot asphalt recycling, *Construction and Building Materials* 98 (2015) 530-536.
- [6] D. Kuang, J. Yu, H. Chen, Z. Feng, R. Li, H. Yang, Effect of rejuvenators on performance and microstructure of aged asphalt, *Journal of Wuhan University of Technology-Mater. Sci. Ed.* 29(2) (2014) 341-345.
- [7] S. Nahar, Phase-separation characteristics of bitumen and their relation to damage-healing, (2016).
- [8] D. Kuang, W. Liu, Y. Xiao, M. Wan, L. Yang, H. Chen, Study on the rejuvenating mechanism in aged asphalt binder with mono-component modified rejuvenators, *Construction and Building Materials* 223 (2019) 986-993.
- [9] H.M. Silva, J.R. Oliveira, C.M. Jesus, Are totally recycled hot mix asphalts a sustainable alternative for road paving?, *Resources, Conservation and Recycling* 60 (2012) 38-48.

- [10] J. Brownridge, The role of an asphalt rejuvenator in pavement preservation: use and need for asphalt rejuvenation, *Compendium of papers from the first international conference on pavement preservation, 2010*, pp. 351-364.
- [11] I. Androjić, Ageing of hot mix asphalt, *Građevinar* 68(06.) (2016) 477-483.
- [12] A. Behnood, Application of rejuvenators to improve the rheological and mechanical properties of asphalt binders and mixtures: A review, *Journal of cleaner production* (2019).
- [13] Z. Sun, J. Yi, Y. Huang, D. Feng, C. Guo, Properties of asphalt binder modified by bio-oil derived from waste cooking oil, *Construction and Building Materials* 102 (2016) 496-504.
- [14] M. Chen, F. Xiao, B. Putman, B. Leng, S. Wu, High temperature properties of rejuvenating recovered binder with rejuvenator, waste cooking and cotton seed oils, *Construction and Building Materials* 59 (2014) 10-16.
- [15] R. Romera, A. Santamaría, J.J. Peña, M.E. Muñoz, M. Barral, E. García, V. Jañez, Rheological aspects of the rejuvenation of aged bitumen, *Rheologica acta* 45(4) (2006) 474-478.
- [16] T.B. Moghaddam, H. Baaj, The use of rejuvenating agents in production of recycled hot mix asphalt: A systematic review, *Construction and Building Materials* 114 (2016) 805-816.
- [17] J. Qiu, M. Huurman, B. de Bruin, E. Demmink, M. Frunt, Towards 90% warm re-use of porous asphalt using foaming technology, *Journal of Cleaner Production* 190 (2018) 251-260.
- [18] I.L. Al-Qadi, M. Elseifi, S.H. Carpenter, Reclaimed asphalt pavement—a literature review, 2007.
- [19] O. Reyes-Ortiz, E. Berardinelli, A.E. Alvarez, J. Carvajal-Muñoz, L. Fuentes, Evaluation of hot mix asphalt mixtures with replacement of aggregates by reclaimed asphalt pavement (RAP) material, *Procedia-Social and Behavioral Sciences* 53 (2012) 379-388.
- [20] Á. García, E. Schlangen, M. van de Ven, G. Sierra-Beltrán, Preparation of capsules containing rejuvenators for their use in asphalt concrete, *Journal of hazardous materials* 184(1-3) (2010) 603-611.

- [21] M. Zaumanis, R.B. Mallick, R. Frank, Evaluation of rejuvenator's effectiveness with conventional mix testing for 100% reclaimed Asphalt pavement mixtures, *Transportation research record* 2370(1) (2013) 17-25.
- [22] A. Ongel, M. Hugener, Impact of rejuvenators on aging properties of bitumen, *Construction and Building Materials* 94 (2015) 467-474.
- [23] D. Lesueur, The colloidal structure of bitumen: Consequences on the rheology and on the mechanisms of bitumen modification, *Advances in colloid and interface science* 145(1-2) (2009) 42-82.
- [24] G. King, M. Anderson, D. Hanson, P. Blankenship, Using black space diagrams to predict age-induced cracking, 7th RILEM international conference on cracking in pavements, Springer, 2012, pp. 453-463.
- [25] J. Lamontagne, P. Dumas, V. Mouillet, J. Kister, Comparison by Fourier transform infrared (FTIR) spectroscopy of different ageing techniques: application to road bitumens, *Fuel* 80(4) (2001) 483-488.
- [26] C. Xing, L. Liu, Y. Cui, D. Ding, Analysis of base bitumen chemical composition and aging behaviors via atomic force microscopy-based infrared spectroscopy, *Fuel* 264 (2020) 116845.
- [27] X. Lu, U. Isacson, Effect of ageing on bitumen chemistry and rheology, *Construction and Building materials* 16(1) (2002) 15-22.
- [28] M. Zaumanis, M.C. Cavalli, L.D. Poulidakos, Comparing Different Rejuvenator Addition Locations in Asphalt Plant Based on Mechanical and Chemical Properties of Binder, 2018.
- [29] R. Jing, Ageing of bituminous materials: Experimental and numerical characterization, Delft University of Technology, 2019.
- [30] G. Rowe, G. King, M. Anderson, The influence of binder rheology on the cracking of asphalt mixes in airport and highway projects, *Journal of Testing and Evaluation* 42(5) (2014) 1063-1072.
- [31] H.R. Katragadda, A. Fullana, S. Sidhu, Á.A. Carbonell-Barrachina, Emissions of volatile aldehydes from heated cooking oils, *Food Chemistry* 120(1) (2010) 59-65.



# 4

## PREPARATION AND OPTIMIZATION OF THE CALCIUM ALGINATE CAPSULES

*Developing a capsule healing system in an asphalt pavement largely relies on the innovation of encapsulation technology. On the premise that the capsules are able to survive the asphalt production and compaction process, optimization of the capsules helps to improve the effectiveness and efficiency of the capsule healing system. This chapter presents the development of the calcium alginate capsules by introducing the preparation process of the capsules and how alginate/rejuvenator (A/R) ratio was adjusted to achieve the optimum capsule behaviour.*

## 4.1. INTRODUCTION

This chapter describes the development of calcium alginate capsule encapsulating rejuvenator. The capsule design was optimized to achieve an appropriate capsule behaviour and efficiency for the application in self-healing asphalt. Based on the alginate encapsulation mechanism, the calcium alginate capsules encapsulating rejuvenator were prepared with varying A/R ratios. The morphology and microstructure of the capsules were characterized using LM and ESEM, respectively. In order to determine the optimum A/R ratio for the calcium alginate capsules, the thermal stability and mechanical property were studied using thermogravimetric analysis (TGA) and micro compressive test. After that, XCT was employed to study the structure and volumetric composition of the calcium alginate capsule with the optimum A/R ratio.

The healing efficiency of the calcium alginate capsules prepared with the optimized A/R ratio was evaluated in asphalt mastic and porous asphalt mortar in Chapter 5, and this calcium alginate capsules healing system was further verified in porous asphalt concrete in Chapter 6.

## 4.2. MATERIALS AND METHODS

### 4.2.1. PREPARATION OF CALCIUM ALGINATE CAPSULES

#### 4.2.1.1. MATERIALS

Sodium alginate was used to provide alginate strands and  $\text{CaCl}_2 \cdot 6\text{H}_2\text{O}$  was used to provide doubly charged ions ( $\text{Ca}^{2+}$ ) in water solution. The encapsulated asphalt rejuvenator R20 is an industrially produced asphalt rejuvenator introduced in Chapter 3. Besides, the poly(ethylene-alt-maleic-anhydride) (PEMA) was used in the blend helped to stabilize the emulsion by creating a phase separated polymer film over the rejuvenator beads [1, 2]. Figure 4.1 shows the chemical structure of PEMA and the schemes of rejuvenator encapsulated by the calcium alginate cross-links in a calcium alginate capsule are shown in Figure 4.2. The chemicals used in the capsule preparation process were supplied from Sigma Aldrich, St. Louis, MO, USA.

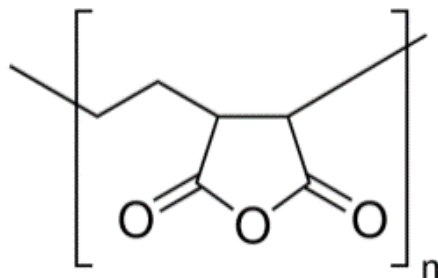


Figure 4.1: The chemical structures of PEMA.

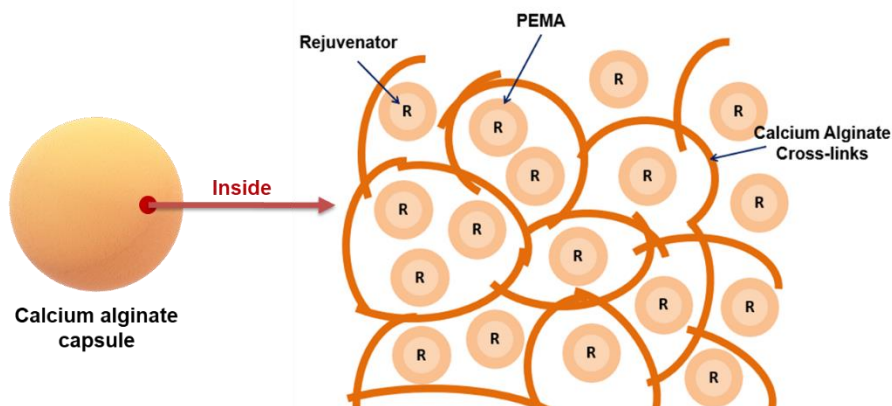


Figure 4.2: Schemes of rejuvenator encapsulated by the calcium alginate crosslinks inside of a capsule.

#### 4.2.1.2. PREPARATION PROCESS

The calcium alginate capsules were produced from an emulsion of rejuvenator suspended solution of sodium alginate. To this aim, 6 wt.% sodium alginate in de-ionized was prepared. At the same time, a 2.5 wt.% solution of PEMA was mixed with the rejuvenator with a ratio of 40% PEMA and 60% rejuvenator, forming a healing agent solution. Then the sodium alginate and rejuvenator solutions, based on seven A/R ratios: 100/0, 60/40, 50/50, 40/60, 30/70, 20/80 and 10/90, were mixed. Each solution was stirred for 30 seconds at a rate of 100 rpm. To remove air bubbles, the blend was processed in a vacuum environment for 60 min. Subsequently, the blend was pumped through a needle dropwise into the  $\text{CaCl}_2$  solution to allow capsule formation. The  $\text{CaCl}_2$  solution was stirred at a low speed for the full duration of the capsule production process. Finally, the calcium alginate capsules can be acquired after drying in an oven. Figure 4.3 shows a schematic diagram which

illustrates the production process of the calcium alginate capsules encapsulating rejuvenator.

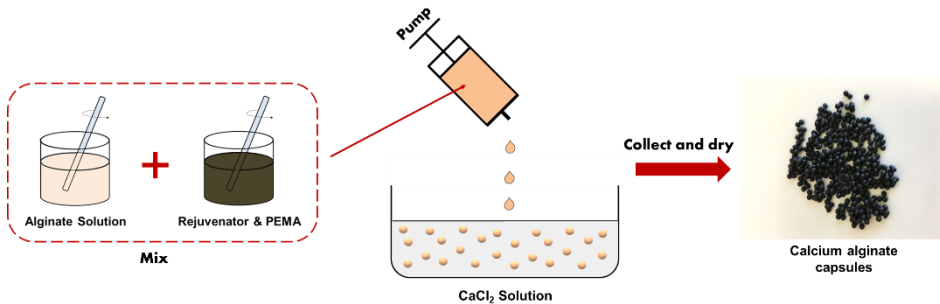


Figure 4.3: Production process of calcium alginate capsules.

## 4.2.2. CHARACTERIZATION OF CALCIUM ALGINATE CAPSULES

### 4.2.2.1. LIGHT MICROSCOPE

A Leica MZ 6 light microscope device made by Leica Microsystems B.V., Amsterdam, Netherlands was used to observe the morphology of calcium alginate capsules. The colour, diameter and morphology of calcium alginate capsules prepared with varying A/R ratio were analyzed using this device.

### 4.2.2.2. ENVIRONMENTAL SCANNING ELECTRON MICROSCOPE

A Philips XL30 ESEM equipment made by Philips, Eindhoven, Netherlands was employed to evaluate the microstructure inside the capsule. The ESEM was operated at 20 kV accelerating voltage and the magnification was 1000 times.

Figure 4.4 shows the tests sample used in ESEM analysis. In order to evaluate the microstructure inside the capsule, several capsules were fixed by pre-coated with epoxy (Figure 4.4 a), and then polished until the cross-sections of the capsules were reached (Figure 4.4 b). In this way, the cross-sectional area of a single capsule is exposed (Figure 4.4 c), as such the inner structure of capsules can be investigated by ESEM.

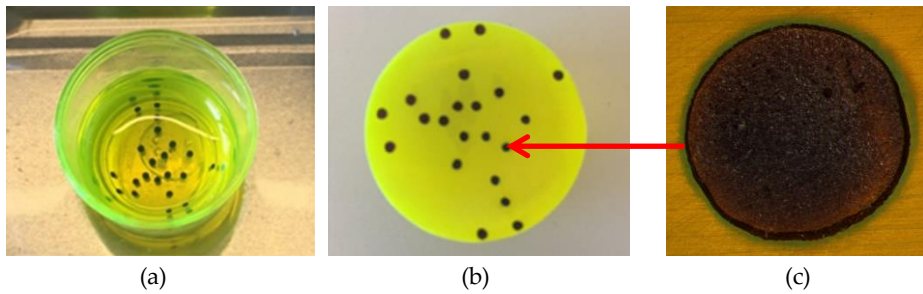


Figure 4.4: Capsules pre-coated with epoxy (a), polished to cross-section (b) and magnified cross-sectional image of a capsule.

#### 4.2.2.3. THERMOGRAVIMETRIC ANALYSIS

The temperature-dependent mass changes of the calcium alginate capsules were evaluated with NETZSCH STA 449 F3 Jupiter TGA system made by NETZSCH, Wormerveer, Netherlands. The analysis was performed in an argon (Ar) atmosphere at a flow of 50 ml/min. As shown in Figure 4.5, a temperature control programme was employed, and the mass changes were recorded with time.

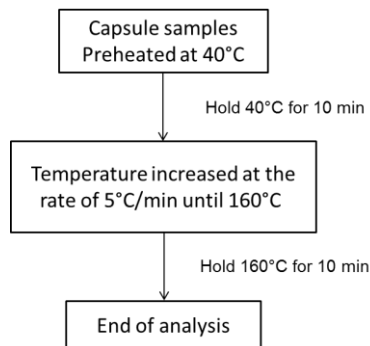


Figure 4.5: Thermogravimetric analysis (TGA) temperature control programme.

#### 4.2.2.4. MICRO COMPRESSIVE TEST

The micro strength testing machine (MSTM) developed by Kamrath & Weiss, Germany shown in Figure 4.6, was used to investigate compressive resistance of the prepared calcium alginate capsules. The tests were performed at the loading speed of 0.01 mm/s and an ambient temperature of  $20 \pm 2^\circ\text{C}$ . In order to analyse the deformation of the capsule during the compression, the whole testing process was recorded by a video camera from the vertical view. Before the compressive tests, capsules were conditioned for 15 min at 10 different temperatures (every  $20^\circ\text{C}$  from

-20°C to 160°C) to investigate the multi-temperature effect on the mechanical performance. The tests were performed after cooling down to 20°C. Minimum five capsules were tested for each temperature condition.

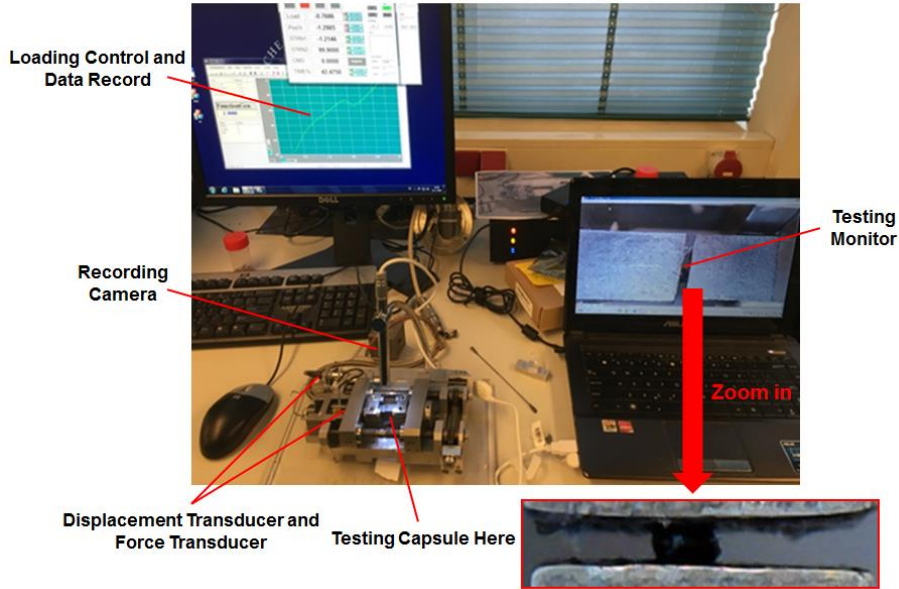


Figure 4.6: The micro compressive test performed by micro strength testing machine.

#### 4.2.2.5. X-RAY COMPUTED TOMOGRAPHY

A Phoenix Nanotom CT scanner made by Baker Hughes, Wunstorf, Germany was employed in order to study the structural and volumetric composition of the calcium alginate capsule. A single capsule was rotated along their longitudinal axis and three x-ray attenuation images were recorded every 0.25°. To fit the lateral dimension of the capsule volume during the scan, the resolution was set as 1.25  $\mu\text{m}^3$  per voxel [3]. After scanning, the image reconstruction was performed with Phoenix Datos|x software and images from the top slices view were analysed to quantify the rejuvenator composition of capsules.

In an X-CT image, individual phases containing different brightness intensities can be segmented by grey level thresholding. The grey level histogram is composed of separate peaks corresponding to distinct phases with heights proportional to the relative fractions of each phase. In this research, within the area of a capsule, the grey level histogram was composed of two phases: rejuvenator and calcium-alginate.

A randomly framed area (400×400 pixels) within the capsule was selected and a feature segmentation algorithm was employed to analyse the images [3]. Two different phases in the framed area can be quantified by cumulating pixels of each phase. To increase the accuracy, ten images from top slices were included in the analysis and the average value of grey level distribution was calculated.

### 4.3. RESULTS AND DISCUSSIONS

#### 4.3.1. CAPSULE MORPHOLOGY

Figure 4.7 presents the microscopic images of the capsule with different A/R ratios. Without rejuvenator, the calcium alginate capsule has a transparent brown colour and ellipsoid shape.

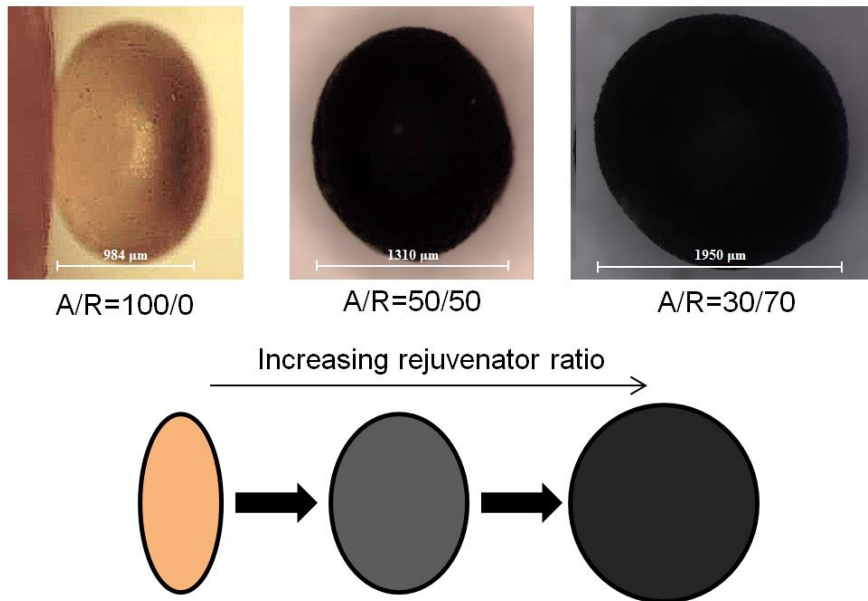


Figure 4.7: Microscopic images of calcium alginate capsules and the trend with various alginate/rejuvenator (A/R) ratio.

With encapsulated rejuvenator, the calcium alginate capsules become black and increasing the amount of rejuvenator results in a more spherical morphology. Table 4.1 summarizes the diameter and morphology information of capsules fabricated with different A/R ratios. At least 12 capsules were measured for each A/R ratio type and since the well-controlled manufacture process, the capsules had the

same diameters for each A/R ratio type. The results indicate that the diameter of capsules increases with rejuvenator content. When the A/R ratio is below 40/60, the shape of capsules is elliptical rather than spherical (circular). This change in morphology might be due to dehydration of the hydrated alginate during the drying process, in which higher alginate content would result in more dehydration and greater deformation, therefore become ellipse.

Table 4.1: Diameter and morphology information of calcium alginate capsules with different alginate/rejuvenator ratios.

Alginate/Rejuvenator ratio (%)	Diameter ( $\mu\text{m}$ )	Minor Axis ( $\mu\text{m}$ )	Morphology
100/0	1500	980	Ellipsoid
60/40	1920	1670	
50/50	1640	1310	
40/60	1740	1600	
30/70	1950	1950	Sphere
20/80	2170	2170	
10/90	2450	2450	

### 4.3.2. MICROSTRUCTURE

The cross-sectional ESEM images of capsules fabricated with A/R ratios in range of 40/60, 30/70, 20/80 and 10/90 are shown in Figure 4.8. In the grey pixels are recognized as alginate (compartmented walls), where dark pixels show the pores for the storage of rejuvenator. These ESEM images show a network of compartments inside of the capsules, which means that the rejuvenator is encapsulated in a number of small compartments rather than one central core compartment. Images from Figure 4.8 (a) to Figure 4.8 (d) illustrated that increasing the rejuvenator volume in the capsule, the size of compartments are increasing which also decrease the alginate network. In a single capsule, a higher volume percentage of rejuvenator indicates a larger rejuvenator carrying capacity, which also means a lower volume percentage of alginate network thus less bone material for mechanical resistance.

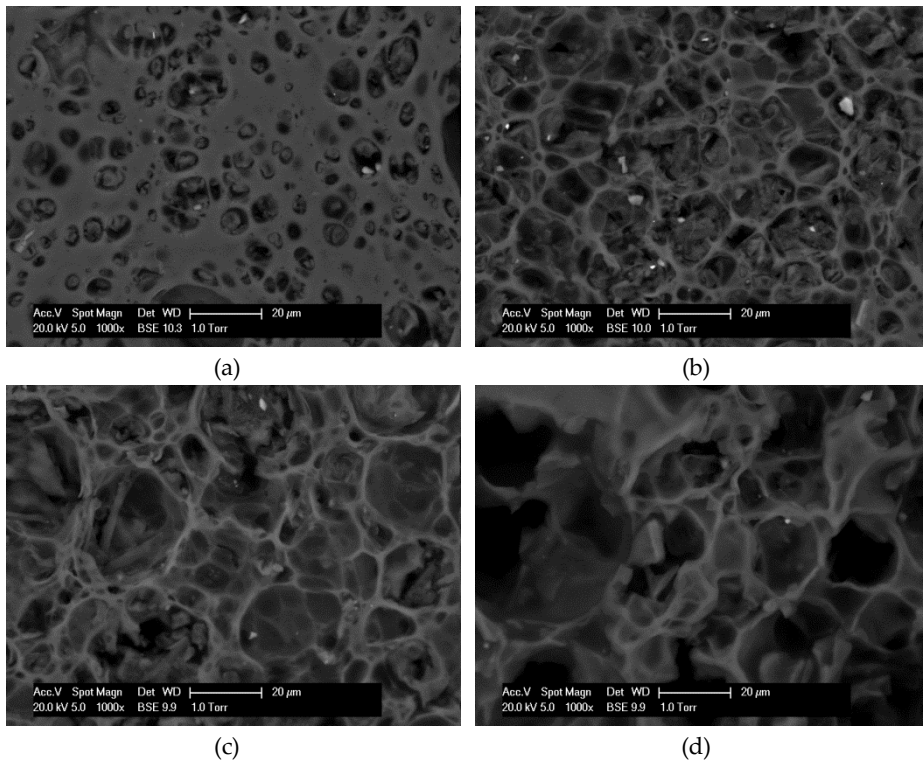


Figure 4.8: The cross-sectional ESEM images of calcium alginate capsules fabricated with A/R ratios of (a) 40/60, (b) 30/70, (c) 20/80 and (d) 10/90.

This special honeycomb-like structure of calcium alginate capsules provides a structural reinforcement that allows the capsule to possess higher thermal and mechanical resistance. Meanwhile, the compartmented rejuvenator storage in porous media could even have a multi-healing function on micro cracks [4].

#### 4.3.3. THERMAL STABILITY

Figure 4.9 shows the TGA results for capsules fabricated with varying A/R ratios. When the testing temperature is below 100 °C (before 25 min), all of the capsules show less than 2% weight loss. When the testing temperature exceeds 100 °C, linear increasing weight loss trends can be observed for capsules with different A/R ratios. Weight loss of capsules in this region is most likely due to the dehydration of calcium alginate gels. Among all the analysed capsules, capsules with an A/R ratio of 10/90 show the lowest weight loss during the tests, and the weight loss trend increases with the alginate contents. As the temperature reaches 160 °C (referred as

the asphalt mixing temperature) and is held for 15 min, the weight loss of the capsules retains a linear trend, and the final weight loss percentages of capsules with A/R ratios of 60/40, 50/50, 40/60, 30/70, 20/80 and 10/90 are 10.5%, 7.9%, 5.6%, 4.9%, 3.8%, and 2.2%, respectively. This indicates that the capsules, except surface moisture evaporation, do not experience any significant degradation at 160 °C. Meanwhile, when the A/R ratio is lower than 40/60, the final weight loss is lower than 5%, which means capsules with these ratios are relatively more stable and are capable of surviving the asphalt mixing temperature.

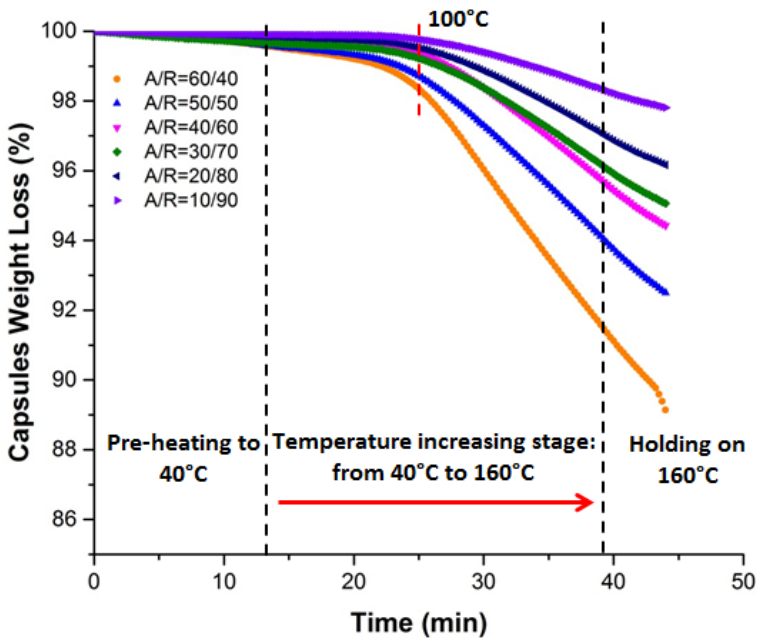


Figure 4.9: TGA results of capsules fabricated with varying A/R ratios.

#### 4.3.4. MECHANICAL RESISTANCE

During the compressive test, a capsule showed elastic behaviour below the yield point. When the stress went higher, permanent deformation was created and the capsule gradually ruptured, along with leaking out of the rejuvenator. As such, the compressive strength at the yield point was used to evaluate the mechanical resistance of a single capsule when subjected to asphalt mixing forces.

Figure 4.10 shows the compressive testing results for different A/R ratios of capsules. In general, with the increase of curing temperature, especially from 100 °C to 160 °C, a decrease of compressive strength can be found. It can also be seen that higher rejuvenator content results in lower compressive strength on capsules, especially under higher curing temperatures. The compressive testing results indicate that the dehydration of the alginate gel results in the degradation of some of the calcium alginate chains and a decrease in the compressive strength of calcium alginate capsules.

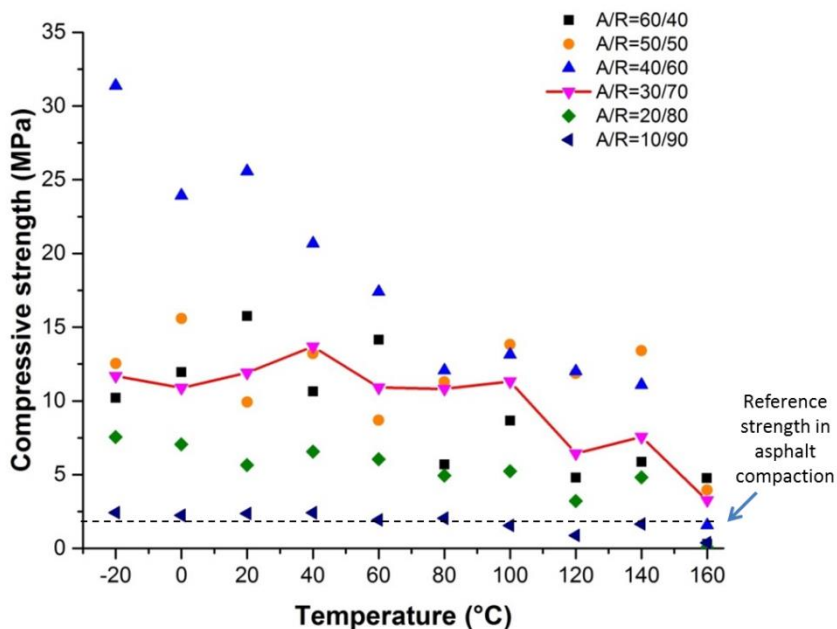


Figure 4.10: Compressive strength of capsules fabricated with varying A/R ratios cured under different temperatures.

The corresponding compression for the mastic mix is about 1.8 MPa, and the vehicle loading pressure is less than 1 MPa [5, 6]. After curing at 160 °C, capsules with A/R ratios of 20/80 and 10/90 showed a compressive strength less than 0.4 MPa, which is insufficient to survive the asphalt production process. Meanwhile, for the capsules with a ratio of 30/70, at the curing temperature of 160 °C, the lowest compressive strength in the curve remains 3.27 MPa. Hence, the capsules fabricated with A/R ratio of 30/70 are expected to show elastic behaviour and survive the asphalt

mixing process and dynamic vehicle loading during the asphalt pavement service life. Although capsules with other A/R ratios also have applicable compressive strength, they contain less rejuvenator. According to the compressive tests as well as the TGA test results, 30/70 is determined to be the optimum A/R ratio.

It is noticed that the compressive test on the calcium alginate capsules can not fully simulate the conditions in the asphalt compaction process in which the capsules will be compressed under 160°C. Hence, for the calcium alginate capsules with the optimum A/R ratio, the ability to survive the asphalt mixing and compaction needs to be further validated with the asphalt compaction tests, which are described in Chapter 5 and Chapter 6.



Figure 4.11: Rejuvenator flowing out of a crashed calcium alginate capsule (A/R ratio of 30/70) after the compressive test.

Figure 4.11 shows the image of a crashed calcium alginate capsule (with A/R ratio of 30/70) after the compressive test. A shining area of liquid rejuvenator can be found in the middle of the crashed capsule, which indicates that the rejuvenator is encapsulated in the calcium alginate capsules and will be released upon damaging of capsules.

#### 4.3.5. VOLUMETRIC COMPOSITION

XCT was performed on the calcium alginate capsules to investigate the volumetric composition so that the rejuvenator content of these capsules can be acquired.

The grey value distribution depending on voxel numbers and the segmented area is shown in Figure 4.12. Only one peak can be found in the voxels grey value

distribution curve, this peak is regarded as a result of superposition from two phases. In the area segmented curve, the maximum slope is located at the grey level of  $T=150$ , which indicates a dramatic change between phases. Hence,  $T$  is recognized as the boundary between the two phases.

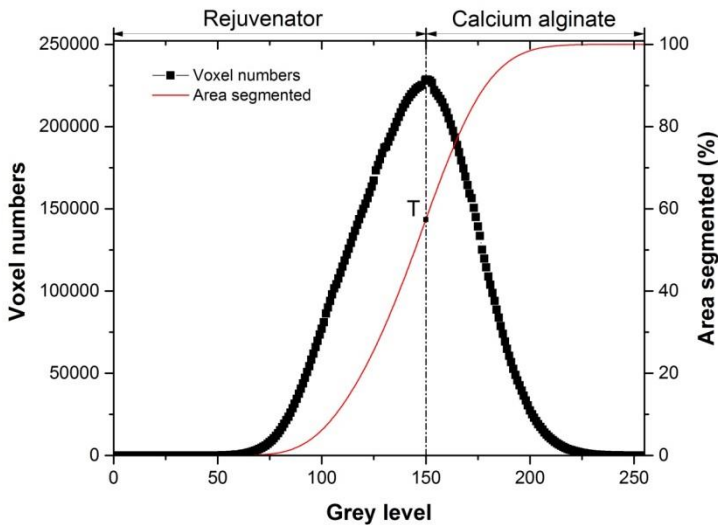


Figure 4.12: Phase evaluation through grey level histogram of CT images

An XCT image is shown in Figure 4.13. The image illustrates the calcium alginate crosslinks, shown as a brighter colour in the image, which means its grey level is distributed in higher values than rejuvenator. When applied with boundary  $T$ , the voxels with a grey level smaller than  $T$  is regarded as rejuvenator and the voxels with a grey level greater than  $T$  is regarded as calcium alginate. As shown in Figure 4.13, for a better view of segmentation in phases, a framed area can be processed to an image in which two different phases are highlighted: rejuvenator in black and calcium alginate in white.

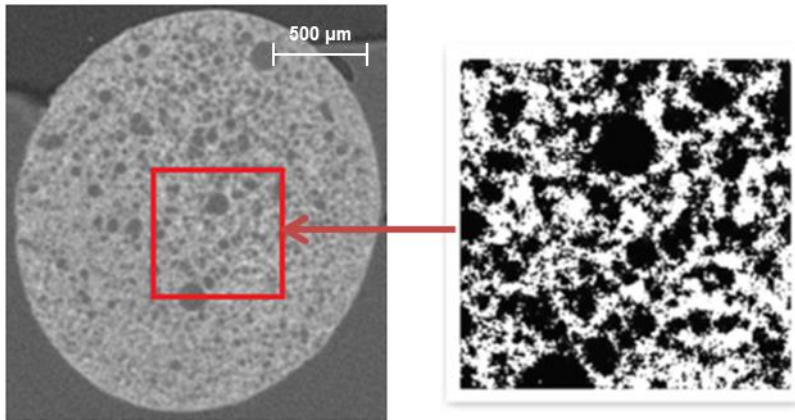


Figure 4.13: (left) X-ray tomography image and (right) image of area segmentation.

Based on the grey level histogram analysis from 10 different CT images, the rejuvenator phase content of the capsule was calculated and the result turned out to be 56% by volume. The 56% rejuvenator content of the calcium alginate capsules shows an advantage over the existing rejuvenator encapsulation technologies for asphalt pavement, which results in a higher healing potential [7-9]. The x-ray tomography image also indicates the porous honeycomb-like structure inside a capsule, which agrees with the ESEM results.

#### 4.4. CONCLUSIONS

This chapter illustrates the preparation process of calcium alginate capsules encapsulating rejuvenator and how A/R ratios affect the properties of these capsules. The following conclusions can be drawn based on the findings:

- The microstructure inside the calcium alginate capsules is presented as a honeycomb-like porous structure and individual rejuvenator droplets are encapsulated in the porous media.
- The A/R ratios used in the capsule production process greatly influence the morphology, internal matrix structure and performance of calcium alginate capsules. In principle, a higher rejuvenator content (lower A/R ratio) results in a larger diameter, larger inside pores, higher thermal resistance, and less compressive strength.

- The optimum A/R ratio is 30/70, as the prepared capsules not only have sufficient thermal and mechanical resistance to survive the asphalt mixing and compaction process but also contain as much rejuvenator as possible.
- The capsules prepared with the optimum A/R ratio have a uniform diameter of 1.95 mm and the rejuvenator content is 56% by volume. Besides, these capsules have proven sufficient thermal and mechanical resistance to survive the asphalt production and compaction process.

The main aim of this Ph.D. project is to develop the combined healing system based on the potential synergy effect of the capsule healing system and the induction heating system. The successful development of calcium alginate capsules including the preparation and the optimization has definitely paved a way to this aim. The optimal calcium alginate capsules with A/R ratio of 30/70 were adopted for further studies presented in Chapter 5 and integrated into the combined healing system (with capsules and steel fibres) in order to achieve a more efficient healing system for asphalt pavement presented in Chapter 6.

## REFERENCES

- [1] M. Prajer, X. Wu, S. Garcia, S. van der Zwaag, Direct and indirect observation of multiple local healing events in successively loaded fibre reinforced polymer model composites using healing agent-filled compartmented fibres, *Composites Science and Technology* 106 (2015) 127-133.
- [2] D. JOHNSON, *New Applications for Poly (ethylene-alt-maleic anhydride)*, Durham University, 2010.
- [3] H. Wong, M. Head, N. Buenfeld, Pore segmentation of cement-based materials from backscattered electron images, *Cement and Concrete Research* 36(6) (2006) 1083-1090.
- [4] S. Xu, A. Tabaković, X. Liu, E. Schlangen, Calcium alginate capsules encapsulating rejuvenator as healing system for asphalt mastic, *Construction and Building Materials* 169 (2018) 379-387.

- [5] A. Tabaković, A. Karač, A. Ivanković, A. Gibney, C. McNally, M.D. Gilchrist, Modelling the quasi-static behaviour of bituminous material using a cohesive zone model, *Engineering Fracture Mechanics* 77(13) (2010) 2403-2418.
- [6] E.R. Brown, P.S. Kandhal, J. Zhang, Performance testing for hot mix asphalt, National Center for Asphalt Technology Report (01-05) (2001).
- [7] Á. García, E. Schlangen, M. Van de Ven, Properties of capsules containing rejuvenators for their use in asphalt concrete, *Fuel* 90(2) (2011) 583-591.
- [8] J.-F. Su, J. Qiu, E. Schlangen, Stability investigation of self-healing microcapsules containing rejuvenator for bitumen, *Polymer degradation and stability* 98(6) (2013) 1205-1215.
- [9] A. Tabaković, W. Post, D. Cantero, O. Copuroglu, S. Garcia, E. Schlangen, The reinforcement and healing of asphalt mastic mixtures by rejuvenator encapsulation in alginate compartmented fibres, *Smart Materials and Structures* 25(8) (2016) 084003.

# 5

## EVALUATION OF THE HEALING EFFECT OF CALCIUM ALGINATE CAPSULES IN POROUS ASPHALT

*The successful encapsulation of asphalt rejuvenator in calcium alginate capsules provides a potential for the build of a more environmentally friendly and economically viable self-healing system in asphalt pavement. Although the thermal and mechanical properties of calcium alginate capsules have preliminarily demonstrated their suitability using in asphalt pavement, questions about the effectiveness and efficiency of this new capsule healing system still remained. Evaluation of the calcium alginate capsules healing system begins with an asphalt mastic mixture, then an asphalt mortar and finally a porous asphalt concrete.*

## 5.1. INTRODUCTION

Previous chapter (Chapter 4) describes the successful preparation of the calcium alginate capsules. Testing results on the capsule's thermal stability and compressive resistance showed that these calcium alginate capsules are able to survive the asphalt production and compaction process. This chapter presents the study on how calcium alginate capsules encapsulating rejuvenator affect the mechanical properties and the healing capacity of an asphalt mix, at mastic, mortar and concrete levels.

The first step in the calcium alginate capsules healing system evaluation was the assessment of the capsule healing system within an asphalt mastic mix. The three-point bending testing protocol was employed to evaluate the mechanical properties of the asphalt mastic and the healing efficiency of the capsule healing system.

The asphalt mortar mix was derived from a porous asphalt aggregate skeleton study [1]. To prove the effectiveness (healing efficiency) of the capsules in an asphalt mortar mix, capsules were embedded in asphalt mortar beams and a bending and healing program was carried out. Except the mortar beams with optimized calcium alginate capsules (A/R ratio at 30/70), mortar beams without capsules were tested as a reference. Besides, mortar beams with blank capsules (A/R ratio at 100/0) were tested to determine that the improvement of healing is from the rejuvenator rather than the capsule shell material.

At a full asphalt mix level, a porous asphalt (PA) mix with capsules was designed and produced. A PA mixture without capsules was used as a reference mixture. Semi-circular bending (SCB) tests were performed to study the fracture resistance of PAC samples. The healing capacity of the porous asphalt mix was evaluated by a bending and healing programme based on SCB tests.

## 5.2. MATERIALS AND METHODS

### 5.2.1. MATERIALS AND ASPHALT MIXTURE DESIGN

The calcium alginate capsules healing system was preliminarily investigated in asphalt mastic which includes three types of mixture with varying content of the calcium alginate capsules (Table 5.1), including control beams (without capsules), beams with 2 wt% capsules (takes 7% volume of bitumen) and beams with 4 wt% capsules (takes 14% volume of bitumen). The capsules were inserted into the asphalt mastic mix design by replacing the bitumen content of the mix.

Table 5.1: Mix composition of asphalt mastic

Mix constituent	Percentage by weight		
	Without Capsules	2% Capsules	4% Capsules
Sand(0~4mm)	50	50	50
Filler(Wigro60k)	25	25	25
Bitumen(70/100)	25	23	21
Capsules	0	2	4

Before evaluation in a full PAC mix, the calcium alginate capsules healing system was tested in an asphalt mortar mix, this is because asphalt mortar is the major composition of the stone-to-stone contact regions in PAC where the stress concentrates and where ravelling would most likely take place [2]. The study in the mortar level also provides a closer and more accurate characterization of the capsule performance.

Table 5.2 shows the asphalt mortar mixture composition derived from a porous asphalt aggregate skeleton study on the RAW specification for porous asphalt [3]. Two types of capsules were used in the mortar mix preparation, including capsules with rejuvenator (A/R ratio at 30/70) and blank capsules (A/R ratio at 100/0). In total three types of mortar mix were prepared, including the control mix (without capsules), 2.6 wt.% capsules mix and 2.6 wt.% blank capsules mix (takes 7% volume of bitumen). The bituminous mortar in the top layer of a porous asphalt mixture contains sand fractions smaller than 0.5 mm [1, 4]. For this reason, the sand used in this study is sieved from the Bestone sand provided by Bontrup, Amsterdam, Netherlands, with a maximum size of 0.5 mm. The filler is type wigro 60k, which consists of 25~35% calcium hydroxide, provided from Bontrup, Amsterdam, Netherlands. The 70/100 bitumen was provided by Latexfalt, Koudekerk aan den Rijn, Netherlands.

Table 5.2: Mix composition of asphalt mortar.

Mix Constituent	Percentage by weight		
	Without Capsules	2.6% Capsules	2.6% Blank Capsules
Sand(0~0.5mm)	34.8	34.8	34.8
Filler(Wigro60k)	32.6	32.6	32.6
Bitumen(70/100)	32.6	30.0	30.0
Capsules	0	2.6	0
Blank Capsules	0	0	2.6

The porous asphalt mix used in this study was based on the standard mix of PA 0/11. Table 5.3 shows the two types of mixtures designed for the study, including a porous asphalt mix with capsules and a reference mix without capsules. Based on the study in Chapter 3, using calcium alginate capsules to replace 7% the volume of bitumen (8% by weight) possesses an optimistic healing efficiency. Thus, to build the calcium alginate capsules healing system, the capsules were added in the porous asphalt mix by replacing 7% volume of the bitumen. The bitumen used in the PAC mixture was the standard paving grade bitumen 70-100 provided by Vitol, London, UK. All the aggregates were Bestone or byproduct of Bestone, provided from Bontrup, Amsterdam, Netherlands.

Table 5.3: Mix composition of porous asphalt concrete.

Mix Constituent	% Content in Mix	
	7% Capsules	Without Capsules
16 mm	8.5	8.5
11.2 mm	66.1	66.1
8 mm	8.5	8.5
5.6 mm	1.9	1.9
2 mm	6.9	6.9
500 $\mu\text{m}$	2.2	2.2
180 $\mu\text{m}$	0.7	0.7
125 $\mu\text{m}$	0.7	0.7
63 $\mu\text{m}$	4.5	4.5
Bitumen (70/100)	4.092	4.4
Capsules	0.363	0

### 5.2.2. LABORATORY AGEING PROCESS

The aim of the capsule healing system is to achieve self-healing by restoring the lost properties of aged asphalt. Hence the healing effect of the capsules also needs to be illustrated in consideration of the influence of ageing on asphalt mixture. Therefore, except for the fresh mortar mixture, some aged asphalt mortar mixtures were prepared by performing a laboratory ageing procedure which was used by Tabaković et al. [5]: the asphalt mixture was cured at 135 °C for 4 hours and then 85 °C for 96 hours in a ventilated oven, which introduces the oxidative ageing of bitumen and simulates the long term asphalt bitumen ageing. The ageing of asphalt mastic mixture followed the same way.

Aimed to achieve an evenly ageing effect on all aged mortar samples, everytime a mortar mixture sample of 421.2 g (density of 1.755 g/cm<sup>3</sup>) was filled into a 400×300×50 mm silicon container to form a 2 mm thin film before the ageing process. A similar strategy to control the uniformity of oven ageing was adopted by Jing [6]. Figure 5.1 shows the mortar mixture samples filled in containers ready for ageing.



Figure 5.1: Asphalt mortar mixture filled in silicon container before the ageing process.

Figure 5.2 shows the laboratory ageing on PAC slabs in a ventilated oven. After mixing and compaction, the PAC slabs were kept in the mould and cured in a ventilated oven at 135 °C for 4 hours and then another 96 hours under 85°C.



Figure 5.2: Asphalt mortar mixture filled in silicon container before the ageing process.

### 5.2.3. BEAM SAMPLE PREPARATION FOR ASPHALT MASTIC AND MORTAR

Figure 5.3 (a) shows the silicon mould used for the preparation of asphalt mastic/mortar beam samples. Figure 5.3 (b) shows the prepared 125 × 25 × 15 mm

asphalt mastic beam. In order to achieve controlled crack propagation, each beam specimen contained a 'v' notch at the centre of the beam. To prepare the hot mixed asphalt mastic/mortar, all of the asphalt mix constituents were preheated in an oven for 2 hours at 160 °C. Then, sand, filler and bitumen were mixed using a Hobart Mixer forming a mastic/mortar mixture. After that, the capsules were gradually added to the mixer during the mixing process. Subsequently, the mastic/mortar mixture was compacted with 2 passes by a steel roller cylinder in a mould to form the beam testing samples.



Figure 5.3: (a) Mould for asphalt mastic beam preparation and (b) the dimensions for the prepared beam sample.

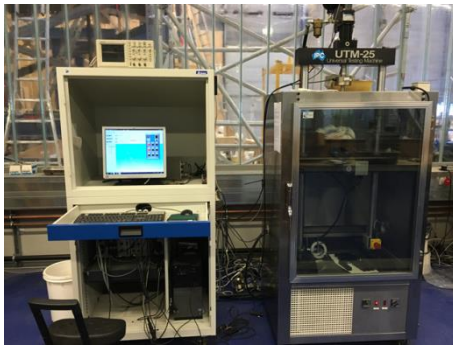
#### 5.2.4. THREE POINT BENDING TEST FOR ASPHALT MASTIC/MORTAR SAMPLES

The 3PB test was used to study the mechanical properties of mastic and mortar beams and the further evaluation of their healing efficiency. A universal testing machine (UTM) with a temperature chamber was employed to perform the 3PB tests. Figure 5.4 shows the experimental setup and parameters. The 3PB tests were performed at the loading speed of 0.01 mm/s under a low testing temperature in order to avoid permanent deformation and to create a brittle fracture in the beam sample. The asphalt mastic beams were tested under 0°C, while the asphalt mortar beams were tested under -5°C since the mortar mix has a fine aggregate composition and higher bitumen content which means it is more temperature-sensitive and prone to permanent deformation under loadings. The bending strength of the beam specimens was calculated with the following equation:

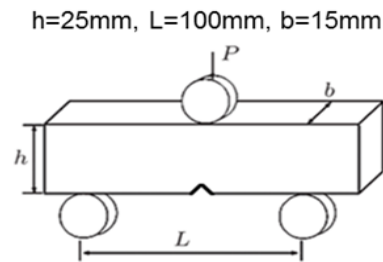
$$\sigma_{max} = \frac{3P_{max}L}{2b(h-a)^2} \quad (5.1)$$

Where

- $\sigma_{max}$  is the bending strength (MPa);  
 $P_{max}$  is the peak load (N);  
 $L$  is the support span (mm);  
 $b$  is the thickness of the beam (mm);  
 $h$  is the height of the beam (mm);  
 $a$  is the notch depth of the beam (mm).



(a)



(b)

Figure 5.4: 3PB test setup: (a) universal testing machine and (b) testing parameters.

### 5.2.5. PREPARATION OF POROUS ASPHALT CONCRETE SLABS

The PAC was produced by making 50 × 50 × 5 cm asphalt slabs in Heijmans infra BV, Rosmalen, Netherlands. To prepare a slab, the designed pre-heated materials were carefully mixed in the laboratory rotating drum mixer (Figure 5.5 (a)). Then, the mixed materials were collected and weighed to meet the required amount of an asphalt slab (Figure 5.5 (b)). Subsequently, the weighed asphalt mix was poured into a mould and compacted with a manual roller compactor (Figure 5.5 (c)). After a series of compaction cycles, the porous asphalt slab was produced (Figure 5.5 (d)).

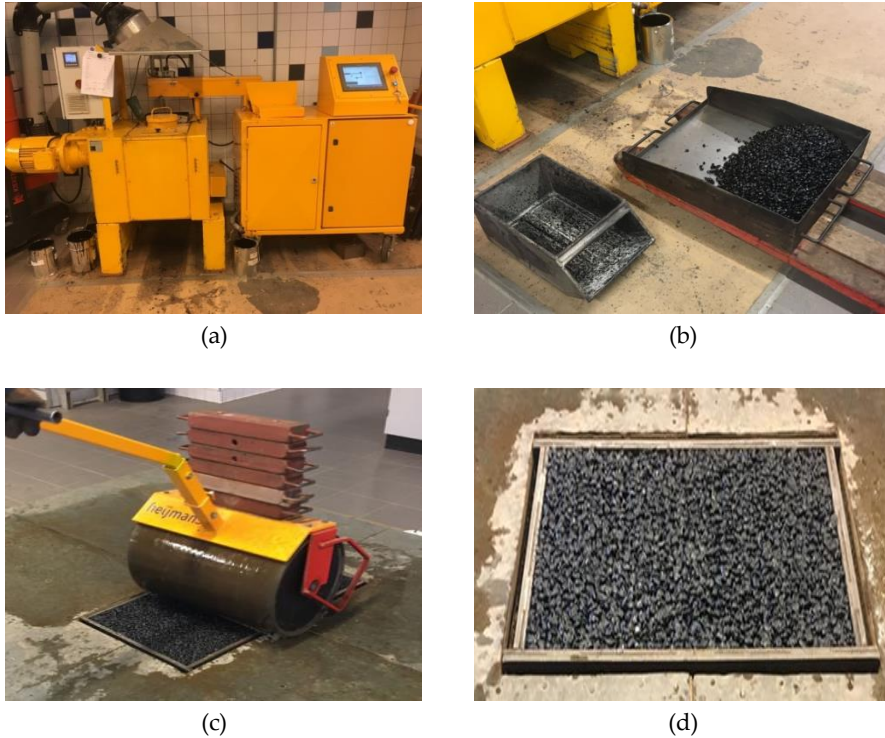


Figure 5.5: Porous asphalt slab preparation procedure: (a) mixing in laboratory rotating drum mixer; (b) weighing the mixture; (c) compaction with manually roller compactor and (d) prepared porous asphalt slab.

### 5.2.6. SEMI-CIRCULAR BENDING AND HEALING TEST FOR POROUS ASPHALT CONCRETE SAMPLES

A UTM with a temperature chamber was employed to perform the SCB tests according to EN 12697-44. As shown in Figure 5.6, the SCB specimens were prepared by sawing the drilled cores from PA slabs, which had a diameter of  $100 \pm 2$  mm, a thickness of  $50 \pm 1$  mm and a height of  $50 \pm 1$  mm. A rectangle notch was placed in the middle of each sample with a length of  $10 \pm 0.2$  mm and a width of  $2 \pm 0.1$  mm. The supporting span for SCB tests is 80 mm and the tests were performed in a temperature-controlled chamber at  $0^\circ\text{C}$  with a loading speed of 5 mm/min. Figure 5.7 (a) shows SCB testing setup and Figure 5.7 (b) shows the fractured specimen after the test.

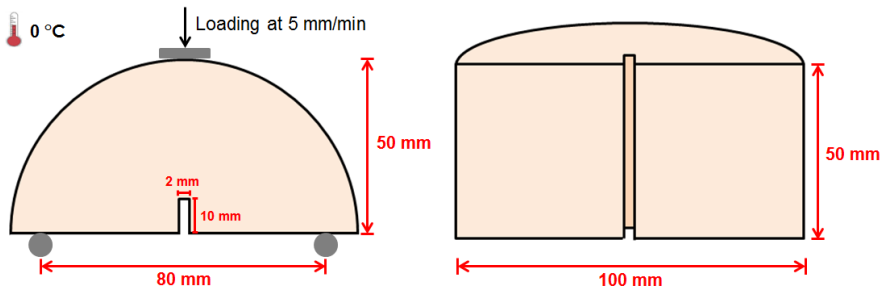


Figure 5.6: SCB specimen dimensions and testing conditions

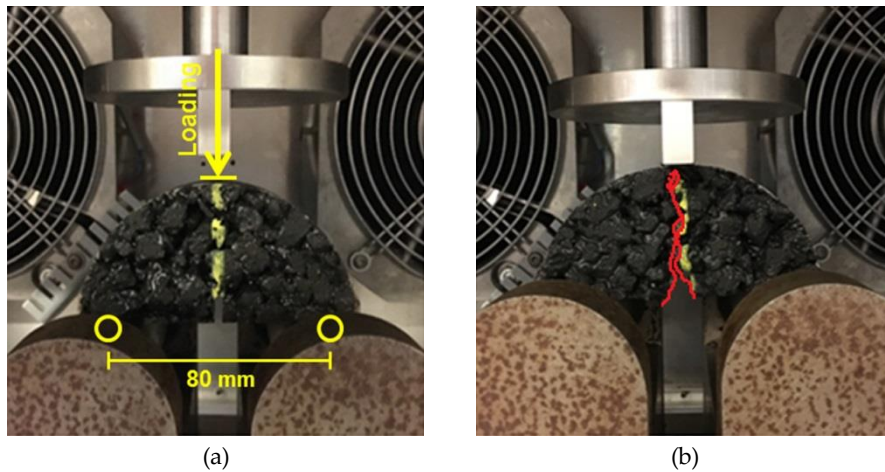


Figure 5.7: (a) SCB testing setup and (b) fractured specimen after test.

The fracture toughness and fracture energy were calculated with the following equations:

$$K_{Ic} = Y_{Ic(0.8)} \frac{P_{max}}{Dt} \sqrt{\pi a} \quad (5.2)$$

$$Y_{Ic(0.8)} = 4.782 - 1.219 \left( \frac{a}{r} \right) + 0.063 e^{(7.045 \left( \frac{a}{r} \right))} \quad (5.3)$$

Where

$K_{Ic}$  is the fracture toughness ( $\text{N}/\text{mm}^{1.5}$ );

$Y_{Ic(0.8)}$	is the stress intensity factor;
$P_{max}$	is the peak load (N);
$D$	is the diameter of the specimen (mm);
$t$	is the thickness of the specimen (mm);
$a$	is the notch depth of the specimen (mm);
$r$	is the radius of the specimen (mm).

$$G_f = \frac{W_f}{A_{lig}} \quad (5.4)$$

$$W_f = \sum_{i=1}^n (u_{i+1} - u_i)p_i + 0.5(u_{i+1} - u_i)(p_{i+1} - p_i) \quad (5.5)$$

Where

$G_f$	is the fracture energy (J/m <sup>2</sup> );
$W_f$	is the work of fracture (J);
$A_{lig}$	is the ligament area which is $(r - a) \times t$ (m <sup>2</sup> );
$p_i$	is the applied load (N) at the $i$ load step application;
$p_{i+1}$	is the applied load (N) at the $i+1$ load step application;
$u_i$	is the displacement at the $i$ step (m);
$u_{i+1}$	is the displacement at the $i+1$ step (m).

## 5.2.7. BENDING AND HEALING PROGRAMME

### 5.2.7.1. THREE POINT BENDING AND HEALING PROGRAMME FOR ASPHALT MASTIC/MORTAR BEAM SPECIMENS

For the 3PB tests performed on asphalt mastic/mortar beams, stress concentration on the notch allows the initiation and propagation of crack through the middle of the specimen, testing the healing function of capsules in the case of cracking. A 3PB bending and healing programme was followed to evaluate the healing efficiency of the calcium alginate capsules healing system. Figure 5.8 (a), (b) and (c) present the images in the bending process.

Since the confining stress on cracking surfaces plays an important role during the asphalt healing process [7], the cracked specimens were placed in the compaction mould to achieve constant healing conditions for all specimens. Figure 5.8 (d) shows the healing of the beam sample in the mould at an ambient temperature of  $20 \pm 2^\circ\text{C}$ .

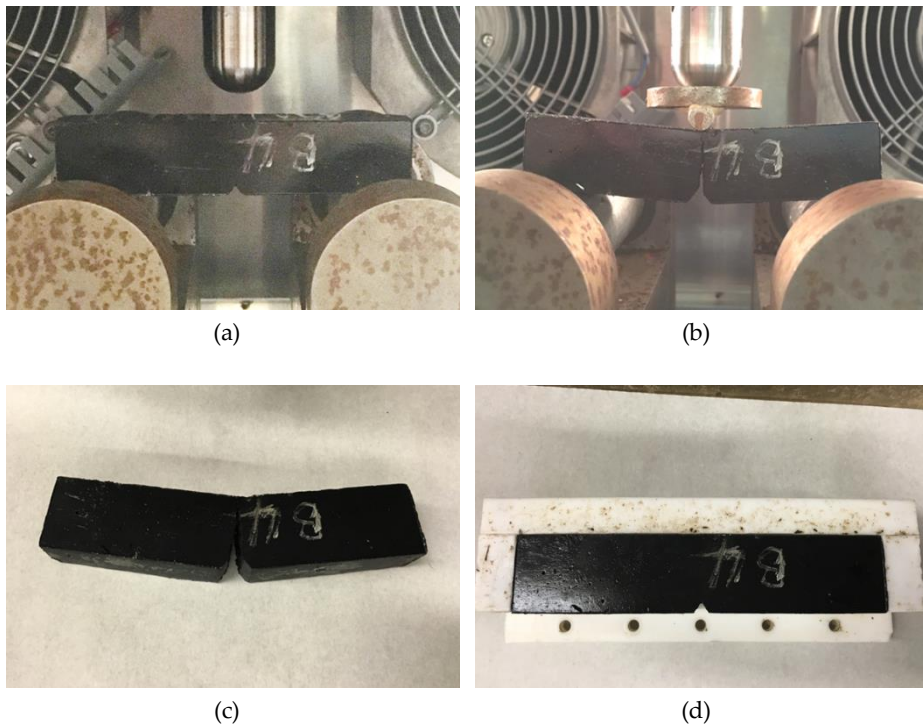


Figure 5.8: 3PB bending and healing images: (a) before the 3PB test, (b) propagation of crack during 3PB test, (c) fractured asphalt beam sample and (d) healing of asphalt beam sample in the mould.

Figure 5.9 illustrates the bending and healing programme: Firstly, a 3PB test was performed to allow crack formation in the beam. After that, the cracked sample was healed for 3 hours and followed by a second 3PB test to acquire the bending strength after the first healing stage. Subsequently, the sample was healed again for 12 hours and followed by a third 3PB test to acquire the bending strength after the second healing stage.

### Bending and healing programme

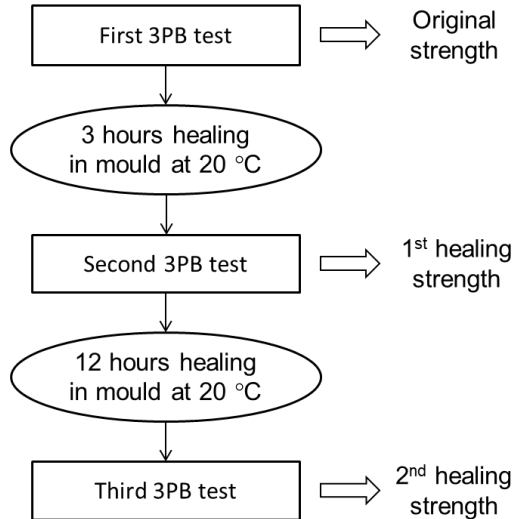


Figure 5.9: 3PB bending and healing programme for asphalt mastic/mortar beam specimens.

#### 5.2.7.2. SEMI-CIRCULAR BENDING AND HEALING PROGRAMME FOR POROUS ASPHALT CONCRETE SPECIMENS

Figure 5.10 shows the fractured SCB specimens self-healed in a temperature chamber conditioned at 23°C on a plain surface. Prior to healing, the fractured specimens were joined to close the fracture face. In order to create constant confinement to ensure the close of cracked surfaces, the specimens were carefully wrapped with tape throughout the healing process, as shown/illustrated in Figure 5.10.



Figure 5.10: Healing of the fractured SCB samples in a temperature chamber

The healing efficiency of calcium alginate capsules healing system in porous asphalt concrete was evaluated with SCB bending and healing cycles illustrated in Figure 5.11:

- First, an SCB test was performed to measure the initial peak load of the specimen;
- Second, the fractured specimen was healed at 23°C for 20 h;
- Subsequently, the second SCB test was performed to acquire the regained peak load of the specimen after healing. Afterwards, the second step was repeated to perform another healing cycle following by the third SCB test.

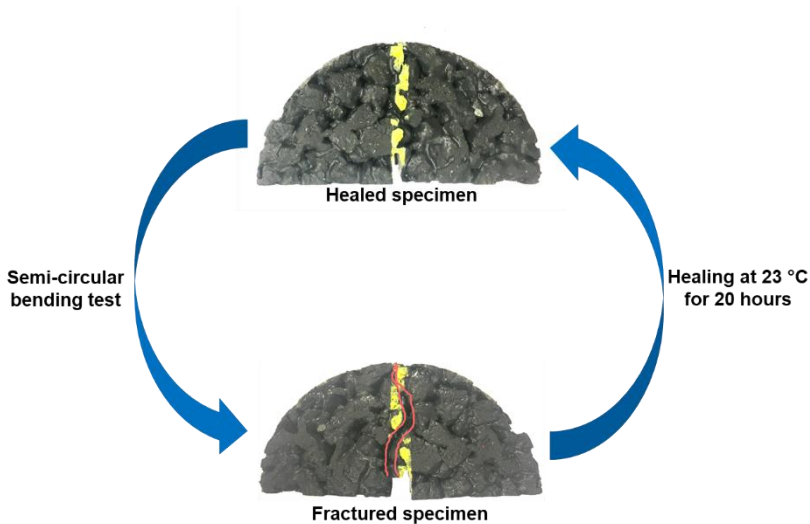


Figure 5.11: Schematic illustration of the SCB bending and healing cycles for porous asphalt concrete specimens.

### 5.2.7.3. EVALUATION OF THE HEALING EFFICIENCY

Healing Index (*HI*) was used to quantify the healing efficiency of the specimens tested through bending and healing programme, which was calculated with the peak load measured from 3PB or SCB tests:

$$HI = \frac{C_x}{C_1} \times 100 \quad (5.6)$$

Where:

- $HI$  is the healing index (%)  
 $C_1$  is the initial peak load (N);  
 $C_x$  is the peak load measured from the  $x$  testing cycle (N).

### 5.3. RESULTS AND DISCUSSIONS

#### 5.3.1. FRACTURE FACES CHARACTERIZATION

##### 5.3.1.1. FRACTURE FACES OF BEAM SAMPLES AFTER BENDING TEST

Images of an asphalt mastic beam sample (with capsules) fractured from 3PB test are presented in Figure 5.12. Figure 5.12 (a) shows the fractured beam sample, Figure 5.12 (b) shows the fracture faces of the beam sample and Figure 5.12 (c) shows the magnified interface image. Figure 5.12 (b) illustrates that broken capsules throughout the depth of the beam and across the crack interface of a beam. These capsules were successfully fractured during the 3PB test. The presence of capsules throughout the crack interface demonstrates that the adhesion between capsules and asphalt binder is strong, which means that cracks are able to propagate through the capsules instead of circumventing them to trigger the release of rejuvenator, as experienced with polymeric capsules [8].

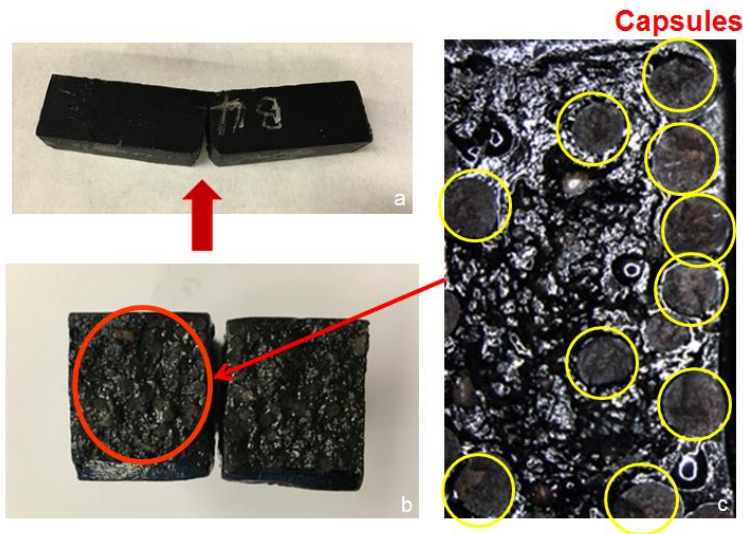


Figure 5.12: Asphalt mastic beam: (a) fractured specimen, (b) cracking interface and (c) magnified interface image.

### 5.3.1.2. FRACTURE FACES OF SEMI-CIRCULAR SAMPLES AFTER BENDING TEST

The fracture surface of an SCB specimen with capsules is shown in Figure 5.13. As shown in Figure 5.13, broken capsules can be found on both sides of the fractured SCB specimens, which indicates that the capsules are able to break upon the propagation of cracks. The reddish shiny regions at the broken capsules indicate the presence of the rejuvenator. This also demonstrates that the calcium alginate capsules have not been crushed by mixing or compaction in this research, which indicates a huge potential for the application in field construction.



Figure 5.13: Fracture surface of a SCB specimen with 7% capsules.

In order to further confirm and track the releasing of rejuvenator from the capsules which were broken in SCB tests, as shown in Figure 5.14, the sample on the right side of Figure 5.13 was exposed to UV light. Since the rejuvenator content of a single capsule is limited, there is no large area distribution of rejuvenator. However, following the locations of broken capsules in Figure 5.13, the brown area can be found which refers to released rejuvenator under UV light.

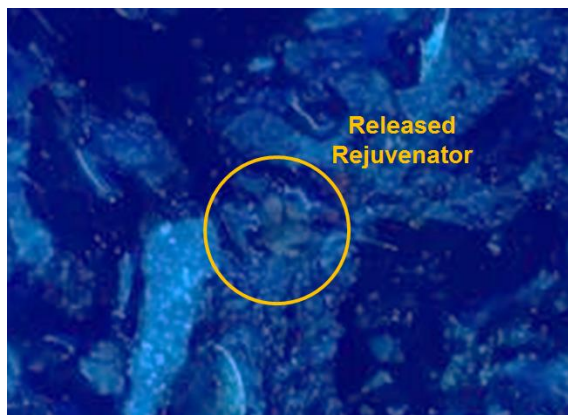


Figure 5.14: Released rejuvenator on fracture face.

### 5.3.2. MECHANICAL RESPONSE OF THE TESTED SAMPLES

#### 5.3.2.1. RESULTS FOR THREE POINT BENDING TEST ON ASPHALT MASTIC SAMPLES

Figure 5.15 summarizes the bending strength of asphalt mastic beams in 3PB tests. Mastic beams containing capsules (including both 2% and 4%) show higher bending strength than those without capsules, indicating the capsule reinforcing effect. This reinforcing effect is proportional to the number of capsules in asphalt mastic beams. Figure 5.15 also shows that the regained bending strength from the healing process is lower than the original bending strength, and decreases with bending times.

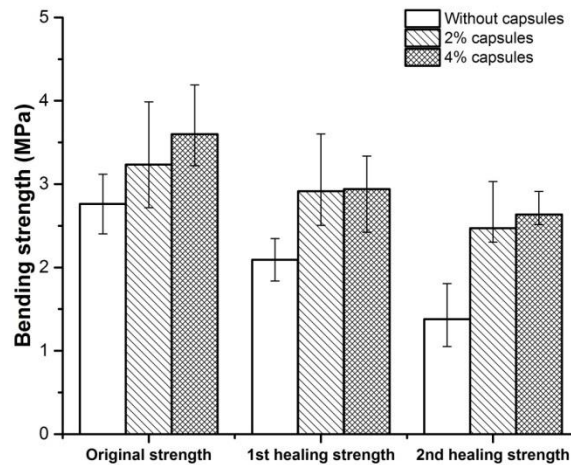


Figure 5.15: Bending strength of asphalt mastic beams.

#### 5.3.2.2. RESULTS FOR THREE POINT BENDING TEST ON ASPHALT MORTAR SAMPLES

Figure 5.16 shows the bending strength of the asphalt mortar beams made with fresh material. During each testing cycle, the bending strengths of all three types of beams are very similar, and the mortar beams still have strengths about 4 MPa after 2 testing cycles, even without capsules or with blank capsules. This means that the healing capacity of the fresh material itself plays the main role in crack healing

(strength recovery). It also demonstrates that the presence of calcium alginate capsules, containing rejuvenator doesn't significantly affect the initial bending strength of the mortar beams. Hence, when the bituminous material possesses sufficient healing capacity, like in fresh bitumen, the capsule healing system could hardly improve the healing efficiency.

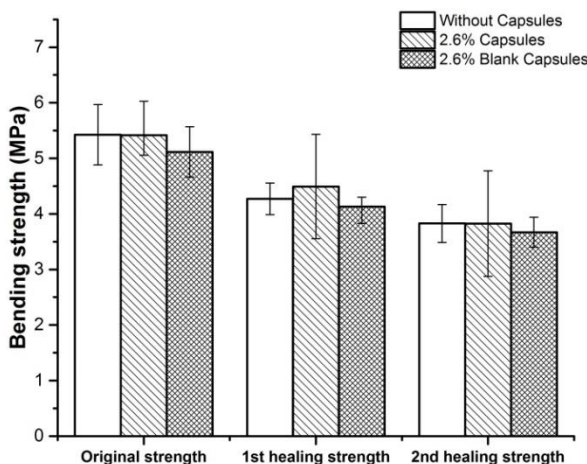


Figure 5.16: Bending strength of fresh asphalt mortar beams.

Figure 5.16 also shows that the mortar beams with blank capsules have a lower bending strength than the other two types of beams, which indicates the blank capsules do not contribute to the fracture resistance nor healing capacity. It is because the blank capsules are made of stabilized calcium alginate cross-links, which perform as a solid material and do not have the ability to reconnect the fracture face. The fractured pieces of blank capsules on fracture face can even create some unbound spots that prevent the contact of bitumen from two fractured faces.

Ageing of the asphalt mixture could not only decrease its stiffness but also decrease its healing capacity [7]. As shown in Figure 5.17, without capsules, the initial bending strength of aged asphalt mortar beams is 4.7 MPa, which is lower than the strength of fresh ones (5.4 MPa). This indicates that the laboratory ageing process decreases the bending strength of asphalt mortar beams. Figure 5.17 also indicates that the first healing strength of beams with capsules are significantly higher than the reference beams, which shows a different trend than the results on

fresh beams. This is because the healing effect from capsules stands out as the asphalt mortar mixture lost its intrinsic healing capacity during the ageing process.

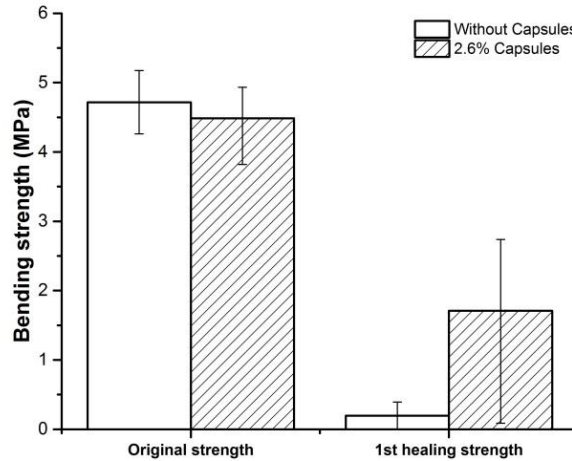


Figure 5.17: Bending strength of the aged asphalt mortar beams

### 5.3.2.3. RESULTS FOR SEMI-CIRCULAR BENDING TEST ON POROUS ASPHALT CONCRETE SAMPLES

The fracture toughness of the SCB specimens, which directly represents the ability for the fracture resistance, are presented in Figure 5.18. In general, both groups of SCB specimens show similar fracture toughness in the first SCB tests, however, SCB specimens with 7% calcium alginate capsules show slightly higher fracture toughness than reference specimens in the second and third bending tests, which indicates that with calcium alginate capsules, the SCB specimens are able to gain a higher toughness from healing. The initial fracture toughness of both types of the mix is much higher than the fracture toughness from second and third SCB tests, which means the 20-hour healing period is not able to provide significant healing for all specimens. It might be because not all the accumulated damages in test samples can be effectively self-healed [9], such as damages on aggregates from the bendings and cracks located out of the effective healing region of capsules.

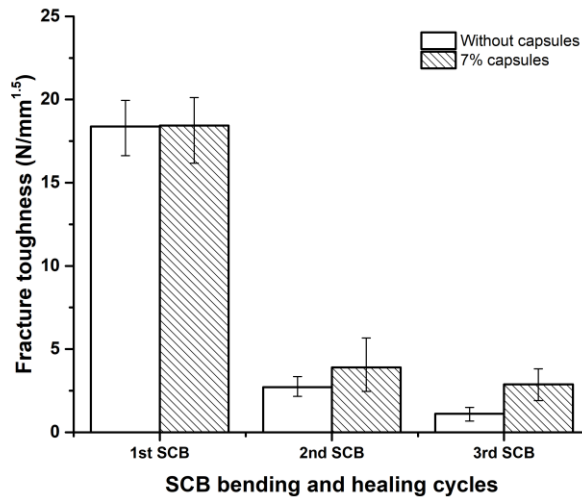


Figure 5.18: Fracture toughness of SCB specimens.

Figure 5.19 presents the fracture energy results from SCB tests. The fracture energy calculation considers the area beneath the load-displacement curve, which is indicative of fracture resistance in the whole testing process from the initiation of crack to the failure of the sample. Similar to the fracture toughness, the first SCB test results are very close, nevertheless, SCB specimens with capsules consume significantly higher energy than reference specimens in both second and third SCB tests. It might be because the encapsulated rejuvenator was released upon fracture, wetted the fracture face and generated more bonds than reference specimens. Hence the SCB specimens with capsules gained more energy during the rest period and showed more healing than reference samples.

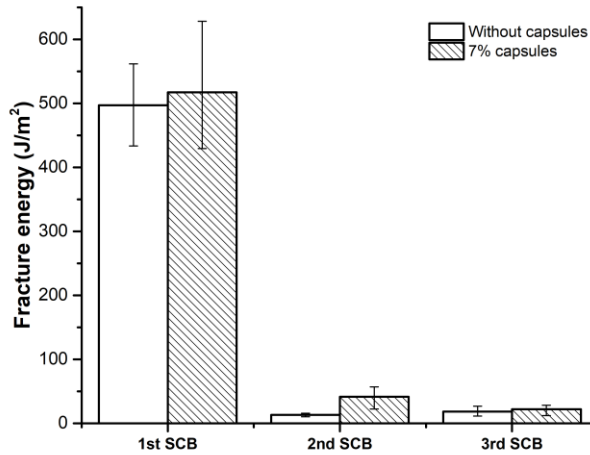


Figure 5.19: Fracture energy of SCB specimens.

### 5.3.3. HEALING EFFICIENCY

#### 5.3.3.1. CAPSULE HEALING EFFECT IN ASPHALT MASTIC

The healing efficiency of the capsules investigated with the 3PB testing and healing programme is presented in Figure 5.20. Because of the intrinsic healing capacity, asphalt mastic beams without capsules are able to recover 75.7% of the original strength in the first healing and 50.0% in the second healing. While with capsules, this healing effect is improved significantly. Addition of 2% capsules, the healing index reaches 90.1% after the first healing and 76.4% after the second. However, the addition of 4% capsules shows less healing effect than 2%, in which the healing index is 81.7% and 73.2% for the two healing stages. These test results demonstrate that the addition of calcium alginate capsules with encapsulated rejuvenator significantly increases the healing efficiency of asphalt mastic. However, to achieve an optimal healing rate of the asphalt mastic mix containing calcium alginate capsules encapsulating rejuvenator, the optimum volume of capsule needs to be determined.

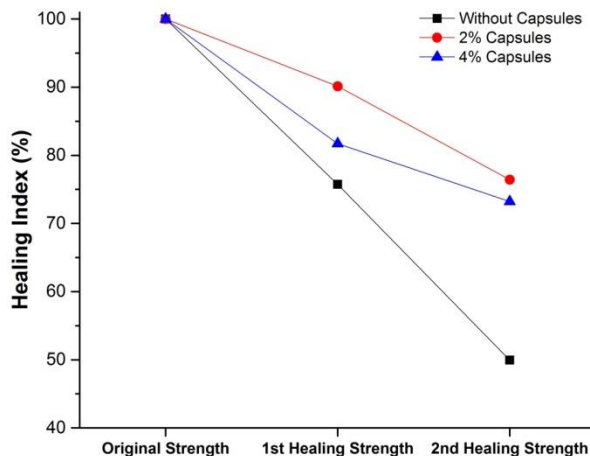


Figure 5.20: Healing index of asphalt mastic beams.

#### 5.3.3.2. CAPSULE HEALING EFFECT IN ASPHALT MORTAR

The bending strength results in Figure 5.16 indicated that, for all mortar beam types, the bending strength decreases after each bending and healing cycle, which indicates that the self-healing effect of the asphalt mortar beams cannot achieve full recovery of strength since the fractured area is prone to crack even after the healing process.

Figure 5.21 shows that after ageing, the asphalt mortar mixture loses most of its healing capacity as the mortar beams without capsules only regain strength of 0.2 MPa (4% of the original strength) during the first healing period. Nevertheless, with calcium alginate capsules encapsulating rejuvenator, the beams recover strength of 1.7 MPa (40% of the original strength) during first healing. This is because the ageing of asphalt mortar greatly decreases its healing capacity, and the aged material could not sufficiently reconnect and provide a sufficient bond between the fracture surfaces. However, with capsules, the encapsulated asphalt rejuvenator can be released when the crack propagates through the capsules which allows localized healing around the broken capsules on the fracture surfaces. Thus, the PA mortar beams with calcium alginate capsules could regain a strength significantly higher than the reference ones.

The bending and healing cycles were intended to be repeated again to measure the second healing strength for the aged beams with calcium alginate capsule

healing system. However, the cycle was not successful as all aged beams could not regain any strength after the second healing process, which indicates the limitation of the calcium alginate capsules healing system that could only be effective in 2 testing cycles for aged PA mortar beams.

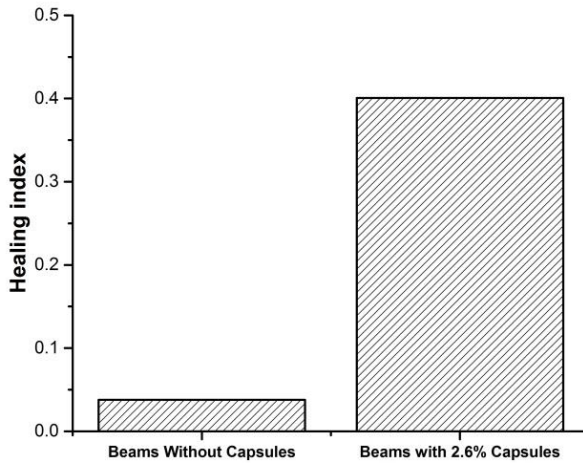


Figure 5.21: Healing index of asphalt mortar beam specimens.

### 5.3.3.3. CAPSULE HEALING EFFECT IN POROUS ASPHALT CONCRETE

The healing efficiency was evaluated by the peak load healing ratio during rest periods. The healing results are presented in Figure 5.22. The results show that the SCB specimens with capsules are able to restore 19.3% of the initial peak load, which is 6% higher than the specimens without capsules. In the third SCB tests, SCB specimens with capsules can still achieve a healing ratio of 14.3%. Without capsules, the healing effect is only 9.9%. Figure 5.22 also illustrates that even with calcium alginate capsules, the healing effect on such a serious fracture is very limited. Although the application of calcium alginate capsules largely improved the healing capacity, the limitation of these capsules as well as other rejuvenation methods lies in the damage level. The calcium alginate capsules are more capable of micro-crack healing, aimed to close crack at an early stage thus preventing serious defects in asphalt pavement. In this way, the calcium alginate capsules possess a healing potential in the application in the construction field.

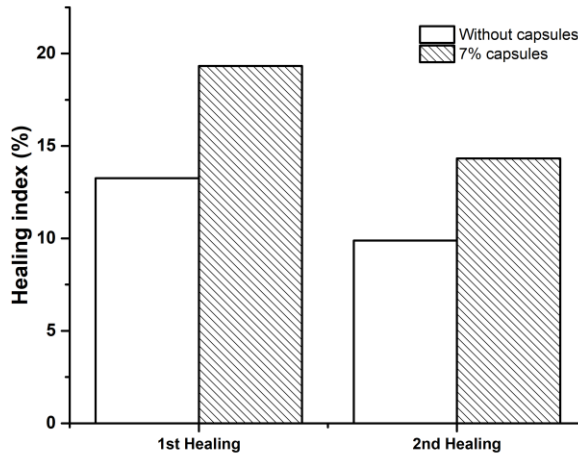


Figure 5.22: Healing index of SCB specimens.

## 5.4. CONCLUSIONS

This chapter presents the evaluation of the calcium alginate capsules healing system in the asphalt mixture. In total three mixture types were tested and conclusions can be drawn as follows:

- The presence of calcium alginate capsules on the fracture surfaces of both beam samples and semi-circular samples indicates that calcium alginate capsules are able to fracture upon the propagation of cracks. Thus, the encapsulated rejuvenator is released to heal the damage site. The presence of capsules in original shape and the witness of the releasing rejuvenator from capsules at fracture faces demonstrate that the calcium alginate capsules are able to survive the asphalt production, compaction and even the oven ageing process.
- The results from the 3PB tests and SCB tests have shown that the calcium alginate capsules have an effect on the mechanical resistance of different asphalt mix. The 3PB testing results for asphalt mastic beams show that calcium alginate capsules have a reinforcing effect by increasing the strength of asphalt mastic by 17%. However, the asphalt mortar beams with or without capsules do not show a significant difference in initial bending strength,

which means calcium alginate, the encapsulation material of these capsules, hardly has a significant contribution to the bending strength of asphalt mortar beams. While the reinforcing effect of the capsules can be found from the SCB testing results for PA samples. In summary, incorporation of calcium alginate capsules in an asphalt mixture could improve its fracture resistance, but this reinforcing effect from capsules can be various depending on the gradations of the target mixture.

- Asphalt ageing has a significant impact on the calcium alginate capsule healing system. Without ageing process, the asphalt mortar beams demonstrated similar bending strengths for all mortar mixture types at each testing cycle, which indicates that the intrinsic healing capacity of the asphalt mortar is relatively high and plays the main role in the healing process of asphalt mortar samples. However, in the aged asphalt mortar beams, the samples with the calcium alginate capsules healing system showed a healing index of 40%, which is much higher than those without capsules. As such, the healing effect of the capsule healing system is largely influenced by the ageing level of the target asphalt mixture and it only effectively contributes to the healing capacity of an aged asphalt mix.
- The healing effect of calcium alginate capsules has been demonstrated in the asphalt mastic, the asphalt mortar and the porous asphalt concrete, which indicates that the capsules are capable of local crack healing, and can increase the healing capacity of an asphalt mix. However, the different healing effects for three types of mixture indicate the impact of mixture gradations to the healing efficiency of the capsule healing system, which agrees with the findings from existing research [7, 9].

In summary, the potential use of calcium alginate capsules in porous asphalt mixture has been explored and the results proved that these capsules can help improve the healing capacity of asphalt mixture and thus prolong its service life. As a healing method in asphalt pavement, the efficiency of the calcium alginate capsules healing system is not as high as the efficiency of the induction heating [10], but the capsule healing system aims at the rejuvenation of the aged binder which may provide a more sustainable option for the asphalt pavement systems. Hence, the calcium alginate capsules hold potential for the development of the combined self-healing asphalt technology in cooperation with the induction heating method, which will be presented in Chapter 6.

## REFERENCES

- [1] M.F. Woldekidan, Response modelling of bitumen, bituminous mastic and mortar, (2011).
- [2] A. Klomp, Life period of porous asphalt, Dutch Road and Hydraulic Engineering Institute report (1996).
- [3] RAW, Standaard RAW Bepalingen 2005, RAW, Ede, 2005.
- [4] P.M. Muraya, Permanent deformation of asphalt mixes, (2007).
- [5] A. Tabaković, W. Post, D. Cantero, O. Copuroglu, S. Garcia, E. Schlangen, The reinforcement and healing of asphalt mastic mixtures by rejuvenator encapsulation in alginate compartmented fibres, *Smart Materials and Structures* 25(8) (2016) 084003.
- [6] R. Jing, Ageing of bituminous materials: Experimental and numerical characterization, Delft University of Technology, 2019.
- [7] J. Qiu, Self healing of asphalt mixtures: towards a better understanding of the mechanism, Delft University of Technology, 2012.
- [8] B. Xue, H. Wang, J. Pei, R. Li, J. Zhang, Z. Fan, Study on self-healing microcapsule containing rejuvenator for asphalt, *Construction and Building Materials* 135 (2017) 641-649.
- [9] A. Tabaković, E. Schlangen, Self-healing technology for asphalt pavements, *Self-healing Materials*, Springer2015, pp. 285-306.
- [10] Q. Liu, E. Schlangen, M. van de Ven, Induction healing of porous asphalt concrete beams on an elastic foundation, *Journal of Materials in Civil Engineering* 25(7) (2012) 880-885.



# 6

## SELF-HEALING SYSTEM EVALUATION IN POROUS ASPHALT

*It is demonstrated that the healing capacity of an asphalt mix can be improved with the utilization of calcium alginate capsules. However, this healing effect does not contribute to a significant damage recovery in asphalt mix, and incorporation of the induction healing system becomes a potential solution. This chapter describes development of the combined healing system which is based on the calcium alginate capsules encapsulating rejuvenator (see chapter 4) and the induction heating approach. The combined healing system is evaluated in the porous asphalt mix and compared with other asphalt healing systems: the capsule healing system, the induction healing system and a reference system without an extrinsic healing method. The results indicate that, the combined healing system has a significant advantage over the other single healing systems in both crack healing and fatigue damage recovery.*

## 6.1. INTRODUCTION

In PA, more than 90% of the distress are initiated by the micro-cracks within asphalt mastic, which means, majority of the damage in PA can be healed with self-healing technologies [1]. As extrinsic healing technologies, both the calcium alginate capsules encapsulating rejuvenator and the induction heating have demonstrated their potential to improve the healing capacity of asphalt pavement [2, 3]. However, both technologies have shown disadvantages, for example: the embedded capsules are capable of aged bitumen rejuvenation however its crack healing abilities within PA are limited and require a long time (20 hours) [4], while the induction heating is a very efficient PA damage healing system, but it does not prevent ageing and with that, the ability to repair damage will decrease in time [5]. It is expected that a hybrid healing system which combines both capsule healing and induction heating should have not only diverse healing mechanisms including aged binder rejuvenation and crack healing, but also an enhanced healing behaviour from their synergistic effects.

To this aim, this chapter introduces the development of a novel combined asphalt self-healing system, in which induction heating serves as the asphalt damage repair mechanism, requiring just 2 minutes heating time and encapsulated rejuvenator will replenish (rejuvenate) aged asphalt binder and reinstate bitumen's healing ability. Moreover, the increased temperature from induction heating could, in turn, accelerate the diffusion process of the released rejuvenator into aged bitumen. The process will involve the insertion of both microcapsules encapsulating rejuvenator and steel fibres into the PA mix.

In this chapter, four different self-healing systems were studied in PA, namely the capsule healing system, the induction heating system, the combined healing system and a reference system without an extrinsic healing method. X-ray computed tomography (XCT) was employed to visualize the distribution of capsules and/or fibres in PA samples with various healing systems.

A laboratory ageing procedure was followed to simulate the condition when healing was needed (after years of serving), and the ageing effect was evaluated by dynamic shear rheometer (DSR) on the extracted binder from PA sample. The indirect tensile test (ITT) including indirect tensile stiffness modulus (ITSM) test and indirect tensile strength (ITS) test was employed to investigate the mechanical properties of asphalt with various healing systems. The cracking resistance of the PA samples was studied using semi-circular bending (SCB) test, and an SCB damaging and healing programme was carried out to evaluate the crack healing efficiency of various healing systems. The fatigue behaviour of PA with various healing systems was studied using the indirect tensile fatigue (ITF) test and four-point bending (4PB)

fatigue test. A 4PB fatigue damaging and healing programme was carried out to evaluate the fatigue damage healing efficiency of various healing systems. In general, the research methodology adopted in this chapter is summarised in Figure 3.3: Schematic of the research methodology for the rejuvenator study.

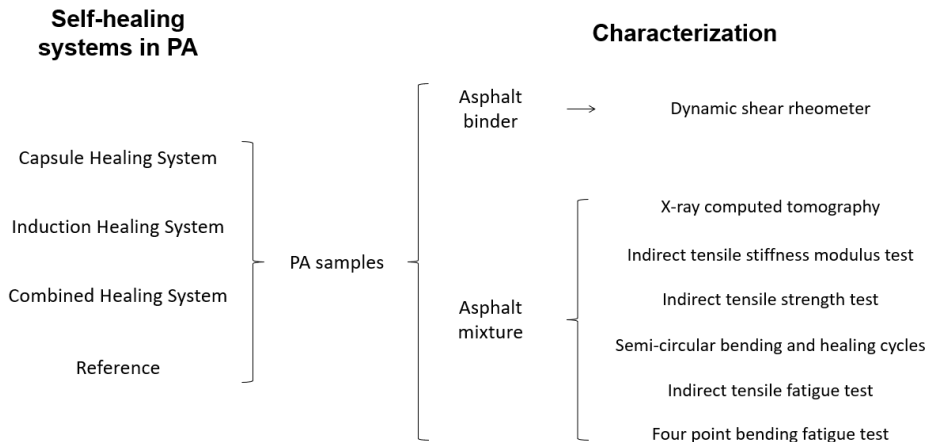


Figure 6.1: The research methodology for self-healing systems evaluation in porous asphalt.

## 6.2. MATERIALS AND METHODS

### 6.2.1. MIXTURE DESIGN AND SAMPLE PREPARATION

#### 6.2.1.1. MATERIALS AND POROUS ASPHALT MIXTURE DESIGN

The calcium alginate capsules and the steel fibres used to build the self-healing systems in PA are shown in Figure 6.2. Aimed to improve the conductivity of PA to achieve induction healing, the steel fibres were used in the induction healing system and combined healing system. The steel fibres with the density of  $7.6 \text{ g/cm}^3$ , an average length of 1.4 mm, the diameter of  $40 \text{ }\mu\text{m}$  and the resistivity of  $7 \times 10^{-7} \Omega \cdot \text{cm}$  were provided by Heijmans Infra BV, Rosmalen, Netherlands.

The calcium alginate capsules encapsulating rejuvenator introduced in Chapter 4 were used in the capsule healing system and the combined healing system. The compositions and the manufacture details of these calcium alginate capsules can be

found in Chapter 4. The calcium alginate capsules are designed to release the rejuvenator upon crack hitting the capsule, thus the capsule healing system can repair damage on demand. Other prospective rejuvenator releasing mechanisms include:

- Squeezing the capsule from fatigue loadings, which will be more significant when bitumen get aged;
- Diffusion of the rejuvenator out of the capsule, which will be faster when temperature increased (induction heated).



Figure 6.2: Steel fibres and calcium alginate capsules used in self-healing porous asphalt.

The PA mix was designed following the Netherlands porous asphalt standard PA 0/11. In total four types of asphalt mix with different healing systems were designed, including capsule healing system mix, induction healing system mix, combined healing system mix and a reference mix (without extrinsic healing system). Table 1 summarises the mix composition of the PA with the different healing systems. In the induction healing system and combined healing system, steel fibres were added as 6% extra volume of bitumen. In the capsule healing system and combined healing system, calcium alginate capsules were added to replace 7% the volume of bitumen.

Table 6.1: The mix compositions of PA.

Mix Constituent	% Content in Mix			Reference
	Capsule healing system	Induction healing system	Combined healing system	
16 mm	8.14	7.97	8.00	8.14
11.2 mm	63.28	62.00	62.21	63.31
8 mm	8.14	7.97	8.00	8.14
5.6 mm	1.82	1.78	1.79	1.82
2 mm	6.61	6.47	6.49	6.61
500 $\mu\text{m}$	2.11	2.06	2.07	2.11
180 $\mu\text{m}$	0.67	0.66	0.66	0.67
125 $\mu\text{m}$	0.67	0.66	0.66	0.67
63 $\mu\text{m}$	4.31	4.22	4.23	4.31
Bitumen (70/100)	3.92	4.32	3.85	4.21
Capsules	0.34	-	0.34	-
Steel Fibres	-	1.88	1.70	-

### 6.2.1.2. ASPHALT SLAB MAKING, LABORATORY AGEING AND SAMPLE CUTTING

The PA slab fabrication process is described in section 5.2.5. Two types of PA slab were fabricated for the study of various healing systems in which Slab\_type\_1 has the dimensions of  $50 \times 50 \times 5$  cm and Slab\_type\_2 has the dimensions of  $60 \times 40 \times 8$  cm. The Slab\_type\_1 was mainly used for the drilling of cylinder samples. The drilled cylinder samples have a diameter of 100 mm and a height of 50 mm which can be used for ITSM, ITS and ITF tests. The cylinder samples can also be further cut into semi-circular samples (as introduced in 5.2.6) for the SCB tests. The Slab\_type\_2 was used to produce beam samples for the 4PB fatigue tests with the dimensions of  $50 \times 50 \times 400$  mm.

After compaction, a laboratory ageing process (described in section 5.2.2) was performed on PA slabs to simulate the condition when healing was needed (after years of serving). Hence, based on the ageing levels and the built-in healing systems, 5 different PA groups are derived, and the detailed group information is presented in Table 6.2. Noted that the 'fresh mixture' means no extra laboratory ageing process was added to the group of samples, while the 'aged mixture' means an extra laboratory ageing process was added to the group of samples. It is also noted that 'No healing' refers to the reference mix.

Table 6.2: PA samples group information.

Sample group name	Laboratory ageing	Built-in healing systems
Induction healing (fresh mixture)	No	Induction
Capsule healing (aged mixture)	Yes	Capsules
Induction healing (aged mixture)	Yes	Induction
Combined healing (aged mixture)	Yes	Capsules and induction
No healing (aged mixture)	Yes	None

Figure 6.3 shows schematic diagrams of the detailed test sample drilling/cutting process. As shown in Figure 6.3, minimum nine PA cylinders were drilled from a Slab\_type\_1 and four PA beams were cut from a Slab\_type\_2. During the drilling/cutting process, the edge 5 cm of the slabs (the light grey area) is ignored to avoid edge effect from the compaction process.

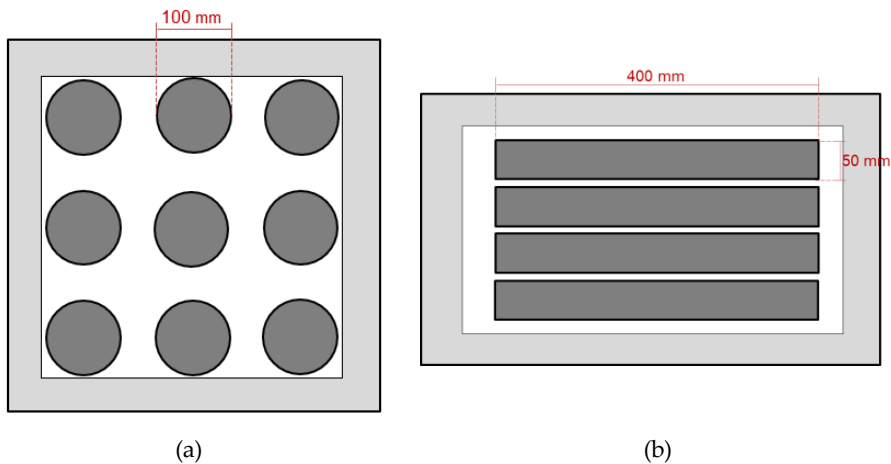


Figure 6.3: Cylinder and beam samples' detailed drilling/cutting schematic: (a) cylinder samples drilled from Slab\_type\_1 and (b) beam samples cut from Slab\_type\_2.

## 6.2.2. ASPHALT BINDER AND MIXTURE CHARACTERIZATION

### 6.2.2.1. MATERIALS DISTRIBUTION STUDY USING X-RAY COMPUTED TOMOGRAPHY

The X-ray computed tomography (XCT) was employed to visualize the capsule and/or fibre distribution within the PA mix. The test will also show whether the capsules can survive the asphalt production process. To this aim, PA cylinder samples

with 33.5 mm in diameter and 48.5 mm in height were drilled from slabs and prepared for XCT scanning. Figure 6.4 shows the Phoenix Nanotom CT scanner (Baker Hughes, Wunstorf, Germany) which was employed to conduct the scans at a resolution of 20  $\mu\text{m}$ .

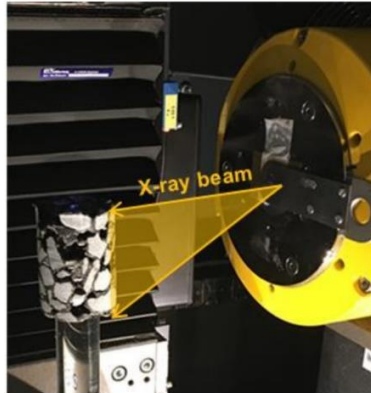


Figure 6.4: XCT scanning system for PA cylinder samples.

#### 6.2.2.2. LABORATORY AGEING EFFECT EVALUATION

DSR testing procedure following the European standard EN 14770 was employed to study the laboratory ageing effect by investigating the change of the rheological properties of bitumen from asphalt ageing [6, 7]. For this purpose, the bitumen samples were extracted from the reference mix before and after laboratory ageing process, and their complex modulus and phase angle were tested.

Figure 6.5 shows the collection process of the PA mixture samples. First, the semi-circular asphalt mix was sawn into four slides (Figure 6.5 (a)) and each slide has a thickness of around 10 mm (Figure 6.5 (b)). Then, a PA slide was peeled into small pieces and collected with a container (Figure 6.5 (c)). Afterwards, the bitumen samples were extracted from the small pieces using Dichloromethane and the extraction process followed the same procedure as Jing [8].

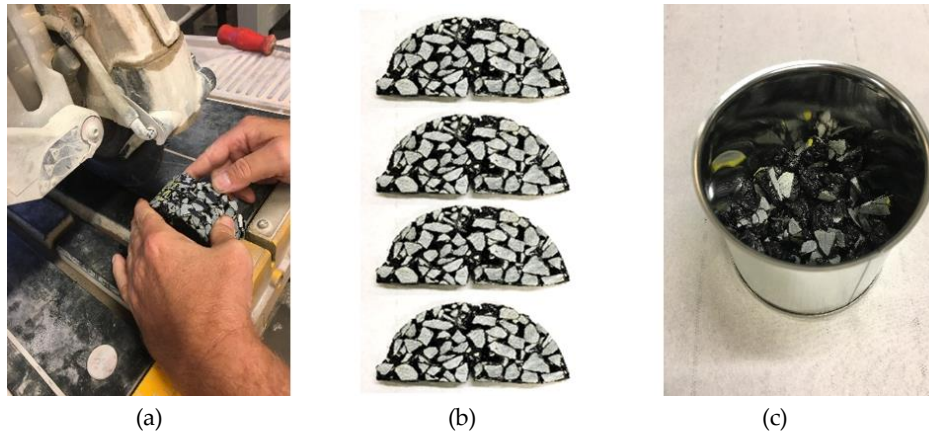


Figure 6.5: PA mixture samples collection process: (a) sawing of the semi-circular into slides, (b) sawed PA slides and (c) collected pieces from the PA slide.

A dynamic shear rheometer (Anton Paar, Graz, Austria) was used to study the rheological properties of the extracted bitumen samples. The frequency sweep tests were performed at the temperature of 0, 10, 20, 30 and 40°C using a range of frequency sweep from 0.01 Hz to 50 Hz. Finally, the master curves of complex shear modulus ( $G^*$ ) and phase angle ( $\delta$ ) were generated at the reference temperature of 20°C based on the Time-Temperature Superposition principle.

### 6.2.3. MECHANICAL PROPERTY TESTS

#### 6.2.3.1. INDIRECT TENSILE TEST

ITT was employed to investigate the mechanical properties of asphalt from all five testing groups. Cylinders with a diameter of 100 mm and a height of 50 mm were tested with both non-destructive ITSM test following the European standard EN 12697-26 and destructive ITS test following the European standard EN 12697-23. Figure 6.6 shows the ITT set up, which was used for ITSM, ITS and ITF tests. A Universal Testing Machine (Industrial process controls LTD, Melbourne, Australia) with a maximum load of 5 kN (UTM 5) with a temperature chamber was employed for the ITT test. As shown in Figure 6.6, a pair of displacement transducers are placed on the front and back of the cylinder sample to measure its horizontal deformation upon vertical loading(s). The cylinder sample is clamped from both sides to ensure the sample and the transducers are not moving during the test.

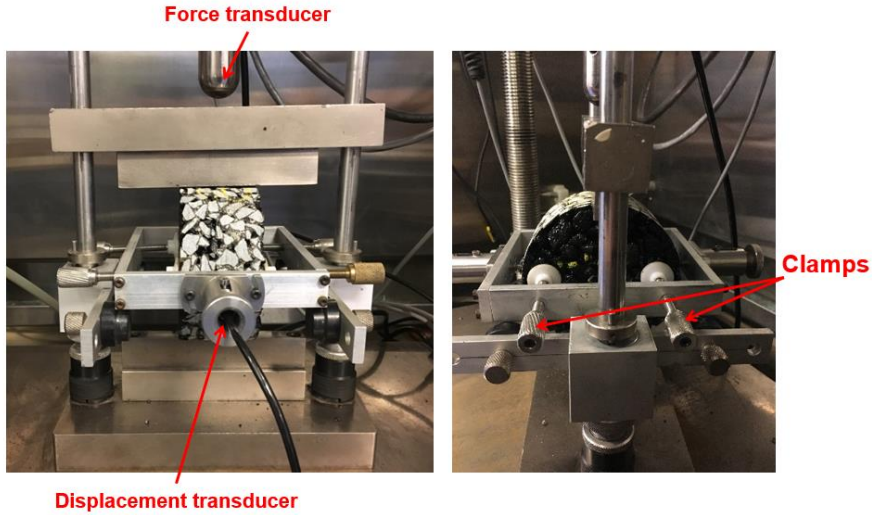


Figure 6.6: ITT testing setups (used for ITSM, ITS and ITF tests).

The ITSM and ITS could be calculated using the following equations:

$$ITSM = \frac{F(v + 0.27)}{Zt} \quad (6.1)$$

Where

$ITSM$  is the indirect tensile stiffness modulus (MPa);

$F$  is the maximum vertical load (N);

$v$  is the Poisson's ratio;

$Z$  is the amplitude of the horizontal deformation during the load cycle (mm).

$t$  is the thickness of the specimen (mm).

$$ITS = \frac{2P}{\pi DH} \times 1000 \quad (6.2)$$

Where

$ITS$  is the indirect tensile strength (kPa);

$P$  is the peak load (N);

$D$  is the diameter of specimen (mm);

$H$  is the height of the specimen (mm).

In this chapter, the indirect tensile stiffness modulus tests were performed at 20°C at four different frequencies (8 Hz, 4 Hz, 2 Hz and 1 Hz). The Poisson's ratio of

0.22 was assumed for this porous asphalt. The indirect tensile strength tests were performed by UTM at 5°C with a loading speed of 0.85 mm/s.

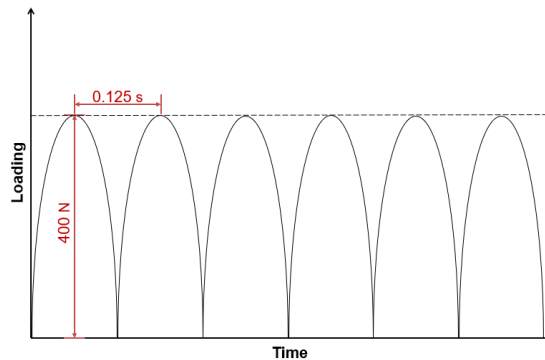
### 6.2.3.2. SEMI-CIRCULAR BENDING TEST

In order to investigate the fracture resistance of PA with various healing systems, the SCB tests were performed following the European standard EN 12697-44. The fracture toughness and the crack healing index were calculated from the SCB test data and the detailed test procedure is described in the section 5.2.6.

### 6.2.4. FATIGUE PROPERTY TESTS

#### 6.2.4.1. INDIRECT TENSILE FATIGUE TEST

ITF tests aim to evaluate the fatigue life of a PA sample by recording the total number of continuous loading cycles that the sample can bear, and the loading mode is selected as stress control. Figure 6.7 (a) shows the loading configuration schematic for ITF tests. Following the European standard EN 12697-24:2018, the ITF tests were carried out by applying a continuous haversine fatigue loadings with a peak value of 400N and the loading frequency of 8 Hz. The ITF tests were performed in a temperature chamber of 5°C to avoid permanent deformation upon loadings. The tests were terminated at the point of the full failure and the number of fatigue loadings leads to the sample failure was recorded. Figure 6.7 (b) shows the data acquired from the ITF fatigue test, where the red dash-line in the graph shows the maximum number of ITF which indicates the fatigue life of the test specimen.



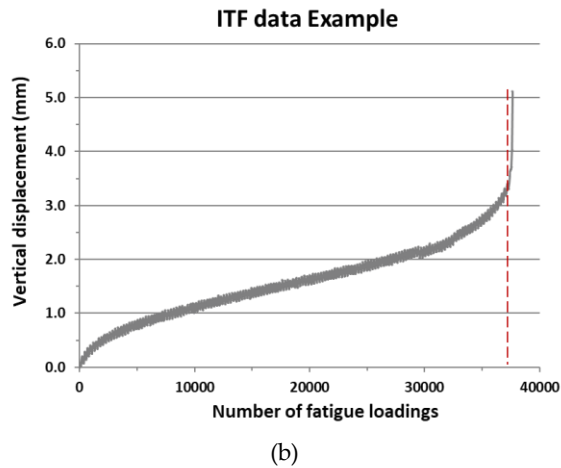


Figure 6.7: The ITF test: (a) the loading configuration schematic and (b) ITF test data example, where the red dash-line indicates the fatigue life.

#### 6.2.4.2. FOUR POINT BENDING FATIGUE TEST

During the service life of asphalt pavement, the asphalt layer will be subjected to a high number of bending loads which leads to fatigue damage, and 4PB test is regarded as the most representative laboratory method which can be used to determine the fatigue performance of an asphalt under controlled bending loads [9, 10]. In this chapter, 4PB test aims to investigate the fatigue behaviour of PA beams incorporating various extrinsic healing systems under strain-controlled fatigue loadings. The 4PB test can also be used to evaluate the healing capacity of the PA beams when the rest period is included [11].

Figure 6.8 shows the 4PB fatigue test samples, test setup and loading configuration. Figure 6.8 (a) shows the testing beams kept on a plain wooden board and stored in the storage room at 5°C. Figure 6.8 (b) shows the 4PB testing setup where the middle of the beam is subjected to a continuous sine shaped loading by the inner two clamps with strain control. Figure 6.8 (c) shows the schematic of the 4PB test schematic and Figure 6.8 (d) shows the loading configuration in which the loading frequency is 8 Hz. The 4PB fatigue tests were performed in a temperature chamber of 20°C and the maximum strain is set as 400  $\mu\epsilon$ . The number of load cycles, at which it decreases to 50% of the initial stiffness modulus, is regarded as the judgment standard of the fatigue test (EN 12697-24).

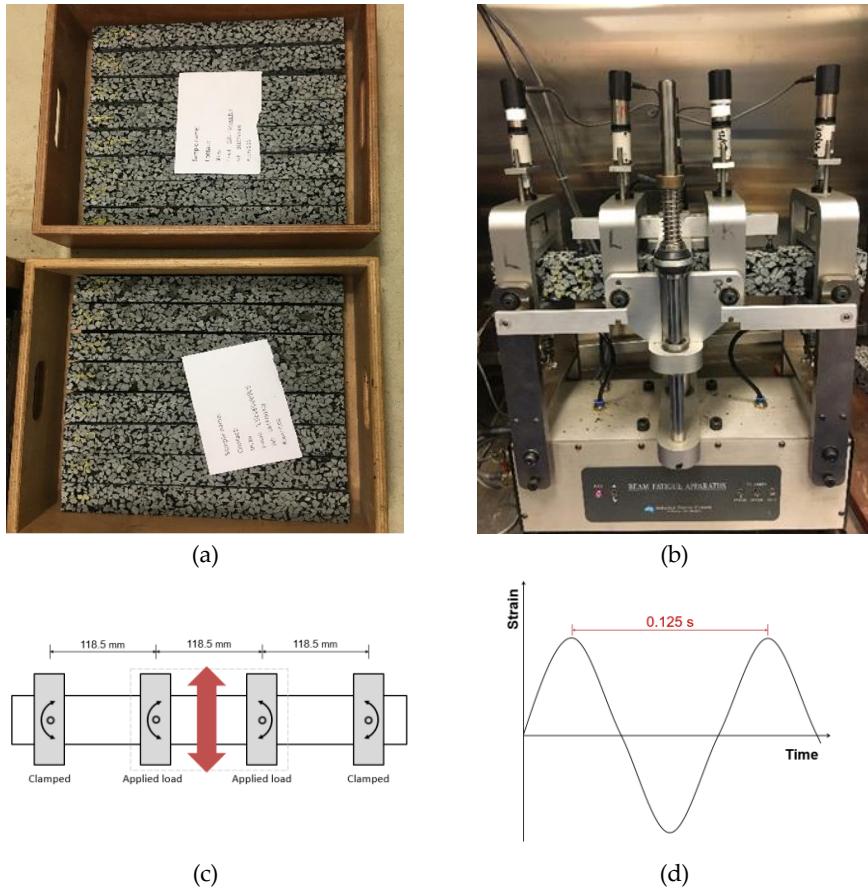


Figure 6.8: 4PB fatigue test: (a) beam samples, (b) 4PB testing schematic, (c) testing setup and (d) loading configuration.

During a 4PB fatigue test, the changes in flexural stiffness of the beam specimen are recorded with the increase of fatigue loadings. Figure 6.9 shows the data acquired from the 4PB fatigue test, which shows the measured flexural stiffness with time. The red dash-line in the graph shows the average decreasing rate of the flexural stiffness whose slope indicates the damage rate ( $D$ ) of the beam specimen. The damage rate ( $D$ ) in a 4PB fatigue test indicates the average decreasing rate of the flexural stiffness of a beam specimen, which means a higher damage rate results in a faster damaging process, therefore shows a lower fatigue resistance. The damage rate of a 4PB test considers both the change in stiffness and the time it takes to make this change, which provides a more comprehensive method to illustrate 4PB fatigue behaviour. The following equations can be used for the calculation of the damage rate ( $D$ ):

$$S_t = \frac{S_0}{2} \quad (6.3)$$

$$t = \frac{N_f}{f} \quad (6.4)$$

$$D = \frac{S_0 - S_t}{t} = \frac{4S_0}{N_f} \quad (6.5)$$

Where:

$S_0$  is the initial flexural stiffness (MPa);

$S_t$  is 50% of the initial flexural stiffness at time  $t$  (MPa) ;

$t$  is the time to reach 50% of the initial flexural stiffness (s);

$N_f$  is the number of loadings to reach 50% of the initial flexural stiffness;

$f$  is fatigue loading frequency which is 8 Hz;

$D$  is the damage rate (MPa/s).

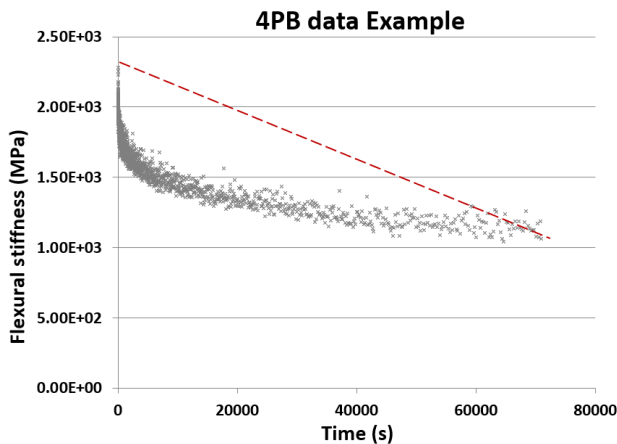


Figure 6.9: 4PB test data example, where the slope of the red dash-line shows the damage rate.

The total number of fatigue loadings ( $N_f$ ), the flexural stiffness ( $S$ ), and the damage rate ( $D$ ) are the key parameters that are used to illustrate the fatigue life, stability and fatigue resistance of the beam specimens in 4PB fatigue test, respectively.

## 6.2.5. HEALING PROCEDURE DESIGN AND HEALING EFFICIENCY EVALUATION

### 6.2.5.1. HEALING PROCEDURE DESIGN

The general principle of the extrinsic healing technology for self-healing asphalt lies in changing the rheology property of the asphalt binder to accelerate the damage healing process, by either increasing the temperature (induction heating) and/or rejuvenating the aged material (capsule healing). Nevertheless, the healing effect is largely affected by the rest period as well as the provided environmental conditions such as time, temperature, humidity, etc. The effect of a rest period in asphalt healing has been proved by the service life extension of asphalt in both laboratory testing and field application [12, 13]. As such, it is important to design a proper healing procedure for each healing system to ensure the results of healing effect are reasonable, feasible and comparable.

To this aim, a 24-hour-rest period is designed which is illustrated in Figure 6.10. The rest period begins with a 20 hours healing period where the majority of healing actions take place by activating the built-in healing system so that the damage healing process is largely accelerated.

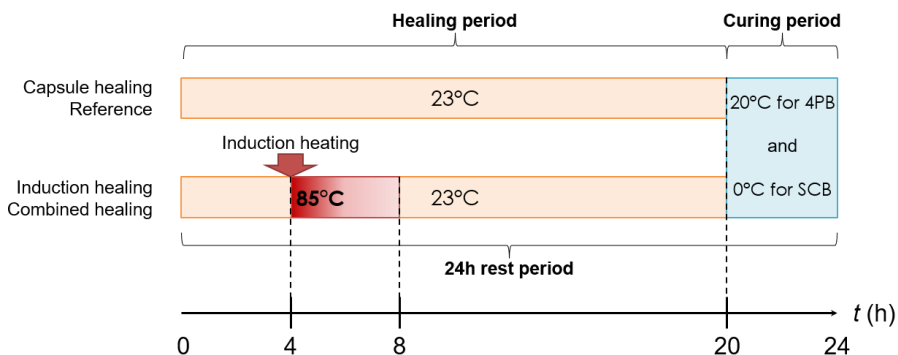


Figure 6.10: The 24-hour-rest period for the healing of various healing systems.

Figure 6.10 shows that, for the healing of damaged samples with the capsule healing system and without healing system, the whole healing period is conditioned in a temperature chamber at 23°C on a plain surface. However, for the healing of damaged samples with the induction heating system and the combined healing system, the first 4 hours is conditioned at 23°C to allow the damaged sample to reach the ambient temperature. After that, the induction heating is applied to increase the sample's surface temperature to 85°C (see section 6.2.5.3) and then followed by a 16

hours period conditioned in the temperature chamber at 23°C to cool down and be further healed.

After the healing period, the sample is cured in a temperature chamber for 4 hours to meet the temperature for the next testing round. In order to evaluate the healing efficiency of PA samples from each testing group, the SCB test and the 4PB fatigue test are selected to investigate the crack healing behaviour and the fatigue damage healing behaviour, respectively. Furthermore, two testing and healing programmes are designed based on the SCB test and the 4PB fatigue test independently.

#### 6.2.5.2. CONFINING SETUPS FOR THE HEALING PROCESS

In order to avoid permanent deformation during the healing process, especially for induction heating which would heat the sample to 85°C, constant confinement is created for all samples throughout the 24-hour-rest period.

For the semi-circular specimen damaged from SCB test, the confinement is also used to ensure the close of cracked surfaces as introduced in 5.2.7.2. Figure 6.11 shows the healing of SCB specimens wrapped with tapes. Figure 6.11 (a) shows the wrapped SCB specimens were carefully placed on a plain surface in a temperature chamber. Figure 6.11 (b) and (c) show the induction heating was added on SCB specimen wrapped with tapes.

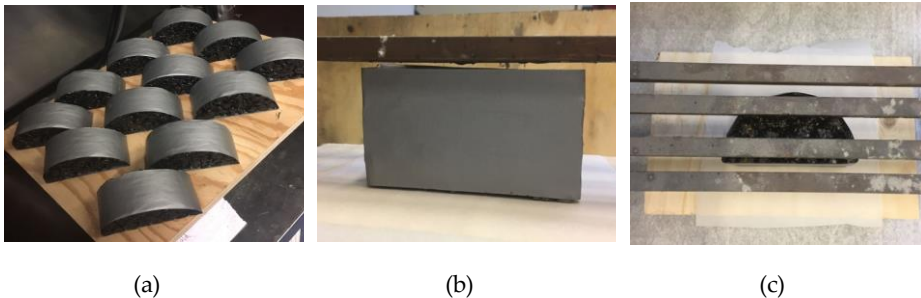


Figure 6.11: Damaged SCB specimens wrapped with tapes: (a) placed in a temperature chamber, (b) front view under the induction coil and (c) top view under the induction coil.

The beam specimens require extra care and more stable confinement for the 4PB fatigue test not only because their larger dimensions make them prone to raveling or even loss of particles during induction heating, transportation and long-term resting process, but also due to the 4PB fatigue test is sensitive to the deformations of the tested specimen. Hence, wooden boxes are designed to provide the confinement for beam specimens for their 24-hour-rest period. The confining process for

beam specimen is presented in Figure 6.12. Figure 6.12 (a) shows that the PA beam specimen is placed in the corner of a wooden frame fixed on three sides first. Afterwards, a wooden bar is added to cover the front side of the beam and a piece of wood with a suitable size is placed at the right side of the beam (Figure 6.12 (b)). Finally, the wooden box is wrapped with tapes to ensure the adjustable two pieces of wood are closely touched with the beam sample (Figure 6.12 (c)). Figure 6.12 (d) shows the image of a beam specimen confined in the wooden box.

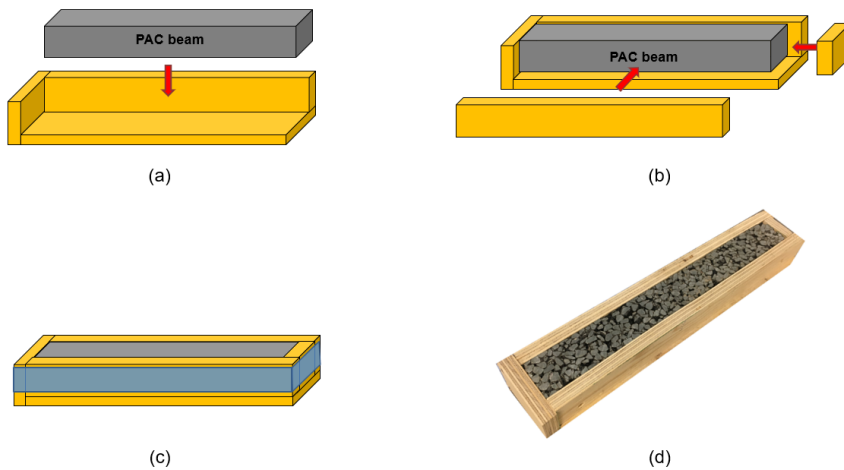


Figure 6.12: The adjustable wooden box for the confining of beam specimen: (a), (b) and (c) shows the schematic confining process for a beam specimen, while (d) shows the image of a beam specimen confined in the wooden box.

### 6.2.5.3. INDUCTION HEATING ON DAMAGED SAMPLES

For the healing of damaged specimens with the induction healing system and combined healing system, an induction heating is applied at the 4<sup>th</sup> hour during the 24-hour-rest period with an induction machine which has a capacity of 50 kW and at a frequency of 70 kHz. An infrared camera was used to monitor the whole induction healing process to control the induction healing process and avoid overheating on SCB specimens.

Figure 6.13 shows the SCB specimen used for the induction heating temperature distribution study. Figure 6.13 (a) shows the top view of the SCB specimen under the induction coil. The distance between the induction coil and the healing specimen was kept at 5 mm (Figure 6.13 (b)). In order to achieve effective healing on the specimen, the induction heating temperature was carefully controlled to reach 85°C

(Figure 6.13 (c)), which is regarded as the optimum temperature for induction heating [3].

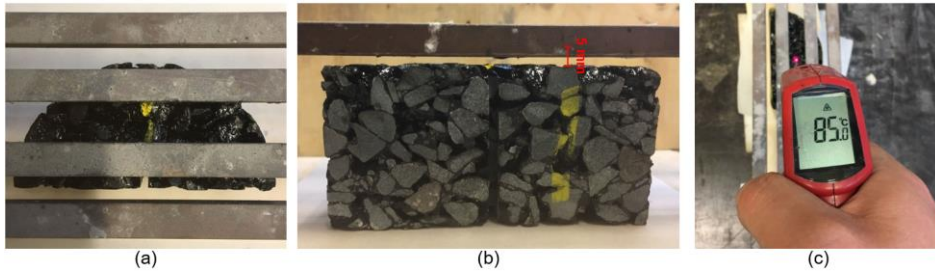


Figure 6.13: A SCB sample under the induction coil: (a) top view; (b) front view and (c) surface temperature.

However, due to the gradient heating effect from induction heating, the temperature at the bottom of the sample might be still low which would result in an inhomogeneous healing effect [5], and this is demonstrated by the temperature distribution images from an infrared camera which are shown in Figure 6.14. To solve this problem, a two-sided heating method for SCB specimens was carried out. Figure 6.14 (a) illustrates an image of a test specimen prior to the heating process at 23°C. The specimen is shown in the same colour as its surroundings under the infrared camera. The two-sided heating method was applied in two steps:

- Step 1. Once the induction heating starts, the alternating current within the coil generates an alternating electromagnetic field, leading to a gradual temperature increase of the SCB specimen from the sample surface to the middle. This step lasted for 90 seconds. Figure 6.14 (b) shows an infrared image which demonstrates that the temperature was the highest at the surface of the test sample;
- Step 2. After one side heating was completed, the SCB specimen was turned over and the induction heating was applied on the other side for 60 seconds (Figure 6.14 (c)). The infrared image shows the SCB specimen, with two-sided heating can achieve a uniform distribution of temperature about 85°C.

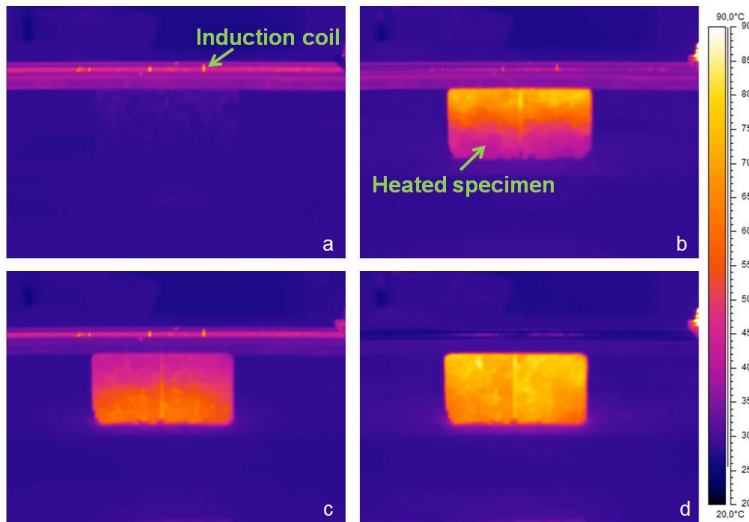


Figure 6.14: The healing process of SCB specimens: (a) heating start on one side; (b) one side heating complete; (c) Turn over and start heating on the other side and (d) the whole heating process complete.

In this way, the test specimen was heated up to 85°C throughout the depth (Figure 6.14 (d)). Thus the overheating and insufficient heating are avoided. In practice (in-situ), uniform heating can be achieved by using a two-layer asphalt structure which has more fibres in the bottom-layer and this concept is discussed in Appendix B.

The two-sided heating method was also adopted for beam test specimen: Step 1, a heating period of 120 seconds was applied at one side of the beam; Step 2, after cooling, the specimen was carefully turned over and another heating period of 120 seconds was applied.

#### 6.2.5.4. HEALING EFFICIENCY EVALUATION IN DAMAGING AND HEALING PROGRAMME

In order to evaluate the healing efficiency of the PA samples with three different asphalt self-healing systems, a damaging and healing programme was developed which was related to both SCB test and 4PB fatigue test.

Figure 6.15 summarises the bending and healing programme for PA sample with various healing systems. First, the initial property of the testing sample was measured, either by SCB test or 4PB fatigue test. Then, the 24-hour-rest period was provided based on the built-in healing system to allow the damaged to be healed, as such a damaging and healing cycle is complete. Afterwards, the bending and

healing programme stopped until the testing sample reached 7 testing cycles or the damages in PA sample cannot be healed anymore.

### Damaging and healing programme

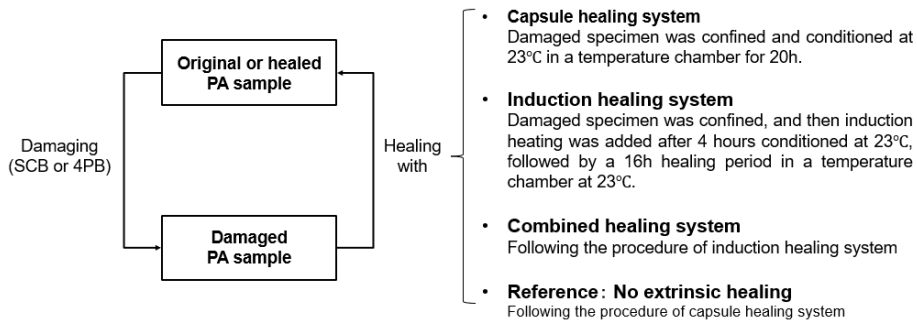


Figure 6.15: The damaging and healing programme for PA samples with various healing systems.

Based on the data acquired from the damaging and healing test cycles, two types of healing index could be calculated from SCB test and 4PB fatigue test separately, which are crack healing index and fatigue healing index. The crack healing index illustrates the ability of PA in crack recovery by analysing the percentage of peak load regained from the healing process. As such, the crack healing capacity of various healing systems can be compared. The crack healing index (*CHI*) can be calculated with the peak load measured from SCB tests, which is the same as the *HI* introduced in section 5.2.7.3 (equation 5.6):

$$CHI = \frac{C_x}{C_1} \times 100\% \quad (6.6)$$

Where:

*CHI* is the crack healing index (%);

$C_1$  is the initial peak load (N);

$C_x$  is the peak load measured from the  $x$  test cycle (N).

The fatigue healing index is used to illustrate the fatigue healing effect of an asphalt pavement. To evaluate the fatigue healing efficiency for all healing systems, the 4PB fatigue damaging and healing cycles were repeated until the test specimen

was fully failed (fractured into two parts). The damage rate ( $D$ ) acquired from the 4PB fatigue tests is used to characterize the durability of a beam specimen under fatigue loadings, and a higher damage rate refers to lower performance in durability. The fatigue healing index ( $FHI$ ) can be calculated with the following equation:

$$FHI = \frac{D_1}{D_x} \times 100\% \quad (6.7)$$

Where:

$FHI$  is the fatigue healing index (%);

$D_1$  is the initial damage rate (MPa/s);

$D_x$  is the damage rate measured from the  $x$  test cycle (MPa/s).

### 6.3. RESULTS AND DISCUSSIONS

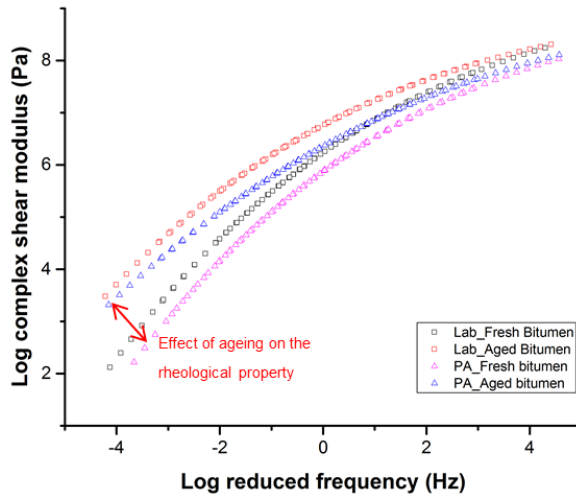
#### 6.3.1. MATERIAL STUDY

##### 6.3.1.1. LABORATORY AGEING EFFECT EVALUATION

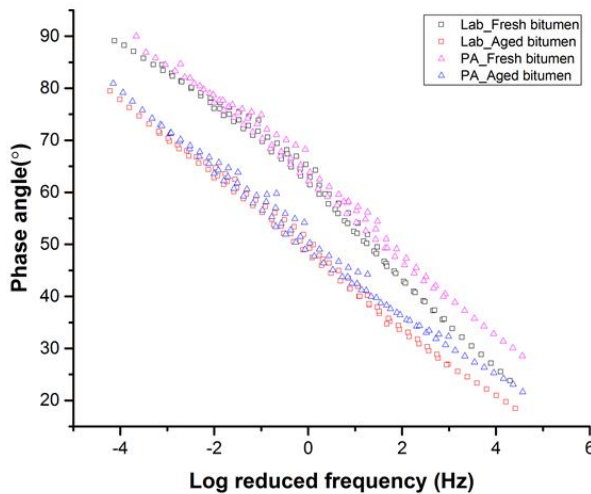
The rheological properties of an asphalt binder are related to its ageing level. As such, DSR tests were performed on the asphalt binder samples extracted from the PA mix without healing system before and after oven ageing. The master curves of complex modulus and phase angle generated from the frequency sweep results are shown in Figure 6.16 (a), in which the standard laboratory Rolling Thin-Film Oven (RTFO) and Pressure Aging Vessel (PAV) aged 70/100 bitumen are plotted as references. Figure 6.16 shows that after ageing, the complex modulus of asphalt binder increased significantly and the increasing amplitude is very similar to the differences in reference curves, which indicates that the ageing procedure described in Chapter 5 and Chapter 6 could accelerate the ageing effect of the PA mixture which is similar to the standard RTFO and PAV ageing process. In Figure 6.16 (b), the phase angle results show that the ageing procedure reduces the phase angle of the asphalt binder in PA and the reducing amplitude is similar to the standard RTFO and PAV ageing effect. As a result, all the PA samples treated with oven ageing were evaluated based on an aged asphalt mix whose ageing level simulates 5 to 10 years field ageing as stated in European standard EN 14769:2012.

The bitumen samples extracted from a different depth of a PA mix were found to have overlapped master curves which means the laboratory oven ageing method showed no gradient ageing effect on PA slabs. This finding differs from the field ageing effect, which mainly because the oven ageing provides a homogeneous heating temperature other than the gradient temperature distribution of the surface layer

in the field. However, this laboratory ageing effect contributes to a more homogeneous asphalt mixture behaviour which may benefit the healing system evaluation with mechanical tests.



(a)



(b)

Figure 6.16: The master curves: (a) complex shear modulus and (b) phase angle.

### 6.3.1.2. ASPHALT MIXTURE CHARACTERIZATION

Figure 6.17 shows the CT-scan image slides of PA sample with three different healing systems. In the capsule healing system Figure 6.17 (a), calcium alginate capsules are found in dark spherical phase which is randomly distributed and attached with asphalt mastic. As a result, the release of rejuvenator from the capsules can easily reach the aged asphalt binder (where it is prone to cracking) to achieve localized binder rejuvenation and eventually crack healing. In the induction healing system (Figure 6.17 (b)), the steel fibres can be found as bright spots within the asphalt mastic area. This fibre distribution allows the induction heat being generated from the asphalt mastic so that cracks that happened in asphalt mastic could be healed. In the combined healing system (Figure 6.17 (c)), the presences of both capsules and steel fibres are found and their distributions follow the same principles as the individual healing systems. It is noticed that steel fibres can always be found in the mastic area near the capsules so that the potential synergistic effects from the capsule healing system and induction healing system are expected during the healing action.

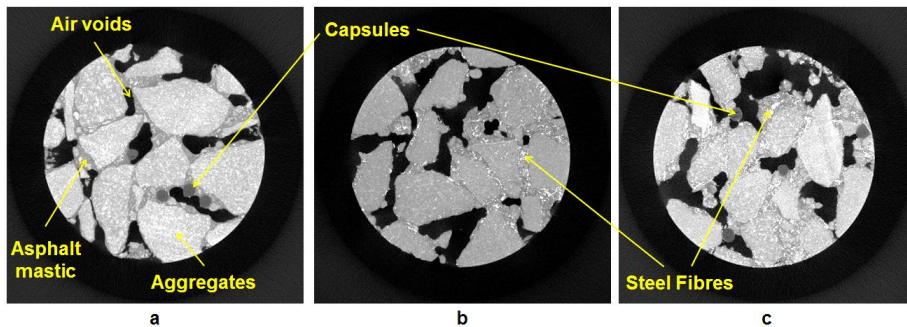


Figure 6.17: CT-scan images of porous asphalt with various healing systems: (a) capsule healing system, (b) induction healing system and (c) combined healing system.

### 6.3.2. MECHANICAL PROPERTIES

#### 6.3.2.1. INDIRECT TENSILE STIFFNESS RESULTS

Figure 6.18 shows the indirect tensile stiffness modulus of the PA samples. Comparing to the induction healing (fresh mixture) group, the cylinders from the induction healing (aged mixture) group show a significant increase in stiffness which indicates that the laboratory ageing can largely increase the stiffness of the PA samples. Out of all four healing systems with aged mixture, the reference mix

shows the lowest stiffness modulus at all loading frequencies, which means the incorporation of a healing system such as calcium alginate capsules and/or steel fibres results in an enhancing effect to make the PA stiffer. These results are in agreement with the conclusions from other research work [3, 14]. Moreover, PA samples incorporated with the combined healing system have the highest stiffness modulus which means the reinforcing effect from calcium alginate capsules and steel fibres can also be combined. The results also indicate that the reinforcing effect from steel fibres is more significant than the calcium alginate capsules as the samples with induction healing system always have a higher stiffness modulus than the capsule healing system.

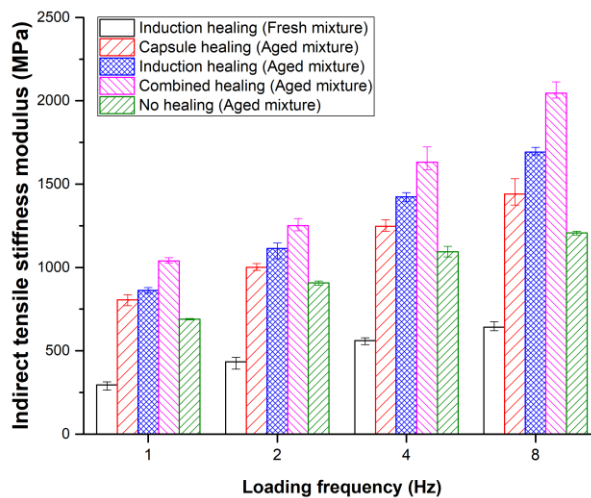


Figure 6.18: Indirect tensile stiffness modulus (ITSM) of PA samples from all testing groups.

### 6.3.2.2. INDIRECT TENSILE STRENGTH RESULTS

As shown in Figure 6.19, the PA samples from different testing groups show similar results in indirect tensile strength, especially between the fresh mixture and the aged mixture. Out of the four aged groups with various embedded healing systems, the combined healing system has the highest strength and all healing systems are stronger than the reference mix. However, the improvement of the indirect tensile strength from the capsule healing system, the induction healing system and the combined healing system is 0.22%, 4.78% and 9.68%, respectively. The results also

indicate that the contribution from the healing systems to the ITS is not that significant compares to ITSM. It might be because the horizontal deformation was not considered in the ITS results, which showed less reinforcing effect in deformation resistance from the capsules and/or steel fibres.

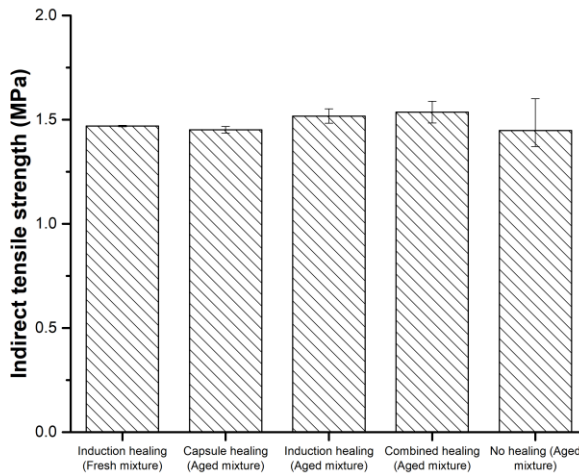


Figure 6.19: Indirect tensile strength of PA samples from all testing groups.

### 6.3.2.3. SEMI-CIRCULAR BENDING RESULTS

The SCB tests were employed to simulate the crack propagation in asphalt and the acquired peak load and fracture toughness were used to evaluate the fracture resistance of the asphalt samples. On the fracture faces of the bent SCB specimens, the remanence of broken calcium alginate capsules are found in both sample groups containing calcium alginate capsules (single and combined healing groups), this indicates that the capsules are activated and rejuvenation and crack healing initiated on demand.

Figure 6.20 shows the fracture toughness of PA samples with various healing systems measured during the SCB bending and healing cycles. In the first cycle, out of all four aged mixture groups, the induction healing system and the combined healing system showed higher fracture toughness than the capsule healing system and the reference group, which means the addition of steel fibres slightly improves the initial fracture resistance of the PA samples. After the first healing, the fractured samples with induction healing system and combined healing system were able to

regain a fracture toughness around  $15 \text{ N/mm}^{1.5}$ , while the fracture toughness of the capsule healing system and the reference group were less than  $4 \text{ N/mm}^{1.5}$ .

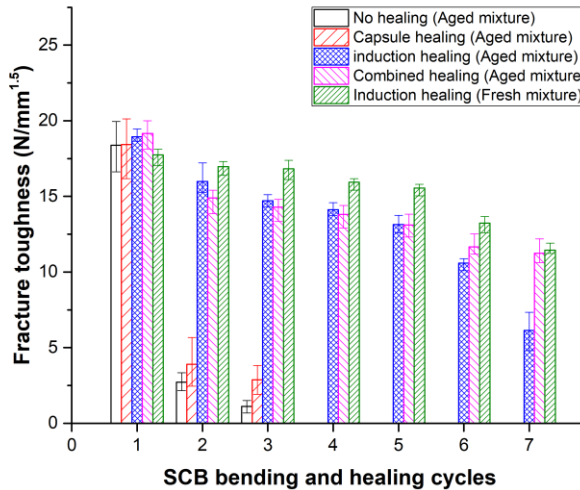


Figure 6.20: Fracture toughness of SCB specimens from all testing groups.

The capsule healing group and the no healing group could not be healed after the third bending cycle, but the fracture toughness recovery in the capsule healing system was higher than the reference group due to the healing effect from the rejuvenator released from the capsules, which is introduced in 5.3.2.3.

As the bending and healing cycles reached the seventh cycle, the induction healing groups and the combined healing group continued to demonstrate effective healing, and as such test samples are managing to reach a fracture toughness greater than  $6 \text{ N/mm}^{1.5}$ . Furthermore, both in aged mixture, the combined healing group has almost twice fracture toughness as much as the induction healing group which proves the positive effect of calcium alginate capsules that can benefit the crack healing in the long-term healing process.

Besides, the induction healing group with aged mixture shows a faster-decreasing trend in fracture toughness and its average final fracture toughness is  $6.1 \text{ N/mm}^{1.5}$  which is much less than the fracture toughness of the fresh mixture group ( $11.4 \text{ N/mm}^{1.5}$ ). Hence, it is demonstrated that the ageing of asphalt mixture has a negative effect on the regain of fracture resistance for the induction healing system, and this effect becomes more significant with the increasing of healing cycles.

Hence, it is believed that the calcium alginate capsules which don't show significant healing in the beginning will benefit the induction healing by providing localised rejuvenation in the aged PA mixture, and in this way, the combined healing system holds more durable and effective healing in the long-term damaging and healing cycles.

### 6.3.3. FATIGUE PROPERTIES

#### 6.3.3.1. INDIRECT TENSILE FATIGUE RESULTS

In the ITF test, the ITF fatigue life of a PA sample is illustrated by the number of loadings that leads to failure. It is also noted that induction heating is not used throughout the continuous fatigue loadings. Figure 6.21 presents the indirect tensile fatigue test results for all testing groups. The PA samples without laboratory ageing show the least fatigue life, which means the laboratory ageing process improves the ITF fatigue life, and this finding agrees with some publications from other researchers [15, 16]. This might be because the ageing increases the stiffness of PA samples, which improves the samples' resistance to deformations under fatigue loadings.

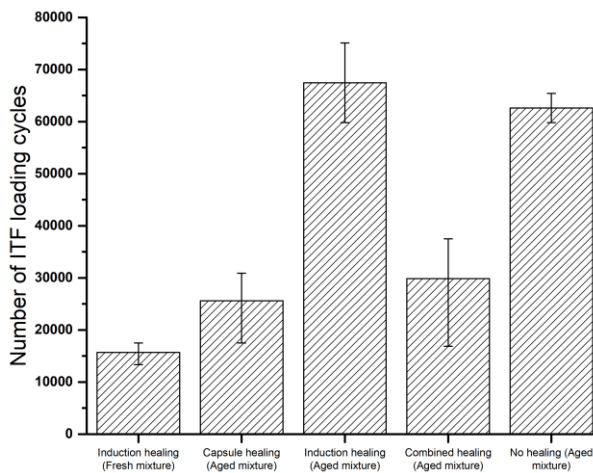


Figure 6.21: Indirect tensile fatigue results of cylinder specimens from all testing groups.

The ITF test results also indicate that the incorporation of induction heating system can extend the ITF fatigue life of PA samples, which can be seen from the

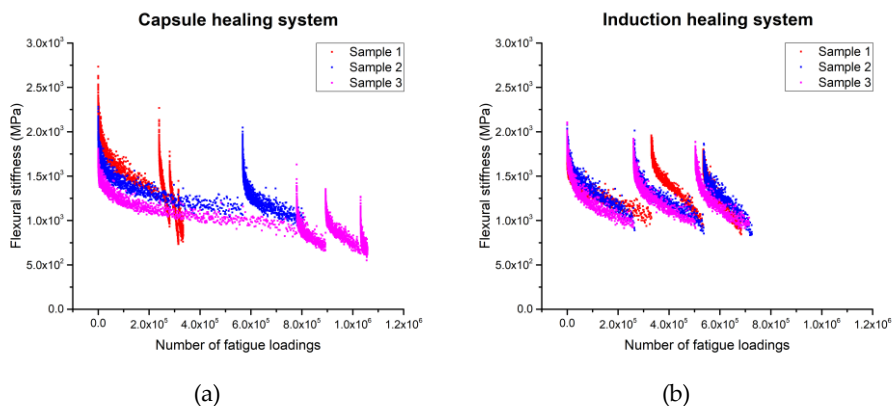
results of aged mixture groups between induction healing and no healing, and between combined healing and capsule healing. This may be due to the reinforcing effect from steel fibres, which are also shown in stiffness (6.3.2.2) and strength (6.3.2.3). A similar ITF fatigue life extension effect of the steel fibres is also reported in the thesis of Liu [3].

However, the PA samples with embedded capsules have much less ITF fatigue life, which indicates that the presence of calcium alginate capsules will reduce the ITF fatigue life of the cylinder specimens under continuous fatigue loadings. This may be due to the released rejuvenator, either from the opened capsules by micro-cracking or being squeezed out by the fatigue loadings, can develop in two ways:

- The released rejuvenator worked. The encapsulated rejuvenator released from capsules and softened the aged binder to reduce the stiffness of the PA sample, and finally resulted in a reduction in ITF fatigue life which behaved like the PA samples with fresh mixture;
- The released rejuvenator didn't work. Due to the continuous fatigue loadings, the released rejuvenator was not able to diffuse into the aged binder especially at low temperature. In this case, the rejuvenator would be located at the damage site in a liquid phase which might cause slippery, and this could be amplified under indirect tensile fatigue loadings.

### 6.3.3.2. FOUR-POINT BENDING FATIGUE RESULTS

Figure 6.22 presents the 4PB fatigue test results for various healing systems built in the aged mixture, from which the fatigue behaviours of each healing system in damaging and healing cycles are illustrated.



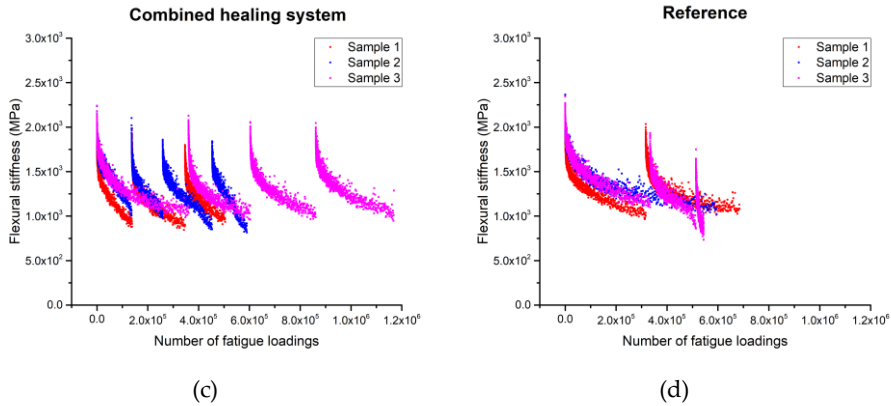


Figure 6.22: Four-point bending fatigue test results for the aged mixture with various healing systems: (a) the capsule healing system, (b) the induction healing system, (c) the combined healing system and (d) the reference mix.

Figure 6.22 (a) shows the 4PB fatigue test results for the capsule healing system. Damages took place in the first 4PB fatigue test were recovered in the rest period which allowed the beam specimen to regain a part of the lost flexural stiffness. However, the healing effect from capsules is limited which results in a continuous reduction in both 4PB fatigue life and flexural stiffness with the increase of testing cycles. Furthermore, the beam specimens with capsule healing system showed a large variety in the 4PB fatigue life results which indicates the calcium alginate capsules have an unstable impact on the 4PB fatigue life tested from 4PB fatigue test cycles.

Figure 6.22 (b) shows the 4PB fatigue test results for the induction healing system. The induction healing system showed a more stable healing effect on fatigue damage than capsule healing system which lies in the recovery of both flexural stiffness and 4PB fatigue life. The results acquired from the third fatigue test cycles could still have an average maximum flexural stiffness of 1845 MPa, which is more than 85% of the average initial stiffness which is 2080 MPa. Besides, the three beam specimens with induction healing systems showed a very similar 4PB fatigue life rather than a large variety for the specimens with the capsule healing system.

Figure 6.22 (c) shows the 4PB fatigue test results for the combined healing system in which the fatigue behaviours of both capsule healing system and induction healing system are found. The combined healing system showed an effective recovery on the flexural stiffness from the rest period and a significant 4PB fatigue life extension effect. However, the combined healing system leads to variety in 4PB fatigue life of the three beam specimens which is similar to the capsule healing system.

For the reference beams without healing systems, the fatigue damage healing actions still took place during the 24-hour-rest period which showed a notable extension of 4PB fatigue life as well as a recovery of stiffness for Sample 1 and Sample 3 (Figure 6.22 (d)). However, the reference beams have a lower number of average possible healing cycles, and the healing effect is limited compare to beams with a built-in healing system.

Figure 6.23 shows the summary of the number of 4PB fatigue loading cycles which leads to failure of the beams. In Figure 6.23, induction healing PA sample without laboratory ageing (fresh mixture) showed the lowest 4PB fatigue life which indicated that the laboratory ageing process improved the fatigue behaviour of PA samples and the same results were found from ITF tests. Among the aged PA samples with various healing systems, beams from the reference group showed the lowest number of loading cycles, thus incorporation of a healing system may result in an increased 4PB fatigue life. Besides, the capsule healing system showed slightly higher average fatigue life than the induction healing system which is different from the results from SCB tests, indicating that healing effect from the calcium alginate capsules can be further activated under fatigue loadings, e.g., rejuvenator squeezed out from fatigue loadings.

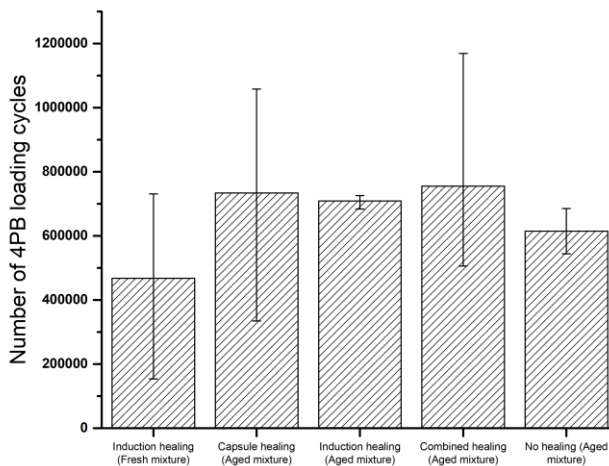


Figure 6.23: Number of 4PB fatigue loadings leads to failure of all beam specimens.

It is also indicated that the PA samples with the combined healing system have the highest fatigue life, however, the data variety is large which is also found in the

results for the capsule healing system. It might be the localised rejuvenation effect from the embedded capsules that softened the aged material at the damage site, and as such slowed down the development of microcrack under repeated fatigue loadings where the rejuvenation took place. As a result, the fatigue damage healing with the capsule healing system is largely determined by the distribution of the opened capsules, whereby leads to the variety in 4PB fatigue life.

Figure 6.24 summarises the developments of flexural stiffness with the 4PB fatigue loadings for all the aged beams. Despite some scattered results from the capsule healing system and the reference group, the general trend for the stiffness of beam specimens developed throughout the damaging and healing programme is clear which shows the stiffness stability of a healing system. The slopes of trendlines in Figure 6.24 illustrate the stiffness stability for the four healing systems, which decreases from combined healing system (red), induction healing system (purple), capsule healing system (blue) to reference group (grey). Hence, the combined healing system shows an advantage in the stiffness recovery under fatigue loadings over the other healing systems.

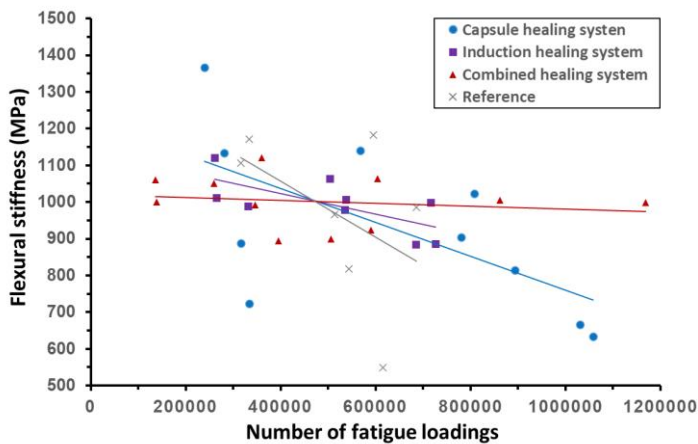


Figure 6.24: Development of flexural stiffness for the various healing systems.

For all testing groups, the damage rate acquired from each 4PB damaging and healing cycles is presented in Figure 6.25. The capsule healing with the aged mixture group showed an increasing trend in damage rate during the 4PB fatigue test cycles which means the beams incorporated only with capsule healing system were easier to lose the regained stiffness in the following fatigue test cycles. Compared to the reference (no healing) group, the capsule healing system showed two advantages in

fatigue damage recovery, which are much lower damage rate after two rest periods and one extra potential healing cycle. It might be because the released rejuvenator showed more significant damage healing effect after two rest periods, and then stimulated the healing of microcracks in beam specimens to be able to conduct the fourth 4PB fatigue test before failure.

The damage rate for the induction healing (aged mixture) group slightly increased with the increase of fatigue test cycles (Figure 6.25), however, it is much lower than the capsule healing group and the reference (no healing) group in the second and the third 4PB fatigue test cycles which indicates the advantage of induction healing system in fatigue damage healing.

While incorporated with a capsule healing system, the combined healing system showed a more stable and durable healing effect than the induction healing system in an aged mixture, which even had a decreased trend in damage rate and the 4PB fatigue test could run up to four cycles. As a result, the combined healing system demonstrated the best performance in fatigue damage healing in comparison to the single extrinsic healing systems (capsule healing and induction healing) and the intrinsic asphalt healing.

The induction healing on fresh mixture also showed a decreased damage rate after a healing period, which means the induction healing could achieve a better fatigue damage healing on a fresh PA mixture (without laboratory ageing).

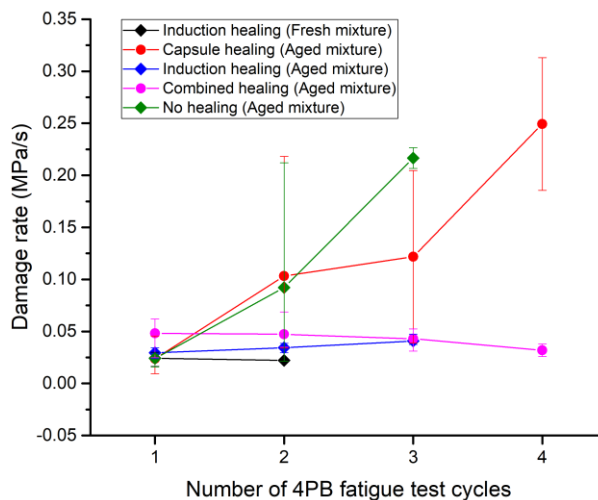


Figure 6.25: The damage rate acquired from each 4PB damaging and healing cycles.

### 6.3.4. HEALING EFFICIENCY

Based on the testing results from the damaging and healing programme conducted with SCB tests and 4PB fatigue tests, the crack healing index and the fatigue healing index for each rest period can be derived and presented in Figure 6.26 and Figure 6.27, respectively.

#### 6.3.4.1. CRACK HEALING INDEX

For the analysis of crack healing index results, the discussion is first addressed on the influence of laboratory ageing on induction healing efficiency. Figure 6.26 shows that induction healing was applied on both fresh PA specimens and aged PA specimens, and showed a decreased crack healing index with the increasing of testing cycles. However, the decreasing rate for the aged PA specimens is much higher which leads to a crack healing index of 25% after 6 healing cycles, while the crack healing index of fresh asphalt specimens still reaches 73%. It might be because, the laboratory ageing deteriorates the self-healing capacity of the PA mix, which makes the high temperature generated from induction heating in the aged PA mix could not provide as much healing effect as the fresh PA mix.

The discussion is then focused on the groups with aged mixture where the crack healing index results from various healing systems are comparable. As shown in Figure 6.26, in the first five damaging and healing cycles, the induction healing system showed a similar healing effect to the combined healing system. Beyond five cycles, a significant decreasing trend in the crack healing index could be found in the induction healing system, while the combined healing system continued a stable trend of healing and did not show a decrease of the crack healing index as observed in the induction healing system. Induction heating is a very efficient crack healing method in PA, but its healing ability is reduced with each healing event. At the fifth damaging and healing cycle, accumulated permanent deformation on fracture faces made the induction healing less effective. However, the capsules in the combined healing system which release the rejuvenator, wet the fracture surface and soften the aged binder, thus promoting the induction healing effect on fractured samples and finally results in a higher crack healing index than the induction healing system in the last two cycles.

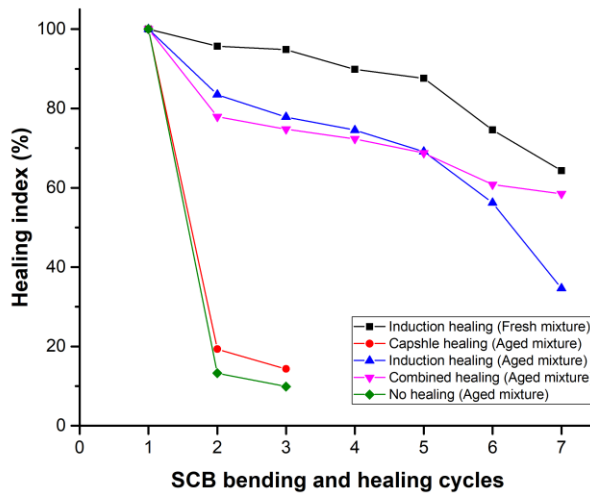


Figure 6.26: The crack healing index for various healing systems.

The SCB damaging and healing results indicate that, with more effective and efficient healing in asphalt, the induction healing technology showed a significant advantage over the capsule healing technology. Although the induction healing can be repeated, the healing efficiency is limited due to the asphalt ageing effect which allows an asphalt gradually loses its intrinsic healing capacity, as such a higher temperature is needed from induction heating to heal the crack.

#### 6.3.4.2. FATIGUE HEALING INDEX

The fatigue healing index for all four healing systems in each healing event is shown in Figure 6.27. Induction healing on the fresh mixture shows the highest fatigue healing index in the first healing event, which is because the induction heating approach has a promising fatigue damage healing effect especially on a fresh mixture, and this healing effect is better than any testing groups with aged mixture.

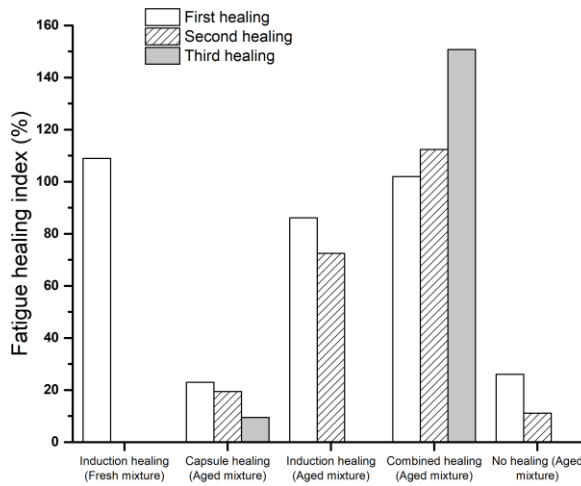


Figure 6.27: The fatigue healing index for various healing systems.

Compared to the no healing group, the capsule healing group showed a lower fatigue healing index in the first healing, but a higher fatigue healing index in the second healing and could also showed effective healing in the third healing event. It indicates that the capsule healing system can improve the healing capacity of an aged PA mixture and achieve a more durable fatigue behaviour in the 4PB test series.

The induction healing (aged mixture) group has a much higher fatigue healing index than the capsule healing group and the no healing group in the first and second healing events, which indicates that induction heating has a much better fatigue damage healing effect than capsule healing. However, the induction healing system can only provide two effective healing cycles which are less than the capsule healing system.

When the capsule healing system and induction heating system are combined, the fatigue damage healing effect is significantly improved (see Figure 6.27). In contrast to the capsule healing system with an aged mixture and the induction heating system with an aged mixture, the combined healing system with an aged mixture shows a much higher fatigue healing index and these values even increases after every healing event. A possible explanation is the gradual healing effect from the calcium alginate capsules whose compartmented rejuvenator is gradually released upon the fatigue loadings so that the induction healing effect is enhanced due to

aged binder rejuvenation time after time. As such, the terrific fatigue damage healing effect from the combined healing system is demonstrated.

In summary, the fatigue properties of beam specimens with all four healing systems have been investigated with 4PB fatigue test in multiple damaging and healing cycles, and the total number of fatigue loadings, flexural stiffness and damage rate are used to illustrate the behaviours of all tested healing systems. The capsule healing system, the induction healing system and the combined healing system showed their inherent healing mechanisms in the fatigue test series and showed advantages over the reference group (mix without an extrinsic healing system). However, the combined healing system demonstrated the best performance in fatigue life, stability, and fatigue resistance.

#### 6.4. CONCLUSIONS

Aimed to explore the potential healing effect of the combined healing system, various healing systems were designed and the mechanical properties, the fatigue properties and the healing efficiency of four healing systems were investigated. Based on the test results, the following conclusions can be drawn:

- The DSR test results show that the laboratory oven ageing procedure used in this chapter refers to an ageing level that simulates 5 to 10 years of field ageing, and this ageing effect is homogeneous throughout the asphalt slab.
- The CT-scan images show that the capsules and steel fibres can be randomly distributed in the porous asphalt and contacted asphalt mastic, this distribution allows both healing systems to function.
- The ITSM results indicate that the incorporation of a healing system in a PA mixture increases stiffness modulus, and the increasing effect from the combined healing system is the most significant. The main reason is the reinforcing effect of calcium alginate capsules and steel fibres. However, the reinforcing effect from the healing systems has a negligible effect on the ITS. Meanwhile, the asphalt ageing also increases the ITSM of PA mixture but not that significant for ITS.
- The designed healing conditions, including the 24-hour-rest period and the provided confinements to the samples, successfully activate the built-in healing system for all PA samples. As a result, the healing effect of various

healing systems can be evaluated and compared by using the damaging and healing programme.

- The results from SCB damaging and healing cycles indicate that the induction heating has a remarkable crack healing effect which is much better than the capsule healing, but this induction healing effect can be largely affected by asphalt ageing. The combined healing system shows a significant advantage over the capsule healing system. Compared to the induction healing system in the aged mixture, although their healing efficiency is very similar in the first 5 cycles, the healing effect of the combined healing system is more stable after that and it might be because of the rejuvenation effect from the embedded capsules.
- The ITF results indicate that the built-in healing systems of PA samples have a significant impact on the fatigue behaviours under continuous ITF loadings, in which the induction healing system shows the positive effect to extend the ITF fatigue life but the capsule healing system shows the negative effect and reduces the ITF fatigue life. It might be because the released rejuvenator from capsules softens the aged material which results in higher deformations under stress-controlled fatigue loadings, therefore a reduced fatigue life. The other possible reason is the released rejuvenator can hardly diffuse and rejuvenate at 5°C under continuous loadings. It is also indicated that the laboratory oven ageing process results in the improvement of the fatigue resistance of PA samples.
- The 4PB fatigue test results from multiple damaging and healing cycles indicate that the extrinsic healing systems namely the capsule healing system, the induction healing system and the combined healing system show their inherent healing mechanisms in the fatigue test series and show advantages over the reference group. The induction healing system can significantly heal the fatigue damages in the rest period, thus a more stable stiffness and an extended 4PB fatigue life. The beam specimens with calcium alginate capsules have the highest number of potential healing cycles, which might be because the rejuvenator released from capsules improves the healing capacity of the aged materials thus a more durable fatigue behaviour in the fatigue test series. However, the beam specimens with the combined healing system have the best performance in fatigue life, stability and fatigue resistance, which even showed increased fatigue healing index in the fatigue

test series. A possible explanation is the gradual healing effect from the capsules that enhanced the induction healing in the damaging and healing cycles time after time.

This chapter presents the key findings of this Ph.D. project including design, evaluation and comparison of different healing systems in PA mixture. The combined healing system shows outstanding performance in both crack healing and fatigue damage healing, in which an important reason is a synergistic effect that the embedded capsules may enhance the induction healing in the long-term damaging and healing cycles. Hence, it is believed that the combination of capsule healing and induction healing system contributes to a more stable and durable healing effect in the PA mixture.

## REFERENCES

- [1] S. Xu, X. Liu, A. Tabaković, E. Schlangen, A novel self-healing system: Towards a sustainable porous asphalt, *Journal of Cleaner Production* (2020) 120815.
- [2] S. Xu, A. Tabaković, X. Liu, E. Schlangen, Calcium alginate capsules encapsulating rejuvenator as healing system for asphalt mastic, *Construction and Building Materials* 169 (2018) 379-387.
- [3] Q. Liu, *Induction Healing of Porous Asphalt Concrete*, Delft University of Technology, 2012.
- [4] S. Xu, A. García, J. Su, Q. Liu, A. Tabaković, E. Schlangen, Self - Healing Asphalt Review: From Idea to Practice, *Advanced Materials Interfaces* (2018) 1800536.
- [5] S. Xu, X. Liu, A. Tabaković, E. Schlangen, The influence of asphalt ageing on induction healing effect on porous asphalt concrete, *RILEM Technical Letters* 3 (2018) 98-103.
- [6] W. Van den Bergh, The effect of ageing on the fatigue and healing properties of bituminous mortars, (2011).
- [7] P.K. Behera, A. Singh, M. Amaranatha Reddy, An alternative method for short- and long-term ageing for bitumen binders, *Road Materials and Pavement Design* 14(2) (2013) 445-457.

- [8] R. Jing, *Ageing of bituminous materials: Experimental and numerical characterization*, Delft University of Technology, 2019.
- [9] M. Huang, W. Huang, *Laboratory investigation on fatigue performance of modified asphalt concretes considering healing*, *Construction and Building Materials* 113 (2016) 68-76.
- [10] F. Pramesti, A. Molenaar, M. Van de Ven, *The prediction of fatigue life based on four point bending test*, *Procedia Engineering* 54 (2013) 851-862.
- [11] Q. Liu, E. Schlangen, M. van de Ven, G. van Bochove, J. van Montfort, *Evaluation of the induction healing effect of porous asphalt concrete through four point bending fatigue test*, *Construction and Building Materials* 29 (2012) 403-409.
- [12] L. Francken, *Fatigue performance of a bituminous road mix under realistic test conditions*, *Transportation Research Record* (712) (1979).
- [13] G. Sun, D. Sun, A. Guarin, J. Ma, F. Chen, E. Ghafooriroozbahany, *Low temperature self-healing character of asphalt mixtures under different fatigue damage degrees*, *Construction and Building Materials* 223 (2019) 870-882.
- [14] S. Xu, X. Liu, A. Tabaković, E. Schlangen, *Investigation of the Potential Use of Calcium Alginate Capsules for Self-Healing in Porous Asphalt Concrete*, *Materials* 12(1) (2019) 168.
- [15] A. Kavussi, M.J. Qazizadeh, *Fatigue characterization of asphalt mixes containing electric arc furnace (EAF) steel slag subjected to long term aging*, *Construction and Building Materials* 72 (2014) 158-166.
- [16] B. Vallerga, F. Finn, R. Hicks, *Effect of asphalt aging on the fatigue properties of asphalt concrete*, *Intl Conf Struct Design Asphalt Pvmnts*, 1967.

# 7

## CONCLUSIONS AND RECOMMENDATIONS

*The two main contributions of this Ph.D. research are the development of calcium alginate capsules encapsulating bitumen rejuvenator and the combined (induction heating and rejuvenation) healing system. This chapter outlines the findings of this research and gives the general conclusions. Finally, recommendations for future studies are given.*

## 7.1. CONCLUSIONS AND PROSPECTS

### 7.1.1. CALCIUM ALGINATE CAPSULES ENCAPSULATING REJUVENATOR

Ageing results in a decrease of bitumen grade: after a short-term ageing process (simulated with RTFO), the PEN 70/100 bitumen decreased to the grade level of PEN 40/60, and this bitumen grade further decreased to PEN 20/30 after a long-term ageing process (simulated with PAV). The bitumen penetration level can be 'upgraded' by using a rejuvenator. For the application in a capsule healing system, the recommended dosages for rejuvenator R, B and O are 3.9%, 2.7% and 2.2%, respectively, which aimed to 'upgrade' the aged bitumen from PEN 20/30 to PEN 40/60. However, bitumen rejuvenated with R showed better rutting and cracking resistance, and had more stable performance after re-ageing, therefore determined as the optimal rejuvenator for a capsule healing system.

Research findings showed that the optimal type and amount of rejuvenator is determined based on the ideal situation that rejuvenator and bitumen are evenly mixed. However, in the capsule healing system, the release of the rejuvenator is triggered by cracking followed by slow rejuvenator-bitumen diffusion. On the other hand, in the combined healing system, the rejuvenator diffusion process is accelerated, by increasing the healing temperature to 85°C.

The calcium alginate capsules encapsulating rejuvenator can be prepared in the laboratory, and the microstructure inside the calcium alginate capsules is presented as a honeycomb-like porous structure and individual rejuvenator droplets are encapsulated in the porous media. The capsule performance is largely determined by the alginate/ rejuvenator (A/R) ratio, and the optimum A/R ratio is 30/70, as the prepared capsules not only have enough thermal and mechanical resistance but also contain as much rejuvenator as possible. These capsules have a uniform diameter of 1.95 mm, and the rejuvenator content is 56% by volume.

The effectiveness of these capsules is investigated using bending and healing tests in asphalt mastic, mortar and PA. After a bending test, the presence of calcium alginate capsules on the fracture surfaces of asphalt samples indicates that these capsules can fracture upon the propagation of cracks. Thus, the encapsulated rejuvenator is released to heal the damage site. It also indicates that these capsules can survive the asphalt production, compaction and even the oven ageing process.

The calcium alginate capsules improve the healing efficiency in all types of asphalt mix, while this effect is largely influenced by bitumen ageing. It is found that these capsules can hardly promote the crack healing in a fresh mix in which the intrinsic healing capacity of virgin 70/100 bitumen plays the main role in the healing

process. However, the capsule healing system becomes more effective in an aged asphalt mix. Research results also showed that the healing efficiency of the calcium alginate capsules is influenced by the gradations of the asphalt mixture which agrees with the findings from existing research [1, 2].

### 7.1.2. EVALUATION OF SELF-HEALING SYSTEMS IN POROUS ASPHALT

When applied in a full PA mix, the calcium alginate capsules and steel fibres are randomly distributed and contacted with asphalt mastic, and this distribution allows both healing systems to function efficiently. Incorporation of a self-healing system in a PA mix leads to an increase in stiffness but shows a negligible effect on the indirect tensile strength.

Results from the SCB bending and healing cycles indicate that asphalt ageing leads to a decrease of crack healing efficiency of the induction healing system, and this situation can be largely improved when a calcium alginate capsules healing system is incorporated so that both thermally induced healing and aged bitumen rejuvenation are combined in the crack healing process. Besides, the induction healing system has a higher crack healing efficiency than the capsule healing system and showed a more stable and durable performance in the SCB damaging and healing cycles.

Based on the results from the 4PB bending and healing test cycles, all extrinsic healing systems, namely the capsule healing system, the induction healing system and the combined healing system, can improve the performance of PA under fatigue loadings. The combined healing system shows the best performance in fatigue life, stability and fatigue resistance, which might be due to the gradual healing effect from the capsules that enhanced the induction healing in the damaging and healing cycles time after time. Besides, the induction healing system shows a higher fatigue damage healing index than the capsule healing system, but the capsule healing system shows a slightly better fatigue life extension effect than the induction healing system, which indicates the healing effect from the calcium alginate capsules can be further activated under fatigue loadings. However, incorporation of the calcium alginate capsules also leads to a scattered fatigue performance, and this might be due to the capsule distribution which determines whether the healing takes place on the damage site or not.

The life-extension prospects of PA with various healing systems are presented in Figure 7.1. Figure 7.1 shows that a PA incorporated with a capsule healing system would have an increased life span than the standard PA, which is because of the

improved crack healing effect from aged binder rejuvenation. Compared to the capsule healing system, the induction healing system has a more durable crack healing performance in PA so that the life span of PA could be further extended. However, for the combined healing system, the comprehensive healing effect lies in not only the advantages of both encapsulated rejuvenator and induction heating, but also the synergistic effects which promote each individual mechanism, namely accelerated rejuvenator diffusion (with induction heating) and improved induction healing (with asphalt binder rejuvenation). As such, the combined healing system shows the longest PA life extension prospect among the three extrinsic healing systems. Following this conclusion, it is recommended that multi-healing method which includes mechanical property recovery and aged material rejuvenation as a research focus for the future development of self-healing technology in asphalt pavement.

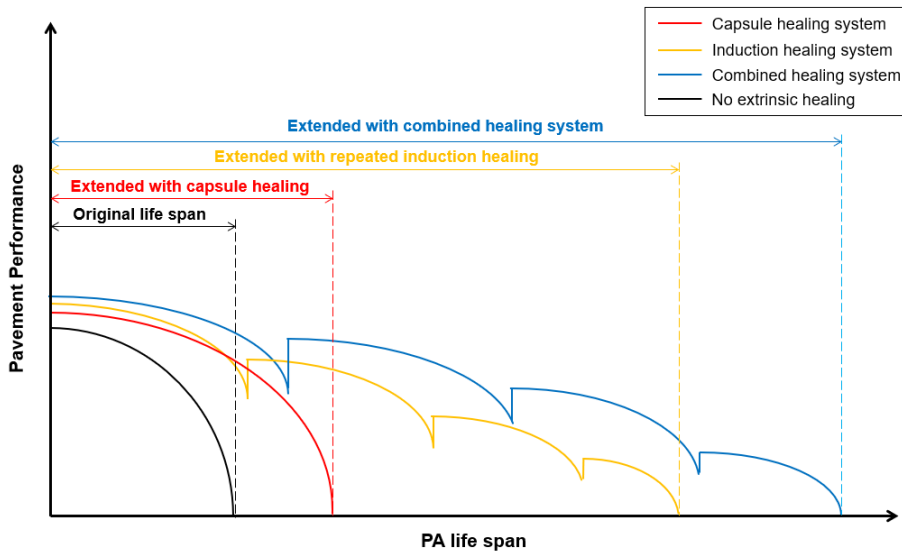


Figure 7.1 Schematic life extension prospects in PA with various healing systems: the capsule healing system, the induction healing system and the combined healing system.

In this research, the laboratory oven ageing test was performed to simulate the ageing of PA in practice which is assumed to be the status of an asphalt mix when healing is needed (after years of service). The efficiency of the healing systems was evaluated based on the healing of two different forms of damage in PA:

- The SCB damaging and healing programme aimed to evaluate the healing of progressive meso or macro cracks in PA (e.g., thermal cracking).

- The 4PB damaging and healing programme aimed to evaluate the healing of microcracks in PA (e.g., fatigue cracking).

However, all these tests only indicate the performance of each healing system under certain conditions and cannot fully represent the situation in practice. The most common damage in PA is ravelling. Although no ravelling test is done in this research, it is believed that the SCB and 4PB are good substitutes. Hence, the advantages of the combined healing system need to be further evaluated in the long-term field application.

## 7.2. RECOMMENDATIONS FOR FUTURE WORK

The calcium alginate capsules and the combined healing system have been developed in this Ph.D. project, however, more optimization work needs to be conducted in the future to further improve the healing efficiency and pavement performance. Hence, recommendations for future research are given as follows:

- Investigation of the rejuvenator diffusion process is recommended. Understanding of the temperature-dependent diffusion behaviour of different types of rejuvenator provides an important basis for rejuvenator ranking, which will help optimize the capsule healing system and other practical uses of rejuvenator (e.g., RAP, fog seal).
- The distribution of calcium alginate capsules in PA needs to be optimized by adjusting the diameter of calcium alginate. It is expected that a smaller capsule may result in a more homogeneous distribution in PA. However, this diameter change will also lead to a different capsule characteristic, such as morphology, thermal stability, mechanical resistance and rejuvenator content. Hence, all these parameters should be considered in the additional optimization process.
- The optimal amount of calcium alginate capsules for the capsule healing system and combined healing system in PA need to be determined. To this aim, the capsule distribution, mechanical response, crack healing efficiency and fatigue damage healing efficiency of PA samples with different amount of calcium alginate capsules should be evaluated. Based on these experimental results, the relation between the number of capsules and the PA performance will be obtained, therefore the optimal amount of capsules for both systems can be determined.

- It is also recommended to develop a numerical model that simulates the cracking and healing process of a capsule healing system in asphalt mastic. The damaging process can be simulated with a finite element based model, with the inputs of material properties, interface bonding and loading conditions. Afterwards, the healing process can be simulated with a rejuvenator transportation model, in consideration of the capillary flow and diffusion of the released rejuvenator. This numerical model can be validated which helps to predict the performance of a capsule healing system.

### 7.3. REFERENCES

- [1] A. Tabaković, E. Schlangen, Self-healing technology for asphalt pavements, *Self-healing Materials*, Springer 2015, pp. 285-306.
- [2] J. Qiu, Self healing of asphalt mixtures: towards a better understanding of the mechanism, Delft University of Technology, 2012.



# EXPERIMENTAL AND NUMERICAL INVESTIGATION OF THE REJUVENATOR-BITUMEN DIFFUSION PROCESS

## A.1. INTRODUCTION

In the laboratory, the rejuvenation of an aged bitumen can usually be achieved by blending the aged bitumen with a rejuvenator, and this process is always accompanied by a stirring procedure under high temperature, therefore a homogeneous rejuvenation effect. However, in the practical rejuvenator applications, mixing of rejuvenator with aged bitumen is achieved by a time-consuming diffusion process, in which the rejuvenator gradually diffuses into the aged bitumen and changes its physical properties [1]. If the diffusion process cannot finish within a given period, the lubricating effect of rejuvenator will remain at the surface of the bitumen which may cause premature failures [1, 2]. Carpenter et al [1] explained the diffusion process of a rejuvenator into the aged bitumen with four steps:

- i. The rejuvenator forms a layer covering the surface of the aged bitumen;
- ii. The rejuvenator starts penetrating the aged bitumen and softens the bitumen;

- iii. The penetration goes deeper and both inner and outer bitumen are gradually softened;
- iv. The equilibrium is reached at the majority depth of the bitumen film.

In 2003, Karlsson and Isacsson [2] reported a study which characterized the rejuvenator diffusion process using FTIR. It was found that the diffusion of a rejuvenator into the aged bitumen is a time-consuming process which takes 48 to 144 hours and this process is influenced by various factors, such as temperature, bitumen film thickness, bitumen type, etc. Karlsson and Isacsson also indicated that the diffusion process can be described using Fick's law.

## A.2. MATERIALS AND METHODS

To further investigate the diffusion process between aged bitumen and rejuvenator, the bitumen-rejuvenator diffusion test was designed which is illustrated in Figure A.1. Figure A.1 shows that the diffusion test was carried out in three steps:

- i. Firstly, to prepare the diffusion test samples, the rejuvenator and the bitumen are contained in a glass bottle in two layers where the rejuvenator on the top and the aged bitumen on the bottom. Rejuvenator R20 and the LTA bitumen described in Chapter 3 were used in the diffusion test.
- ii. Afterwards, the glass bottle was sealed with rubber plugs and the diffusion process was conditioned in an oven at 140°C. The samples were scanned using a Nano CT with a resolution of 12  $\mu\text{m}$  at 40, 60, 120 and 360 min of the diffusion process, to characterize the mass transfer during the diffusion process.
- iii. Finally, after 8 days of diffusion FTIR was employed to detect the chemical composition of the liquid samples which were taken from the surface of the rejuvenator phases after 8 days of diffusion.

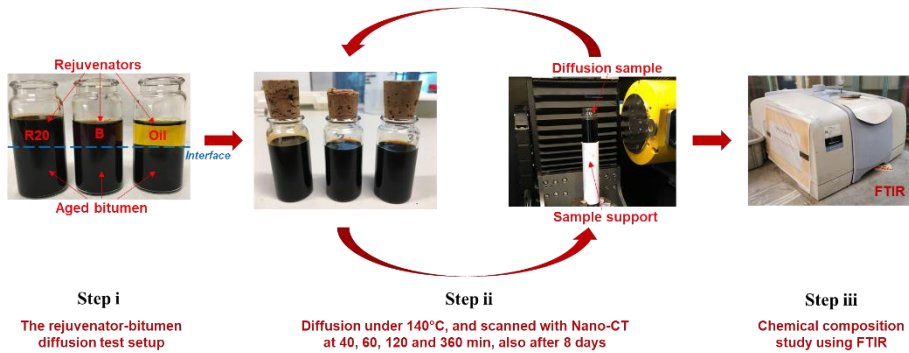


Figure A.1 The setup used for the diffusion coefficient study.

A numerical diffusion model was developed and validated in this study to simulate the rejuvenator-bitumen diffusion process.

### A.3. RESULTS AND DISCUSSION

#### A.3.1. NANO CT

Figure A.2 shows the diffusion process characterized using CT-scan. In a CT scan image, individual phases can be distinguished with different brightness intensities which can be referred to the density at each pixel. Figure A.2 (a) shows a CT-scan image which illustrates the various phases in the diffusion test setup, and the grey value of the rejuvenator phase ( $g_r$ ) and bitumen phase ( $g_b$ ) and their difference ( $\Delta g$ ) in the dashed rectangle area was studied. Figure A.2 (b) presents the CT-scanned images and the relative grey value difference. It was found that  $\Delta g$  gradually decreases with the diffusion time which indicates density of the two phases were getting closer during the diffusion process and this grey value change can almost be observed with the naked eye. Figure A.2 (c) presents the development of  $g_r$  and  $g_b$  with diffusion time. It shows that  $g_r$  decreases during diffusion, while  $g_b$  increases at the same time, which indicates an increase of density in rejuvenator phase and a decrease of density in the bitumen phase. However, the interface between the two phases remained at the same level throughout the diffusion process. It means components exchange happened, by passing through a stable boundary between the two phases, and finally results in the change of density in the two phases without changing their colloidal structure. This could be caused by two different diffusion mechanisms:

- i. Heavy component diffuses from bitumen to rejuvenator;

- ii. Heavy component diffuses from bitumen to rejuvenator and light component diffuses from rejuvenator to bitumen at the same time.

Since both Karlsson and Qiu have reported a presence of rejuvenator composition at the bottom of the bitumen layer, mechanism ii would be the more possible case in this study. However, further investigations are needed to understand this diffusion behaviour, and future diffusion study includes more diffusion cases, such as various types of rejuvenator and bitumen, and different diffusion temperatures, is recommended. Besides, the diffusion model may also need to be validated with the experimental results.

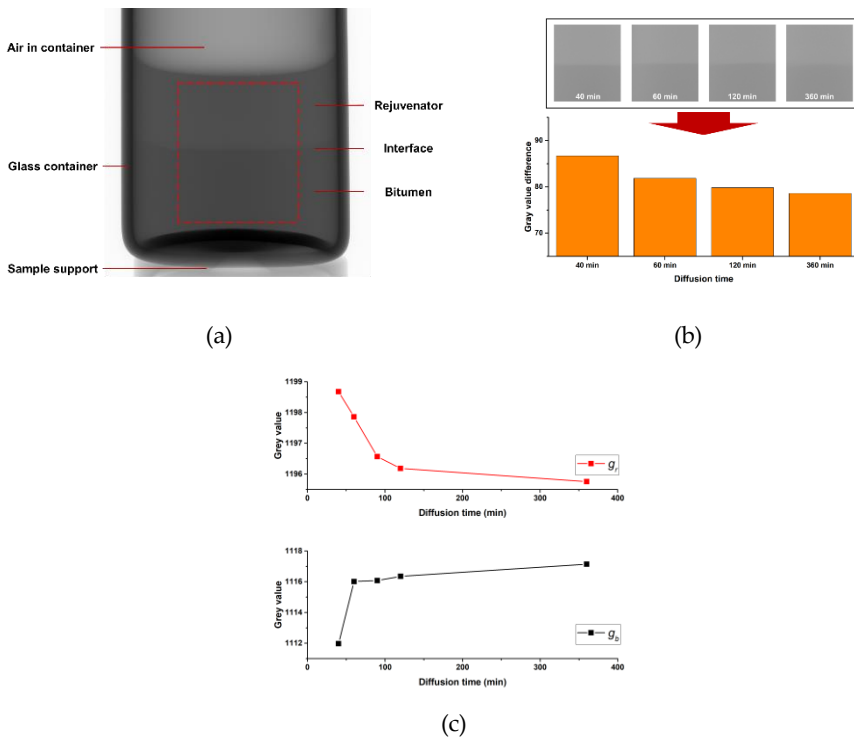


Figure A.2 Liquid phases differential characterization: (a) The focused area of a CT scan image, (b) the grey value difference between rejuvenator and bitumen phases in the diffusion process and (c) the development of  $g_r$  and  $g_b$  with time.

### A.3.2. FTIR

Figure A.3 shows the FTIR spectrogram of the samples taken from the surface of the rejuvenator phases after 8 days of diffusion (R8d), and the FTIR spectrograms of the long-term aged bitumen (LTA) and Rejuvenator (Rej\_R) are presented as references. As shown in Figure A.3, the absorbance band at  $743\text{ cm}^{-1}$  was found in the spectrogram of the rejuvenator phase which also presented in LTA, but not in rejuvenator R20. It indicates that the bitumen phase could diffusion into the rejuvenator as well (mechanism ii).

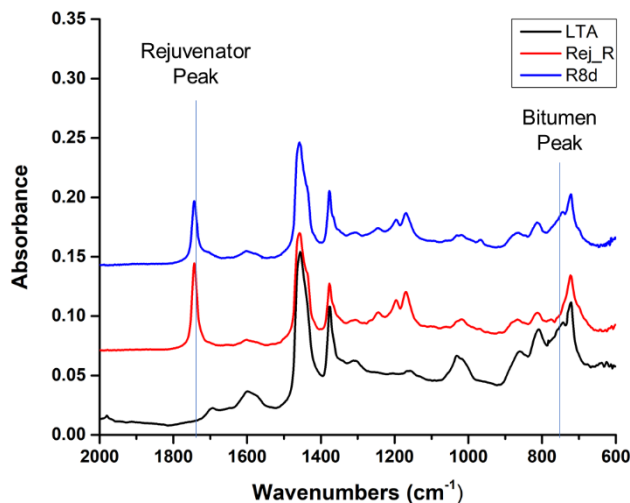


Figure A.3 FTIR spectrogram of the samples taken from the surface of the rejuvenator phases after 8 days of diffusion.

### A.3.3. DEVELOPMENT OF THE DIFFUSION MODEL

A lattice model was employed to simulate this diffusion process. This diffusion model was developed based on the Fick's second law by Šavija et al [3], which was originally designed to simulate the chloride diffusion in concrete, from the higher concentration zones to the lower concentration zones.

Figure A.4 shows the validation of the diffusion model with the experimental results from project IOP SHM 012019 which was reported by Qiu et al [4, 5]. In that study, the rejuvenator-to-bitumen diffusion process was investigated using an in-situ FTIR setup, where the rejuvenation concentration at the bottom of the bitumen

was obtained with time, in a temperature-controlled condition. Qiu et al reported a diffusion coefficient ( $D$ ) of  $3.5 \times 10^{-10}$  m<sup>2</sup>/s which was measured at 140°C, with rejuvenator on the top at a thickness of 0.25 mm and bitumen on the bottom at a thickness of 0.75 mm. Figure A.4 (a) shows the input for the diffusion model in which the same parameters from the experimental setup were used. Figure A.4 (b) shows the experimental results reported by Qiu et al and the simulation results from the diffusion model. After about 30 minutes, the experimental results show a peak rejuvenator concentration value of 30%, and then the rejuvenation slowly decreased to around 26% at 100 minutes. While the diffusion model predicted that the rejuvenator concentration at the bottom of the bitumen gradually increased to 25% at 60 minutes and kept at 25% afterwards. The main reason for the difference between the measured curve and the simulated curve lies in the period it takes to reach equilibrium, in which the simulated results show a more smooth process. It is also noticed that the volume loss during the real diffusion process, such as rejuvenator component evaporation at a high temperature, was not considered in the diffusion model, which is the reason that experimental results have a higher final rejuvenator concentration due to a less total volume. Hence, following the Fick's law, the diffusion model can predict the rejuvenator diffusion process smoothly and stably.

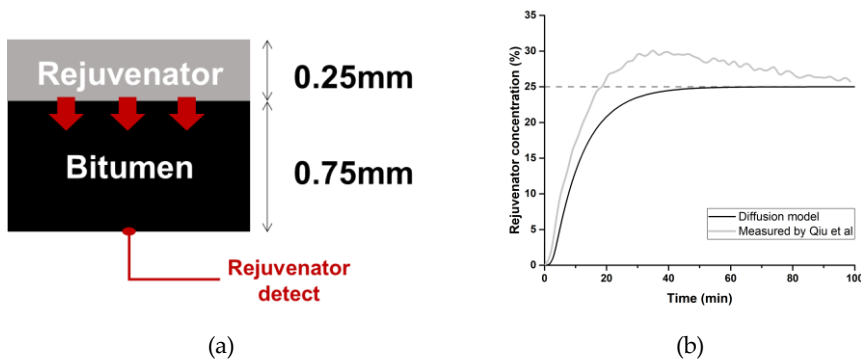


Figure A.4 Diffusion model validation with the results from Qiu et al: (a) the bitumen-to-rejuvenator diffusion setup and (b) simulated results vs tested results [5].

#### A.3.4. CONCLUSIONS AND REMARKS

The rejuvenator-bitumen diffusion process can be investigated with CT-scan and FTIR in which CT-scan can capture the mass transfer during the diffusion

process and FTIR can detect the change of chemical components. The rejuvenator-bitumen diffusion process exists in two directions, namely from rejuvenator to bitumen and bitumen to rejuvenator. In future research, more diffusion tests will be carried out to investigate the influence of different rejuvenator types, temperature and thickness of liquid phases. The CT-scan results will be further analysed to determine the diffusion coefficient for both diffusion directions. Besides, the diffusion model validated in this research will be employed to simulate the diffusion behaviour in future research.

## REFERENCES

- [1] S.H. Carpenter, J.R. Wolosick, Modifier influence in the characterization of hot-mix recycled material, *Transportation Research Record* (777) (1980).
- [2] R. Karlsson, U. Isacson, Application of FTIR-ATR to characterization of bitumen rejuvenator diffusion, *Journal of Materials in Civil Engineering* 15(2) (2003) 157-165.
- [3] B. Šavija, J. Pacheco, E. Schlangen, Lattice modeling of chloride diffusion in sound and cracked concrete, *Cement and Concrete Composites* 42 (2013) 30-40.
- [4] J. Qiu, H. Schlangen, M. Van de Ven, M. Shirazi, Reintroducing the intrinsic self-healing properties in reclaimed asphalt by rejuvenation, (2013).
- [5] J. Qiu, E. Schlangen, M. van de Ven, T. Scarpas, M. Shirazi, Reintroducing the Intrinsic Self-healing Properties in Reclaimed (Polymer Modified) Asphalt (RISP2RA), IOP SHM 012019, Delft, 2014.



# B

## IMPROVED INDUCTION HEALING ON TWO-LAYER POROUS ASPHALT

As described in Chapter 6, induction heating on an asphalt sample usually results in a gradient temperature distribution which may lead to an uneven damage healing effect and the overheating risk on the asphalt surface. The main reason is the gradient distribution of magnetic field generated from the alternating current which mainly concentrated near the induction coil. In principle, this situation can be improved by an improved induction healing system which has a gradient steel fibres distribution that responds to the concertation of magnetic field, for instance, the region close to the coil contains a lower amount of steel fibres.

Fortunately, a special two-layer porous asphalt system is well suited for this improved induction healing system. In the Netherlands, the two-layer PA system is widely used in the surface course with a 25 mm fine graded top layer and a 45 mm coarse graded bottom layer, and this two-layer structure shows a better noise reduction effect than the single-layer porous asphalt [1, 2]. In this study, the two-layer porous asphalt was incorporated with the improved induction healing system by applying 3% of steel fibres in the top layer and 6% of steel fibres in the bottom layer (B). A two-layer PA with 6% steel fibres in both layers was tested as a reference.

Figure B.1 summarises the mix compositions of layers from the two-layer PA system. The top layers (T1 and T2) contained finer aggregates were prepared following the standard PA 4/8 with modified 45/80 bitumen and the bottom layer (B) were prepared following the standard PA 8/11 with virgin 70/100 bitumen. T1 was designed for the top layer of the original induction healing system with 3% steel

fibres while T2 for the improved induction heating system with 6% steel fibres, and mixture B was used for the bottom layer for both induction heating systems.

Table B.1: The mix compositions of the two-layer PA system.

Mix Constituent	% Content in Mix		
	T1 (PA 4/8)	T2 (PA 4/8)	B (PA 8/11)
16 mm	-	-	7.97
11.2 mm	8.21	8.12	62.00
8 mm	42.68	42.18	7.97
5.6 mm	29.13	28.79	1.78
2 mm	7.85	7.74	9.86
63 $\mu$ m	5.61	5.55	4.22
Bitumen	5.34	5.27	4.32
Steel Fibres	1.18	2.33	1.88

Based on the mix design in Table B.1, three types of PA slabs were prepared in Heijmans, and the detailed slab making procedure is described in Chapter 5. Figure B.1 (a) shows the individual asphalt beams with dimensions  $25 \times 50 \times 500$  mm and  $45 \times 50 \times 500$  mm cut from the slabs, which referred to the top layer and bottom layer, respectively. The two-layer system was simulated by placing the top layer in contact with the bottom layer and both beams had a plain surface to ensure a close contact in between. Figure B.1 (b) shows the induction heating on a two-layer porous asphalt system simulated in laboratory: the two layers were stacked together and placed 5 mm below the induction coil. The induction heating test lasted for 2 minutes, and in this period, an infrared camera was employed to record the surface temperature of the two-layer system in the front direction.

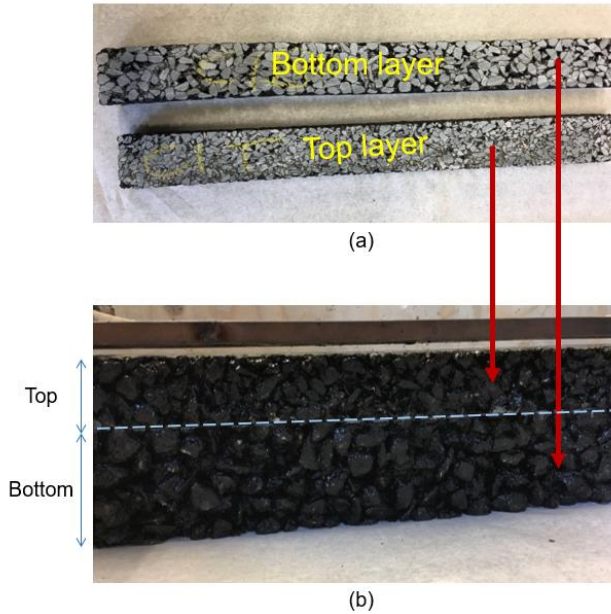


Figure B.1 Induction heating of the two-layer porous asphalt system simulated in laboratory: (a) individual beams to simulate asphalt layers and (b) the stacked layers under induction coil.

Figure B.2 shows the infrared images of the two-layer system under induction heating. For both systems, the surface temperature gradually increased during heating, developed from the top layer and into the bottom layer. In general, the original system showed higher heating speed, as the surface temperature was higher than the improved system after 1-minute heating. However, the heat was more concentrated in the top 2 cm for the original system, and this temperature segregation became more significant after 2-minute heating which caused an overheating (temperature over  $90^{\circ}\text{C}$ ) on the surface but the bottom remained below  $50^{\circ}\text{C}$ . With the improved induction system, the temperature segregation was significantly reduced as the upper half of bottom layer presented a similar infrared colour as the top layer.

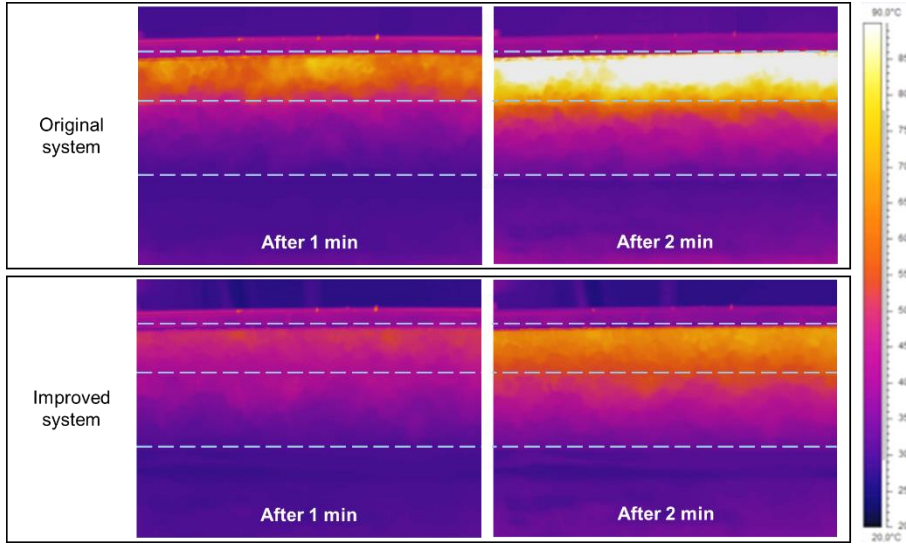


Figure B.2 The infrared images of the two-layer porous asphalt heated with the original system (top) and the improved system (bottom).

Hence, applying an improved induction heating in a two-layer PA holds great potential to achieve deeper and more homogeneous heating, thus a better overall healing effect which has a significant field application prospect.

## REFERENCES

- [1] M. Liu, X. Huang, G. Xue, Effects of double layer porous asphalt pavement of urban streets on noise reduction, *International Journal of Sustainable Built Environment* 5(1) (2016) 183-196.
- [2] M. Li, *Tyre-road noise, surface characteristics and material properties*, Delft University of Technology, 2013.

# C

## **USING MICROWAVE HEATING AS A SUPPLEMENT TOWARDS A FASTER AND DEEPER CRACK HEALING**

Microwave healing, with excellent heating speed and less energy consumption, was also investigated in this study. The aim of this study is to use microwave healing as a supplement for the combined healing system to solve the potential practical problems from induction healing, i.e., limited heating depth and heating speed. To this aim, the microwave healing efficiency was investigated with the SCB bending and healing programme which is described in Chapter 6.

The preparation procedure of the SCB samples is described in Chapter 5, and the mix compositions of the SCB samples are described in Table B.1. Hence, this microwave healing system study includes three different mixture groups, namely T1, T2 and B, and as such two mixture types and two steel fibres contents are considered in this study. Figure C.1 shows images of an SCB specimen (mixture type T1) before bending test and after bending test.

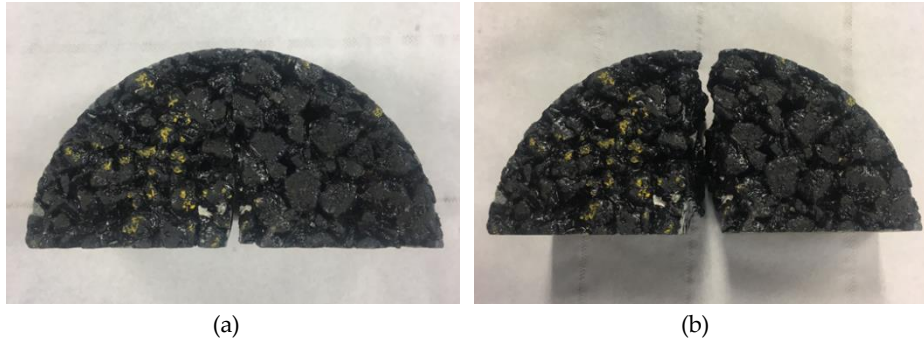


Figure C.1 The SCB specimen: (a) before bending test (after healing) and (b) fractured after bending test.

X-CT was employed to study the steel fibre distribution in the PA mix. Figure C.2 presents the steel fibres distribution in a PA with mixture type B, where the yellow particles in the CT scan image (right) illustrate the positions of the steel fibres in the PA cylinder (left). It indicates that when 6% steel fibres are added, they are homogeneously distributed in the PA mix since no significant cluster is found.

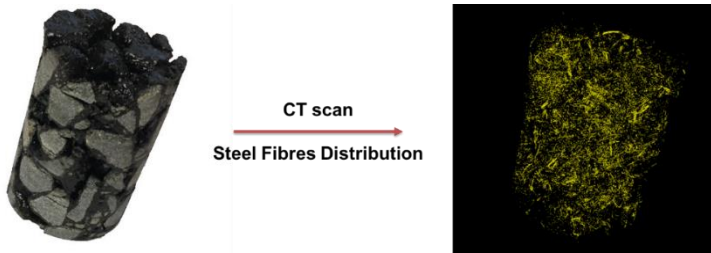


Figure C.2 Steel fibre distribution study with CT scan.

Aimed to determine the microwave heating time for this study, five SCB specimens (type B) were heated in a microwave oven for 30, 45, 60, 75 and 90 seconds, respectively, and the highest surface temperature of the heated specimen are shown in Figure C.3 (a). It is found that a microwave heating period of 75 seconds leads to the highest surface temperature at 84°C which almost reaches the optimum temperature for thermally induced crack healing behaviour [1], and as such the microwave heating time was determined as 75 seconds. Figure C.3 (b) shows the average temperature measured from the infrared camera during all microwave healing cycles. The dash-lines in Figure C.3 (b) show the average healing temperatures of SCB specimens from groups T1, T2 and B, which are 60.4, 97.3 and 77.1°C,

respectively. The specimens in group T2 showed the highest microwave heating temperature, this may be due to its greatest steel fibres content among the three test groups. For the same reason, B showed higher microwave heating temperature than T1.

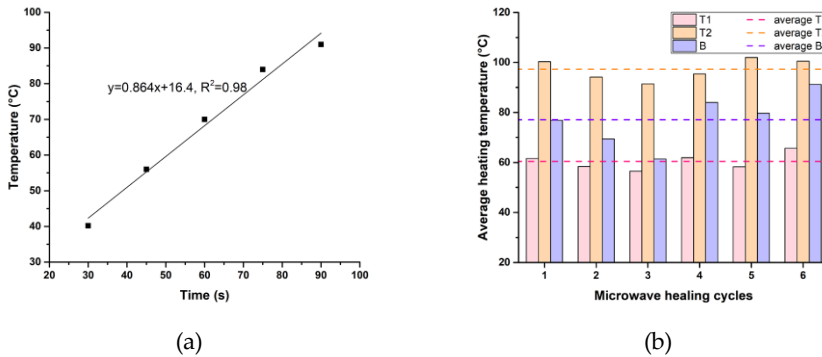


Figure C.3 Maximum temperature after microwave heating: (a) temperature vs heating time and (b) maximum temperature during healing cycles.

Figure C.4 illustrates the temperature distribution of SCB specimens with different mixture types after microwave heating. Although T1 (Figure C.4 (a)) showed a lower heating temperature than T2 and B, its temperature was more evenly distributed and did not show a temperature concentration area which was presented in the other two groups (Figure C.4 (b) and (c)). Besides, it is noticed that the temperature inside the sample is sometimes much higher than on the surface, and this can be observed from both Figure C.4 (b) and (c) where some area behind the surface aggregate showed brighter colours. As such, the microwave healing technique holds a damage healing potential deeper inside the PA.

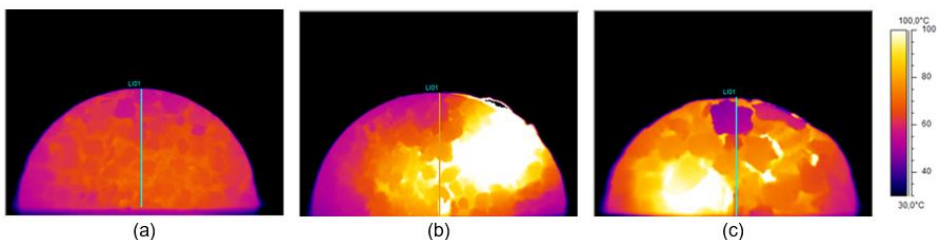


Figure C.4 images of SCB specimens with different mixture types after microwave heating: (a) T1, (b) T2 and (c) B.

Figure C.5 presents the development of maximum stress of SCB specimens during the bending and healing cycles. Figure C.5 (a) shows that T1 and T2 have much higher initial maximum stress than B which indicates PA 4/8 has a higher fracture resistance than PA 8/11. During the SCB bending and healing cycles, some specimens from group T1 could not gain any strength from microwave healing after the third bending test, and the maximum stress of these specimens was regarded as 0 N/mm<sup>2</sup> in the following cycles which caused large errors of group T1 from cycle 4. The same situation was also found in group B where some specimens could not be healed after cycle 5. However, all specimens from group T2 could regain a maximum stress around 0.3 N/mm<sup>2</sup> after all the microwave healing cycles. Moreover, the regained strength in T1 (after cycle 2) was significantly lower than B and T2, and this finding might be related to the microwave heating temperature shown in Figure C.5 (b) as well as the steel fibres content in PA mix. Figure C.5 (b) presents the healing index of T1, T2 and B during the bending and healing test cycles which shows a similar trend as the maximum stress. It was found that T1 had the lowest healing efficiency, and B showed a rapid decrease of healing index at cycle 6 which might be due to the unrecoverable specimens in group B.

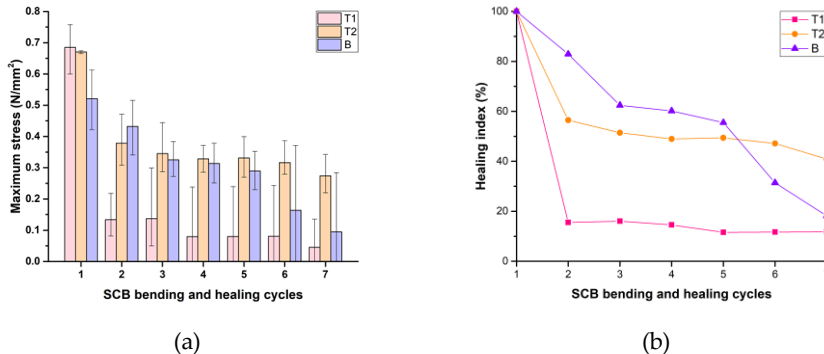


Figure C.5 the development of maximum stress of SCB specimens during the bending and healing cycles: (a) the average maximum stress and (b) the healing index.

Figure C.6 shows the side effects of microwave heating on the healed specimens. Figure C.6 (a) shows the image of SCB specimen from group T2 whose bitumen overflowed out of the surface after microwave heating, which might be due to the heat concentration inside of the PA. Figure C.6 (b) summarised the vertical deformation of all the specimens after all the bending and healing cycles. Specimens from group B (PA 8/11) contained larger particles in the mix and showed the highest

vertical deformation. The deformation of specimens in group T2 was higher than those in T1, which might be because of the higher microwave heated temperature for specimens in T2. The change of asphalt structure during microwave heating was also reported by Norambuena-Contreras et al [2].

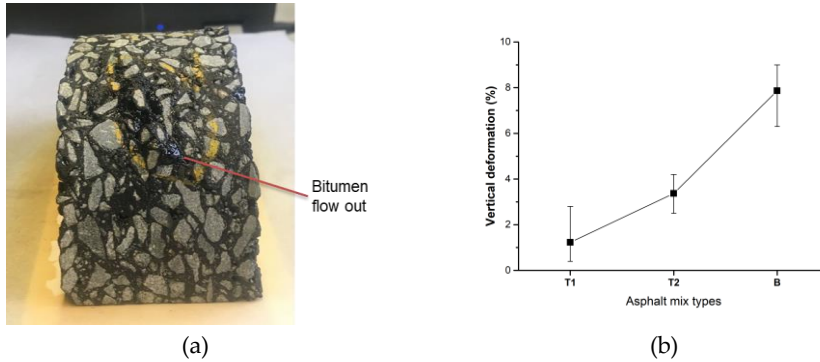


Figure C.6 Side effects of microwave heating: (a) bitumen flow out and (b) summarise of the vertical deformation.

Figure C.7 shows the crack healing efficiency of microwave healing system in comparison with other healing systems discussed in this Ph.D. project. In Figure C.7, the healing index of specimens from group B is used to represent the healing efficiency of microwave healing system as B followed the same mixture design principle as the other healing systems. It indicates that the microwave healing showed lower efficiency than the induction healing when tested on the same mix (without laboratory ageing). Moreover, this microwave healing efficiency was even lower than the induction healing system and combined healing system with laboratory aged mixture in most of the healing cycles. This might be due to the uneven heating effect from microwave which means the damaged area is not always covered by the high-temperature region from microwave heating, and this uneven heating could further change the void distribution in PA mix. However, since the microwave heating technique can heat up the PA structure below the surface, it is believed that, after improvement, the microwave healing system can be an effective supplement for induction healing system towards a deeper damage healing in asphalt.

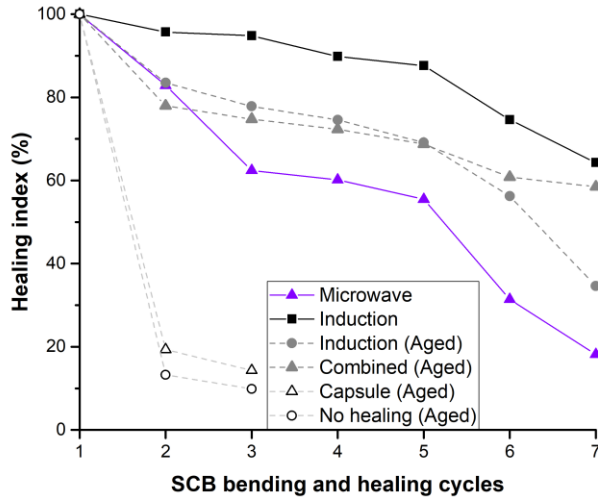


Figure C.7 The healing efficiency of microwave healing system in comparison with other healing systems.

## REFERENCES

- [1] Q. Liu, E. Schlangen, M. van de Ven, Induction healing of porous asphalt concrete beams on an elastic foundation, *Journal of Materials in Civil Engineering* 25(7) (2012) 880-885.
- [2] J. Norambuena-Contreras, A. Garcia, Self-healing of asphalt mixture by microwave and induction heating, *Materials & Design* 106 (2016) 404-414.

## SUMMARY

Porous asphalt, due to its advantages of noise reduction and water drainage, is widely used in the surface layer of the highway in the Netherlands. However, the porous structure makes it prone to ravelling, therefore more frequent maintenance and reconstruction than other asphalt mixtures. The porous asphalt service life can be extended with self-healing technology, such as: induction heating and encapsulated rejuvenator, but both methods have their limitations: induction heating becomes less effective when bitumen oxidises, ages and loses its healing/recovery abilities, while encapsulated rejuvenator usually has a limited crack healing efficiency. Hence, this research aims to develop a unique self-healing system that combines two self-healing methods (induction heating and rejuvenator encapsulation), and the advantages of the above two methods further extend the service life of the porous asphalt. For this purpose, the development of the combined healing system was conducted in two research stages:

- Development of the calcium alginate capsules healing system

The healing mechanism of a capsule healing system largely relies on the performance of the encapsulated rejuvenator. Aimed to determine the optimal rejuvenator type and amount for a capsule healing system, three different types of bitumen rejuvenator were evaluated based on the physical, rheological and chemical properties of the rejuvenator-bitumen blends. Among them, the rejuvenator R20 was determined as the best performing rejuvenator which was selected to be used for encapsulation purpose.

The calcium alginate capsules encapsulating rejuvenator were prepared and optimized by adjusting the alginate/rejuvenator (A/R) ratio in the production process. It was found that calcium alginate capsules prepared with a A/R ratio of 30/70 possessed the highest rejuvenator content and showed sufficient mechanical resistance and thermal stability to survive the asphalt production and compaction. These capsules are furthermore not harmful to the environment and therefore seem very good candidates to be used for the capsule healing system in porous asphalt.

The calcium alginate capsules healing system was evaluated in asphalt mastic, asphalt mortar and full porous asphalt mix. It was found that the incorporation of these capsules improved the healing efficiency in all types of asphalt mix, while this effect is largely influenced by bitumen ageing since a fresh bitumen might play the main role in the healing process.

- Development of the combined healing system

The combined healing system which includes both calcium alginate capsules healing system and induction healing system was incorporated in a porous asphalt mix. The mechanical properties, fracture resistance and fatigue life of the combined healing system were evaluated and compared with the capsule healing system, induction healing system and the reference mix (without extrinsic healing method). It was found that incorporation of calcium alginate capsules and/or steel fibres would not compromise the mechanical properties of porous asphalt.

Among these healing systems, the combined healing system showed outstanding performance in both crack healing and fatigue damage healing, which might be because of the synergistic effect that the embedded capsules may enhance the induction healing in the long-term damaging and healing cycles. Besides, the induction healing system showed a higher and more durable healing performance than the capsule healing system. It was also found that the capsule healing system showed a slightly higher fatigue life than the induction healing system, but the results were a bit scattered which might be caused by the capsule distribution which determines whether the healing takes place on the damage site or not.

Based on findings in this Ph.D. project, the calcium alginate capsules have been proven to be a reliable rejuvenator encapsulation mechanism and an asphalt pavement healing system. However, combined self-healing system showed an excellent self-healing performance demonstrating the service life extension of PA. However, to perfect the damage healing efficiency of the combined healing system further optimization is recommended in future research.

# SAMENVATTING

Zeer open asfaltbeton (ZOAB) wordt veelvuldig toegepast voor de deklagen van de Nederlandse snelwegen wegens de uitstekende prestaties in zowel geluidsreductie als waterafvoer. De poreuze structuur maakt het wegdek echter vatbaar voor rafeling, hierdoor heeft een ZOAB-toplaag een verkorte levensduur in vergelijking tot deklagen bekleed met dichtasfaltbeton. Met als gevolg dat de wegverhardingen met ZOAB-deklagen frequenter onderhoud en vervanging vereisen. Doormiddel van toepassing van zelfhelend asfalt technologie (i.e. inductiebehandelingen en verjongingscapsules) is het mogelijk de levensduur van de ZOAB-deklaag te verlengen.

Beide zelfhelende asfalttechnieken hebben echter hun beperkingen. Zo hebben de verjongingscapsules meestal een beperkte scheurherstelefficiëntie. En worden inductie-behandelingen op den duur minder effectief als gevolg van de veroudering (i.e. het verlies van herstellend vermogen) van het bitumen dat onder meer optreedt door oxidatie.

Het doel van dit onderzoek is een optimaal zelf herstellend asfalt systeem te ontwikkelen dat beide technieken en hun voordelen (inductiebehandelingen en verjongingscapsules) combineert waardoor het mogelijk wordt om de levensduur van de ZOAB-deklagen drastisch te verlengen.

Om dit doel te verwezenlijken is het onderzoek opgezet in twee onderzoeksfasen:

- i. Het ontwikkelen van de calcium alginaat capsules

Het herstelmechanisme van de capsules is grotendeels afhankelijk van de prestaties van het in de capsules verwerkte verjongingsmiddel. Om het optimale type en hoeveelheid verjongingsmiddel te bepalen, zijn er drie verschillende type bitumenverjongers onderzocht op basis van de fysische, reologische en chemische eigenschappen. Uit het onderzoek is voortgekomen dat de R20 variant het beste resultaat opleverde, en dit type verjongingsmiddel is daarom geselecteerd om in de capsules te verwerken voor het vervolgonderzoek.

Bij de productie van de calcium alginaat capsules zijn voor optimalisatie doeleinden verschillende verhoudingen alginaat/rejuvenator (verjongingsmiddel) (A/R) onderzocht. Uit het onderzoek is geconstateerd dat de calcium alginaat capsules bereid met een A/R-verhouding van 30/70 het hoogste verjongingsmiddelgehalte bevatten, en voldoende mechanische weerstand en thermische stabiliteit bieden om de asfaltproductie en het verdichtingsproces te overleven. Deze capsules zijn bovendien niet schadelijk voor het milieu en lijken daarom zeer goede kandidaten om te worden toegepast voor het zelfhelend asfalt systeem.

De calcium alginaat capsules zijn in asfaltmestiek, asfalt mortel en in een zeer open asfalt mengsel beproefd. Hieruit is gebleken dat de toevoeging van de capsules in alle gevallen leiden tot een groter herstellvermogen van de verschillende types asfaltmengsels.

ii. Het ontwikkelen van een gecombineerd zelfhelend systeem

In de tweede fase van het onderzoek zijn beide zelfhelend asfalt technologieën (i.e. de calcium alginaat capsules en de inductiebehandeling systeem) simultaan toegepast in een poreus asfaltmengsel. Dit mengsel is vervolgens gekarakteriseerd op mechanische eigenschappen, gevoeligheid op scheurvorming en vermoeiingslevensduur. De verkregen resultaten zijn vervolgens vergeleken met de uitkomsten van beproevingen verricht op een referentie mengsel (i.e zonder extrinsieke herstel-methode) en mengsels waarin beide zelfhelende systemen afzonderlijk zijn toegepast. Hieruit volgde dat de toevoeging van de calcium alginaat capsules en/of de staalvezels geen negatieve gevolgen heeft op de mechanische eigenschappen van het poreuze asfalt.

Het mengsel waarin beide zelfhelende asfalt technologieën simultaan zijn toegepast leverde de beste prestatie wat betreft het scheurherstel en het herstel van de vermoeiingschade. Dit is mogelijk het gevolg van het synergistisch effect verkregen door de gecombineerde toepassing van de technieken. De simultane toepassing van beide technieken biedt zowel een oplossing voor bitumenveroudering als haar gevolgen. Aangezien de capsules het herstellend vermogen van het bitumen in stand houdt, behouden de inductie handelingen hun effectiviteit, ook op de lange termijn (i.e. de gevorderde schade-herstel cycli).

Uit de laboratoriumexperimenten is ook vastgesteld dat wanneer beide technieken afzonderlijk werden toegepast, de inductiebehandelingen tot een beter en duurzamer herstellend vermogen resulteerde dan het enkel toepassen van de capsules. De mengsels waarin enkel capsules werden toegepast vertoonde echter een iets langere vermoeiingslevensduur ten opzichte van het inductieherstel systeem. Er

zat echter een spreiding in de resultaten, wat mogelijk te verklaren is door de verdeling van de capsules in het mengsel. Deze verdeling is bepaald of er capsules aanwezig zijn op de beschadigde locatie en of er daardoor herstel plaatsvindt.

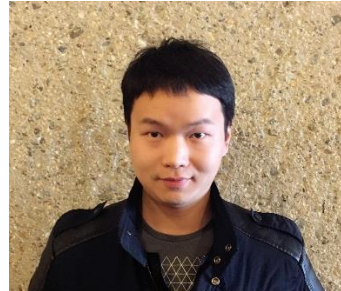
Gebaseerd op de bevindingen in dit proefschrift kan worden geconcludeerd dat het toegepaste calcium alginaat inkapselingproces een betrouwbare methodiek is om het verjongingsmiddel te integreren in het mengsel en dat zowel de capsules als de inductiebehandelingen een bevorderend effect hebben op het herstellend vermogen en levensduurverlenging van het asfalt. Ook kan worden geconcludeerd dat de voordelen van simultane toepassing van beide technieken (zowel inductiebehandelingen als de verjongingscapsule) dus groter zijn dan die van de som van haar delen.

Tot slot wordt er aanbevolen om in de toekomst verder optimalisatie onderzoek te verrichten om de herstelefficiëntie van het gecombineerde systeem te bevorderen.



# CURRICULUM VITAE

**Shi Xu**



11-10-1989      Born in Wuhan, China

## EDUCATION

- Sep 2007 - Jun 2011      B.Sc. student in Computer Sciences  
Wuhan University Luojia college, China
- Sep 2012 - Jun 2015      M.Sc. student in Materials Science  
School of Materials Science and Engineering  
Wuhan University of Technology, China
- Mar 2013 - Sep 2013      M.Sc. exchange programme  
Section of Pavement Engineering  
Delft University of Technology, The Netherlands
- Oct 2015 - Nov2020      Ph.D. candidate  
Section of Materials and Environment  
Delft University of Technology, The Netherlands



# LIST OF PUBLICATIONS

## JOURNAL PUBLICATIONS

1. **S. Xu**, A. Tabaković, X. Liu, E. Schlangen, Calcium alginate capsules encapsulating rejuvenator as healing system for asphalt mastic, *Construction and Building Materials* 169 (2018) 379-387.
2. **S. Xu**, A. García, J. Su, Q. Liu, A. Tabaković, E. Schlangen, Self-healing asphalt review: from idea to practice, *Advanced Materials Interfaces* 5(17) (2018) 1800536.
3. **S. Xu**, X. Liu, A. Tabaković, E. Schlangen, Investigation of the potential use of calcium alginate capsules for self-healing in porous asphalt concrete, *Materials* 12(1) (2019) 168.
4. **S. Xu**, X. Liu, A. Tabaković, E. Schlangen, A novel self-healing system: towards a sustainable porous asphalt, *Journal of Cleaner Production* 259 (2020) 120815.
5. **S. Xu**, A. Tabaković, X. Liu, D. Palin, E. Schlangen, Optimization of the calcium alginate capsules for self-healing asphalt, *Applied Sciences* 9(3) (2019) 468.
6. **S. Xu**, X. Liu, A. Tabaković, E. Schlangen, The influence of asphalt ageing on induction healing effect on porous asphalt concrete, *RILEM Technical Letters* 3 (2019) 98-103.
7. **S. Xu**, X. Liu, A. Tabaković, P. Lin, Y. Zhang, B. Lommerts, E. Schlangen, The Role of Rejuvenators in Embedded Damage Healing for Asphalt Pavement, *Materials and Design*. (Accepted)
8. **S. Xu**, X. Liu, A. Tabaković, E. Schlangen, Characterization of the extrinsic asphalt healing technologies under fatigue loadings, *Journal of Cleaner Production*. (Under Review)

9. Y. Zou, S. Amirkhania**n**, **S. Xu**, Y. Li, Y. Wang, J. Zhang, Investigation of the behavior of oxidation, dissolution and migration of base asphalt during aqueous solution erosion, *Construction and Building Materials*. (Accepted)
10. **S. Xu**, X. Liu, A. Tabaković, E. Schlangen, An improved induction healing system in porous asphalt, *Construction and Building Materials*. (Submitted)
11. **S. Xu**, X. Liu, A. Tabaković, E. Schlangen, Microwave healing of asphalt pavement, *Processes*. (Submitted)
12. P. Lin, X. Liu, P. Apostolidis, S. Ren, **S. Xu**, S. Erkens, T. Scarpas, W. Huang, On the Rejuvenator Dosage Optimization for Aged SBS Modified Bitumen, *Construction and Building Materials*. (Under Review)

## CONFERENCE PROCEEDINGS

1. **S. Xu**, A. Tabaković, X. Liu, E. Schlangen. Alginate capsules encapsulating rejuvenator as self-healing system for porous asphalt concrete. Proceedings of the EU-funded HEALCON project final conference, Delft, The Netherlands, 2016.
2. **S. Xu**, A. Tabaković, X. Liu, E. Schlangen. Preparation of Calcium Alginate Capsules and the Application in Asphalt Mastic. Proceedings of the 6th International Conference on Self-healing Materials, Friedrichshafen, Germany, 2017.
3. **S. Xu**, X. Liu, A. Tabaković, E. Schlangen. Investigation of the Potential Use of Calcium Alginate Capsules for Self-healing in Porous Asphalt. Proceedings of the 4th International Conference on Service Life Design for Infrastructures, Delft, The Netherlands, 2018.
4. **S. Xu**, X. Liu, A. Tabaković, E. Schlangen. Alginate Capsules Encapsulating Rejuvenator as Self-healing System for Porous Asphalt Concrete. Proceedings of the 5th Chinese European Workshop on Functional Pavement Design, Changsha, China, 2018.
5. **S. Xu**, X. Liu, A. Tabaković, E. Schlangen. Investigation of the Potential Use of Calcium Alginate Capsules for Self-healing in Porous Asphalt Concrete. Proceedings of the 98th Transportation Research Board, Washington, United States, 2019.

6. **S. Xu**, X. Liu, A. Tabaković, E. Schlangen, Application of Induction Heating and Encapsulated Rejuvenator in Self-healing Asphalt. Proceedings of the 7th International Conference on Self-healing Materials, Yokohama, Japan, 2019.